Integrating 3D Printing and Injection Molding for Mass Customization: Advancements in Hybrid Manufacturing

TUS
**Technological University of the Shannon:
Midlands Midwest**
Ollscoil Teicneolaíochta na Sionainne:
Lár Tíre Iarthar Láir

A thesis submitted for PhD Viva

of

Technological University of Shannon: Midlands and Midwest

By

Ke Gong

Based on the research carried out under the supervision of

Dr. Ian Major

Co-supervisors: Dr. Declan Devine, Dr. Zhi Cao, Dr. Evert Fuenmayor

PRISM Research Institute

Technological University of Shannon: Midlands and Midwest

Athlone

Co. Westmeath

Ireland   August 2023

Declaration

I hereby declare that this thesis submitted to the Technological University of Shannon: Midlands and Midwest for the Ph.D. Viva, is a result of my own work and has not in the same or altered form, been presented to this university or any other institutes in support for any degree other than for which I am now a candidate.

Ke Gong   August 2023

Acknowledgement

Light travels like an arrow, and time like a shuttle. The research study, which lasted for five years, is finally completed. During this time, I gained a lot of valuable experience, not only in terms of research skills, but also through the kind and patient individuals I met who provided me with a lot of support.

First and foremost, I would like to express my sincere gratitude to my principal supervisor, Dr. Ian Major, due to his invaluable advice, patience, motivation and immense knowledge. He has provided me guidance and support for my progress to date in my own ability and thus having the opportunity to progress my studies to PhD registration and even the PhD award. Apart from his mentorship he has been instrumental in expressing confidence and encouraging me to undertake this research course.

I would like to thank my co-supervisors Dr. Declan Devine, Dr. Zhi Cao and Dr. Evert Fuenmayor for their insightful comments and encouragement which helped me wide my research from various perspectives.

I would like to thank all the staff members of Office of Research, International Office, MRI, APT, CISD as well as my fellow researchers for their support and advice.

Last but not least, I would like to thank my family for their love, support, encouragement and for all the help from Ms. Linghong Li, my landlord Mr. Denis Cronin, my housemates of mine in Athlone, and friends when in need.

Abstract

Additive manufacturing (AM) is renowned for its ability to create complex geometries and customized products but is limited by low throughput. Conversely, injection molding (IM) excels in high-volume production but struggles with cost-effective customization due to mold tooling constraints. This thesis investigates hybrid manufacturing (HM), which combines the strengths of AM and IM, as a solution for mass customization - the production of personalized products at costs comparable to mass production. The focus is on integrating fused deposition modeling (FDM), a form of AM, with IM to achieve mass customization. The study is divided into two main sections: overmolding and overprinting.

In the overmolding section, FDM-fabricated preforms are integrated into the mold cavity. The study examines how various parameters, such as infill density, joint configuration, interface direction, and material choice, affect the mechanical properties of the hybrid products. The results indicate anisotropic maximum tensile strength between half-length (25.47 MPa in HL-FT 25 for Acrylonitrile Butadiene Styrene (ABS) batches and 30.11 MPa in HL-FT 75 for Polylactic Acid (PLA) batches) and half-thickness specimens (48 MPa in HT-FT 50 for ABS batches and 68.38 MPa for HT-FC 75 in PLA batches) for single-material overmolding specimens. As for the dual-material overmolding, a worse tensile performance (46.1 MPa in 75-FT-60) in comparison to the half-thickness series for single-material ones can be found.

The overprinting section explores the integration of FDM components onto injection-molded substrates. While this approach showed inferior tensile performance (47.1 MPa in 25-70-220 batch for ABS pieces and 56.3 MPa in 50-70-210 batch for PLA pieces) compared to pure IM and overmolding, it demonstrated potential benefits including reduced manufacturing costs and enhanced design flexibility.

In conclusion, this thesis establishes a groundwork for future HM techniques that demand higher design flexibility and fabrication efficiency. Overmolding and

overprinting have demonstrated their potential in producing customized products at lower costs. Future research could explore the integration of Stereolithography (SLA) for creating tailored molds with thermosetting polymers, combining higher design flexibility with cost efficiency.

Abbreviation

ABS	Acrylonitrile Butadiene Styrene
AM	Additive Manufacturing
AM-CNC	Additive Manufacturing-Computer Numerical Control
ANOVA	Analysis of Variance
ASTM	American Society for Testing Materials
CAD	Computer Aided Design
CNC	Computer Numerical Control
CSA	Cross Section Area
DLP	Digital Light Processing
FDM	Fused Deposition Modelling
FFF	Fused Filament Fabrication
Hybrid-AM	Hybrid-Additive Manufacturing
HM	Hybrid Manufacturing
HYM	Hybrid Manufactured Sample
IM	Injection Molding
IMM	Injection Molding Machine
IT	Information technology
LOM	Laminated Object Manufacturing
MC	Mass Customization
MFI	Melt Flow Index
MPa	10^6 Pascal
N	Newton
PC	Polycarbonate
PS	Polystyrene
PET	Polyethylene Terephthalate
PLA	Polylactic Acid

RP	Rapid Prototyping
SEM	Scanning Electron Microscopy
SFF	Solid-Freeform
SI	International System of Units
S_o	Cross Section Area
SPSS	Statistical Product and Service Solutions
STL	Standard-Triangle-Language
TS	Tensile Strength
UTS	Ultimate Tensile Strength
3DP	3D printing
σ	Tensile Strength
"ϵ"	Tensile Strain
δ	Extension
ΔL	Change in Length
e	Elongation
E	Young's Modulus
k	Stiffness
l	Final Length after deformation
L	Original Length
L_K	Original Length in Elongation
L_o	Final Length for Elongation
F_b	Maximum Force

Table of Contents

List of Tables

List of Figures

Chapter 1: Introduction

1.1 Research Context

Traditional manufacturing, particularly in the context of plastics processing, has been squarely focused on high-volume production, to produce the largest number of articles in the least amount of time. Thus, much manufacturing research has been concerned with increased efficiency through faster cycle times or by lowering energy input. However, for specific items, consumers are showing an increased desire for articles that are better suited to their individual needs or tastes. Custom items have always been considered a luxury purchase, be that furniture or clothing, and conversely come with a higher price tag. Over the last decade, companies have become engaged in a concept known as mass-customization, aiming to provide a tailored choice for the consumer while maintaining a lower cost.

The trend for custom products that meet individual needs and tastes gathered pace with the advent of the personal computer, largely generated by consumer pressure on suppliers (Aigbedo, 2007; Duray, 2002; Fogliatto et al., 2012). Nike pioneered the production of custom footwear by offering both custom-fit and fully tailored with the launch of NikeiD in 1999; custom-fit kept much of the base units the same (mass-volume) could be tailored easily in very specific areas such as color and size which were specified by the customer at purchase, whereas the fully tailored batch manufactured for each customer (Salvador et al., 2009). NikeiD offers a variety of customized goods, such as shoes and clothing, with shoes classified into basketball, soccer and other categories. Hybrid manufacturing, combining additive and subtractive manufacturing in a single part, has been widely applied in several fields and has gradually obtained popularity in the last two decades (Feldhausen et al., 2021; J. Ma et al., 2021; Merklein et al., 2016a; Strong et al., 2018). The additive manufacturing process offers great freedoms of design, while the subtractive manufacturing possesses a high efficiency in production. To date, several studies have discovered the possibility of varied additive processes in hybrid manufacturing (Kerschbaumer & Ernst, 2004; Sreenathbabu et al., 2005), but few have investigated the potential of fused deposition modelling applied in the combination. In addition,

injection molding has been extensively utilized in manufacturing industry since it can produce massive items in short. Thus, the implementation of hybrid manufacturing is expected to enhance the productivity of customizable items using injection molding.

1.2 Research Questions

Injection molding (IM) is a technique being widely employed in the area of plastics owing to its outstanding capability to produce 3D articles with adequate dimensional accuracy and high-volume characteristics allowing users to manufacture several products in a relatively short time (Dalgarno et al., 2001; Sha et al., 2007). The higher density of the material in the injection molded samples is considered to be the reason for the excellent mechanical properties of the injection molded parts. However, there are still a number of issues that limit the use of IM, including the high cost and long lead times of manufacturing new mold tooling.

Additive manufacturing, also well known as 3D printing, is a method that can be used to manufacture several complex three-dimensional articles, facilitate the design improvement and rapidly manufacture tailored components (Casavola et al., 2016; Domingo-Espin et al., 2015; S. H. Huang et al., 2013; Melenka et al., 2016; Stansbury & Idacavage, 2016; Sugavaneswaran & Arumaikkannu, 2015; Tymrak et al., 2014). FDM technique is the most applied technique amongst all 3DP manufacturing methods, which prints specimens by controlling the location of extruded molten filament and thereafter collecting onto the build platform in which layers are fused together (Wang et al., 2017). Its low operating costs, ease of use, and multi-material capacity enable it to be widely used in a variety of applications, including pharmaceutical and household industries (Araújo et al., 2019; Fuenmayor, Donnell, et al., 2019; Goyanes et al., 2015a; Lim et al., 2016; Martinez et al., 2018; Melchels et al., 2012; Sadia et al., 2018). In particular, the ability to fabricate customized objects with complex geometry while governing the internal structure of 3D printed objects has made it popular with most users. However, some defects, such as the poor mechanical performances for products having low infill density, the voids formed during the manufacturing and the necessary

preparation of material filament prior to the printing process, are still challenging the users (Weng et al., 2016). Given the importance of mechanical properties in manufactured composites, recent studies have looked at the relationships between printing settings and the resulting printing quality (Anitha et al., 2001; Lee et al., 2005; Rodríguez et al., 2001, 2003a; Vaezi & Chua, 2011).

Given these phenomena, existing techniques have reached a standstill, creating a fitting moment to introduce a novel hybrid manufacturing approach. This innovative method could effectively address the limitations inherent in both injection molding and 3D printing.

1.3 Research Objectives

- Determine the effect of fused deposition modelling and injection molding on the hybrid manufactured part performance
- Determine the effect of two different hybrid manufacturing approaches - overmolding and overprinting – on part performance.
- Determine the key factors that underpin successful additive-molding based hybrid manufacturing.

1.4 Project Output

1.4.1 Academic Journal Papers

1. Hybrid Manufacturing of Acrylonitrile Butadiene Styrene (ABS) via the Combination of Material Extrusion Additive Manufacturing and Injection Molding

Gong, K.; Liu, H.; Huang, C.; Cao, Z.; Fuenmayor, E.; Major, I. Hybrid Manufacturing of Acrylonitrile Butadiene Styrene (ABS) via the Combination of Material Extrusion Additive Manufacturing and Injection Molding. Polymers 2022, 14, 5093. doi: 10.3390/polym14235093

2. Mass Customization of Polylactic Acid (PLA) Parts via a Hybrid Manufacturing

Process

Gong, K.; Liu, H.; Huang, C.; Jiang, Q.; Xu, H.; Cao, Z.; Fuenmayor, E.; Major, I. Mass Customization of Polylactic Acid (PLA) Parts via a Hybrid Manufacturing Process. Polymers 2022, 14, 5413. doi: 10.3390/polym14245413

3. Hybrid Manufacturing of Mixed-Material Bilayer Parts via Injection Molding and Material Extrusion 3D Printing
K. Gong, H. Xu, H. Liu, Z. Cao, E. Fuenmayor, I. Major, J. Appl. Polym. Sci. 2023, e53972. https://doi.org/10.1002/app.53972

4. Optimizing process parameters of a material extrusion-based overprinting technique by Taguchi method for the fabrication of tensile specimens
Gong, K., Liu, H., Xu, H. et al. Optimizing process parameters of a material extrusion–based overprinting technique for the fabrication of tensile specimens. Int J Adv Manuf Technol (2023). https://doi.org/10.1007/s00170-023-11720-7

5. Parameter Optimization for PETG/ABS Bilayer Tensile Specimens in Material Extrusion 3D Printing through Orthogonal Method
Chen, Z., **Gong, K.**, Huang, C., Hu, S., Xu, H., Fuenmayor, E., Major, I. Parameter optimization for PETG/ABS bilayer tensile specimens in material extrusion 3D printing through orthogonal method. Int J Adv Manuf Technol (2023). https://doi.org/10.1007/s00170-023-11515-w. **Zhixin Chen and Ke Gong have contributed equally to this work and share first authorship.**

6. Hybrid Manufacturing of Oral Solid Dosage Forms via Overprinting of Injection-Molded Tablet Substrates
Xu, H.; Ebrahimi, F.; **Gong, K.**; Cao, Z.; Fuenmayor, E.; Major, I. Hybrid Manufacturing of Oral Solid Dosage Forms via Overprinting of Injection-Molded Tablet Substrates. Pharmaceutics 2023, 15, 507. doi: 10.3390/pharmaceutics15020507

1.4.2 Conferences and Seminars

1. AIT Research series (Athlone Institute of Technology, Ireland, May 2019): Poster presentation on the experiments for FDM-IM hybrid manufacturing in ABS pieces.

2. AIT Research series (Athlone Institute of Technology, Ireland, November 2019): Poster presentation on the experiments for hybrid manufacturing in ABS and PLA pieces.

3. AIT Research series (Remote, June 2020): Poster presentation on the findings in the mechanical performances of hybrid manufactured ABS and PLA pieces.

4. Shannon Region Postgraduate Research Conference (Remote, May 2021): Poster and slide presentation on the overmolded ABS and PLA pieces.

5. Irish Polymer Group (IPG) Polymer Seminar (Athlone, April 2023): Presentation on the two routes of FDM-IM hybrid manufacturing in pursuit of mass customization.

Chapter 2: Literature Review

2.1 Manufacturing

Manufacturing is the production of goods and can directly indicate a country's productivity and is a significant determinant of global competitiveness and an advanced economy's national output (Kalpakjian & Schmid, 2010). Advanced manufacturing encompasses both the traditional manufacturing industry that has integrated new technologies, especially information technology (IT), and new manufacturing techniques such as bio-manufacturing, micro and nanomanufacturing. One advanced manufacturing technique is 3D printing. The development of 3D printing will lead to the manufacturing industry's significant growth as it offers a simple method to make complicated goods in demand by customers (Srinivasan et al., 2018). In combination with digitalization, IT implementation and new energy efficiencies, this manufacturing technology will bring fundamental change to national economies.

Traditionally, manufacturing has been defined as the process of transforming raw resources into finished goods. This transformation involves the use of physical and chemical techniques to alter the form and properties of the raw materials. The manufacturing of components typically involves machine tools, energy, cutting tools, and manual labor, and it may incorporate assembly techniques such as robotics and automated machinery. In the past, manufacturing was often associated with larger economic operations, and it was primarily seen as a process that added value to raw materials by changing their shape and properties (physical and chemical) (Mital et al., 2014).

In the context of today's economic landscape, the traditional manufacturing process, which simply transforms raw materials into products with desired geometries, has become inadequate (Lauwers et al., 2014). Instead, the transformation process must be swift, convenient, cost-effective, and efficient, resulting in high-quality products that meet consumer demands. To secure a larger market share, it's crucial to introduce a product to the market as quickly as possible. In this view, a product must be unique and offer great value and utility to the customer; otherwise, it has little chance of surviving in the present global market for comparable items.

Manufactured products can be divided into two categories: a) consumer products, such as vehicles, lights, and televisions, which are generally used by the public, and b) producer capital items, like railroad cars and drilling machines, which are used to produce consumer products. The manufacturing industry comprises enterprises and organizations that use capital assets to manufacture consumer goods. Manufacturing processes refer to the procedures used to transform raw materials into finished goods with desired properties via specific methods, which can be shown in Figure 2-1 (Mital et al., 2014).
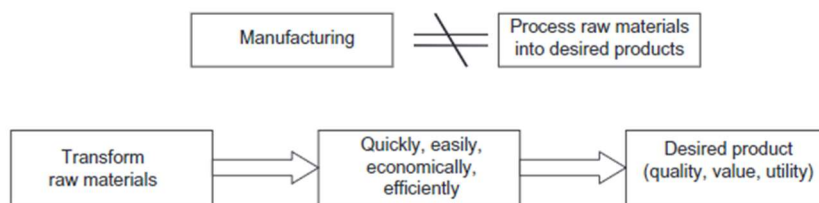
Figure 2-1 Definition of manufacturing (Mital et al., 2014).

Manufacturing is composed of the design, planning, operation, the control of manufacturing and the final outputs (Kalpakjian & Schmid, 2010). Figure 2-2 indicates a manufacturing system is an organization that includes marketing, finance, human resources, and accounting in addition to manufacturing processes and production, aiming to generate the final products. This demonstrates that the customer is at the heart of the manufacturing infrastructure, regardless of the techniques or utilities involved. Essentially, manufacturing combines appropriate design, technology, materials, processes, labor, and energy to produce desired goods in an efficient and economical manner (Robert H. Todd, Dell K. Allen, 1994). This needs a thorough rethinking by manufacturing firms, as producing bespoke items has become critical for survival in the global market.

(6)
Manufacuring infrastructure
(5)
People—Materials—Tools—Resources—Information—Technology—Suppliers

Life cycle transitions (4) Business definition

Customer services

System design

Sales and promotion

Shared knowledge (3)

Component design

Customer support

Product/process

Distribution

(2)

People

Teamwork

Continuous improvement

Global organization

(1)

Customer

Documentation and release

Organization

Resource planning

Material management

Systems

Manufacturing

Employee—Investor—Community—Responsibilities—Regulatory—Ethical—Environmental

Assembly and rest

Component fabrication

Operations planning

Figure 2-2 The manufacturing enterprise wheel (Society of Manufacturing Engineers, 1994).

2.2 Custom Manufacturing via 3D Printing

2.2.1 Introduction

Additive manufacturing (AM) is a manufacturing process that uses computer-aided design to produce a three-dimensional object, using an additive (or deposition) process (Tofail et al., 2018), usually layer-by-layer. This technology was invented and first commercialized by Charles Hull in the 1980s with the stereolithography (SLA) technology (Patrick et al., 2017). The AM technique has been utilized in several fields, including medical, automotive, and aerospace (Arif et al., 2018; Chen et al., 2018; C. Liu et al., 2018; Sugavaneswaran & Arumaikkannu, 2015; Tian et al., 2017). Several AM techniques are available such as Stereolithography (SLA) (Cooke MN, Fisher JP, Dean D,

Rimnac C, 2003), Selective Laser Sintering (SLS) (Kruth et al., 2005), Laminated Object Manufacturing (LOM) (Giannatsis & Dedoussis, 2009), Digital Light Processing (DLP) (Cooperstein et al., 2015), and Fused Deposition Modelling (FDM) (Syed, 1996).

To date, seven categories in AM processes have been identified in ISO/ASTM 52900: 2021 (Additive Manufacturing — General Principles — Fundamentals and Vocabulary, 2021), in which the material extrusion (Braconnier et al., 2019), material jetting (Giorleo et al., 2022), vat photopolymerization (Zhuo et al., 2022), and binder jetting (Van Der Walt et al., 2022) are extensively employed in polymer materials, while the powder bed fusion (Oliveira et al., 2020), sheet lamination (Z. Huang et al., 2023), and direct energy deposition (K. Liu et al., 2023) are mostly utilized in metals and ceramics.

AM fabricates articles by creating successive cross-sectional layers. The process begins with a 3D model constructed via CAD software and translated to a Standard-Triangle-Language (STL) extension file. Such a file is normally sliced into various pieces, containing the necessary information for each desired layer of the model, like the number of layers (relying on the resolution) by the preparation software. Each single layer then stacks altogether to generate the finished products.

This technique offers a good deal of advantages compared with those conventional manufacturing methods: near-net form capabilities; product geometry flexibility; superior levels of design sophistication with more minor or single-step manufacturing required; reduced tooling and fixtures; shorter cycle times for both designs and processing; multiple material manufacturing; savings in energy and start-up expense (Gao et al., 2015), in which its rapid design and fabricating ability make it popular in the research and manufacturing industry (Melenka et al., 2016). The disadvantages of AM involve slow manufacturing rates compared to other manufacturing processes like injection molding. There is also a limit to the size of the 3D printed parts, and the mechanical properties are poor compared with other manufacturing processes. Lastly, the discontinuous nature of the process prevents savings via economies of scale.

2.2.2 Fused Deposition Modelling

FDM, which is also referred as Fused Filament Fabrication (FFF), Modelling Extrusion (ME) and Fused Layer Manufacturing (FLM), is one type of 3DP process on the grounds of extruding material, in which the material selected is normally deposited through a nozzle (Popescu et al., 2018). FDM was a patented technology of Stratasys up until 2009 (Crump, 1992), and although the name is still trademarked by the company, the technology was adapted for making affordable desktop printers under the name FFF and especially through the efforts of the RepRap project. Despite some main FDM applications, like visual aids, presentation or educational models, and assembly models, its ability to manufacture helpful articles has increasingly attracted much interest in various fields (Wong & Pfahnl, 2014).

The filament is generally fed through the heating area in which melting the filament into a semi-melted phase occurs. The material is then forced through the nozzle and then deposited on the printing platform. The extrusion nozzle moves relating to the STL file and the file instructions obtained from the software that it rises on the Z axis and works in the X-Y plane. The extrusion nozzle repeats the same procedure to deposit material in a layer-by-layer action to produce a 3D model (Wang et al., 2017).

The substratum is originally lying on the table, which is available to move in the Z axis. The printing platform moves down to deposit the following layer after one layer has been successfully fabricated, whose distance based on the layer thickness. All layers are composed of specific roads of deposition, whose dimensions are controlled with the flow rate of material and extrusion head movement. Rodríguez et al., (2001) showed that molecules' action constructs the bonding between the rasters or layers due to the thermal energy of material in molten phase. These layers were stacked in basis of two phenomena: intimate contact and molecular interdiffusion, which will be more discussed in Section 2.2.3. The value of layer thickness can be varied in accordance with the types of FDM machine and is floating from 0.05 mm to 0.76 mm as for the Prodigy FDM 1000 ® from Stratasys ® (Rosas, 2013). The part is finally

constructed after all acquired layers have been fabricated and shown as the model imported from the CAD file. On some special occasions, the process of FDM needs a support structure underneath the building material. The material for such structure is similar to that for the model. However, it should be considered more on the brittle material compared with the model one as this makes support easily removed after the model finishes. Usually, the FDM 3D printer fabricates the support for the area with the overhanging angle less than 45 degree in horizontal (Montero et al., 2001). As shown in Figure 2-3, the usual FDM printer carries two nozzles employed to extrude the model material and the one for support.
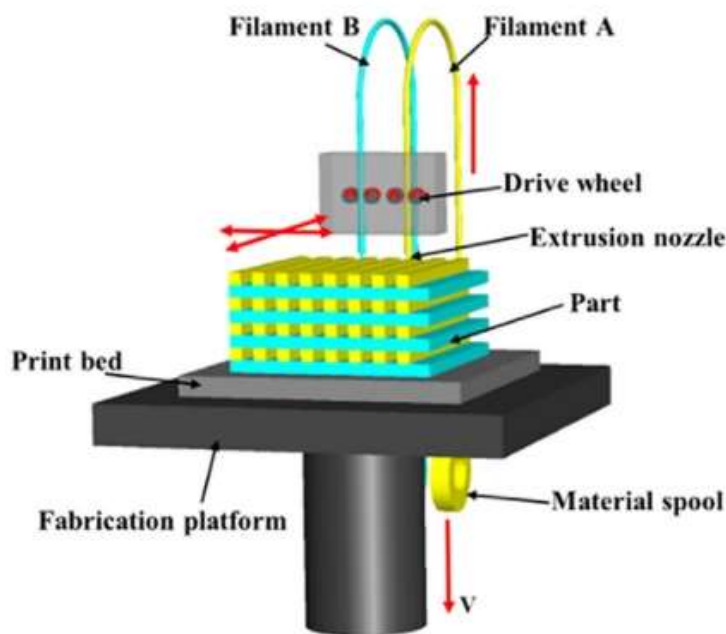
Figure 2-3 Schematic representation of FDM (Wang et al., 2017).

Various types of thermoplastic material like Polycarbonate (PC), Acrylonitrile Butadiene Styrene (ABS) and Polylactic Acid (PLA) (Drummer et al., 2012), Nylon (Masood & Song, 2004; Pei et al., 2015), and their blends (Rocha, C., Torrado Perez, A., Roberson, D., Shemelya, C., MacDonald, E., & Wicker, 2014) are generally utilized mainly owing to their low melting temperature and other particular characteristics. For instance, those material soluble in water can be employed to fabricate as the interim support during the model being constructed.

Several advantages, such as low cost, high speed, and simplicity during the

process of FDM, have offered it a wide range of applications, equipment building (Hutmacher et al., 2001), prototyping (Kalita et al., 2003), numerical simulation through finite analysis (Zhang & Chou, 2008), and houseware (Weng et al., 2016). Notwithstanding these benefits, there are still some drawbacks concerned with FDM, including the limited material range, the process feeding constraints, and the need for support structures.

The quality of articles by FDM can be varied under the modification of printing parameters, including infill density, layer thickness, orientation of building, raster angle and raster width (Sood et al., 2010). Several previous publications have concluded that various 3DP parameters may influence the mechanical properties of objects produced through FDM technique, in which some researchers demonstrated some terms, low feeding speed and low layer height, can enhance the mechanical properties of final manufactured objects (Christiyan et al., 2016). Chacón et al. (2017) investigated the influence of some process parameters, printing orientation, the thickness of each manufactured layer and printing speed upon the tensile and flexural specimens of PLA material. They found that those printed in upright orientation led to the worst mechanical property amongst all three, while those manufactured in the orientations of edge and flat attributed to excellent strength and stiffness, respectively. This result can be explained from the perpendicular direction in fusion area and tensile/flexural loading in edge and flat batches and parallel situation in upright ones. Ziemian et al., (2012) demonstrated the influence of raster orientation on ABS objects' mechanical properties fabricated by FDM technique and found such changed with an anisotropic behavior based on raster orientation and directionality, showing a similar behavior in Chacón et al. (2017): upright results in a poor tensile strength but flat and edge leads to a 3 to 4 times value. Meanwhile, Durgun and Ertan (2014) studied the effect of raster angles and build orientations on final articles' mechanical properties. Wu et al. (2015) investigated the influence of layer thickness and raster angle on the mechanical properties of Polyether ether ketone (PEEK) samples and suggested 300 μm layer thickness and 0° raster angle could result in excellent profiles for final PEEK products.

Below Figure 2-4 describes the FDM layers in details: Akessa et al. (2017) performed an investigation on the effect of air gap, raster width and raster angle upon the mechanical properties (tensile and flexural properties) of ABS material. They concluded that lower 3DP parameters could improve the tensile and flexural properties. Onwubolu and Rayegani (2014) made an investigation into the influence of layer thickness, air gap, raster width, raster angle and build orientation on the final printed samples. They found the following factors could trigger improved tensile strength, minimum layer thickness, negative air gap, minimum raster widths, zero-part orientation and increased raster angle. Deng et al. (2018) found the optimal combination of 3DP parameters, which is 60 mm/s printing speed, 0.2 mm layer height, 370 °C nozzle temperature and infill density of 40 %, utilized on the tensile properties of PEEK products fabricated by FDM. Birosz et al. (2022) fabricated batches of samples in function of the infill pattern and infill density and found a honeycomb and gyroid pattern could result in a great mechanical performance. However, both patterns need amount of manufacturing time in fabrication, indicating a cost-performance balance is a necessity in manufacturing. Huang et al. (2014) did some comparisons in the effect of raster angle in the FDM-fabricated specimens and found a $\pm 45°$ raster angle would benefit in the tensile performance (tensile strength and Young's Modulus).
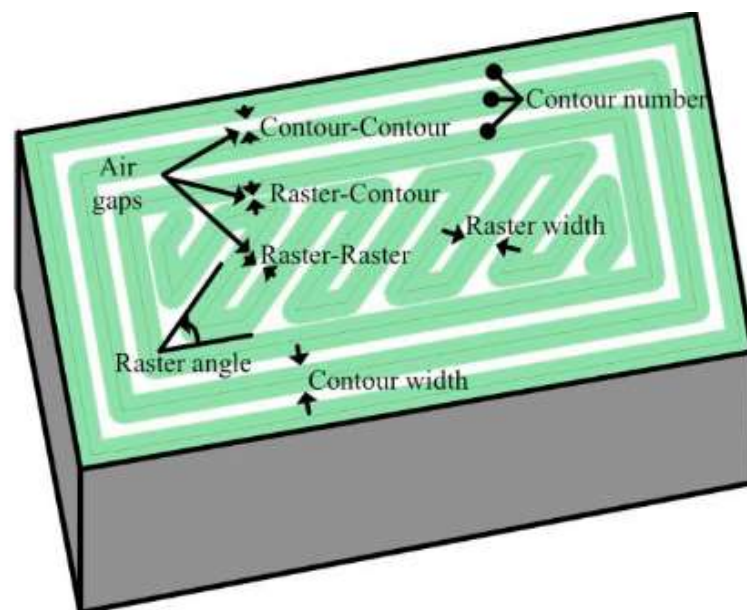
Figure 2-4 Fused Deposition Modelling process parameters (Gebisa & Lemu, 2019b).

Furthermore, one common advantage of FDM lies in its capacity to create components with unrestricted geometric configurations through layer-by-layer construction. Consequently, this technique allows for intentional design of interfaces between diverse materials, which can potentially be concealed in the final product, thereby facilitating optimal interconnection or interlocking between these materials. Ribeiro et al. (2019) investigated the geometries of interfaces between materials of different compositions within the context of multi-material 3D printing, utilizing two sets of materials with varying degrees of compatibility. Three interface mechanisms (shown in Figure 2-5)were proposed in this study to figure out the impact of geometry in the finalized specimens. The microscopic interfaces, depicted in Figure 2-5(a), are referred to as chemical interfaces. They emerge from the chemical bonding that occurs across adjoining surfaces of distinct materials. The efficacy of this phenomenon is closely contingent upon the molecular characteristics and arrangement of the employed materials, alongside their respective viscosities and processing temperatures. As anticipated, such interface occurrences are notably more prevalent among materials demonstrating heightened compatibility or a substantial degree of chemical affinity. The macroscopic interfaces shown in Figure 2-5(b) were bonded in mechanical structure/interlocking mechanisms, which suit in materials with low compatibility. In the case of mesoscopic interface (Figure 2-5(c)), this presents an interface mechanism between chemical bonding and mechanical interlocking.
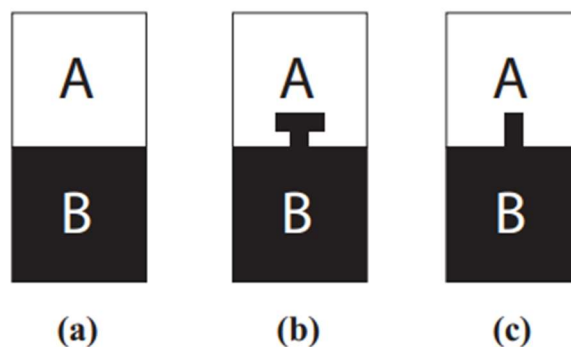
Figure 2-5 Discrete interface mechanisms proposed in the study: a. Microscopic; b. macroscopic; c. mesoscopic (Ribeiro et al., 2019).

2.2.3 Reptation Theory

The process of FDM fabrication/fusion bonding in thermoplastics can be involved into two phenomena: intimate contact and healing. Liquid material is pressurized and introduced onto a foundational surface. This procedure guarantees close interaction between the materials. Healing, also referred to as autohesion, pertains to the mutual diffusion of polymer molecules occurring at the juncture where bonding takes place. The onset of healing is prompted by the elevation of temperature beyond the glass transition temperature (T_g) within amorphous thermoplastics, or the melt temperature (T_m) within semi-crystalline thermoplastics. For instance, the temperature of the interface between the fused glass fiber reinforced PC and PC filled with carbon black needs to be above the T_g of PC to confirm a good cohesion and great chain entanglement (Akué Asséko et al., 2016).

This theory involving intimate contact and healing to describe the healing process of thermoplastics was introduced by de Gennes in the 1970s, with a name of reptation theory (de Gennes, 2003). The reptation model serves as a representation elucidating the spatial arrangement and mobility of large-scale macromolecules within amorphous polymers (Eslami & Grmela, 2008). These macromolecules, possessing a chain length denoted as L, are enveloped within a confined region termed the tube, functioning as a steric boundary separating them from neighboring molecules. Upon surpassing a critical temperature threshold (T_g or T_m), the macromolecular chains commence a process of deviating from this tubular confinement. Initially, the terminal segment of the chain (l), referred to as the minor chain, disengages from the tube, followed by a gradual liberation of successive portions of the chain. The temporal duration required for the complete escape of the entire macromolecular chain from the tube (l = L) is designated as the reptation time, as depicted in Figure 2-6. Notably, the reptation time to a certain degree encapsulates the transformation of the polymer chain from one state of equilibrium to another. Noteworthy research by Wool et al. (Wool et al., 1989) indicates that the relaxation time, deduced from viscosity measurements, can be employed as an approximation for the reptation time.

17
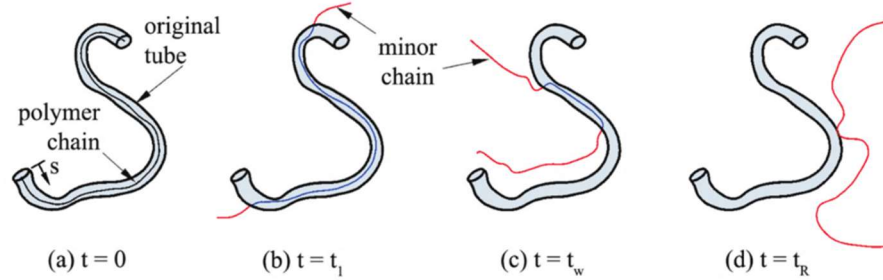
Figure 2-6 Reptation movement of a linear polymer chain, and reptation time, in which the whole chain escapes from the original tube (Szuchács et al., 2022).

To date, several analytical models were proposed to figure out the bonding between two thermoplastic components and these models can be described as the degree of healing (D_h):

$$D_h = \frac{s}{s_\infty}$$

in which s is the actual bonding strength and s_∞ is the strength of a single-piece part.

The applicability of the reptation model proved effective in the assessment of adhesive potency within various contexts, including instances such as weld lines in injection molding, the fusion of polymer films (Grewell & Benatar, 2008), the amalgamation of polymers through fusion bonding (Bastien & Gillespie Jr., 1991), and the establishment of bonds among the strata comprising Thermoplastic Composites (TPC) through processes like Automated Fiber Placement (AFP) and Automated Tape Placement (ATP) (Yassin & Hojjati, 2017).

2.2.4 Application of Additive Manufacturing

AM has greatly reduced the lead time needed for traditional manufacturing, making prototyping in hours rather than weeks, and at a very low cost. Two main industries, automotive and aerospace, have taken advantage of this advanced producing technique, even if conventional manufacturing shall be most cost-effective in mass production. In cases where products are not mass-produced, AM is ideal because it can be produced relatively cheaply on a small batch or case-by-case basis. Similarly, advances in AM technology have facilitated the improvement of materials

and processes, that this sort of novel method is appropriate not only with the product prototype, but also with the fabrication of finalized products.

Several corporations have now provided cloud-based AM service as cloud computing has been popular all over the world, allowing those who wish to fabricate goods and items remotely without the necessities of purchasing a 3D printer and assembly (Srinivasan et al., 2018), demonstrating companies now offering the theory of mass customization, in which clients or consumers will be available to tailor items by means of some novel system and order their favorite items.

In the past few years, many applications of AM have been emerged in the medical field, ranging from bio-printing, integrating some certain biomaterials, like cells, to produce semi-tissue structures that mimic their individuals to medical devices such as prosthetics (additive manufactured teeth). It is deemed as a fantastic technique for us human to produce prosthetics befitting with one unique patient. Under the background of 3DP, unique prosthetics shall be designed and then fabricated at a quite lower expense. Previously, children requiring a prosthetic limb were fraught with concerns about its potential for becoming ill-fitting over time. However, advances in prosthetic technology have enabled the expeditious fabrication of replacement prostheses.

The research of AM has been split into five major fields, that is, implants, in vitro drug testing, oral drug administration, transdermal and rectal/vaginal routes, what's more, numbers of publications discussing about its application on medicine area have continually come up since 2014 (Lim et al., 2018). Several relevant literatures have proved its significant effect upon medicine, like perfect control of release rate on tablets in basis of the amount of polymer binder offered in the producing (Katstra et al., 2000), highly appropriate content of drug per unit was achieved as well by 3DP. Meanwhile, one of potentials utilized in 3DP is and has always been considered in the customization on drug treatment for individual patients (Goyanes et al., 2017) as those ongoing productive methods based on mass production for tablets had no idea to achieve tailor treatment for individuals. Certain research papers have indicated that

modifications to factors such as infill density, dosage form quantity, and internal geometry can hold significant potential for altering the final therapeutic outcome for diverse patients (Goyanes et al., 2015b). These modifications can be implemented without requiring adjustments to the formulation itself. This approach enables healthcare professionals to consider various patient characteristics such as age, weight, and sex, thus facilitating the prescription of an appropriate medication dosage. 3DP offers a promising strategy for expediting medication production, with the capability to generate medicinal constructs ranging from minutes to hours (Skowyra et al., 2015). This technology also permits the creation of innovative composite structures containing multiple active ingredients tailored for the treatment of various conditions within a single dose, which enhanced patient adherence (Khaled et al., 2015). Furthermore, the manipulation of drug release profiles is feasible through adjustments in the geometric attributes of the manufactured form, necessitating only a novel computer-aided design (CAD) without any additional prerequisites.

2.3 High-Volume Manufacturing via Injection Molding

2.3.1 Introduction

Injection molding (IM) is a rapid and flexible processing system employed for different kinds of materials and mostly for the thermoplastics to manufacture items with various profiles, including size and shape (Bryce, 1996) and is a shaping procedure that forces molten polymer at high pressure into a mold. In 2016, this plastic processing method constituted 27% of the world's plastic supply (Florian, 2016), with an estimated global market size of USD 261.8 billion in 2021 (Grand View Research, 2020), despite the Covid-19 pandemic. This technique offers several advantages, including high precision in the final products, predictable repeatability, low per-unit cost, and the ability to manufacture in large volumes. Nevertheless, some limitations associated with this approach, such as expensive mold design, limited finished product size, and extended lead times, still impede its utilization.

2.3.2 Process of Injection Molding

In the process of IM, a part of molten plastic is forced into a cavity with the ideal form, accompanied by solidification and cooling of the molten material (H. S. Park et al., 2019). The two main parts of an injection-molding machine (IMM) are the plasticizing zone which softens the material, conveys it forward, and then the mold area where the material is molded and cooled.
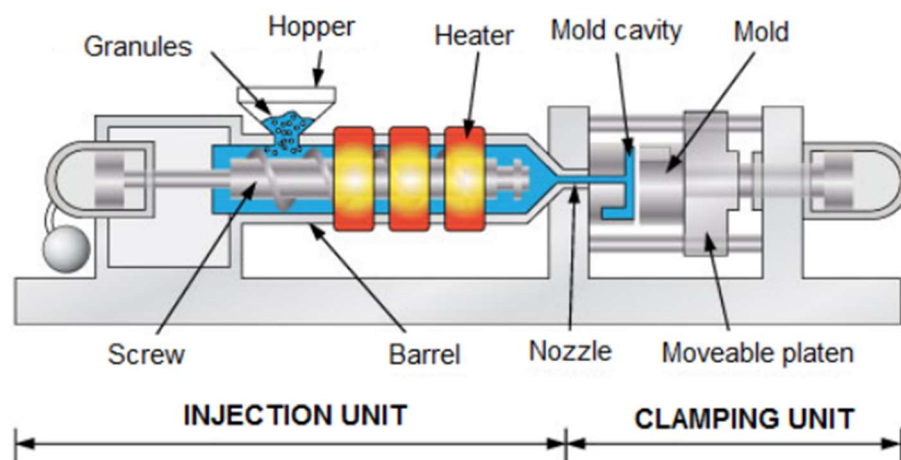
Figure 2-7 Schematic graph of IMM (Svečko et al., 2013).

During the molding cycle materials are placed in a hopper and fed to the injection barrel in which heat is applied via conduction from the regulated heated zones along the barrel combined with shear stresses from the rotation of the screw (Rosato & Rosato, 2000) resulting in the softening of the material. The molten material is conveyed by the reciprocating screw which pulls the molten material through the nozzle as the material accumulates in front of it and a non-return valve at the front of the screw prevents the molten material from moving backwards. The melt is injected into the mold while being pushed along by the screw which uses high pressure to fill the cavity. The now formed part is allowed to cool down for a period which varies depending on the material and processing conditions before the mold opens and the part is ejected. The loop repeats since the mold closes and begins over again (Campo, 2006).

Plasticizing area is consisted of a feeding hopper, a heated barrel in which polymer heats, mixes, compresses and melts. The screw-type barrel generates the pressure needed by its forward movement, whereas whose rotation leads to the movement of melted polymer and the increasing heating temperature caused of shear forces. The metering screw is a preferred type used in the barrel as it is designed with a smaller-diameter section for feeding, which allows more material to be driven into a gradually narrow area for more heating.

IMM has a broad range of available sizes and designs. However, the operating parameters for injection machines are dominated by three variables: temperature, pressure, and time (Bryce, 1996). Temperature involves the melting temperature of the material along the barrel in the injection unit as well as the temperature of the injection unit itself, the hydraulic system, and the surrounding environment.

Pressure relates to the amount of energy expended during the processes and stages of the IM process (Sreedharan & Jeevanantham, 2018; Zema et al., 2012). The most important pressure in an IM cycle is the primary injection pressure that is the force exerted by the tool at the beginning of the injection, which is determined by tool size and material viscosity (Ozcelik et al., 2010). In addition, the pressure required to fill a mold at the start of cooling and maintain the material in a densely packed state is known as holding pressure(Fuenmayor, Donnell, et al., 2019). Backpressure refers to the energy applied to the material while being prepared for injection. As the screw rotates, its reciprocating design pushes material forward in front of it and the amount of material accumulating pushes the screw back and this back pressure is applied to the screw to counteract this. Lastly, the clamping unit applies a certain amount of force when opening and closing the mold. The main force is known as clamping pressure, whose energy is applied to keep the mold closed during injection. Usually, this pressure is applied to match the injection pressure, as its main function is to prevent the material entering the mold from opening the tool.

Time is determined by the process cycle and is illustrated by the time employed in the single part fabrication (Rashid et al., 2020). There are a few significant terms

connecting time, for instance, the injection time which begins as the mold's closure with precise clamping pressure indicating the movement of injection unit to drift the screw forward, employing to force the material into the cavity. Holding time begins as the injection finished and presents a pressure's drop in comparison between the time when force applied in the injection. Cooling time represents the time required to fully shape the product at a constant temperature after the cavity has been filled with the plastic melt (Dai & Zou, 2002; Y. Liu, 1999). The cooling time depends mainly on the thickness of the product, but also ensures that the product does not cause changes when it is released from the mold, it is deemed as an imperative time of the process as this indicates the curing of the part (Sreedharan & Jeevanantham, 2018). Ejection time encompasses the period from the mold's open to the ejector's push.

2.3.3 Application of Injection Molding

IM is a valuable method for the manufacturing of various plastic items, such as plastic cartons to fill with milk, containers, caps, pocket combs, automotive dashboards, and most of plastic products available today. The usage of IM provides the greatest productivity in achieving mass output. In addition, the work of IMM would be used in AC drives to provide hydraulic oil pressure to operate the hydraulic oil pressure pump. Besides, the injection screw is required for the servo drives to work properly, as this will regulate the precision through injection stage. Finally, IM introduced in the electric drive systems will greatly save the energy under the replacement of hydraulic system, which is a modern way fitting for the current situation.

Moreover, IM can be commonly applied in the usage of cosmetic/pharmaceutical packaging to promote the development of biomedical products, such as scaffolds and microneedles (Ghosh et al., 2008; Gomes et al., 2001; Haugen et al., 2006; Kramschuster & Turng, 2009; Sammoura et al., 2007; Zhang et al., 2011). IM has been recommended for use in medication dosage formulations by Speiser (Zema et al., 2012). It is apparent that IM can be utilized in automated cycle process, and that a

single mold (more than two units) is adequate to manufacture several products concurrently, which dramatically decreases the processing period and improves the performance.

2.4 Hybrid Manufacturing

2.4.1 Introduction

To date, several manufacturing processes are utilized in producing goods for numerous industrial sectors. These techniques include CNC machining, AM, transformative processes such as forming, joining, and dividing operations, welding and sawing, etc. (Kalpakjian & Schmid, 2010).

However, these manufacturing techniques have drawbacks resulting in poor product quality and cannot be eliminated during fabrication. This indicates a single manufacturing technique does not suit in producing different items in terms of geometry, dimension, and strength at the meantime (Kolleck et al., 2011; Tawakoli & Azarhoushang, 2008). For example, the stair-step effect occurring during FDM process is challenging to produce high-quality products, particularly the inner structure (Rossi & Lanzetta, 2020). In addition, FDM-fabricated objects can only be manufactured using materials with low melting temperature and their performance is inferior to that of IM-fabricated objects (Boros et al., 2019; Dawoud et al., 2016; Lay et al., 2019). As for IM, it is still limited due to the high cost of design change, as compared to the FDM approach. Also, the long setup lead time and restricted design change are two additional disadvantages of it.

In light of the aforementioned issues, hybrid manufacturing (HM), which can be defined as the merging of two or more manufacturing processes, has emerged as it incorporates the best features of both (Le et al., 2017). The objective to improve these HM techniques is to maximize their benefits while minimizing their drawbacks (Karunakaran et al., 2010a). For instance, the HM combining CNC machining and AM offers a novel and considerable solution to the limitations of AM technique from the

high precision and processing speed of machining technique (Liang et al., 2002). Fuenmayor et al. (2019) discovered an HM technique combining FDM and IM to manufacture tailored tablets but in short production time. A lower cutting force and tool wear rate can be investigated in the combination of ultrasonic vibration and drilling (Heisel et al., 2008).

The above studies demonstrate that HM technique owns an enormous development potential in terms of generating more complex components with more flexibility and retaining high precision in a reasonably quick production period. The HM technique brings up new research possibilities for strengthening the capabilities of processes, minimizing their shortcomings, and expanding their application areas.

2.4.2 Definitions of hybrid manufacturing

To date, there is no specific consensus for an HM definition even if few researchers have made various suggestions on its design and had divided it based on several aspects, joining, dividing, subtractive, transformative and additive technology (Nassehi et al., 2011).

HM was first developed in a similar way to hybrid machining in the work by Rajurkar et. (1999) and defined as the combination of two or more machining actions for the material separation process. In Kozak and Rajrkar's description, the performance parameters of hybrid machining technique need to be significantly varied from those of the component processes when they are conducted individually (Kozak & Rajurkar, 2000). In 2001, it was also described as the combination of machining processes utilized in a single unit in simultaneous manner (Aspinwall et al., 2001). Menzies and Koshy (2008) referred to as the integration of two or more machining actions with different principles to remove material. In addition, Curtis et al. (2009) gave a restricted definition, indicating that the word "hybrid" may only be used to a system in which two or more material removal processes operate concurrently.

However, HM was referred in a prototype-oriented way that the prototype was built using varied techniques, typically the rapid prototype and conventional technique

(Rivette et al., 2007). Nau et al. (2011) broadened HM in terms of energy consumption as a strategy in which varied energy or forms of energy created in different ways are utilized simultaneously at the same zone of effect. The International Academy for Production Engineering (CIRP) described HM processes as methods involving deliberate and coordinated interactions between process mechanisms and energy sources, which exert a substantial effect on the finished performance of the process (Pragana et al., 2021). This definition can be viewed in publication from Lauwers et al. (2010), in which HM needs to show a significant effect on the process features. These can be found in the combination of laser and milling (Dandekar et al., 2010) and the one with laser and water-jet cutting (Molian et al., 2008). Also, HM has been referred to the combination of effects which are typically induced using varied techniques in a single process simultaneously based on the literatures (Klocke et al., 2011; Lauwers et al., 2010). An improved hybrid set-up was carried out by Araghi et al. (2009), in which two plastic deformation processes were integrated, indicating the HM need not be limited to the combination of two disparate techniques.

The combination of manufacturing techniques and AM processing, which can be referred as hybrid additive manufacturing (HAM), involves processing mechanism in manner of materials deposited as well as raw materials that have undergone conventional manufacturing techniques.

Moreover, the HM combining conventional techniques and AM can be employed in diverse fields since these may overcome the limitations from individuals, including greater quality in surface and dimension (Nielsen & Martins, 2021) and the opportunity to lessen the constraints of technique (Karunakaran et al., 2010b). These can be found in the enhanced performance in HM compared to the individual technique, such as the material removal rate and tool wear (Karunakaran et al., 2010c; Zhu et al., 2013).

2.4.3 Typical examples on hybrid additive manufacturing

The integration of forming processes with HAM has been identified as a promising approach for imparting customized properties to products fabricated through forming

processes. This can be achieved through a multi-stage procedure, where preforms are first produced and then further processed using other techniques (Merklein et al., 2016b). This route can benefit diverse characteristics into the finished parts, such as improved mechanical performance in manufacturing industry and customer-oriented drug delivery in medicine field (Fuenmayor, Donnell, et al., 2019).

A mechanical performance improvement was the first noticeable advantage found in the products manufactured using HAM. Overmolding, in which the preforms are subsequently injection molded to complete the whole fabrication, is being utilized in the HAM since a high efficiency in fabrication from IM technique and tailored features from AM can be offered in the finished products. Boros et al. (2019) developed a special injection mold in this technique shown in Figure 2-8 and discovered that the bonding strength of the sample improved as the melt temperature increased, indicating its potential applications in the manufacturing industry.

A further investigation was carried out by Rajamani et al. (2021), in which the 3DP preforms were inserted into the special mold shown in Figure 2-8 to finish the entire manufacturing process. This mold with a slider able to accommodate the 80 mm$\times$80 mm$\times$2mm preforms was designed by this lab team to determine the bonding strength (tensile strength between the base plate and rib). The reference batches could be also manufactured using this mold to compare with the experiment batches. In this study, some methods which can deliver greater bonding strength were proposed: proper parameter sets (printing speed, layer height and orientation) in 3DP process, reduced infill density in 3DP preforms, direct contact and larger contact area between ribs and preforms.
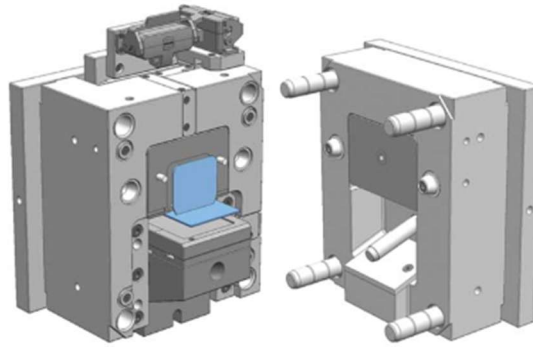
Figure 2-8 Injection mold with the slider for overmolding (Boros et al., 2019).

This overmolding route also finds a potential application in the medicine field as a means of personalized drug delivery (Fuenmayor, Donnell, et al., 2019). In this trial, the integration of FDM and IM produces a bilayer tablet (Figure 2-9) which releases two cardiovascular disease drugs based on the surface area-to-volume ratio control from the FDM layers, while a promising fabrication efficiency can be enabled from IM.

Figure 2-9 Bilayer tablet fabricated using HAM combining IM (Fuenmayor, Donnell, et al., 2019).

Fernandez et al. (2022) performed another route of AM-IM hybridization, in which a polymeric mold was fabricated using AM and then placed into the IM machine to proceed the manufacturing process. This study addresses two main challenges in mold design (long lead time and high manufacturing cost) and shows a promising future in fabricating mold with desired geometry.

Friction stir welding (FSW) was integrated into a Ham process to join FDM-fabricated workpieces by (Vidakis et al., 2022). The finished components displayed a significant improvement in mechanical properties compared to batches that did not undergo a welding stage. These findings indicate a promising future for the combination of FDM and FSW technologies in enhancing the industrial value of such processes.

Pokkalla et al. (2022) first analyzed the deformation mechanism of AM-

compression molding (CM) fabricated components using finite element analysis (FEA) and furtherly investigated methods to manufacture finished metal polymer composites with enhanced mechanical properties, in which a promising approach to the fabrication of metal-polymer composites exhibiting enhanced mechanical characteristics while minimizing manufacturing costs was identified. The findings of this study provide a basis for further utilizing metal-polymer components with diverse functionalities, such as energy (MacDonald & Wicker, 2016), control (Baranowski et al., 2022) and automotive engineering (Grujicic et al., 2008, 2009; Pokkalla et al., 2023).

However, certain drawbacks of metal-polymer composites, particularly the weak strength of interfaces, continue to pose challenges for researchers. Consequently, an alternative approach combining AM and joining techniques was proposed to advance this investigation. This idea was first conducted into manufacturing industry by Katayama et al. (2018) and biomedicine field by Wang et al. (2010) under laser-assisted joining method. Two recent published articles utilized this method to join metal and polymer using laser-assisted metal surface treatment (F. Ma et al., 2019) and ultrasonic welding (Tang et al., 2018) to produce finished metal-polymer components with significant improved interface strength.

This addjoining processing can be also observed in a study by Silva et al. (2019) to manufacture mortise-and-tenon fixture metal-polymer joints using aluminum and polycarbonate sheets, extending the future applicability to connect two portions with varied chemical, mechanical, and thermal properties.

Deshpande et al. (2016) put forward a proposal to enhance the power generation efficiency of a Darrieus type vertical axis wind turbine by incorporating AM and joining process. This adjoining technique was progressed by Falck et al. (2018) to fabricate metal-polymer composites, in which the polymer was fused deposited onto the metal substrate (Figure 2-10). This proposal was experimentally employed into the aluminum-ABS hybrid joints (Falck et al., 2019) and ordered the effects of parameters in the finished specimens as deposition speed, ABS coating concentration, contour number and road thickness. These resulting samples exhibited a foundation for a

subsequent study aimed at fabricating hybrid single lap joints with superior bonding at an appropriate building temperature (Falck & Amancio-Filho, 2022).
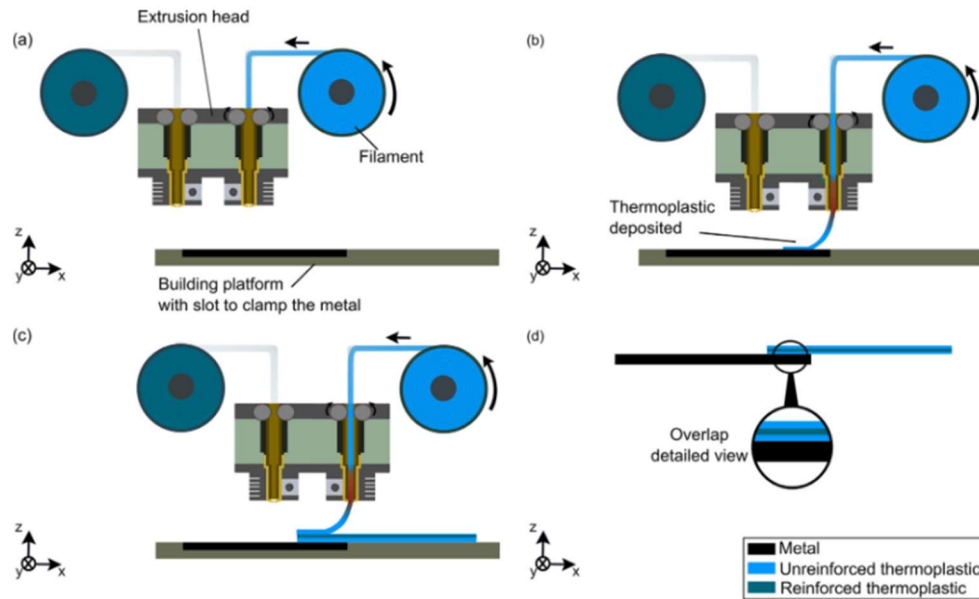
Figure 2-10 Schematic representation of the addjoining processing employed by Falck et al. (2018).

Material extrusion and CNC are two common techniques utilized in the AM and subtractive techniques, respectively, due to their promising competitiveness. Therefore, integrating both techniques can be highly effective in fabricating high-quality single articles with minimal material waste (Ribeiro et al., 2019). Several experiments were conducted by Paz et al. (2018) and discovered specimens with greater hardness and accuracy were achieved through greater layer thickness, while lower infill density resulted in a stiffer structure. In addition, CNC process could improve two main aspects of finished specimens, roughness and flatness defect. This guiding study can be analyzed in further investigations related to the FDM-CNC process and other approaches suitable for specific projects, such as the production of ceramic components (Hinton et al., 2019).

Femtosecond laser was carried out in the polymer HAM with subtractive process (Sugioka et al., 2015) to fabricate some functional biochips (Figure 2-11) to allow for some specific fields (fluid chemistry and aerospace regimes) (Wu et al., 2014), and extensively delivered an investigation to approach in lab-on-chip (LOC) device (Jonušauskas et al., 2017) and produce deformable and intertwined polymer

components (Jonušauskas et al., 2019).
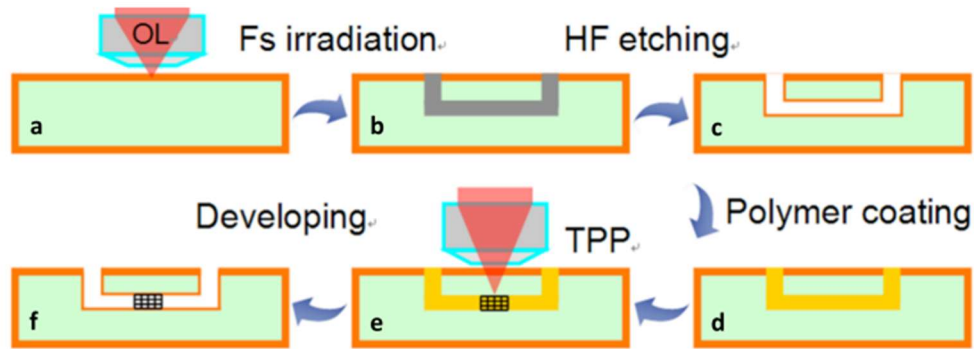
Figure 2-11 Schematic illustration of femtosecond laser fabricating biochips: (a) Fs laser machine fabricating specific base; (b) thermal treatment; (c) HF etching; (d) polymer filling; (e) two-photon polymerization, and (f) developing (Sugioka et al., 2015).

Tala et al. (2020) extended this AM-subtractive technique in production of porous PGS-M (Polyglycerol sebacate-methacrylate) scaffold with personalized porosity and enhanced mechanical properties, aiming to carry out more applications in tissue engineering. Other investigations related to the virgin polymer products in this route were conducted to figure out the possibility in agriculture field from the polydimethylsiloxane (PDMS) oxygen-permeable films (Kunwar et al., 2020), highlighting the broad applicability of AM-subtractive system.

Similar to the AM-forming system, metal-polymer components can be produced using this integration based on the designed joint interface (shown in Figure 2-12), as demonstrated by Ozlati (2019) through the hybridization of FDM and drilling to enhance the quality of finished specimens. The findings highlighted the significant impact of the fill pattern on the mechanical performance of the finished specimens, with improved quality observed in samples with a larger joint interface area.
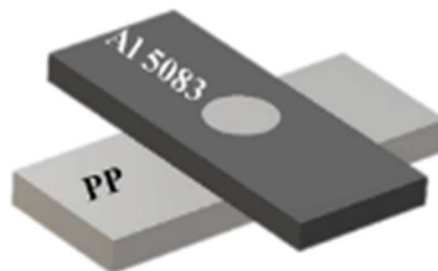
Figure 2-12 Joint Interface designed in the AM-forming system, reproduced from (Ozlati et al., 2019).

In a subsequent investigation, Weflen and Frank (2021) utilized a combination of AM and subtractive manufacturing (cutting) to produce metal-polymer components, where interlocking mechanisms (shown in Figure 2-13) mechanically joined the two materials. Their investigation revealed that cooling to some extent could improve the strength of AM-fabricated components, while the interlocking features led to diverse material characteristics, such as strength, in the transition regions. This study broadens the usage of multi-material components and sheds light on the factors contributing to distinctive features in transition regions.

Figure 2-13 Mechanical Interlocking employed in the combination of AM and cutting, reproduced from (Weflen & Frank, 2021).

Integrations that combine multiple AM techniques face challenges for future applications, primarily due to the use of different communication languages for each technique (Roach et al., 2019). Hence, two routes were considered in their study: (a) AM techniques employed in consecutive stages; (b) developing an innovative algorithm.

Polymer composites can be fabricated using HAM techniques where two AM are utilized in consecutive stages. This route was conducted by Anandkumar et al. (2021), in which the FDM machine was modified allowing shape deposition modelling (SDM) stage (Figure 2-14). This process developed the multi-material sublayers and thus, an improved bonding strength could be observed, offering more potentials in the material research.
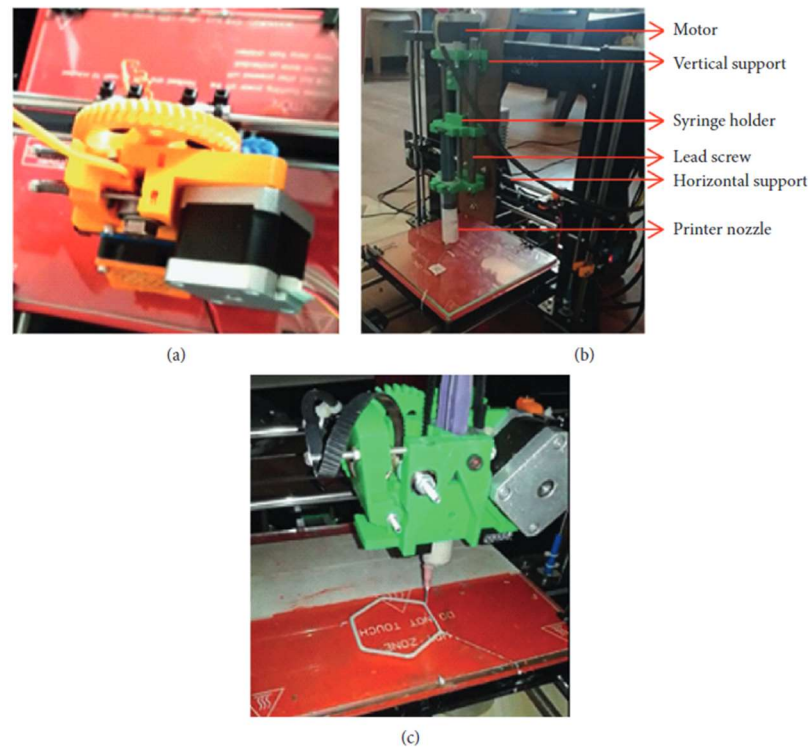
Figure 2-14 3D printer employed in FDM-SDM hybridization: (a) 3D printer with FDM printing head; (b) first iterated printing head and (c) second iterated printing head (Anandkumar et al., 2021).

Baranowski et al. (2022) fused deposited polymers onto SLA derived preforms, resulting in a unique set of material properties. They found a proper insert selection (SLA batch instead of thermoplastic one) could enhance adhesion and suggested that an automation system could further increase manufacturing efficiency, which was in line with the conclusion shown in (Fuenmayor, Donnell, et al., 2019).

Moreover, some studies related to the thermosetting materials were carried out due to the strong chemical bond and high temperature resistance in finished specimens in comparison to the thermoplastic ones. For example, an integration of direct writing and VAT Polymerization was conducted using thermally cured epoxy and photopolymer resins to fabricate high-mechanical property products with precise dimensions (Alrashdan et al., 2020).

A drug delivery system combining SLA and inkjet printing studied by Konasch et al. (2019) demonstrated promise in incorporating individual drugs within the matrix, resulting in optimized release profiles and a patient-centric scheme for drug

production. Bernasconi et al. (2022) expanded on this integration by incorporating a consecutive stage of SLA to fabricate accelerometers, followed by inkjet deposition for the piezoelectric layer (Figure 2-15). This approach enabled the production of electromechanical devices with exceptional characteristics at the mesoscale.
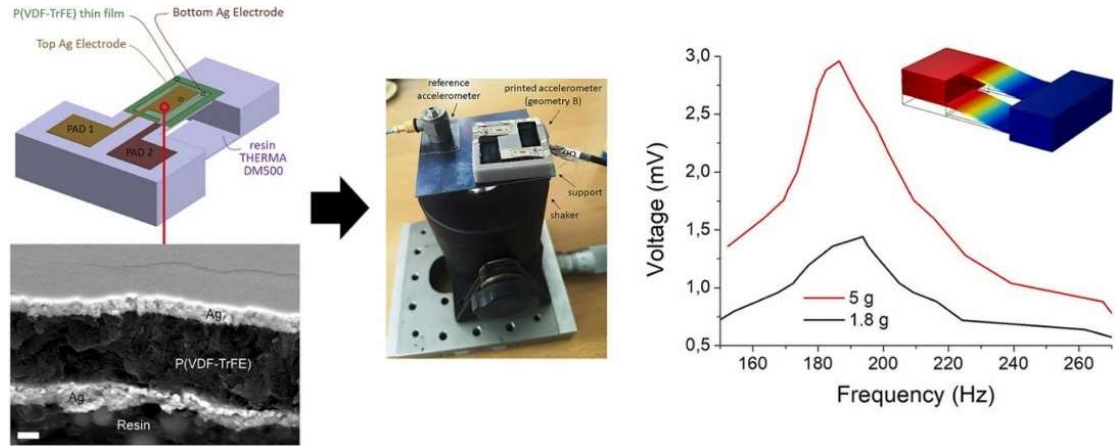
Figure 2-15 Schematic representation of SLA and inkjet integration and the characteristics of finished specimens (Bernasconi et al., 2022).

Moreover, a UV-DIW hybridization was performed by Marzi et al. (2022) to fabricate high-quality freeform silica glass components, building on previous literature (de Hazan et al., 2012; Faes et al., 2016; Kretzschmar et al., 2019). In this study, the completed 3D honeycomb products exhibited enhanced characteristics with minimal weight, suggesting that this HAM could be utilized in applications requiring lightweight components.

For metal-polymer components, they can also be fabricated using this approach, such as through an integration of selective laser melting (SLM) and SLA (M. R. Silva et al., 2019). In this study, the SLA technique was employed to fill the voids in the SLM-fabricated metal base. A significant improvement in mechanical performance was observed at the metal-polymer interface compared to resin, opening up opportunities in areas where lightweight products with promising mechanical properties and customized features are in demand (M. Silva et al., 2017).

Englert et al. (2022) presented a laser powder bed fusion (LPBF)-FDM technique to fabricate metal-polymer composites and assessed their mechanical properties through tensile and edge shear tests (Figure 2-16), finding an acceptable method to

improve mechanical bonding under intricate interlocking geometries and faster filling structures. A similar trial was carried out by Chueh et al. (2019) to fabricate multi-material components with enhanced interface and surface quality in flexible solution.
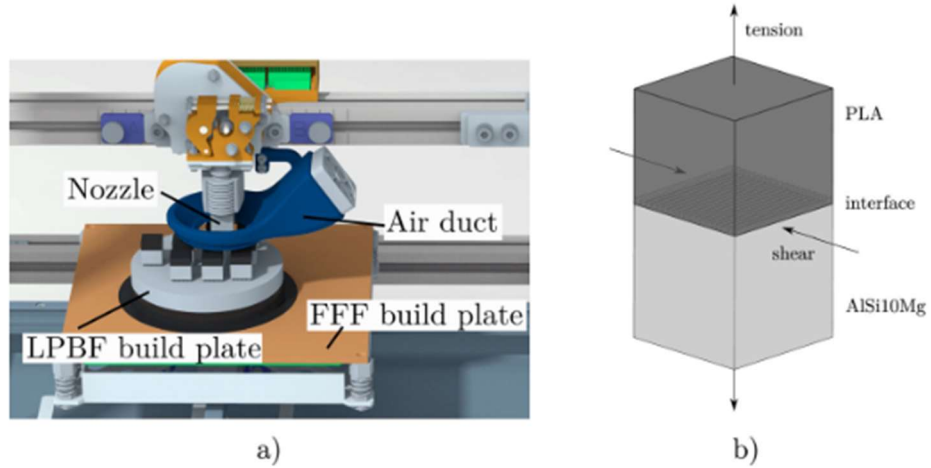
Figure 2-16 (a) LPBF-FDM manufacturing setup; (b) CAD model of finished specimens (Englert et al., 2022).

Czink et al. (2023) stacked $AlSi_{10}Mg$ onto an FDM-fabricated ABS base and discovered that a form-fit bond (shown in Figure 2-17) enhanced the interfacial strength in the components. These studies offer valuable insights for designing interlocking structures and facilitate the production of customized specimens by adjusting parameters in both stages of the fabrication process.
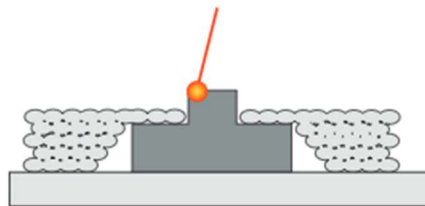
Figure 2-17 Schematic diagram of form-fit bond, reproduced from (Czink et al., 2023).

Farzad et al. (2017) first proposed a hybrid system combining powder-bed binder-jetting (PBBJ) and material micro-dispensing methods to fabricate cylindrical artifacts using silicone, a non-Newtonian viscous material that is challenging to use in AM techniques. This study laid the groundwork for integrating material jetting and material extrusion techniques, enabling the high-quality production of finished silicone products at a significantly accelerated fabrication rate, ranging from 10 to 20

times faster than previously possible (Liravi & Toyserkani, 2018).

A workflow and complicated algorithm were brought in the integration (Roach et al., 2019) where four AM techniques (inkjet, FDM, DIW, and aerosol jetting) involved to design an M^4 3D printer. This advancement increased the applicability of 3D-printed components in various fields, including medicine, biology, and electronics.

Furthermore, this led to another experiment in which FDM, DIW, and SLS were combined to manufacture metal-polymer components, with several investigations into the effects of processing parameters on electrical conductivity. This developed process has practical applications in everyday life, such as creating circuits with power sources (Wałpuski & Słoma, 2021).

In addition to the aforementioned HAM types, several studies present unique processes, highlighting the promising capabilities of HAM in fabricating products, even under challenging conditions.

Gackowski et al. (2022) introduced the incorporation of buckypapers in a layer-by-layer fashion for the current HAM processing. This method resulted in enhanced tensile behavior and interlaminar shear strength in the finished specimens, with a 50 % reduction in manufacturing costs compared to the traditional FDM method.

A similar method to improve the interlayers of FDM specimens was conducted by Andreu et al. (2022), in which a heated roller compressed each stacked layer to allow for an increased adhesion. A significant positive effect from heated roller was found in the quality of finished specimens since increased contact surface area and neck growth, reducing the number of voids and improved bonding behavior in the samples.

Moetazedian et al. (2021) were the first to employ chemical treatment in HAM, where the physical and mechanical properties of extruded PLA and ABS samples could be altered based on the parameter sets in the immersion stage.

Another HAM (FDM-metal spray) can be found in the study from Kumar et al. (2022), where an aluminum spray was employed between the PLA deposited layers to improve the mechanical properties of finished products with a recommended process setting as five spray layers, 70% infill density, and 100 Celsius platform temperature to

enable mass production fabrication of objects. The findings of this study serve as a foundation for further research on manufacturing products tailored for mass customization in a competitive market.

Another case of metal-polymer composites can be found in the hybridization of FDM and ultrasonic consolidation technique (Wu et al., 2022), where an improved bond strength could be observed. This enhanced bonding strength can be explained from the ultrasonic strengthening, re-fusing the pores inside the sample and forming a strong molecular chain to increase the contact surface fusion area to resist the tensile deformation. However, two main problems were found in this integration: the detrimental impact of recurrent ultrasonic consolidation on the tensile strength of the final specimens, and a notable reduction in strength resulting from the ultrasonic stage when the thickness of samples was increased since the increasing rate of ultrasonic cannot manufacture well-fabricated layers (some voids may be found). The advantage of this integration lies in establishing a foundation for the fabrication of heterogeneous-material products with promising performance.

2.5 Mass Customization

Mass customization (MC) refers to the capability to offer products or items tailored to consumer preferences at a low-to-moderate cost (Da Silveira et al., 2001; Fogliatto et al., 2012; Hu, 2013; Piller, 2004). This contemporary concept, developed nearly four decades ago, emerged in response to a growing demand for variety (B Joseph II, 1993; Hu, 2013; Hu et al., 2011). Davis first originated the concept of MC (Davis, 1989; Saleh et al., 2009), but it was Pine (1993) who popularized it more broadly, establishing it as a prevailing trend across various industries (Hart, 1995; Hu et al., 2011), especially in pharmaceutical and manufacturing fields. This term underpins the development of processes used to deliver customized products at a reasonable level of customization, and encompasses tailored specifications across diverse fields such as electronic appliances (Davis, 1989; Trattner et al., 2019), food industry (McIntosh et al., 2010), customized nutrition (Boland, 2008), engineering (Lu et al., 2009),

housebuilding (Barlow et al., 2003), and foot orthotics (Pallari et al., 2010). However, it is essential that these customized offerings be priced competitively with mass-produced alternatives to remain viable in a competitive market.

2.5.1 Mass Production

Mass production was first proposed in 1913 (Gu & Koren, 2018; Hu, 2013; Mourtzis, 2016), but first achieved wide adoption in 1955 (Gu & Koren, 2018; Mourtzis, 2016). This concept emerged in response to a growing global population and an increased standard of living, resulting in a higher demand for commodities from potential customers and subsequently driving productivity (Mital et al., 2014). Mass production provides reliable and affordable access to standardized products (e.g., televisions, laptops) to customers, leveraging economies of scale (cost-effective production of large quantities) (Govender, 2021). The efficiency and cost-effectiveness of manufacturers are confirmed by the economies of scale characteristic, achieved through fixed and specialized production lines for standardized items (robotics) and high-volume manufacturing of products with precise tolerances (e.g., injection molding). Additionally, the interchangeability of certain components enhances the potential for worldwide mass production.

The effectiveness and economies of scale in mass production explain why it is presently the leading blueprint in the manufacturing industry, which is based on expanding customer access to manufactured goods throughout the population. The core attributes of mass production (high-quality items manufactured economically) ensured its continued popularity despite the growing demand for customized goods (Govender, 2021). Currently, mass production still prioritizes high-volume manufacturing with low product variety. However, the industry can benefit from increased product diversity and flexibility to meet the demand for customization.

2.5.2 Customization

Some manufacturing processes, such as AM, allow for customization based on an individual's personal needs and preferences. Several sectors, such as open architecture product (OAP) (Koren et al., 2013), product simulation, and supply and assembly techniques, enable consumers and manufacturers to collaborate on the creation of goods, allowing manufacturers to quickly meet client expectations.

An OAP refers to products that are designed with several components that can be added or removed from the original structure, allowing for the modification of features (Koren et al., 2013). In context of MC, the foundation of product family design methodologies lies in the concept of common modules and customized modules (Jiao et al., 1998; Simpson, 2004). In general, personalized goods consist of three distinct modules: common modules that are shared among the product platform, customized modules that offer options for customers to choose from, and personalized modules that enable customers to design their own features (Hu, 2013).

2.6 Materials of Interest

The polymer materials chosen for this work were selected based on their exceptional properties suitable for 3D printing (3DP) and injection molding (IM) processes. The following is a description of the specific polymer utilized in the manufacturing.

2.6.1 Acrylonitrile Butadiene Styrene (ABS)

Acrylonitrile butadiene styrene (ABS), as a ternary copolymer, is composed of three monomers, acrylonitrile (A), butadiene (B) and styrene (S), which possesses the characteristic properties of three components (Figure 2-18).
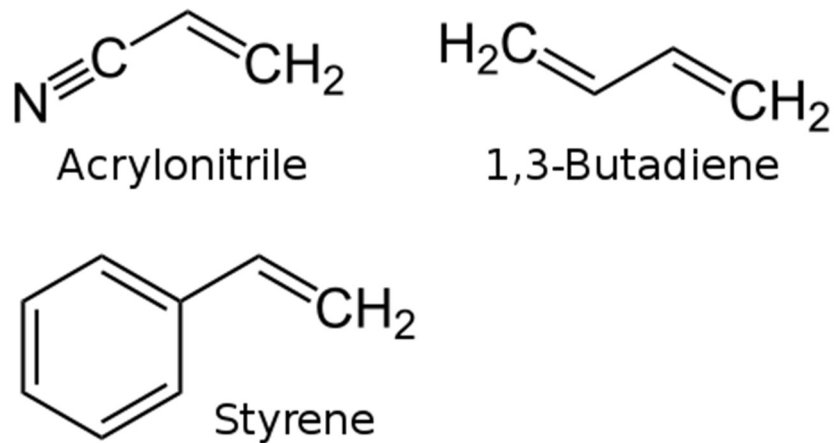
Figure 2-18 Presentation of all three monomers for ABS production.

ABS is an amorphous polymer and has no exact glass transition temperature (around 110 °C) and melting temperature (210 °C to 235 °C). For example, the Real-Filament Corporation found the elongation at break value was 2.5 %, and a 2280 MPa tensile modulus. These features resulted in a recommended temperature scope while fabricating articles. The difference in monomer ratio results in the final components of ABS have numerous properties and many new forms of ABS have been obtained including heat tolerant, light weight, ease to form, and good strength, making it commonly employed in many fields including construction, science and manufacturing (a typical example of FDM-fabricated lizard made with ABS shown in Figure 2-19). However, this material still finds some challenges in the FDM fabrication process: the harmful smell while melted and the shrinkage and warpage due to the large temperature difference between the melted and solidified states (Sreedharan & Jeevanantham, 2018).
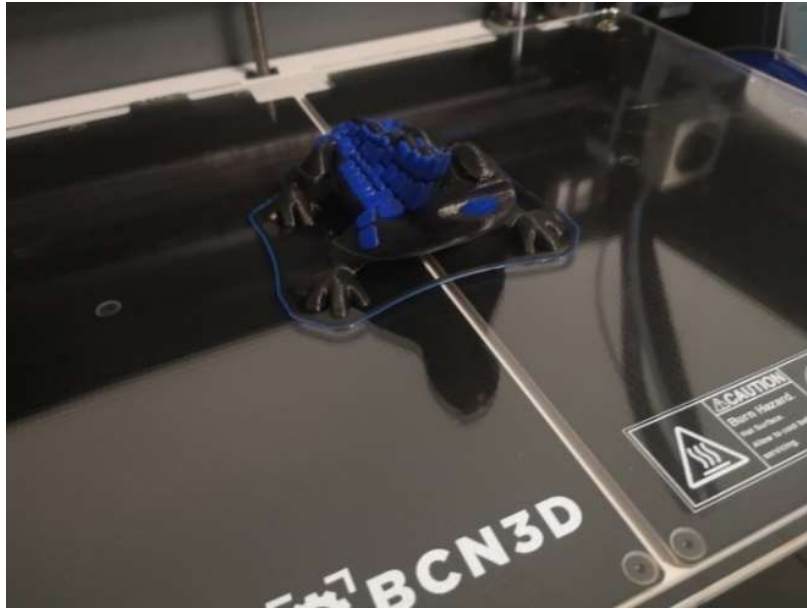
Figure 2-19 Lizard fabricated via 3DP with ABS Material.

In the context of household appliances, ABS is commonly employed due to its desirable characteristics of luster and shaping. It finds applications in appliances such as household coffee machines, audio systems, and media players. In the field of engineering plastics, ABS holds significant importance. It is extensively utilized in automotive, electronic, office, and communication equipment, among other areas. ABS is particularly well-suited to meet specific requirements, including its prominent position in the market for electronics and electrical appliances that require flame retardancy and high heat resistance. Its versatile properties make it a preferred choice for applications where durability, impact resistance, and a balance of mechanical properties are crucial.

2.6.2 Polylactic Acid (PLA)

PLA, a biodegradable material made from lactic acid (Figure 2-20), has attracted a great deal of interests in the area of biotechnology. It is considered a polymer comparable to everyday plastics derived from petrochemicals, such as polystyrene (PS) and polyethylene terephthalate (PET) (C. G. Silva et al., 2019). PLA offers several advantageous properties, including non-toxicity, biocompatibility, high mechanical strength, and thermal plasticity. These qualities have positioned PLA as one of the

most competitive polymers utilized in packaging applications. Moreover, its biodegradability makes it an environmentally friendly choice, aligning with sustainability goals in various industries (Karamanlioglu et al., 2017).
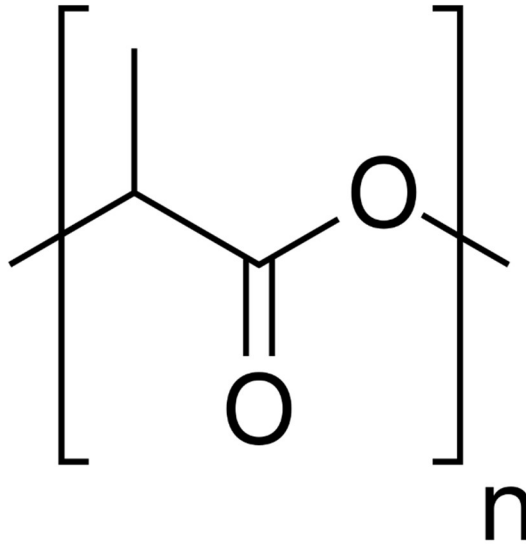
Figure 2-20 Monomer for PLA material.

This material is a semi-crystalline polymer, indicating it easy to find a proper temperature selection (Zhao et al., 2019). For example, the printing temperature and melting point can be scoped in 190 to 210 °C and 145 to 160 °C. Many researchers have made investigations about PLA, for example, Lim et al. (2008) researched the structural, thermal, crystallization and rheological properties in regard to its manufacturing process. The advantages of PLA have made it a popular choice for 3D printing, particularly as a filament. It exhibits low levels of shrinkage, which minimizes residual stress in printed articles and reduces the risk of deformation. Additionally, PLA has a low melting temperature, enabling higher productivity during the printing process (Kuznetsov et al., 2018a). Research has also highlighted the excellent mechanical properties and processability of PLA (Auras et al., 2003; Datta & Henry, 2006).

PLA finds applications in various fields, including extrusion, injection molding (IM), film drawing, spinning, and more. Two notable applications of PLA are heart stents and disposable products. Soluble PLA stents offer advantages over metal stents, as they do

not leave behind "metal spiders" during x-rays, reducing the risk of blood clots and interference with future tests and surgeries. Figure 2-21 depicts heart stents made with PLA.
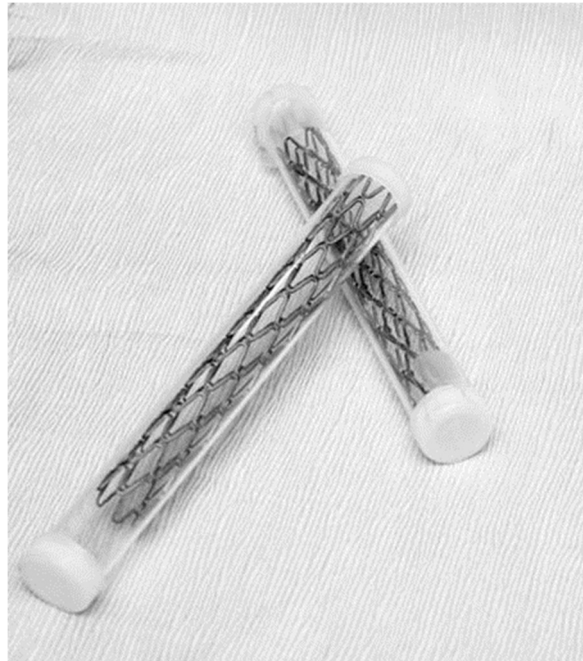
Figure 2-21 Heart Stents made from PLA.

In the realm of disposable products, PLA's biocompatibility and complete biodegradability make it a desirable choice for disposable tableware, food packaging materials, and other single-use items. It aligns with environmental protection efforts worldwide, particularly in the European Union, the United States, and Japan. However, PLA-based disposable tableware may have some limitations, such as reduced temperature and oil resistance, leading to functional drawbacks. These limitations can result in shape deformation and brittleness, leading to a higher number of defective goods during transportation and use as shipping medium.

2.7 Conclusion

The literature review shown above indicates that HM can combine the advantages of both techniques to compensate the individual disadvantages. In this context, overmolding, where FDM preforms with varied geometries were manufactured first and then overmolded, and overprinting, in which an IM substrate

could be overprinted using FDM technique, were conducted in this study in achievement of the FDM-IM hybrid manufacturing. A greater design flexibility and mass production capability can be achieved in this technique. The FDM and IM literature review assisted in the optimized parameters employed in this study to fabricate the controlled and experimental batches, aiming to expand the applicability of this study. The joint configurations designed in this study were based on the previous FDM study and was expanded in two series: half-length and half-thickness, showing a similar role in building orientations of FDM-fabricated articles. In case of HM, some previous studies related to this FDM-IM hybrid manufacturing focused on the improvement of bonding strength via several methods, such as increased surface roughness, infill density, mechanical interlocking, and even fiber-reinforcement in the contact area. However, this study finds another route in basis of greater design flexibility in FDM stage to determine the methods to employ this HM technique in manufacturing field while offering a high degree of design flexibility and mass production.

Chapter 3: Methodology

3.1 Introduction

In the first stage, the overmolding technique is explored using Acrylonitrile Butadiene Styrene (ABS) as the primary material (Chapter 4). ABS is a popular choice in the industry due to its impressive mechanical properties, such as impact resistance, toughness, and rigidity. The second stage involves employing the overmolding technique with Polylactic Acid (PLA) (Chapter 5), a polymer known for its composability, high mechanical strength, and the semi-crystalline structure with amorphous and crystalline area included. Chapters 4 and 5 lay the groundwork for dual-material overmolding, where FDM-fabricated preforms made of PLA are overmolded with ABS. This stage aims to evaluate the characteristics of the dual-material samples and explore their potential applications in future manufacturing (Chapter 6).

The third stage focuses on the overprinting technique, which is essentially the reverse of overmolding (Chapter 7). This involves initially creating substrates through injection molding, followed by the addition of components using the FDM process. The final stage of the study examines the customization options available through the FDM process, including the variation in geometries of the FDM preforms used in the overmolding stage and the different parameter sets employed in the FDM process. Additionally, the study highlights the cost-effectiveness of both hybrid manufacturing routes due to the utilization of the IM technique in overmolding and the fabrication of injection-molded substrates in overprinting.

The study also discusses the mechanisms through which these hybrid manufacturing techniques influence the performance of the final products. This insight is crucial for understanding the potential applications of combining FDM and IM in future manufacturing industries.

The methodology section provides a detailed overview of the materials (such as filaments for FDM and pellets for IM), equipment, testing procedures, and software used for data analysis. This section is structured according to the stages of the study and includes a list of the main parameters and equipment used, enabling readers to replicate the experiments.

3.2 Methodology for Chapter 4

3.2.1 Materials

ABS filament with a diameter of 1.75 mm used in the FDM stage of this project was supplied by Real Filament Company (Wateringen, Netherlands) and was shown in Figure 3-1. The virgin ABS pellets utilized in the IM processing were supplied by LOTTE Advanced Material Corporation (Seoul, South Korea). The ABS pellets were first placed in the tray and dried at the temperature of 70 °C for 4 hours prior to the IM processing.

Figure 3-1 Filament utilized in the fabrication of ABS printed samples/inserts.

3.2.2 Sample Preparation

Three sets of samples (FDM, IM and hybrid manufactured, HYM, samples) were produced in this study to compare their mechanical performances. All manufactured specimens in this study were fabricated following the ASTM-D638-3 Standard, dimensions of the fabricated samples have been shown in Figure 3-2.
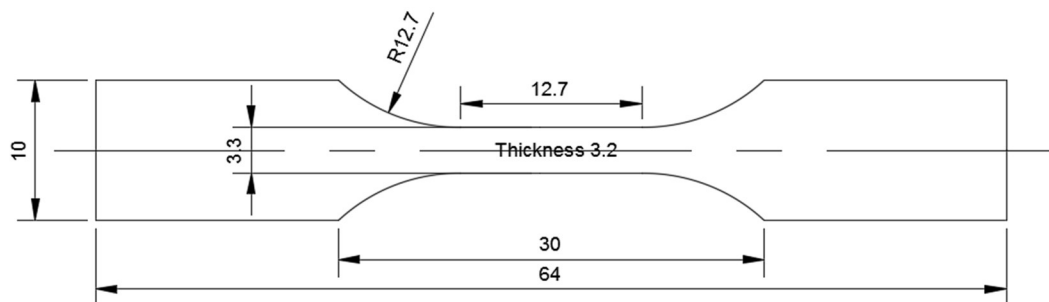
Figure 3-2 Detailed dimensions of tensile bar specimens produced for characterization in this study (unit in millimeter).

Three batches of FDM samples and varies of inserts applied in the overmolding processing were produced by FDM technique using an Orion Delta 3D Printer (SeeMe CNC, Indiana, USA) shown in Figure 3-3, the software suite used to control the printer was Simplify 3D Software Version-4.1.1 (Cincinnati, Ohio, USA). All CAD models, which were displayed in Figure 3-4 and Figure 3-5 were designed using SolidWorks 2016 Software (Dassault Systèmes, Waltham, USA). These CAD software-designed files were determined from the studies from Ribeiro et al. (2019) and our lab team to determine the impact of joint configuration and overmolding direction on the tensile performances of finalized specimens.
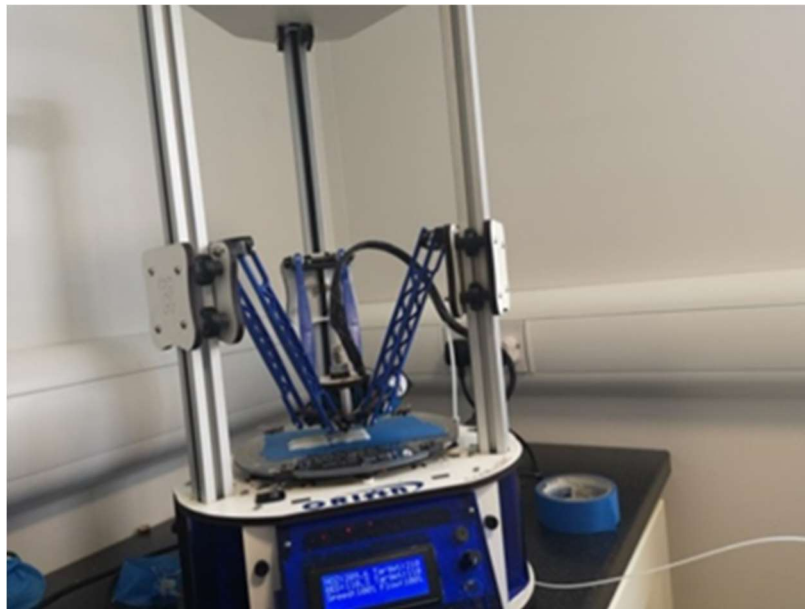
Figure 3-3 SeeMe CNC 3D Printer printing samples.
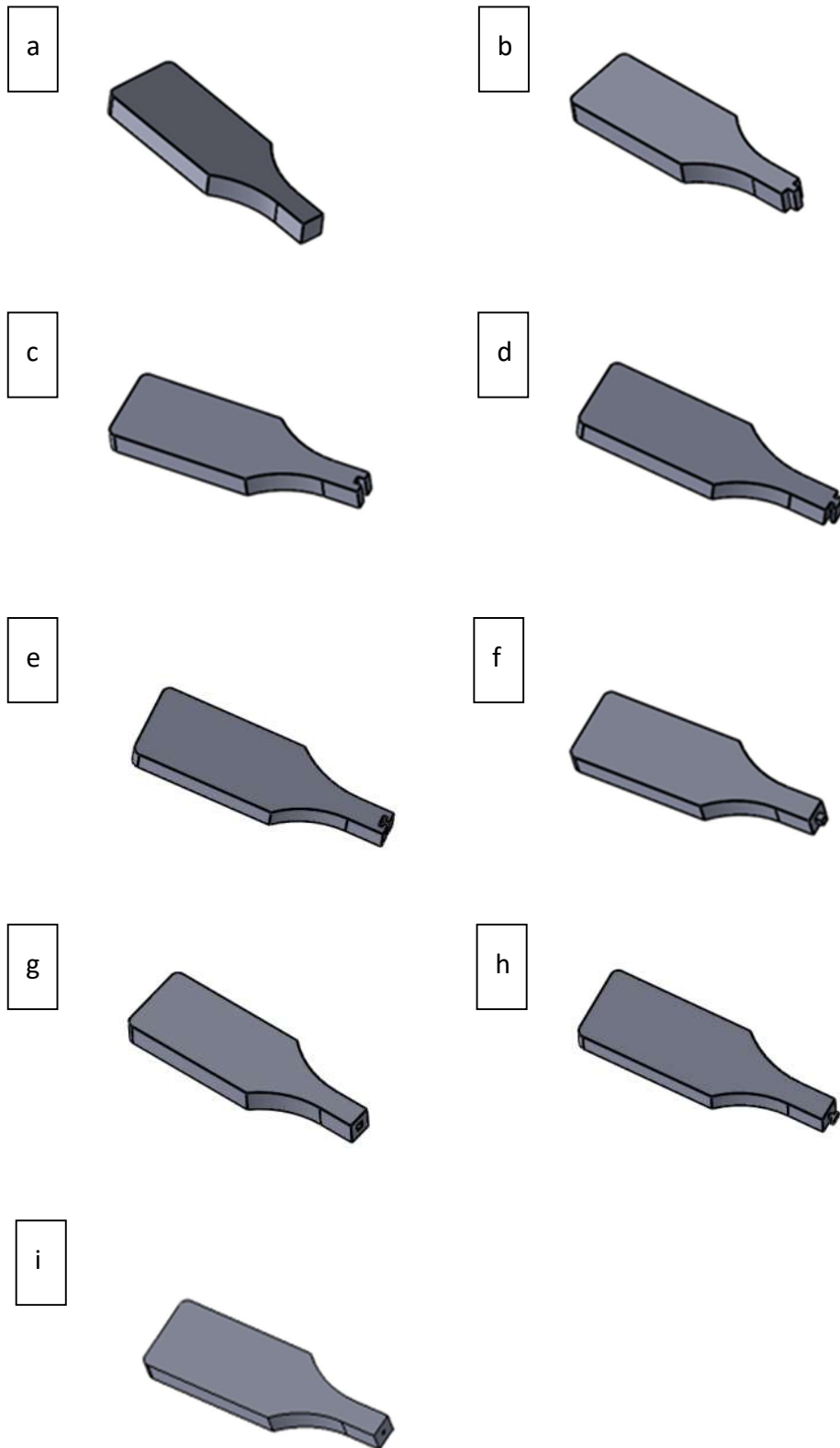
Figure 3-4 CAD models for all HL series inserts: a)half-length; b)half-length male cube; c)half-length female cube; d)half-length male T; e)half-length female T; f) half-length male cube outset; g)half-length female cube inset: h)half-length male T outset: i) half-length female T inset.
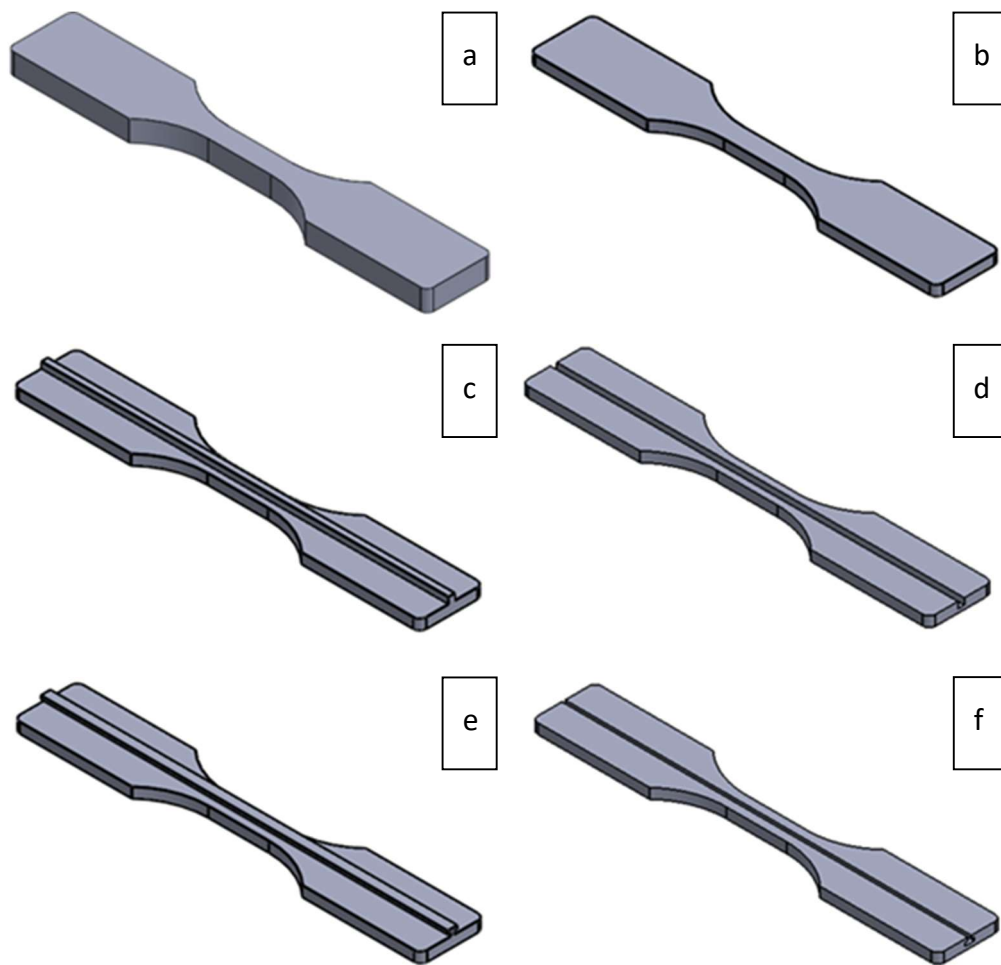
Figure 3-5 CAD models of FDM articles, in which (a) normal, FDM sample; (b) half-thickness without joint; (c) half-thickness male cube type joint; (d) half-thickness female cube type joint; (e) half thickness male T type joint; (f) half thickness female T type joint.

The main parameters applied in the FDM processing were selected based on some previously published literature (Fuenmayor et al., 2018; Mohamed et al., 2015; Patterson et al., 2019; Sood et al., 2010; Tymrak et al., 2014) and manufacturing resolution test plate (pins and voids) (shown below in Figure 3-6) prior to the fabrication, these parameters were shown in Table 3-1. These resolution test models were found in Simplify3D Website to offer the proper parameter settings employed in the FDM stage.

Table 3-1 FDM parameters applied in the study.

FDM Parameters	
Printing speed (mm/min)	3000
Infill Orientation (degrees)	± 45
Outline Overlap (%)	20
Number of top solid layers	1
Number of bottom solid layers	1
Number of outline/perimeter shells	2
Infill extrusion width (%)	100
Minimum infill length (mm)	5
Extruder temperature (°C)	210
Printing bed temperature (°C)	110
Retraction distance (mm)	8.4
Retraction vertical lift (mm)	0.1
Retraction speed (mm/min)	3600
Diameter of Nozzle (mm)	0.5
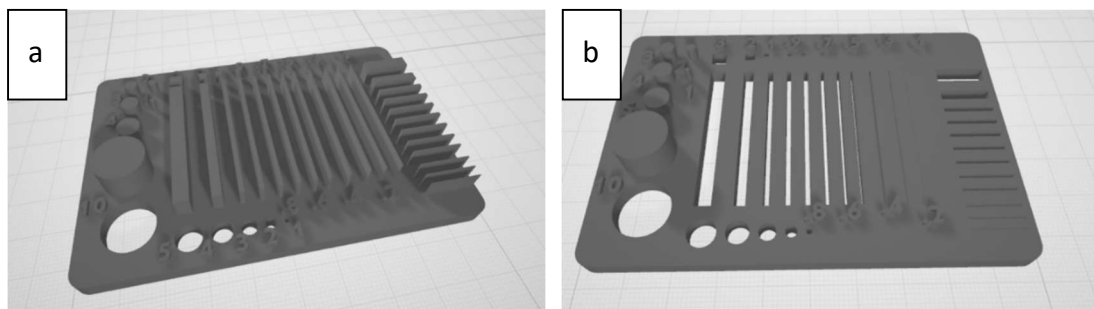
Figure 3-6 CAD files for resolution plate:(a) pins ;(b) voids.

Besides, one sort of phenomenon happened in FDM processing was the material shrinkage. A shrinkage test had been carried out prior to the sample production, in which the tested samples with size of 100 % had shrinkage phenomenon by nearly 5 % and had shown in Table 3-2 below in which the parameters of fabricated specimens were 10 mm, 3.2 mm and 32 mm, respectively. Thus, the sample models utilized in the production were set for 105 % size.

Table 3-2 Shrinkage condition in the production of ABS samples (mm).

	25 % infill	50 % infill	75 % infill
1	9.68 3.07 31.45	9.33 3.01 30.89	9.51 3.03 31.16
2	9.63 3.04 31.03	9.62 3.06 31.52	9.49 3.08 30.66
3	9.5 3.07 31.06	9.64 3.03 31.3	9.56 3.01 30.3
4	9.67 3.06 31.56	9.47 3.1 31.14	9.4 3.02 30.52
5	9.37 3.03 30.69	9.43 3.12 31.01	9.42 3.13 30.58

The FDM specimens, inserts employed in the overmolding processing were all fabricated using flat building orientation, which had been shown in Figure 3-7.
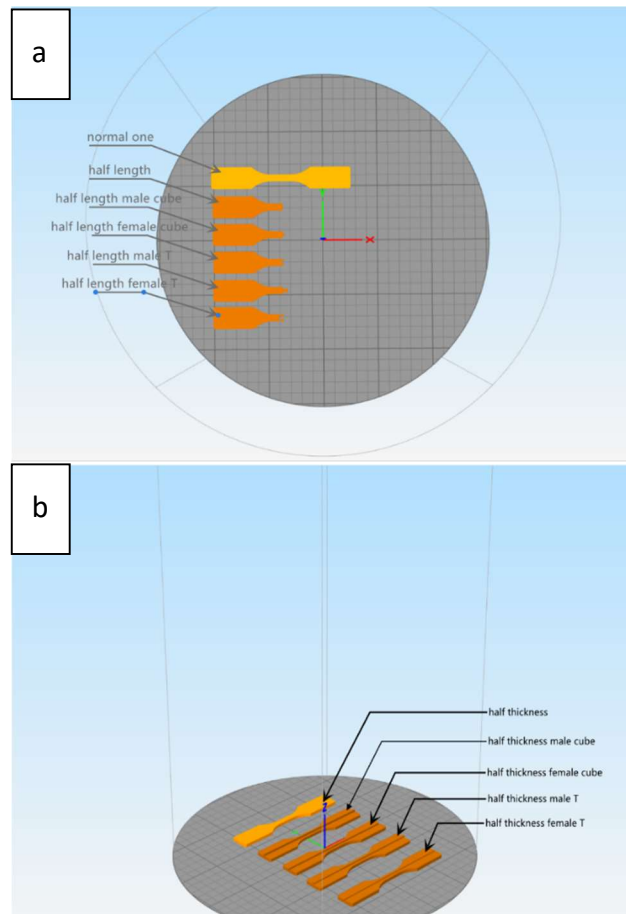
Figure 3-7 Building orientations for fabricated specimens/inserts using FDM technique: (a) normal and half-length series; (b) half-thickness series.

The IM processing was carried out via Babyplast 6/P injection molding machine (Rambaldi Company, Molteno, Italy), which has been displayed in Figure 3-8. The working parameters in the overmolding stage are listed as follows: shot size (mm) at 40 for IM batch and 30 for HYM batches, cooling time (sec) at 20, plasticizing zone temperature (°C) at 190, chamber temperature (°C) at 180, nozzle temperature (°C) at 170, mold temperature (°C) at 50, 1st injection pressure (bar) at 100, 1st injection pressure time (sec) at 3.5, 2nd injection pressure (bar) at 50, 2nd injection pressure time (sec) at 3, 2nd pressure setting (mm) at 3, decompression (mm) at 2, injection speed (%) at 95, 2nd injection speed (%) at 50, and 2nd speed point (mm) at 4. The required shot size for IM processing was set and determined by the volume of material necessary per shot to fill all sections, including runners, gates and cavities (Fuenmayor, Forde, et al., 2019). All IM settings were optimized prior to the production of samples. The FDM-fabricated preforms need to be manually inserted into the mold cavity tightly to confirm the success of overmolding stage. In some cases, the shrinkage of preform fabrication would result in the failed overmolding trials.

Figure 3-8 Babyplast IMM utilized in IM processing.

3.2.3 Tensile test for the specimens

All tensile tests were carried out using a Lloyd LRX Material Testing Machine (JLW

Instruments Corporation, Chicago, USA), at a movement speed of 5 cm/min at room temperature, where the tensile stress and Young's Modulus of all parts were collected and analyzed using the NEXYGEN™ software to obtain their individual average values and standard deviations (Douglas C. Montgomery, 2009).

Tensile strength (TS), also known as ultimate tensile strength (UTS) or σ within equations, is the maximum stress that a measured object will endure until cracking which is not influenced by the scale of checked specimens. In brittle materials, TS is close to the yield point, while it will be higher in ductile materials. The symbol of TS is referred as σ with its unit in International System of Units (SI) as MPa (10^6 Pascal), whereas its definition equation listed as $\sigma = F_b / S_o$, in which F_b refers to the maximum force for the tensile bar under the condition of deformation with a unit of N (Newtons), while S_o refers to the original cross section area (CSA) of samples.

Figure 3-9   LRX single column, bench mounted materials testing system machine utilized for test.

Tensile strain (ϵ), which is the ratio of change in length due to deformation of the tested specimen, it is also called as engineering strain, which is normally positive as the samples are forced with stretching, whose definition equation referred as $\epsilon = \frac{\Delta L}{L} =$

$\frac{l-L}{L}$, in which ΔL means the change in length, L means the original length of specimen,

and l means the length of sample after the deformation.
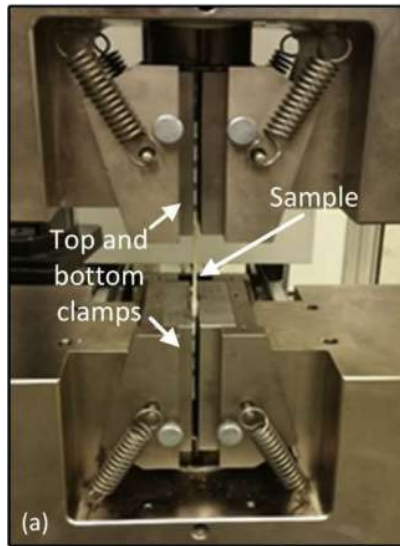
Figure 3-10 Pictorial illustration of tensile specimen fixture (Byberg et al., 2018).

3.2.4 Dimensional Accuracy Study

A Nikon Digital Microscope (Firmware ShuttlePix P-MFSC) from Japan with a magnification of (*20) was used to measure the parameters of fabricated samples and observe their macrostructures, providing the size accuracy of parts produced in this study.

Figure 3-11 Nikon ShuttlePix P-MFSC observing the specimen.

3.2.5 Statistical Analysis

Minitab 18 software (MiniTab Inc., Pennsylvania, USA) was utilized to analyze the tensile stress and Young's Modulus through analysis of variance (ANOVA) (Douglas C. Montgomery, 2009) and to figure out the impact of joint configuration on HYM samples' mechanical performances (Cao et al., 2016; Hutmacher et al., 2001). The p-value was defined at 0.05 (Byberg et al., 2018).

3.2.6 Composite Morphology

A Mira FE scanning electron microscopy (SEM) was used to illustrate the microstructure and dispersion morphology of the samples after testing on the fracture areas, with a 20 kV acceleration voltage and the magnification of (* 50) to visualize the dispersion via a back scattered electron detector. Prior to the SEM investigations, the samples observed were gold coated using a Baltec SCD 005 Sputter Coater (Cao et al., 2016).

Figure 3-12 Mira FE scanning electron microscopy utilized in the study.

Figure 3-13 Baltec SCD 005 Sputter Coater utilized before SEM observation.

3.3 Methodology for Chapter 5

3.3.1 Materials

The PLA filament (neutral color, 1.75 mm diameter) assembled in the filament reel was purchased from the Real Filament Company in Wateringen, Netherlands. The virgin PLA 4043D biopolymer utilized in the IM process were supplied from Nature-Works Corporation in 15305 Minnetonka Blvd., Minnesota, USA.

3.3.2 Preparation of samples

All manufactured samples were separated into three series in this study, the FDM, IM and hybrid manufactured (HYM) specimens, whose dimensions comply with the ASTM-D638-3 Standard, a schematic of the samples is shown in Figure 3-14. The fabrication of HYM specimens can be divided into two stages, in which the FDM inserts were created firstly and pushing these FDM preforms into the mold cavity to proceed the overmolding process.
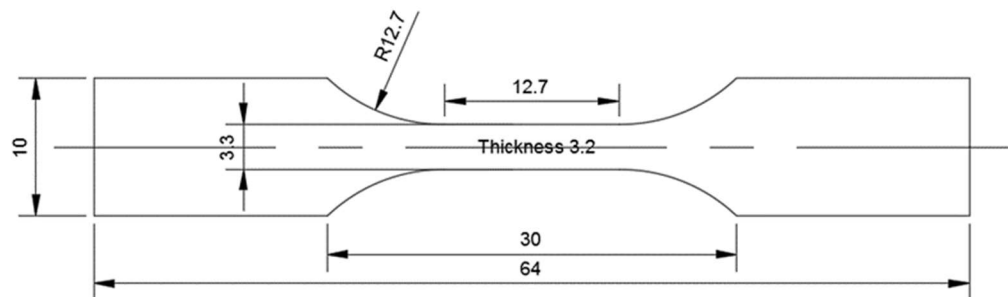
Figure 3-14 Dimensions of tested specimens produced in this study (unit in millimeter).

A total of 552 samples (42 batches of HYM samples, 3 batches of FDM samples and 1 batch of IM one were consisted of 12 specimens each) were prepared, the infill density for FDM inserts (25 %, 50 % and 75 %), the interface direction, the joint configurations for overmolding processing were used to evaluate the effect of FDM and IM on the mechanical performance of HYM samples, which can be found in Figure 3- 15 for half-length series and in Figure 3-16 for half thickness series.
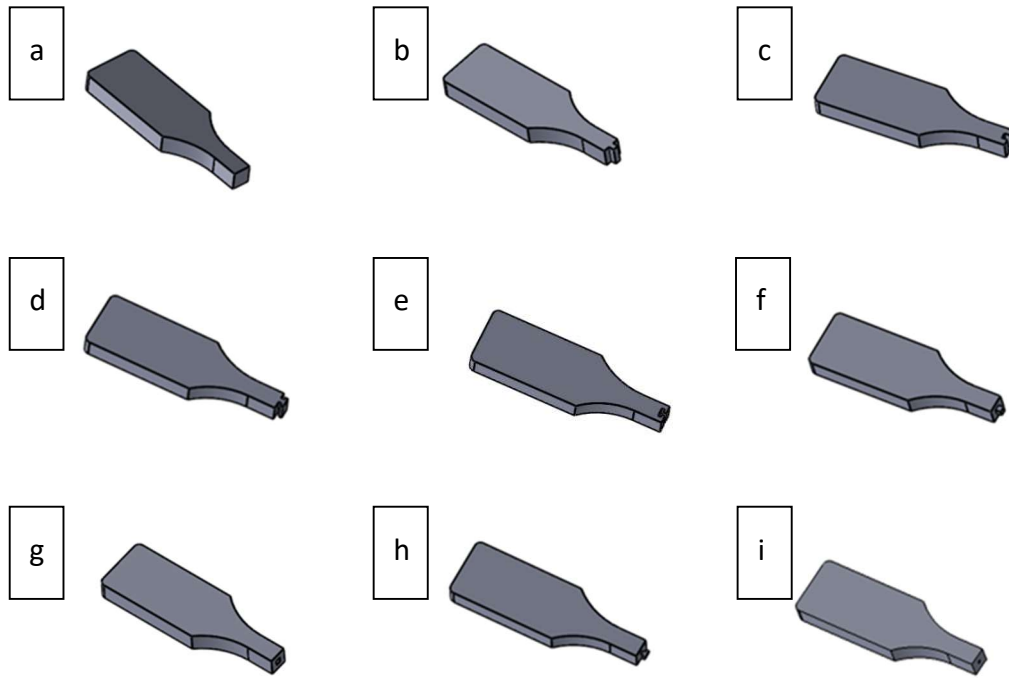
Figure 3- 15 CAD models for all HL series inserts: a) half-length; b) half-length male cube; c) half-length female cube; d) half-length male T; e) half-length female T; f) half-length male cube outset; g) half-length female cube inset: h) half-length male T outset: i) half-length female T inset.
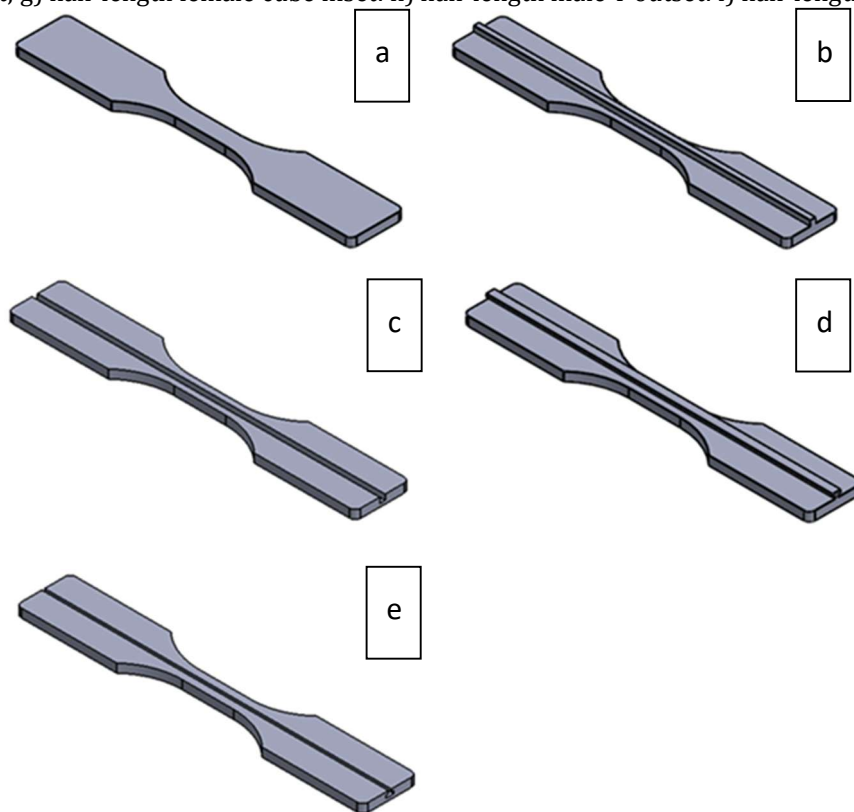
Figure 3-16 CAD models of all HT-series articles, in which (a) half-thickness without joint; (b) half-thickness male cube type joint; (c) half-thickness female cube type joint; (d) half thickness male T type joint; (e) half thickness female T type joint.

The additive manufacturing technique utilized in the fabrication process was FDM. The PLA filament used here was first dried in the oven using 60 °C for 4 hours due to PLA's moisture absorption which can adversely affect the mechanical output of fabricated samples (Kim et al., 2016), and then used in the FDM process. SolidWorks 2016 Edition Software (Dassault Systèmes, Waltham, USA) was used to design the CAD models of FDM tensile dumb-bell and FDM preforms/inserts and export them into the corresponding STL. Files. The STL. Files were then imported into MakerGear M2 Rev. E. (M2e) 3D printer machine (MakerGear LLC, Beachwood, Ohio, USA), which is shown in Figure 3-17, through Simplify 3D Software (Cincinnati, Ohio, USA) to operate the 3D printer.

Figure 3-17 MakerGear M2 machine used in the FDM stage.

The optimal parameters utilized in the process of FDM were derived in previous publications (Dizon et al., 2018; Fuenmayor et al., 2018; Hossain et al., 2014; Kozior & Kundera, 2017; Ning et al., 2016; Zaldivar et al., 2017), and kept constant in the study, these include layer thickness (0.1mm), infill density (25 %, 50 %, 75 %), infill orientation (45 °), number of top solid layers (3), number of bottom solid layers (3), number of outline/perimeter shells (2), infill extrusion width (100 %), extruder temperature (210 °C), printing bed temperature (60 °C), nozzle diameter (0.35 mm), retraction

distance (1 mm), retraction speed (2400 mm/min), default printing speed (6400 mm/min).

The building orientation in this research had been shown below in Figure 3-18 and the dimension of the cube was set as 1*1*1 (mm) for inset and outset shapes, respectively.
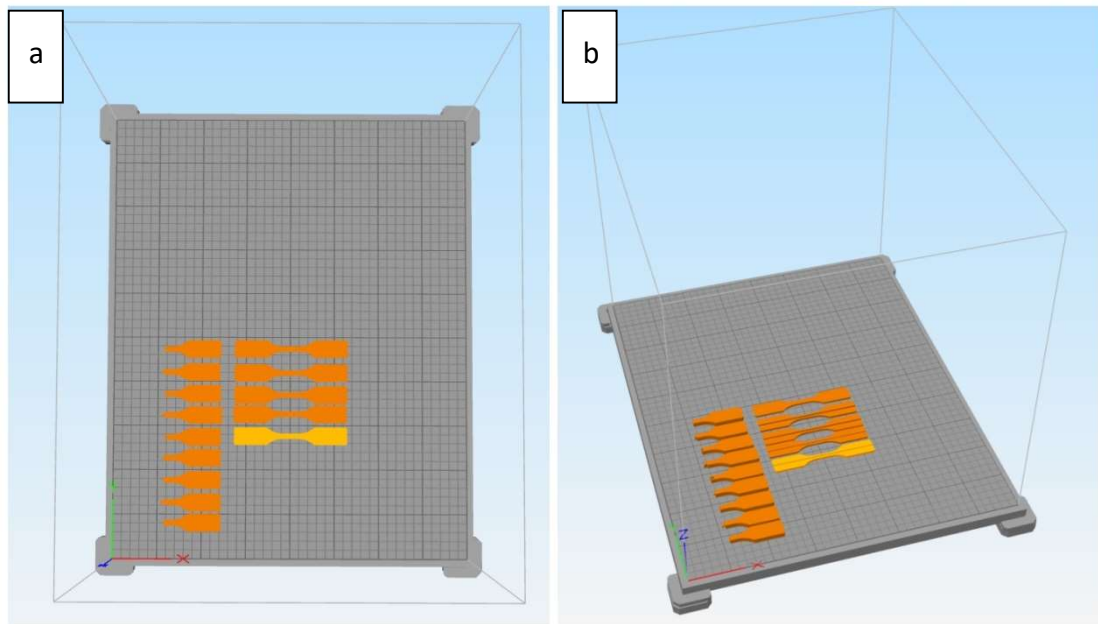
Figure 3-18 Layouts of samples/inserts in PLA specimens for FDM printing platform, in which (a) top view; (b) side view.

Besides, one sort of phenomenon happened in FDM processing was the material shrinkage, similar with what happened in ABS material. Hence, a shrinkage test had been carried out prior to the sample production, in which the tested samples with a size of 100 % nearly had no shrinkage condition due to specification of PLA material (Boros et al., 2019) and had shown in Table 3-3 below in which the example was half-length (flat-to-flat) batch, whose dimensions were 10 mm, 3.2 mm and 32 mm, respectively. Thus, the sample models utilized in the production were set for 100 % size.

Table 3-3 Shrinkage results for PLA printed samples (mm).

	25% infill	50% infill	75% infill
1	9.95 3.19 64.02	9.93 3.21 63.98	9.97 3.19 63.99
2	9.98 3.18 64.03	9.96 3.17 64.04	9.99 3.21 64.03
3	10.01 3.21 64.02	10.01 3.18 64.03	10.02 3.23 64.01
4	9.98 3.18 64.01	9.97 3.21 64.02	10.01 3.19 63.99
5	10.01 3.21 64.03	10.00 3.19 64.01	10.03 3.21 63.98

Injection Molding was performed on a Babyplast 6/12 injection molding machine from Rambaldi Corporation from Molteno, Italy. The temperature of plasticizing zone, chamber and nozzle were controlled and set at 185 °C, 180 °C and 170 °C, respectively. To obtain great-precision samples, the shot size was set at the same volume that is needed to fill the entire cavity (Fuenmayor, Donnell, et al., 2019). Similar with the parameters used in FDM, the settings used in the IM process were determined via preliminary screening trials and are presented as follows: shot size (28 mm for HYM samples and 40 mm for IM samples), cooling time (20 seconds), 1st injection pressure (100 bar), 1st injection pressure time (3.5 seconds), 2nd injection pressure (50 bar), 2nd injection pressure time (3 seconds), 2nd pressure setting (3 mm), decompression (2 mm), injection speed (95 %), 2nd injection speed (50 %). Furthermore, the virgin PLA material utilized to IM was firstly dried in the heating oven with a temperature of 60 °C for 4 hours due to the material's tendency for moisture absorption (Kim et al., 2016), and were then applied in prior to the process of the IM process. All FDM preforms were firstly pushed into the mold and then injection molded using the PLA material to fill the cavity to produce corresponding HYM samples.

3.3.3 Tensile Test

The mechanical properties of the samples based on ASTM-D638-3 were

determined through the Lloyd LRX Universal tester from Lloyd Instruments Ltd, Bognor Regis in UK at a movement speed of 5 cm/min. All samples were placed in a dryer using 40 °C for a night prior to the tensile test.

The equations shown as follows were utilized to determine the tensile stress (σ); strain (ϵ); and Young's Modulus (E).

$$\sigma=P/A,$$

$$\epsilon =\Delta L/L,$$

$$E=\sigma/\epsilon,$$

$$A=w*t,$$

in which P is the test loading, A is the cross-sectional area of the gauge, $_\Delta$L is the displacement of the crosshead, L is the gauge length, w and t are the width and thickness of sample gauge. In this study, a vernier caliper measured the length and thickness of gauge prior to the tensile test.

3.3.4 Macrostructure Observation

The macrostructures of all fabricated samples/cross sections of gauges for inserts were observed by a Nikon ShuttlePix P-MFSC Firmware Digital Microscope with a range of * 20 magnitudes prior to the tensile tests.

3.3.5 Statistical Analysis

The data analysis was carried out through GraphPad Prism 9 (GraphPad Software Inc., San Diego, CA, U.S.). The data was imported into the software, in which the mean and standard deviation values were obtained from the replicated data. In addition, a one-way analysis of variance (ANOVA) with a Tuckey's Multiple Comparison Test focusing on the joint configurations was applied here to determine the significance of the differences between each batch, where the p-value was set as 0.05.

3.3.6 Scanning Electron Microscopy

The scanning electron microscopy (SEM) was carried out with a Mira SEM (Tescan Oxford Instruments, UK) with a magnification of * 50 to observe the surface morphology of samples after the tensile test using secondary electron. Samples tested via SEM were placed on aluminum stubs and were then gold coated with Baltec SCD 005 sputter coater (BAL-TEC GmbH, Germany) to mollify charging's impact on the observation (Fuenmayor, Forde, et al., 2019).

3.4 Methodology for Chapter 6

3.4.1 Materials

The 1.75mm-diameter PLA filament with the natural color employed in the FDM technique was purchased from the Real Filament Company in Wateringen, Netherland. It was first dried at 40 °C for 8 hours and kept in the vacuum package before the fabrication (Kim et al., 2016). The virgin ABS pellets were purchased from the LOTTE Advanced Material Corporation in Seoul, South Korea. These pellets were first dried at 80 °C for 4 hours and then proceeded in IM technique.

3.4.2 Sample Preparation

Prior to the FDM processing, the Computer-Aided-Design (CAD) models in the FDM were first designed with the SolidWorks 2016 Edition Software (Dassault Systèmes, Waltham, USA) and then exported to the STL extension files. The STL files were opened under the control of Simplify3D Software (Cincinnati, Ohio, USA). Four models designed here (a. male cube; b. female cube; c. male T; d. female T) were shown in Figure 3-19. The FDM technique was carried out by a MakerGear M2 FDM Machine (MakerGear LLC, Beachwood, Ohio, USA) to produce all inserts. The parameters utilized in the FDM had been firstly determined via preparatory trials and kept in the fabrication: layer height (0.1 mm), infill percentage (25 % and 75 %), infill orientation (± 45 °), outline overlap (15 %), number of top solid layers (3), number of

bottom solid layers (3), number of outline/perimeter shells (2), infill extrusion width (100 %), minimum infill length (5 mm), extruder temperature (210 °C), printing bed temperature (60 °C), nozzle diameter (0.35 mm), retraction distance (1 mm), retraction speed (2400 mm/min) and default printing speed (6400 mm/min) without the raft and support.
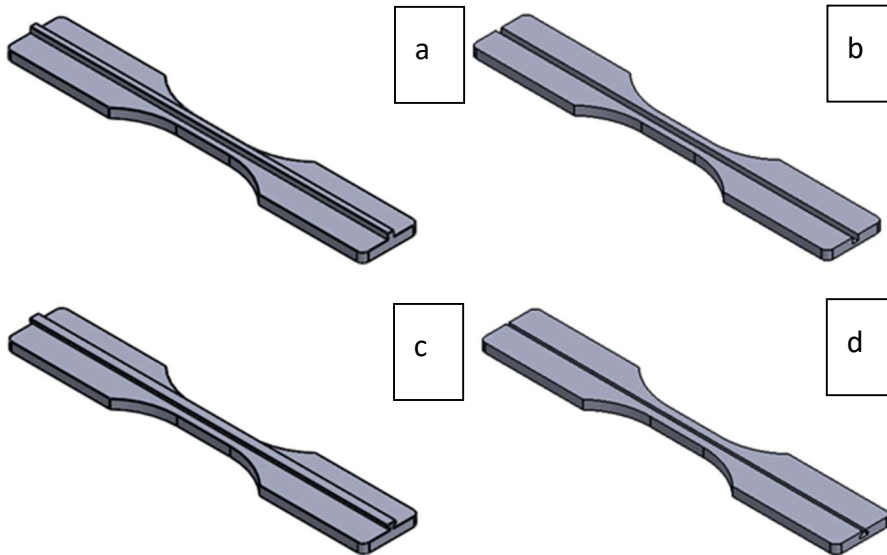
Figure 3-19 CAD models designed in this study, where the thickness for 3.2, length for 64, gauge width for 3.3, width at two ends for 10, cube size for 1*1*1, T size for 1.5*0.5*0.5*0.5 (all units for millimeter).

The overmolding stage accomplishing the full fabrication was employed by a Babyplast 6/12 Injection Molding Machine (Rambaldi Company, Molteno, Italy) with a 14 mm-diameter piston. The temperature of plasticizing zone, chamber, and nozzle were set as 190 °C, 180 °C and 170 °C. All IM parameters had been firstly determined under preliminary trials and then utilized in the production of final specimens and were shown as follows: injection pressure (60 bar and 100 bar), time in injection pressure (3.5 s), decompression (2 mm), injection speed (95 %), mold temperature (50 °C) and cooling time (20 s). Meanwhile, the shot size utilized in the process was set as a stroke of 28 mm to fill sectors of machine, including runners, gates, and cavities. All FDM substrates were first placed into the mold cavity and then directly injected molded using ABS pellets to finish the overmolding processing. These finished specimens were subjected to ASTM-D638-3 and shown in Figure 3-20 (CAD diagraphs).
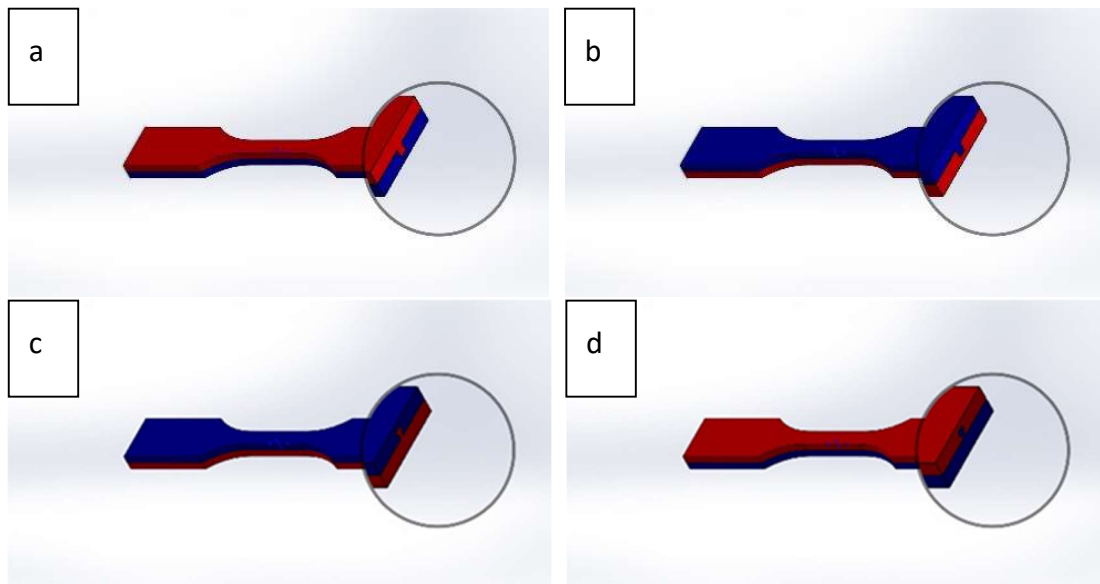
Figure 3-20 CAD diagraphs for all finished specimens, in which red parts were fabricated using FDM and blue ones were overmolded: a) male cube; b) female cube; c) male T; d) female T.

3.4.3 Tensile Test

All finished specimens were determined their tensile performances under the ASTM D638-Ⅲ standard, in which the 5 kN Lloyd LRX Universal tester (Lloyd Instruments Ltd, Bognor Regis, UK) at the fixed speed of 5 cm/min in loading stage was employed. These fabricated samples were firstly placed in the drying oven with the temperature of 40 °C for a night and taken into the tensile tests. The experimental data were all measured based on the ASTM D638-Ⅲ to figure out the specific performances in these specimens, maximum tensile strength (σ) and the Young's Modulus (E). A vernier caliper was applied to measure the dimensions of samples.

3.4.4 Statistical Analysis

The experimental data (σ and E) determined in the test were analyzed via the GraphPad Prism 9 Software. The three-way analysis of variance, one type of multivariate statistical technique to figure out the correlations amongst all variables with the results, was utilized to obtain the statistical significance of several factors. The IM pressure and infill density in this analysis were classified as the quantitative factors, whereas the joint configuration had been considered as the categorical factor. The p-

value indicates the parameters' degree of significance and quantifies the chance of a factor impacting the responses. Significant factors are defined as those with a p-value less than 0.05.

3.4.5 Fracture Observation

The fracture surface analysis was performed via a Mira Scanning Electron Microscope, SEM under 20 kV and the magnitude of 70 ×, (Tescan Oxford Instruments, UK). All tested specimens were cut from the fractured sections to proceed the SEM observation. These specimens were all firstly put on aluminum stubs and then gold coated with Baltec SCD 005 sputter coater (BAL-TEC GmbH, Germany) prior to the observation, aiming to prevent the side effect of charging in the examination.

3.5 Methodology for Chapter 7

3.5.1 Specimens Preparation

Samples in this study were fabricated in two stages: 1. The stainless inserts with the same dimensions of IM base were pushed into the cavity and continued the IM processing to produce the preforms with specific dimensions shown in Figure 3-21 below; 2. The material was overprinted onto the IM preforms to finish the manufacture of all overprinted samples, which were twice the thickness and were shown in Figure 3-22.

IM Base	Dimension (mm)					
	a	b	c	d	e	f
Measurement	64	30	12.7	1.6	3.3	10
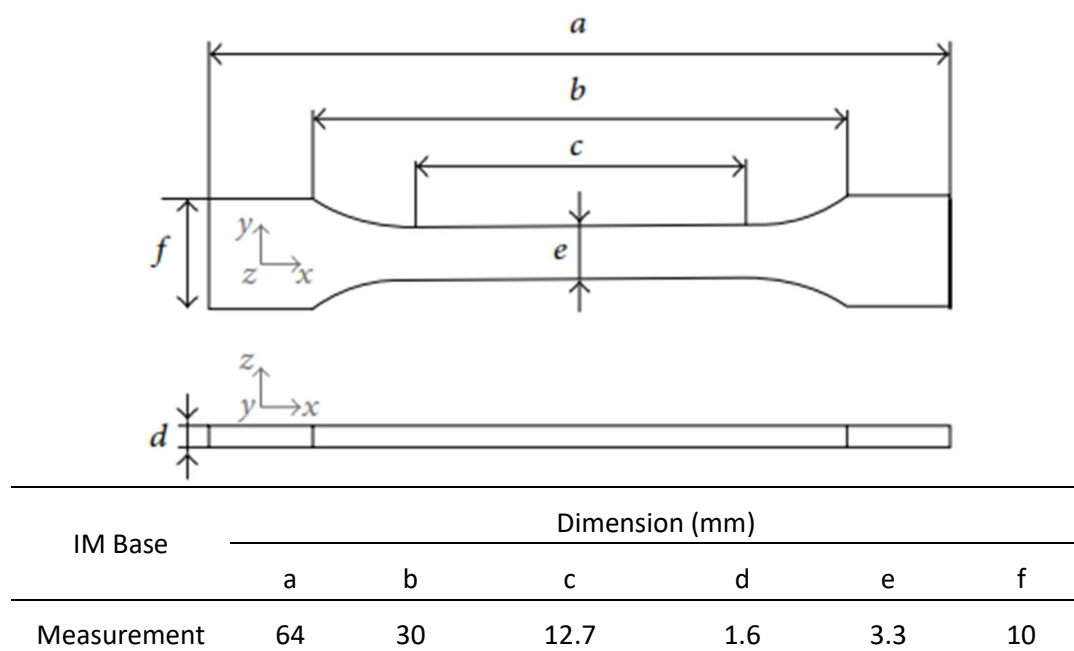
Figure 3-21 Dimensions of IM base.
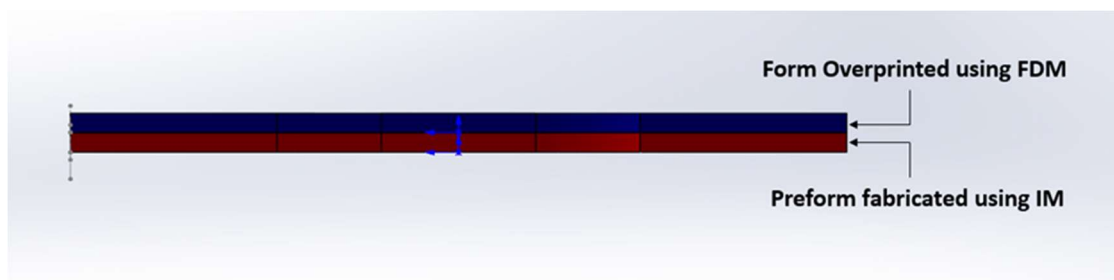
Figure 3-22 CAD design of the finished specimens.

3.5.2 Materials and Instruments

In this study, the virgin ABS pellets used in the IM processing were starex ® ABS

HF-0660IW from Samsung SDI Co., Ltd (Seoul, South Korea). The ABS filament (white color) with a diameter of 1.75 mm supplied by Real Filament Company (Wateringen, Netherlands) was used in the FDM stage for overprinting technique. As for the PLA samples, the virgin PLA 4043D pellets were supplied from NatureWorks Corporation at 15305 Minnetonka Blvd., Minnesota, USA. And the PLA filament (neutral color, 1.75 mm diameter) used in overprinting stage was purchased from the Real Filament Company in Wateringen, Netherlands. The 1.2083 stainless inserts applied in the fabrication of preforms were supplied by Midland Technical Tools Ltd in Athlone, Ireland.

Injection molding technique was carried out using a Babyplast ® 6/12 (Rambaldi Company, Molteno, Italy) equipped with a 14 mm diameter piston. Three temperature-controlled areas, plasticizing zone, chamber and nozzle, were included in the machine and the temperatures were 210 °C, 200 °C and 190 °C for ABS specimens and 190 °C, 180 °C and 180 °C for PLA specimens, respectively. The ABS and PLA pellets were first dried at 40 °C for one night prior to the IM processing. In addition, several trials were brought prior to the IM iteration production to optimize the IM parameters, which were displayed as follows: mold temperature at 50 (°C), shot size at 25 (mm), cooling time at 20 (sec), 1st injection pressure at 60 (bar), 1st injection pressure time at 3.5 (sec), 2nd injection pressure at 50 (bar), 2nd injection pressure time at 3.5 (sec), and decompression at 2 (mm).

In this case, a tailored building platform with half thickness as the building platform of MakerGear FDM machine was manufactured first, which can be found in Figure 3-23: The location of the tensile bar was determined using SolidWorks software and then converted to a CNC laser machine-compatible format. The original platform was placed in the laser machine's working area, and laser processing was initiated to create the building platform suitable for overprinting techniques. The building platform that can be employed in the overprinting technique is created. All injection molded preforms were manually inserted into the cavities with FDM fabricating onto the substrates to complete the overprinting stage.
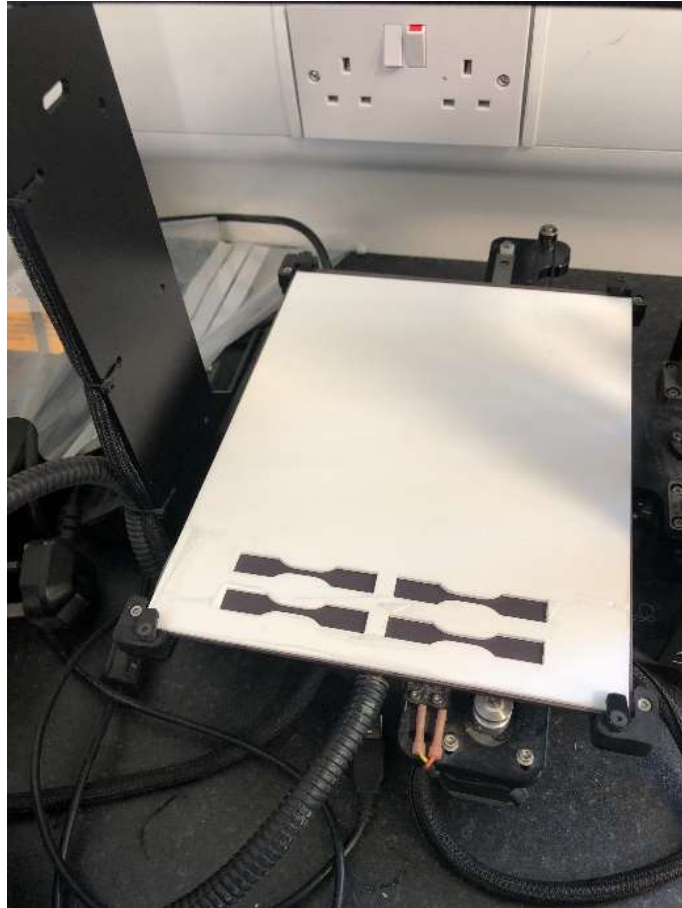
Figure 3-23 Tailored building platform designed for overprinting.

The overprinting technique was carried out using a MakerGear M2 (MakerGear LLC, Beachwood, Ohio, USA) 3D printer under the control of Simplify 3D Software Version-4.1.1 (Cincinnati, Ohio, USA). The CAD model utilized here was designed using SolidWorks 2016 Software (Dassault Systèmes, Waltham, USA). Three main parameters in the fabrication, infill density, printing speed and extrusion temperature, were designed using Taguchi methodology and were shown in Table 3-4. Other main FDM parameters were kept constant in this stage: nozzle diameter at 0.35 mm, layer height at 0.1 mm, top and bottom solid layers at 0, outline shells at 2, the infill outline overlap at 15 %, raster angle at ± 45 ° and infill pattern at rectilinear. This Taguchi methodology makes it possible to improve the quality of products in minimum variability and a reduced impact of external factors due to the S/N ratio determination.

Table 3-4 Experimental plan based on the Taguchi L9.

Run Order	Infill Density (%)	Printing Speed (mm/s)	Extrusion Temperature (°C) for ABS/PLA specimens
1	25	40	210/190
2	25	70	220/200
3	25	100	230/210
4	50	40	220/200
5	50	70	230/210
6	50	100	210/190
7	75	40	230/210
8	75	70	210/190
9	75	100	220/200

3.5.3 Dimension Observation

The dimensional measurements on fabricated specimens were carried out through a Nikon ShuttlePix P-MFSC Digital Microscope to confirm the accuracy of this study. Three main parameters in the tensile bar model were compared, thickness, total length, and width at two ends.

3.5.4 Mechanical Performance

To evaluate the mechanical properties of fabricated samples, tensile test was applied here. Tensile testing was carried out based on the ASTM D638-Ⅲ using an LRX single column, bench mounted materials testing system (JLW Instruments Corporation, United Kingdom) under the movement speed of 5cm/min at room temperature. The maximum stress values, strains and Young's Moduli were collected from the NEXYGEN™ software.

3.5.5 Statistical Analysis

The matrix experiments were conducted on evaluating the effects of parameters in the DOE (Taguchi, 1990). In addition, Minitab 18 software (MiniTab Inc., Pennsylvania, USA) was employed here to analyze the results from tensile test.

Chapter 4: Hybrid Manufacturing of Acrylonitrile Butadiene Styrene (ABS) via the Combination of Material Extrusion Additive Manufacturing and Injection Molding

4.1 Introduction

Acrylonitrile Butadiene Styrene (ABS) is a common thermoplastic polymer that has been widely employed in manufacturing industry due to its impact resistance, tensile strength, and rigidity. In this chapter, we introduced a hybrid manufacturing (HM) process combining materials extrusion additive manufacturing (AM) and injection molding (IM) to create a single article using ABS material, through which the high-volume manufacturing, great design freedom can be offered.

Three manufacturing techniques, fused deposition modelling (FDM), IM, and HM were employed here to produce forty-six batches of specimens, in which the hybrid manufactured (HYM) samples were made by inserting FDM substrates into the IM tool and were varied in infill density and geometries of preforms. The FDM and IM specimens were fabricated and tested first and following with the process for HYM specimens. These comparisons include the manufacturing cost, dimensions, tensile performances, and fracture observations in the determination of their characteristics. This study lays a foundation on the effect of HM in the finished specimens based on the varied infill densities and geometries of FDM preforms employed in overmolding processing.

4.2 Results and Discussion

In this study, the most important batches are those manufactured according to the MC principle, taking into account the sustainability of the process and the mechanical integrity of the parts. The AM-IM hybrid manufacturing process achieves the MC strategy in specimen fabrication: the FDM machine generates multiple inserts with specific properties (infill density and shape), and the IM process completes the creation of HYM specimens. FDM was used to fabricate parts that would be put into the IM tool with a high degree of geometrical freedom. Additionally, IM completes the HYM specimens at faster production rates than FDM alone.

Fabrication time of specimens was the first concern in this investigation, with a

single tensile specimen fabricated using FDM taking an average of 12 minutes to build, depending on processing parameters, particularly infill density, whereas the IM process fabricates two specimens in 1.5 minutes (this is the molding cycle length). In this investigation, each batch comprised of 12 specimens, and it took around 144 minutes to build each batch of FDM specimens, but just 9 minutes to fabricate each batch of IM specimens. In contrast, the current HM method took 72 minutes for insert fabrication plus 9 minutes for IM, for a total of 81 minutes per batch via HM, indicating that HM manufacturing requires less time than FDM. In this investigation, the customizability of 3D printing allowed for the manufacture of different inserts during the overmolding step resulting in the inclusion of multiple batches of HYM samples, which are listed in Table 4-1.

Table 4-1 The range of specimens fabricated in this study.

Batch Name	Type of Samples/Inserts	Infill Density (%)
FDM 25/50/75	FDM Sample	25, 50, 75
IM	IM Sample	100
HL/HT-NJ 25/50/75	Half of Length/Thickness (No Joint Configuration)	25, 50, 75
HL/HT- MC 25/50/75	Half of Length/Thickness Male Cube Joint	25, 50, 75
HL/HT- FC 25/50/75	Half of Length/Thickness Female Cube Joint	25, 50, 75
HL/HT- MT 25/50/75	Half of Length/Thickness Male T Joint	25, 50, 75
HL/HT- FT 25/50/75	Half of Length/Thickness Female T Joint	25, 50, 75
HL-MCO 25/50/75	Half of Length Male Cube Joint, Outset	25, 50, 75
HL-FCI 25/50/75	Half of Length Female Cube Joint, Inset	25, 50, 75
HL-MTO 25/50/75	Half of Length Male T Joint, Outset	25, 50, 75
HL-FTI 25/50/75	Half of Length Female T Joint, Inset	25, 50, 75

4.2.1 Dimensional Accuracy

All fabricated specimens for tensile test were observed via Nikon ShuttlePix P-

MFSC machine in which gauge length, specimen thickness, specimen length were considered and measured following the ASTM-638-3 standard, dimensions shown in Table 4-2, some cross sections of joint configurations for typical FDM inserts as well as the parameters of the gauges for final samples are shown below in Figure 4-1 and Figure 4-2, respectively. These results indicate an enhanced dimension precision and high design flexibility can be offered based on the combination of FDM and IM technique.

Table 4-2 Parameters of sections for all samples.

Parameter	IM batch	FDM batches	HYM batches
Thickness (mm)	3.2±0.1	3.2±0.1	3.2±0.1
Total Length (mm)	64±0.2	64±0.2	64±0.2
Gauge Width (mm)	3.3±0.2	3.3±0.1	3.3±0.1
Width at two ends (mm)	10±0.2	10±0.2	10±0.2
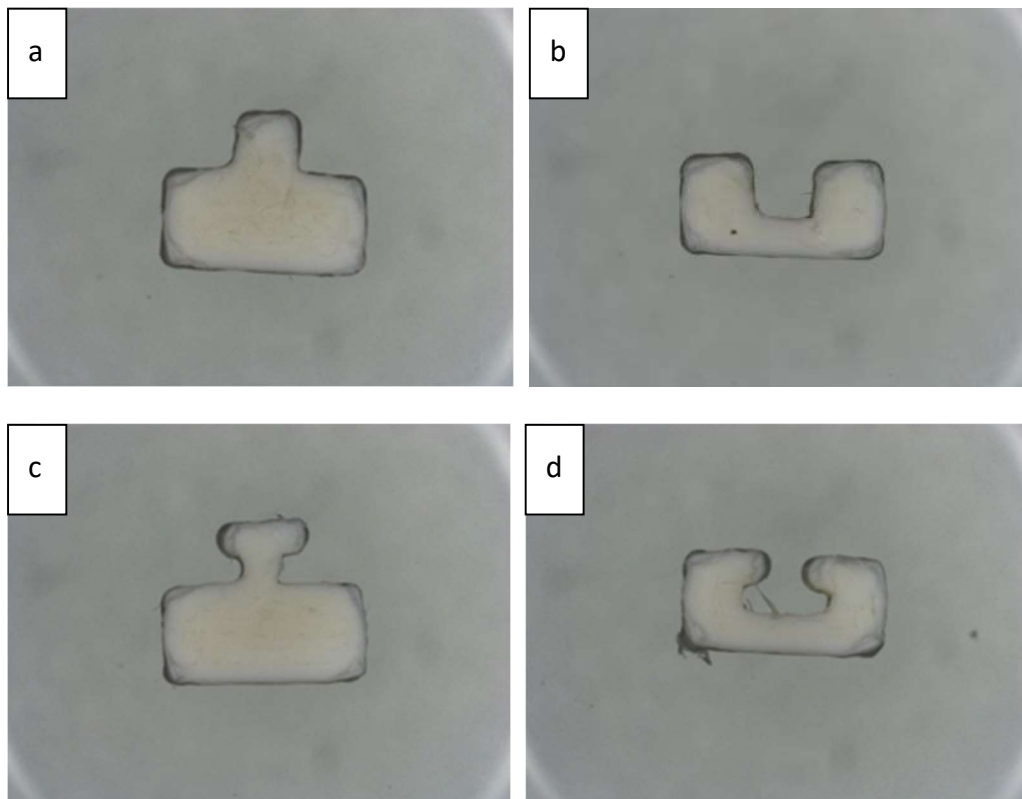
Figure 4-1 Cross sections of some FDM inserts:(a) HT-MC 50; (b) HT-FC 50; (c) HT-MT 50 and (d) HT-FT 50.
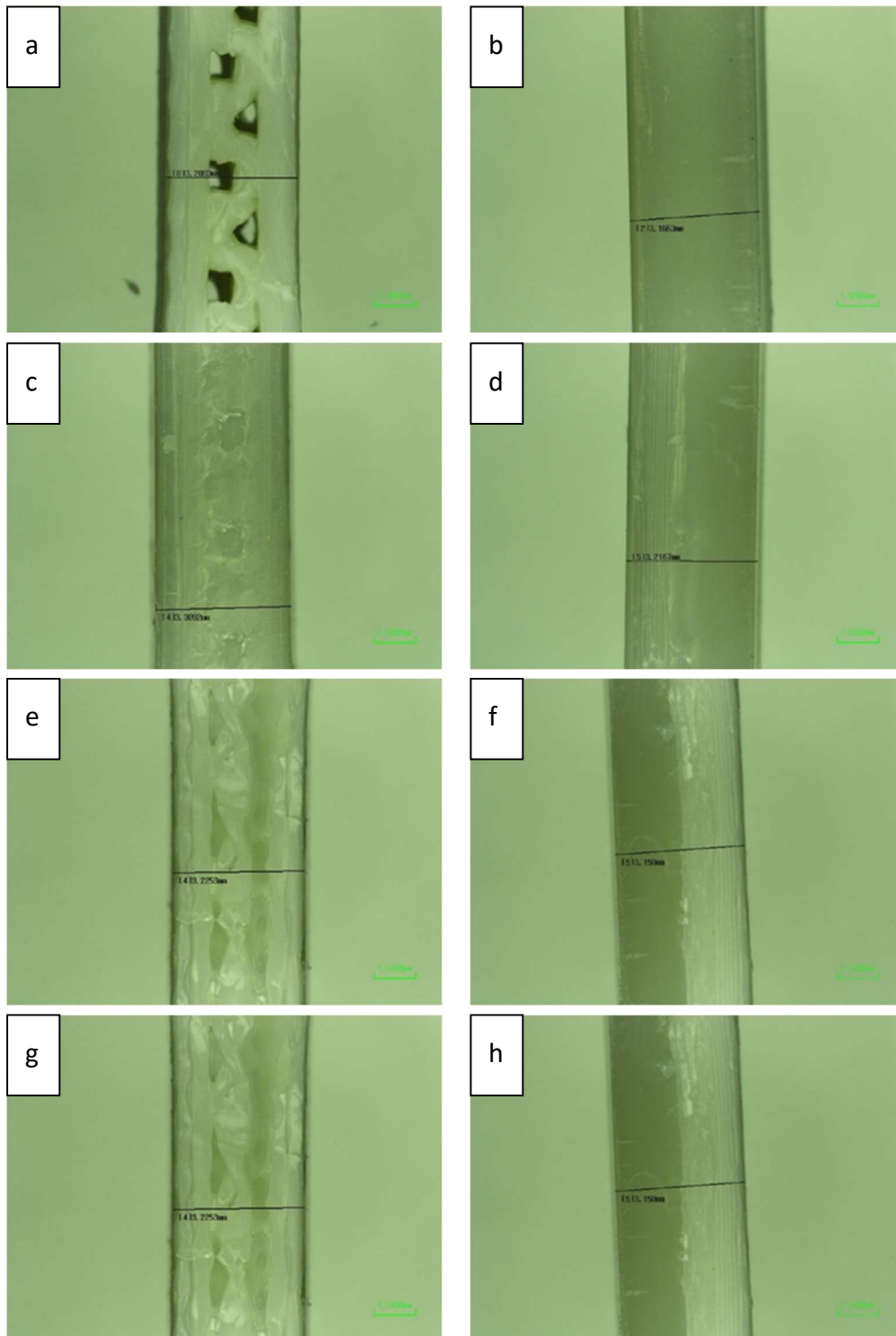
Figure 4-2 Images by Nikon Microscope for macrostructures and parameters of FDM, IM, and HT-series samples: (a)FDM 50, gauge width for 3.2083 mm; (b)FDM 50, thickness for 3.1438 mm; (c) IM, gauge width for 3.4501 mm; (d) IM, thickness for 3.1663 mm; (e) NJ 50, gauge width for 3.3092 mm; (f) NJ 50, thickness for 3.2167 mm; (g) FC 50, gauge width for 3.2253 mm; (h) FC 50, thickness for 3.158 mm.

4.2.2 Ultimate Tensile Strength and Stiffness

The test results, including mean and standard deviations, of the maximum tensile stress/strengths (σ) and Young's Modulus (E) for all ABS samples are tabulated in Table 4-3 for FDM and IM batches, Table 4-4 for HL-series specimens and Table 4-5 for HT-series specimens.

Table 4-3 Average tensile test results for all FDM and IM batches, whose standard deviations have been shown as well.

Batch Name	σ(MPa)	E(MPa)
FDM 25	22.85± 2.97	446.42± 86.86
FDM 50	32.26± 1.56	675.97± 79.17
FDM 75	37.91± 4.66	689.19± 95.01
IM	49.95± 0.61	887.49± 136.19

Table 4-3 displays the tensile test results for specimens fabricated through FDM or IM only, where all average maximum tensile stress and Young's Modulus progressively fell as the infill density decreased in the FDM specimens and the best mechanical property was observed in IM batch, which is in line with previous publications (Ahn et al., 2002; Alafaghani et al., 2017; Rodríguez-Panes et al., 2018) that samples with higher infill density will show greater mechanical performance than lower-infill density FDM parts. In addition, a low deviation in maximum tensile stress for IM batch can be found here. This phenomenon can be explained in the high-density internal structure and high material compaction of IM specimen, offering a stable withstanding while loaded with the tensile. This low deviation indicates a promising applicability in this IM technique (Zhai et al., 2021).

Table 4-4 Average tensile test results for half-length series specimens, whose standard deviations have been shown as well.

Batch Name	σ(MPa)	E(MPa)	Batch Name	σ(MPa)	E(MPa)	Batch Name	σ(MPa)	E(MPa)
HL-NJ 25	11.56±2.82	634.12±70.64	HL-NJ 50	8.55±2.52	625.72±121.93	HL-NJ 75	8.11±2.55	644.08±187.19
HL-MC 25	16.55±5.29	578.77±125.93	HL-MC 50	13.54±5.50	642.35±161.27	HL-MC 75	11.73±2.78	639.90±175.81
HL-FC 25	18.55±2.58	735.09±138.15	HL-FC 50	15.02±3.07	707.59±92.45	HL-FC 75	12.14±4.07	749.77±141.08
HL-MT 25	22.04±2.17	644.54±115.06	HL-MT 50	19.56±6.76	609.35±(99.47)	HL-MT75	14.94±7.27	667.17±122.42
HL-FT 25	25.47±3.64	745.71±55.18	HL-FT 50	21.41±3.42	717.95±82.84	HL-FT 75	20.16±3.70	738.62±119.11
HL-MCO 25	11.20±3.83	710.34±117.17	HL-MCO 50	12.20±2.53	657.56±110.39	HL-MCO 75	12.07±2.99	716.31±80.52
HL-FCI 25	21.19±2.53	765.53±149.24	HL-FCI 50	15.68±2.33	741.72±149.57	HL-FCI 75	13.69±2.58	806.35±96.70
HL-MTO 25	16.90±4.16	772.78±135.62	HL-MTO 50	12.78±6.12	732.15±133.90	HL-MTO 75	15.12±4.05	637.19±89.82
HL-FTI 25	18.98±2.70	848.85±95.03	HL-FTI 50	16.21±4.30	755.38±149.80	HL-FTI 75	14.91±4.51	691.30±124.37

Table 4-5 Average tensile test results for half-thickness series specimens, whose standard deviations have been shown as well.

Batch Name	σ (MPa)	E (MPa)	Batch Name	σ (MPa)	E (MPa)	Batch Name	σ (MPa)	E (MPa)
HT-NJ 25	45.09±2.90	724.96±47.37	HT-NJ 50	46.62±0.87	745.03±24.63	HT-NJ 75	45.62±1.23	690.35±68.90
HT-MC 25	44.06±5.29	824.07±123.02	HT-MC 50	46.30±0.81	746.07±60.62	HT-MC 75	43.50±1.43	681.86±47.83
HT-FC 25	45.55±1.48	723.05±24.62	HT-FC 50	47.42±0.97	737.62±15.43	HT-FC 75	44.79±1.98	778.00±111.42
HT-MT 25	41.80±2.15	854.26±63.99	HT-MT 50	42.62±2.14	861.23±64.63	HT-MT 75	44.39±2.22	818.90±121.19
HT-FT 25	46.39±1.30	752.70±15.24	HT-FT 50	48.00±1.07	727.92±37.09	HT-FT 75	46.50±0.94	709.53±20.78

Figure 4-3 shows representative stress-strain curves for all FDM and IM batches in which the maximum tensile strength varies from 22.85 to 49.95 MPa and it clearly depicts that an increasing tendency for tensile strength with the rise of infill density, agreeing with the result in Table 4-3. In addition, the FDM 25 shows the highest value of strain amongst all FDM samples, reaching around 12 %. These phenomena can be explained by two statements: (1) parts with higher infill density will be more rigid and fewer cavities (Rodríguez-Panes et al., 2018), this makes FDM 75 show the greatest mechanical performance amongst the FDM samples; (2) the higher degree of internal defects for the lower in-fill-density samples will result in greater elongation at break due to the poor bonding force amongst fiber in FDM samples (Rodríguez-Panes et al., 2018).
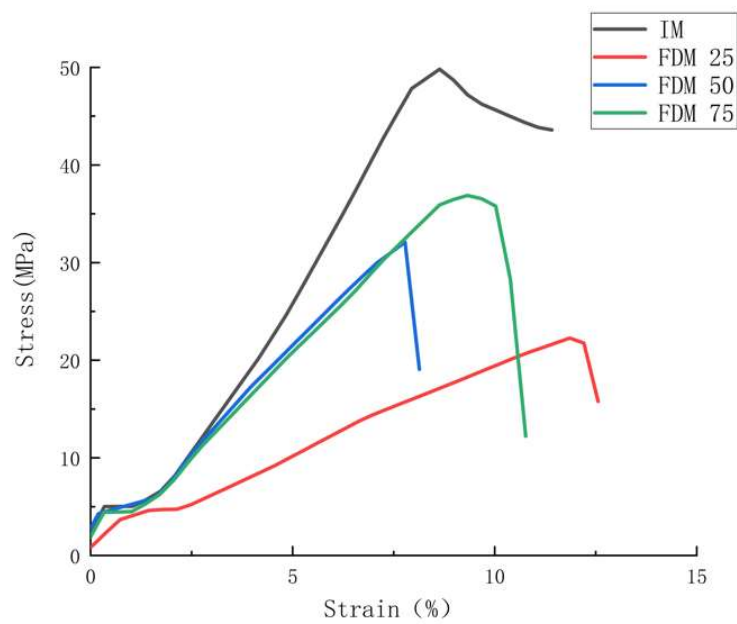
Figure 4-3 Representative stress-strain curves for tensile test amongst FDM and IM batches.

Moreover, IM's outstanding mechanical performance can be found in IM batch based on Figure 4-3 and Table 4-3, with a high-value difference when compared to all FDM batches, this can be explained by two factors: (1) the high-density structure of ABS samples in addition with the strong polymer chain can be created through IM processing, which agrees with some previous studies (Ahn et al., 2002; Lay et al., 2019; Weng et al., 2016); (2) the layer-by-layer formation in FDM parts results in the stress concentration at the fusion line, which further aligns with previous findings (Hossain et al., 2013; J. Ma et al., 2021; Roberson et al., 2015).

Half-Length Series Specimens:

Table 4-4 displays both the average maximum tensile strengths and Young's Modulus for half-length series specimens and demonstrates discrepancies between the samples processed under various conditions, which is related to the infill density and specifications of 3DP inserts. The HL-FT 25 batch showed a significant maximum tensile strength amongst all shown here, with a value of 25.47 MPa. HL-NJ 75 batch carried the worst average maximum tensile strength for this series (8.11 MPa), which was less than 1/3 of the maximum tensile strength observed for this lot (25.47 MPa). As for the stiffness, HL-FTI 25 batch showed the largest Young's Modulus (848.85 MPa) comparing with other batches, indicating its most significant stiffness amongst this sequence, whereas HL-MC 25 batch possessed the worst stiffness, with a Young's Modulus of 578.77 MPa.

It can be clearly found from Table 4-4 that the varied infill densities and geometries of FDM preforms can affect the tensile performances of finished specimens, with the female T joint resulting in the greatest tensile performance if compared to other joints and the flat-to-flat joint (NJ) having the worst performance. In addition, a gap in tensile performance (average tensile strength) can be identified due to the specification difference in cube/T series and cube/T inset or outset series. For instance, the greatest tensile strength for HL series with cube joints can be found in HL-FC 25 (18.55 MPa), while the greatest tensile strength in the HL series with T

joints can be determined in HL-FT 25 (25.47 MPa). As for the cases in HL series with cube inset and outset joint configuration, the greatest tensile strength can be found in 21.19 MPa for HL-FCI 25 batch. Regard to the HL series with T inset and outset joint configuration, this can be determined in the HL-FTI 25 batch, with a value of 18.98 MPa. These results for tensile strength were consistent with the findings for Young's Modulus, indicating the specimens with greater maximum tensile strength exhibited greater stiffness. The stress-strain curves for all half-length series specimens are shown separately in function of their joint configurations, which are in line with the results shown in Table 4-4.

Figure 4-4 displays the stress-strain curves for HL-NJ series specimens with 25 %, 50 %, and 75 % infill density, respectively. It can be found that the batch with 25 % infill density are offered the greatest tensile performance (11.56 MPa for maximum tensile strength) amongst all. In addition, a decreasing tendency of maximum tensile strength value can be determined if the infill density increases, in which the maximum tensile strength value of HL-NJ 50 is 8.55 MPa, and the one for HL-NJ 75 is 8.11 MPa. This value transition can be explained from the greater quantity of polymer overmolded with FDM preforms, resulting in a stronger bond between FDM and overmolded material, and thus, a higher value of maximum tensile strength will be allowed for.
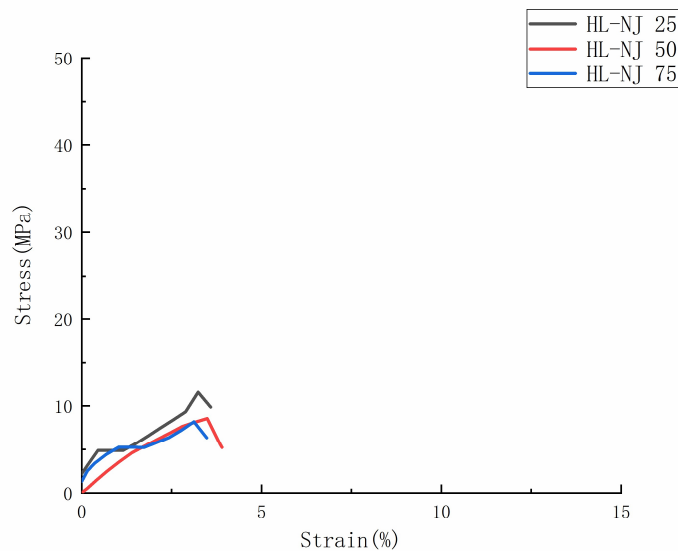
Figure 4-4 Representative stress-strain curves for tensile test amongst HL-NJ series.

Figure 4-5 displays the stress-strain curves for HL-MC and HL-FC series specimens with 25 %, 50 %, and 75 % infill density, respectively. It can be found from Figure 4-5 (a) and (b) that the batch with 25 % infill density are offered the greatest tensile performance (16.55 MPa for maximum tensile strength in HL-MC series and 18.55 MPa for maximum tensile strength in HL-FC series) amongst all. In addition, a decreasing tendency of maximum tensile strength value can be determined in HL-MC series if the infill density increases, in which the maximum tensile strength value of HL-MC 50 is 13.54 MPa, and the one for HL-MC 75 is 11.73 MPa. In the case of HL-FC series, the maximum tensile strength value of HL-FC 50 is 15.02 MPa, and the one for HL-FC 75 is 12.14 MPa, which agree with the conditions in HL-NJ series and HL-MC series.

Furthermore, an interesting phenomenon can be observed from the effect of joint configurations in the overmolding technique that specimens with female joint configurations will have a greater tensile performance if compared to the ones with male joint configurations. This condition can be explained from following two statements: 1. a female joint configuration would offer the stronger mechanical interlock based on the overmolding processing than the male ones; 2. a higher volume of the molten polymer was able to enter the female joints compared to the male ones.
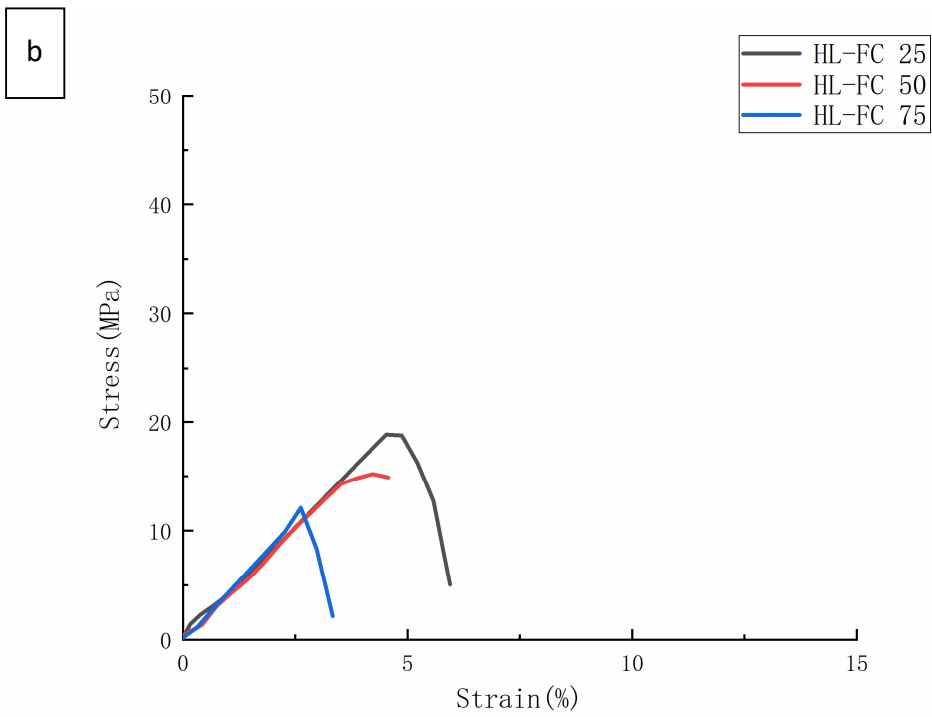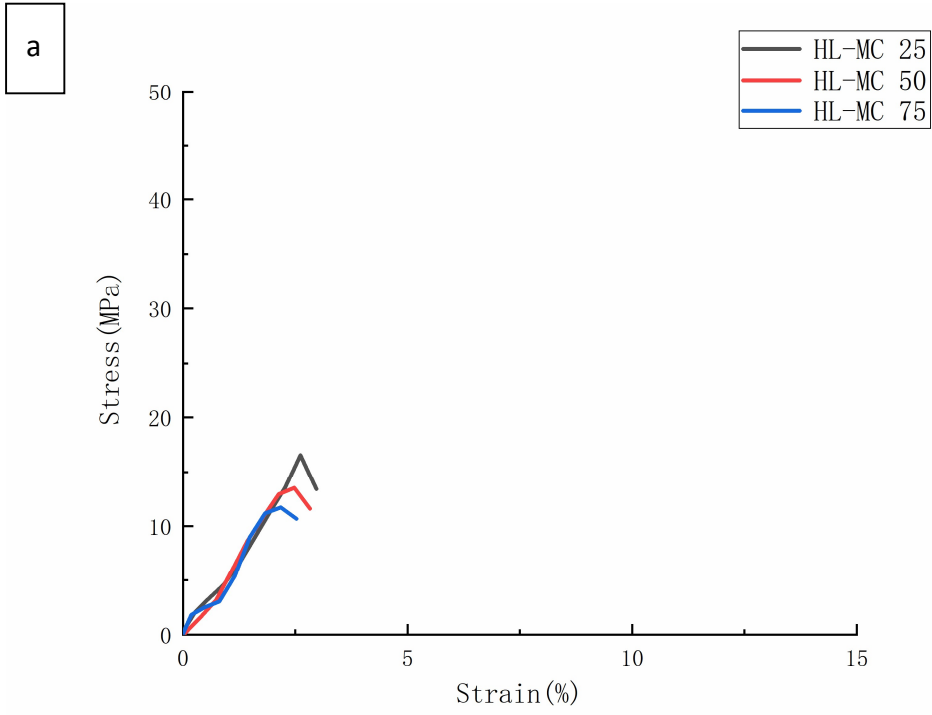
Figure 4-5 Representative stress-strain curves for tensile test amongst half-length series with cube joint configuration: (a) male ones; (b) female ones.

Figure 4-6 displays the stress-strain curves for HL-MT and HL-FT series specimens with 25 %, 50 %, and 75 % infill density, respectively. It can be found from Figure 4-6 (a) and (b) that the batch with 25 % infill density are offered the greatest tensile performance (22.04 MPa for maximum tensile strength in HL-MT series and 25.47 MPa for maximum tensile strength in HL-FT series) amongst all. In addition, a decreasing tendency of maximum tensile strength value can be determined in HL-MT series if the infill density increases, in which the maximum tensile strength value of HL-MT 50 is 19.56 MPa, and the one for HL-MT 75 is 14.94 MPa. In the case of HL-FT series, the maximum tensile strength value of HL-FT 50 is 21.41 MPa, and the one for HL-FT 75 is 14.94 MPa, which are in line with the findings in the above sections.
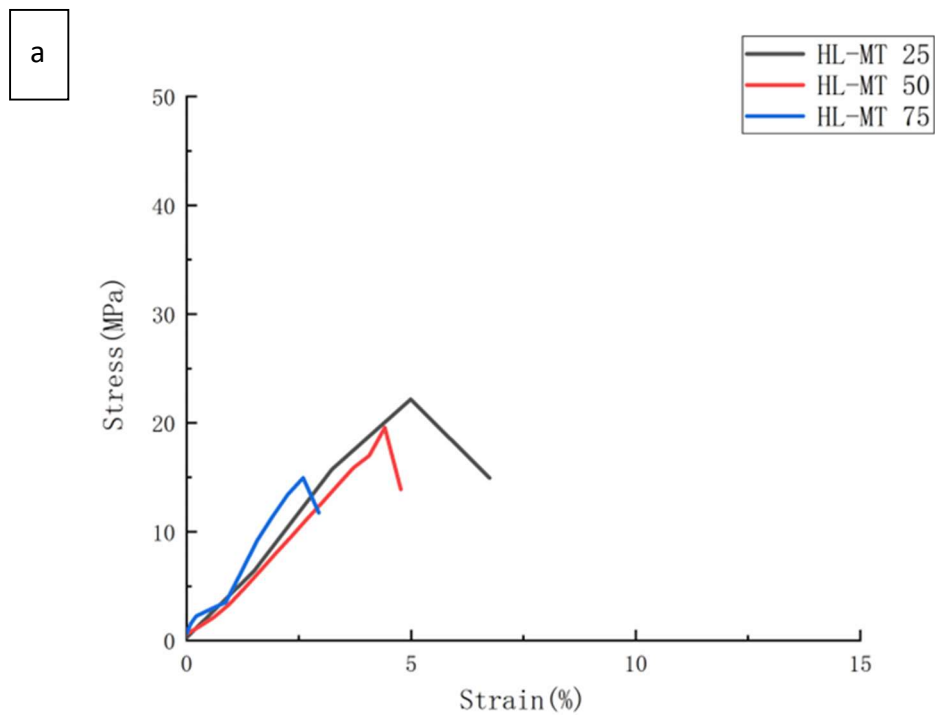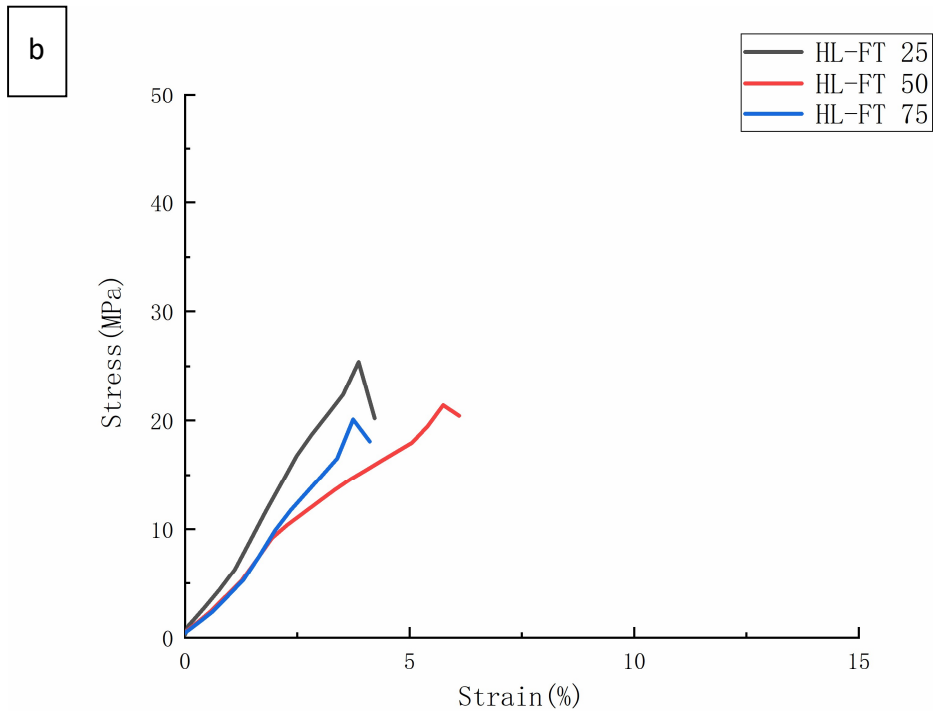
Figure 4-6 Representative stress-strain curves for tensile test amongst half-length series with T joint configuration: (a) male ones; (b) female ones.

Furthermore, the same phenomenon from joint configurations can be observed in this series, in which the specimens with female T joint configuration will have a greater tensile performance if compared to the ones with male T joint configuration. This condition can be explained from following two statements (shown in Figure 4-7): 1. a female joint configuration would offer the stronger mechanical interlock based on the overmolding processing than the male ones; 2. a higher volume of the molten polymer was able to enter the female joints compared to the male ones.
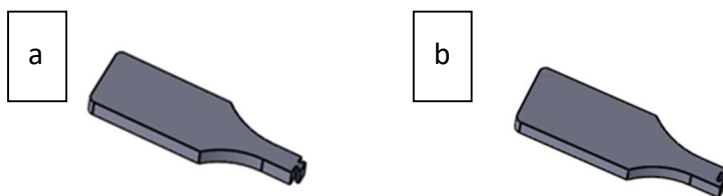
Figure 4-7 Schematic graph of cube inserts applied in overmolding processing: (a) male T; (b) female T.

Figure 4-8 displays the stress-strain curves for HL-MCO and HL-FCI series specimens with 25 %, 50 %, and 75 % infill density, respectively. It can be found from Figure 4-8 (a) that the HL-MCO batch with 50 % infill density is offered the greatest tensile performance in the series (12.20 MPa) and the specimen with 75 % infill density owns a value of maximum Young's Modulus at 716.31 MPa, while the one with 25 % infill density shows the lowest value (11.20 MPa) in this group, but still higher than the HL-NJ 50 and HL-NJ 75. As for the condition in HL-FCI series, Figure 4-8 (b) and Table 4-4 display a decreasing tendency of maximum tensile strength value can be determined from the increase of infill density, in which the maximum tensile strength value of HL-FCI 25 is 21.19 MPa, HL-FCI 50 is 15.68 MPa, and the one for HL-FCI 75 is 13.69 MPa.
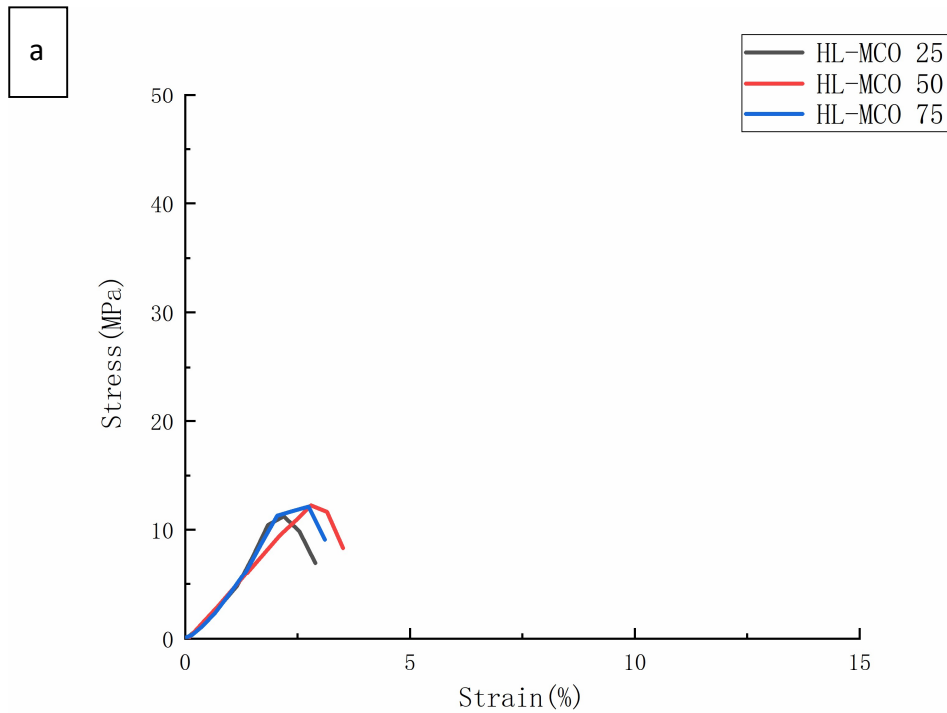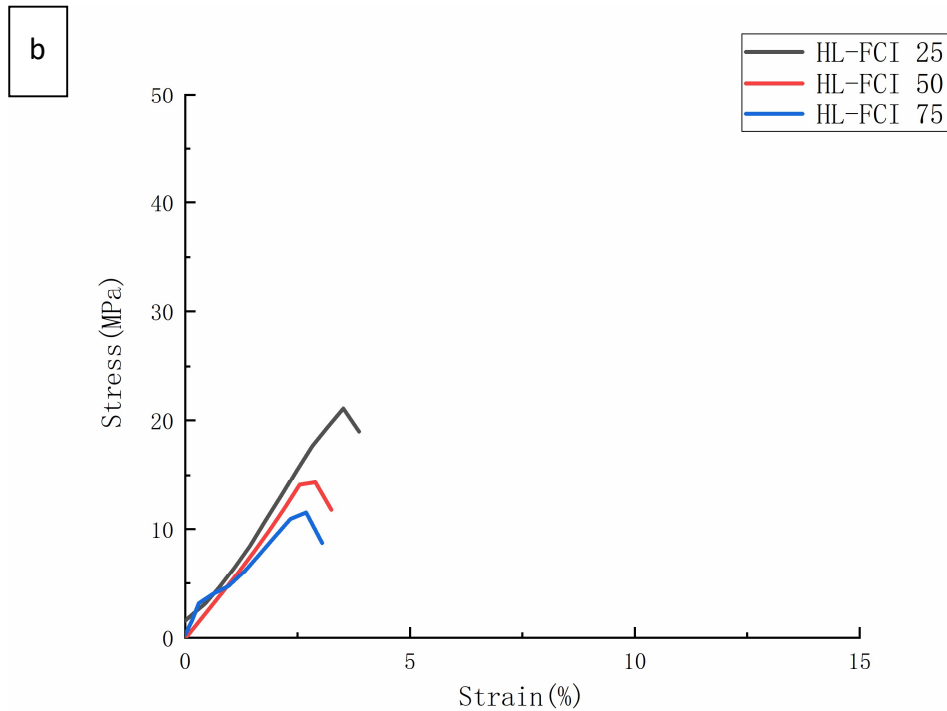
Figure 4-8 Representative stress-strain curves for tensile test amongst half-length series with cube (outset and inset) joint configuration: (a) male ones; (b) female ones.

These phenomena can be explained from the following claims: 1. a female joint configuration would offer the stronger mechanical interlock based on the overmolding processing than the male ones; 2. More contact area can be offered from female joint configuration and thus more interlock can be established in the overmolding period; 3. a higher volume of the molten polymer was able to enter the female joints compared to the male ones.

Figure 4-9 displays the stress-strain curves for HL-MTO and HL-FTI series specimens with 25 %, 50 %, and 75 % infill density, respectively. It can be found from Figure 4-9 (a) that the HL-MTO batch with 25 % infill density is offered the greatest tensile performance in the series (16.90 MPa) and the specimen with 75 % infill density owns a value of maximum tensile strength at 15.12 MPa, while the one with 50 % infill density shows the lowest value (12.78 MPa) in this group, but still higher than the three specimens in HL-MCO series. As for the condition in HL-FTI series, Figure 4-9 (b) and Table 4-4 display a decreasing tendency of maximum tensile strength value determined from the increase of infill density, in which the maximum tensile strength

value of HL-FTI 25 is 18.98 MPa, HL-FTI 50 is 16.21 MPa, and the one for HL-FTI 75 is 14.91 MPa.
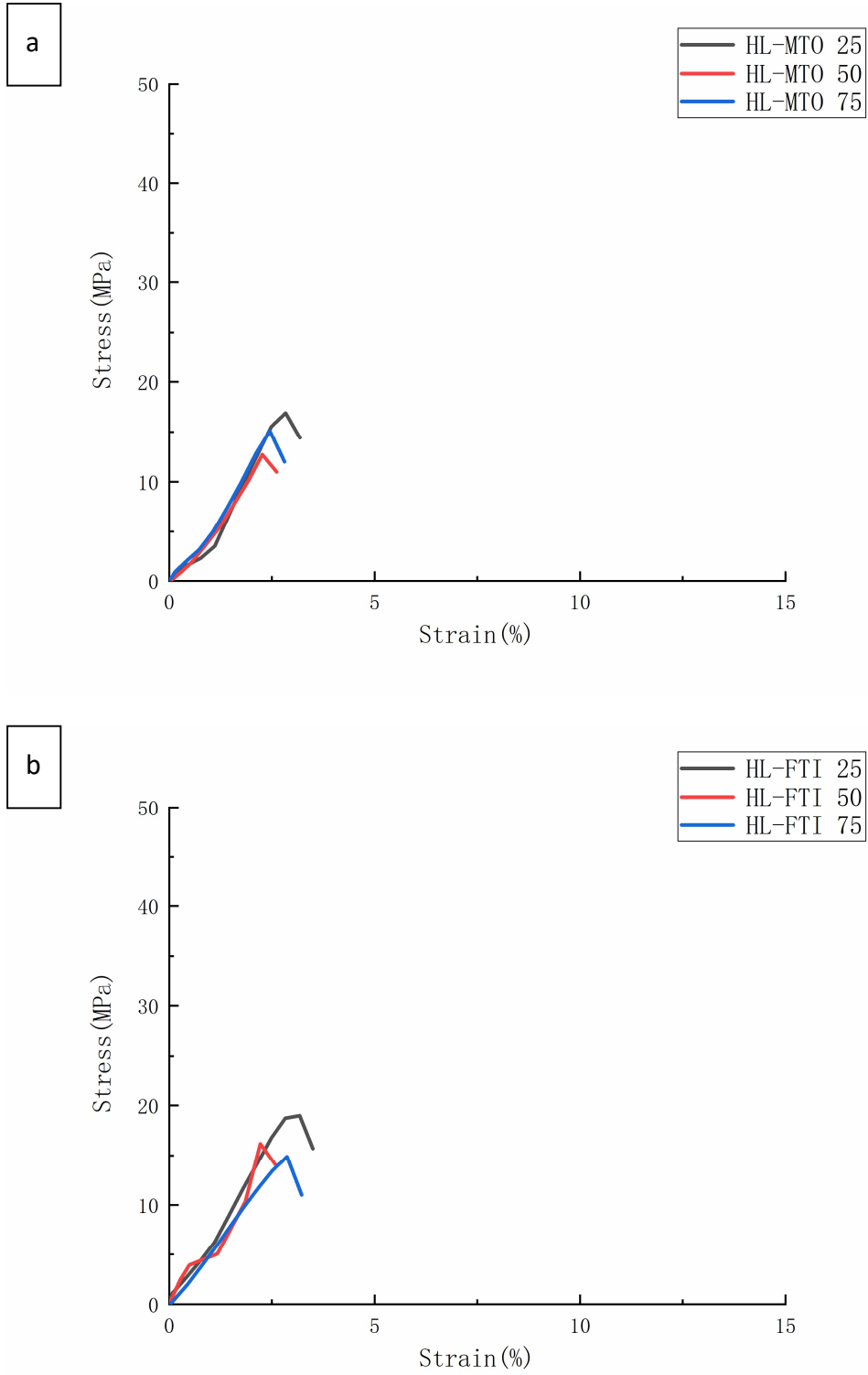
Figure 4-9 Representative stress-strain curves for tensile test amongst half-length series with

T (outset and inset) joint configuration: (a) male ones; (b) female ones.

These findings are in line with the previous sections that a female joint configuration will offer a higher mechanical performance if compared to the male joint configuration. In addition, as can be seen in Figure 4-9 (a) and (b) that the majority of specimens with T joint types will show a greater tensile performance compared to the ones with cube type except the comparison between HL-FCI 25 and HL-FTI 25. This situation is mainly attributed to the more contact area between preforms and overmolded material, which enhances the resistance to tensile loading by increasing the quantity of interlock in the interface zone.

Half-Thickness Series Specimens:

A first glance at the results of HT-series specimens without joint configurations reveal that a 50 % infill density in FDM preforms results in a great tensile performance if compared to the specimens with 25 % and 75 % infill density. Thus, a deep discussion in HT-series specimens with 50% infill density has been identified as follows:

Table 4-5 compares the mechanical properties of all HYM samples during the tensile test, in which FT 50 showed the highest value of average tensile strength, 48 MPa, almost equal to that for IM batch in Table 4-3, while the average tensile strength of FC 50 was slightly lower than 48 MPa, with a value of 47.42 MPa. MT 50 showed the worst average tensile strength of all HYM samples with a value of 42.62 MPa but was remarkably better than all FDM samples. In relation to the value of Young's Modulus, MT 50 carried the highest amongst HYM samples (854.54 MPa) while the worst belonged to HT-NJ 75 (690.35 MPa).

What can be found firstly in Figure 4-10 related to the specimens without joint configurations is that these samples show their significantly higher tensile stress if compared with all batches of FDM samples in Figure 4-3. Even the batch with the greatest tensile performance amongst FDM samples (FDM 75) still shows a worse tensile stress than the worst batch amongst the NJ group (37.91 MPa<45.09 MPa), showing HYM samples have superior tensile properties compared to FDM samples. In

addition, Figure 4-10 shows a different condition in relation to the infill density that NJ which is fabricated from 50 % infill density inserts shows the greatest tensile performance compared with NJ 25 (25 % infill) and NJ 75 (75 % infill). This result agrees with the performances shown in Table 4-5 and can be attributed to the outstanding ductility for ABS material, offering the strongest fusion bonding upon 50 %-infill density insert.
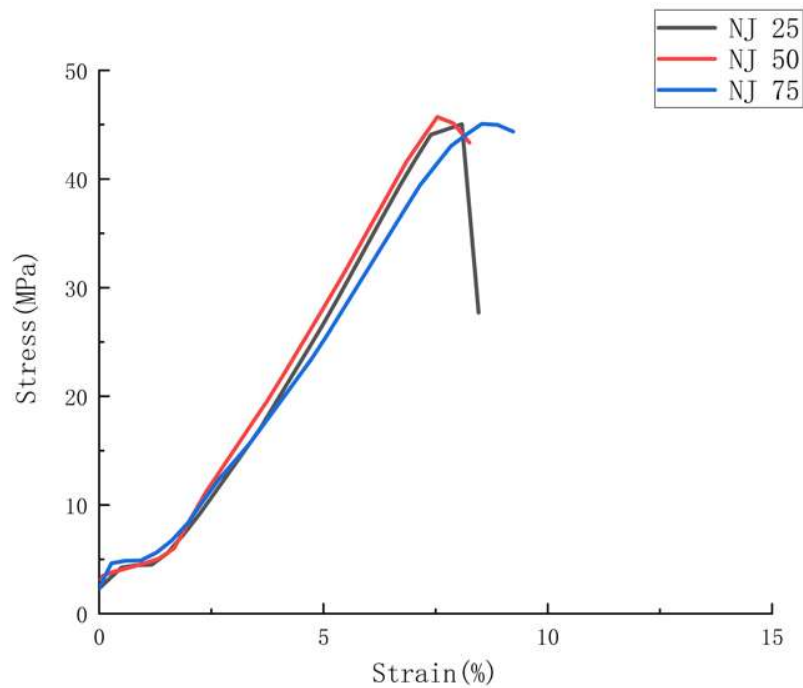
Figure 4-10 Representative stress-strain curves for tensile test amongst HT-NJ batches.

Figure 4-11 shows representative stress-strain curves for the HYM samples with joint configurations, through which the impact of joint configurations on the HYM samples' mechanical performances can be compared. The joint configurations' effort in mechanical performance can be mainly categorized into two aspects, the type (male and female) and geometry (cube and T shapes). It can be found in Figure 4-11 and Table 4-5 that the female joint configuration resulted in a greater tensile stress than the male joint configuration (47.42 MPa>46.30 MPa for cube ones and 48 MPa>42.62 MPa for T ones).
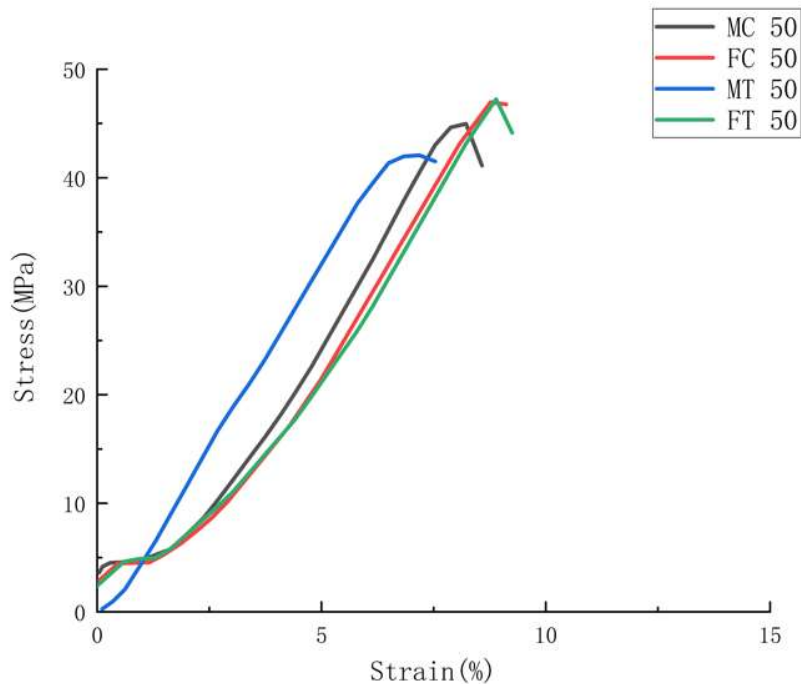
Figure 4-11 Representative stress-strain curves for tensile test amongst all 50% HT-series HYM samples with joint configurations.

In relation to the brittle and ductile performance during fracture, FC 50 and FT 50 had more ductile performances (8-10 % strain) while MC 50 and FC 50 displayed more brittle behaviors (6-8 % strain). In addition, an interesting phenomenon can be found that the standard deviations for the female joints on the maximum stress value and Young's Modulus were lower than those for the male joints, respectively, which indicates a greater reliability on female joints than the male joint (Zhai et al., 2021). Simultaneously, the result of ANOVA has been shown in Table 4-6, where the degree of freedom, sum of squares, mean square, f-ratio and p-value are included. The p-values of the ultimate tensile stress and Young's Modulus are less than 0.05, indicating significant impacts of joint configuration on tensile stress and Young's Modulus. The phenomena can be attributed to two main factors and have been discussed as follows: 1. female joint configuration (cube), which had been shown in Figure 4-12 (b) would offer stronger mechanical interlock based on the overmolding processing than the male cube shown in Figure 4-12 (a); 2. a higher volume of molten polymer was able to enter the female joints compared to the male ones. This illustrates that a greater

92

emphasis on tailored characteristic is required for an increase in the tensile strength of HYM specimens and may be used in certain elements, such as assembly-based toys or parts such as LEGO brand, gears in manufacturing industry and cup holder tray in coffee machine.

Table 4-6 ANOVA of the model for Ultimate Tensile Stress (σ)and Young's Modulus (E). Degree of Freedom for DF, Sum of Squares for SS, Mean Square for MS, F-Ratio for F and P-Value for P.

Source	DF	σ				E			
		SS	MS	F	P	SS	MS	F	P
Model	4	176.91	44.23	24.66	0	121323	30331	20.01	0
Residual	45	80.7	1.793			68221	1516		
Total	49	257.61				189544			
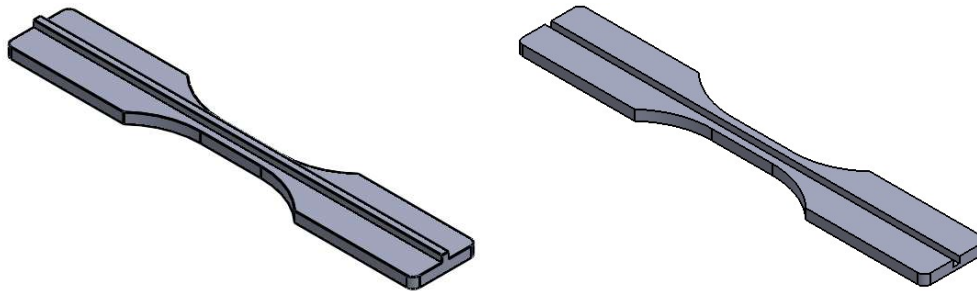
Figure 4-12 Schematic graph of cube inserts applied in overmolding processing: (a) male cube; (b) female cube.

Figure 4-13 shows SEM images of the fractured tensile interfaces of the typical HYM specimens. The comparison of fractured morphologies displays that both the infill density of FDM inserts and the joint configurations employed in the HM technique affect the tensile performance. It can be found in Figure 4-13 (a-c) that several cracks could be found during the tensile loading, with a greater behavior in NJ 50 if compared to NJ 25 and NJ 75, especially in the fractured interlayer area, which proved the greatest mechanical performance of the HYM samples with 50% infill density inserts. During the tensile test, the first few cracks were generated in the overmolded polymer, which possessed a greater hardness than the FDM area to inhibit the fracture. However, more cracks were created to keep the tensile loading process. More tensile loading would be required and result in more new cracks and finally the tensile stress increased (Zhai et al., 2021). Besides, the damage in the MC 50 and FC

50 showed more brittle morphologies due to the cube-shape joint configuration than the MT 50 and FT 50, which agrees with the results obtained in the tensile test. Failures for these HYM samples were in relation to the trans-interlayer tensile failure by the fracture of polymer fusion bonds themselves, leading to the ductile morphologies and greater stiffness (Tábi et al., 2021). The failure could be illustrated into the following three steps: 1. Primary cracks happened in the FDM-fabricated area; 2. The primary crack was inhibited by the IM-fabricated area; 3. Secondary crack was generated and then inhibited by the IM area also, but the tear step was allowed. The phenomena of Young's Modulus and strain deliver a solution in some certain bespoke appliances requiring higher stiffness in several fields, such as frames of bicycles, chairs, television support and even some specific assembled parts in aircraft.
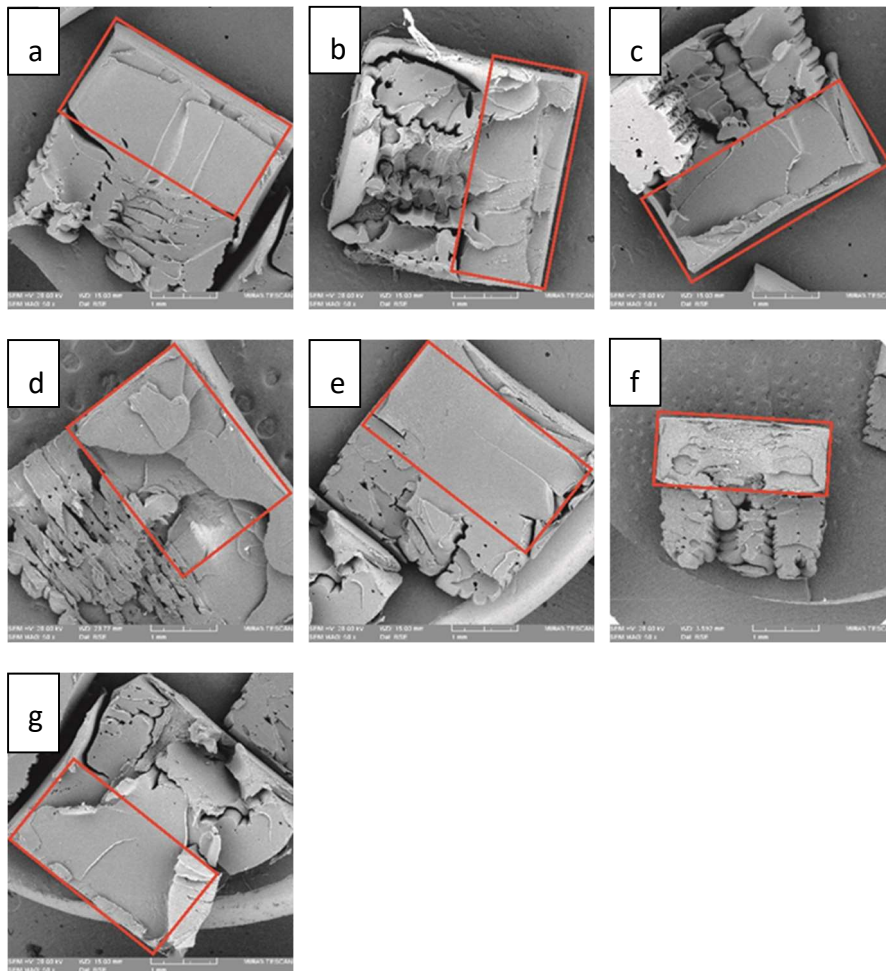
Figure 4-13 SEM images showing the fracture sections of specimens, in which the IM part is marked in red square: (a) NJ25; (b) NJ50; (c) NJ75; (d) MC50; (e) FC50; (f) MT50; (g) FT50.

Comparison of Tensile Performance between HL and HT series:

What can be interpreted from the results shown in Table 4-4 and Table 4-5 on overmolded samples is that the half-length series specimens had worse mechanical properties when compared with half-thickness series ones. A comparison between the stress-strain curves for HL-NJ and HT-NJ specimens reveals that the HT series has much higher tensile strength than the HL series, almost four times. As for the values of strain, it obviously depicts an evident phenomenon that the value of strain for HL-NJ series were nearly half if compared with the HT-NJ series.

This phenomenon can be explained from the varied tensile failure for both series, in which the failures for half-thickness series batches were in relation to trans-layer tensile failure by the fracture of polymer fusion bonds themselves, leading to ductile morphologies and better stiffness (shown in Figure 4-13). In contrast, the damage in half-length series batches showed brittle morphologies due to the interlayer bonding failure (shown in Figure 4-14), which is similar to the result in upright orientation samples from Chacón's study (2017).
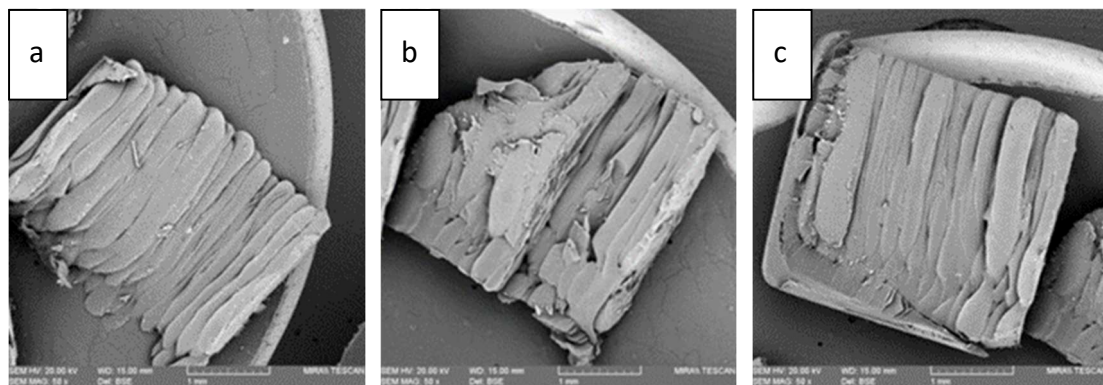
Figure 4-14 SEM images showing the fracture sections of specimens, in which a) HL-NJ 25; b) HL-NJ 50; c) HL-NJ 75.

4.3 Summary

Through comparative tensile tests on FDM, IM, and HYM samples, the effect of AM-IM hybrid manufacturing on the mechanical properties of ABS samples has been investigated in this work. Consideration was given to the infill density of inserts (25 percent, 50 percent, and 75 percent) and joint configurations, both of which were

employed in HM processing (4 types of joint configurations along with one series have no joint configurations).

The study provides evidence for the following claims:

(1) Mechanical properties of IM samples surpassed those of other samples due to the nature of the IM process, which results in strong material compaction and enhanced internal morphology.

(2) The infill density of FDM inserts had a significant impact in determining the mechanical performance of HYM samples, with the good flexibility of ABS material providing superior mechanical performance for HYM samples with a medium infill density (50 percent for half-thickness series samples).

(3) The female T-shape joint showed the strongest interlayer bonding and the biggest interlayer surface compared to the other joint types, resulting in the greatest tensile performance compared to other HYM samples and FDM specimens. This makes HM particularly attractive for employment in manufacturing products with bespoken features and great mechanical characteristics, such as some butterfly models fabricated on the fridge handler, hence addressing one of the drawbacks of FDM specimens' low mechanical properties if compared to the IM parts.

(4) HYM samples showed anisotropic mechanical properties between half-length series and half-thickness series samples. This is related to the direction of tensile loading versus the polymer bonding that is in the parallel direction for half-thickness series but in a perpendicular direction for half-length series.

(5) Manufacturing cost is a big topic in the market: HYM samples demonstrated their ability to achieve cost reduction as well as execute a facile, personalized feature, which is present in all HYM samples. A reduction in manufacturing time can be found in specimen fabrications using HM technique if compared to the FDM technique. This expands the availability in manufacturing of goods with customized characteristics and high quality at a reasonable cost if compared to the high expense in mold design and manufacture in IM technique.

Chapter 5: Mass Customization of Polylactic Acid (PLA) Parts via a

Hybrid Manufacturing Process

5.1 Introduction

The previous chapter introduced the employment of Acrylonitrile Butadiene Styrene (ABS) material in this overmolding technique to figure out the properties of finished specimens, such as the dimension and tensile tests. In this chapter, another common material utilized in polymer industry, Polylactic Acid (PLA), is employed here. Three types of specimens fabricated using the same formulations, including fused deposition modelling (FDM), injection molding (IM), and HM, are compared here. The main objective of this phase in this study is to determine the properties of PLA specimens in the dimension and mechanical performances and compare them based on our previous study in ABS specimens.

This phase of study is an extended stage of previous chapter, demonstrating the impact of varied material employed in this technique. Three parameters were varied and were repeated in this study to determine the effect of HM in the finished specimens. These parameters included infill density of FDM preforms (25 %, 50 %, and 75 %), joint configurations (10 types in half-length series and 5 types in half-thickness series), both of which have been found their significant effects in the finished specimens.

This study lays the groundwork for using HM to produce bespoke and mechanically improved parts over FDM alone and exploits the impact of varied material utilized in the overmolding technique in the finished specimens.

5.2 Results and Discussion

The Mass Customization (MC) philosophy separates sophisticated manufacturing processes into several distinct stages to offer customers bespoken products at reasonable costs (Alford et al., 2000; Deradjat & Minshall, 2017; Fuenmayor, Donnell, et al., 2019). The HYM batches were produced in line with the MC theory using FDM-IM hybrid manufacturing technique which combines the customized manufacturing from FDM and mass manufacturing ability from IM. In our manufacturing technique,

batches of FDM inserts with varied joint configurations were firstly acquired in the first stage, these inserts were then delivered to the injection molding machine to commence the overmolding process, where the final HM samples could be created shortly.

Manufacturing cost has always been a hotspot in modern industry (Chacón et al., 2017). In this study, one tensile bar needed 6 minutes to fabricate on average, which mainly de-pended on the infill density, whereas the IM technique took 1.5 minutes to produce two specimens, this made one FDM batch run 72 minutes to finish fabrication but 9 minutes for the IM batch for a batch consisting of 12 samples. However, the HM technique applied in this study would save cost since it took 36 minutes on producing inserts plus 9 minutes on overmolding process, with a total of 45 minutes for each batch. Moreover, even two inserts in different batches, could be pushed into the cavity to proceed the overmolding technique at the meantime and this would be finished under 2 minutes for each fabrication.

Figure 5-1 shows all batches of HYM samples, where the red part is fabricated using FDM and the blue part is finished through IM. Table 5-1 lists all specimens fabricated in this study and these were labelled based on their individual manufacturing routes and parameters.
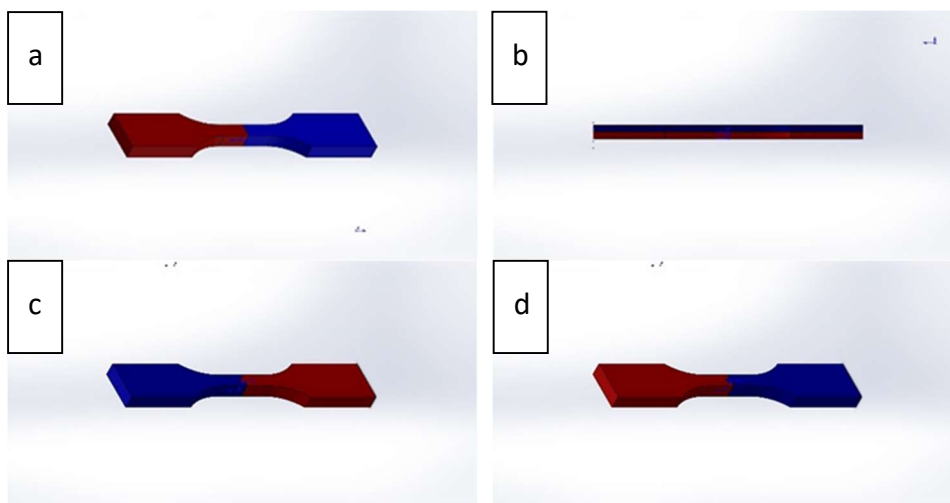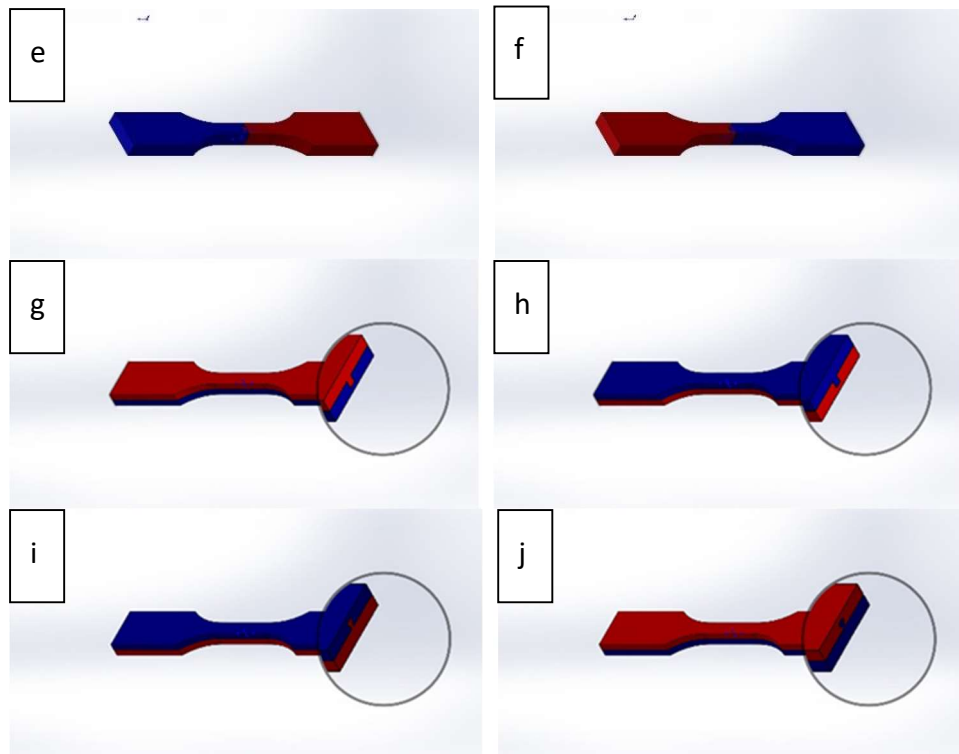
Figure 5-1 CAD diagraphs for all finished specimens, in which red parts were fabricated using FDM and blue ones were overmolded: a) half-length without joint; b) half-thickness without joint; c) half-length with male cube joint; d) half-length with female cube joint; e) half-length with male T joint; f) half-length with female T joint; g) half-thickness with male cube joint; h) half-thickness with female cube joint; i) half-thickness with male T joint; j) half-thickness with female T joint.

Table 5-1 The range of fabricated specimens.

Batch Name	Type of Samples/Inserts	Infill Density (%)
FDM 25/50/75	FDM Sample	25, 50, 75
IM	IM Sample	100
HL/HT-NJ 25/50/75	Half of Length/Thickness (No Joint Configuration)	25, 50, 75
HL/HT- MC 25/50/75	Half of Length/Thickness Male Cube Joint	25, 50, 75
HL/HT- FC 25/50/75	Half of Length/Thickness Female Cube Joint	25, 50, 75
HL/HT- MT 25/50/75	Half of Length/Thickness Male T Joint	25, 50, 75
HL/HT- FT 25/50/75	Half of Length/Thickness Female T Joint	25, 50, 75
HL-MCI 25/50/75	Half of Length Male Cube Joint, Inset	25, 50, 75
HL-FCO 25/50/75	Half of Length Female Cube Joint, Outset	25, 50, 75
HL-MTI 25/50/75	Half of Length Male T Joint, Inset	25, 50, 75
HL-FTO 25/50/75	Half of Length Female T Joint, Outset	25, 50, 75

5.2.1 Macrostructure Observation for all fabricated samples

Some FDM preforms in HL-series, which were employed in the overmolding stage, were displayed in Figure 5-2, emphasizing the customization features brought from high design flexibility in FDM technique.
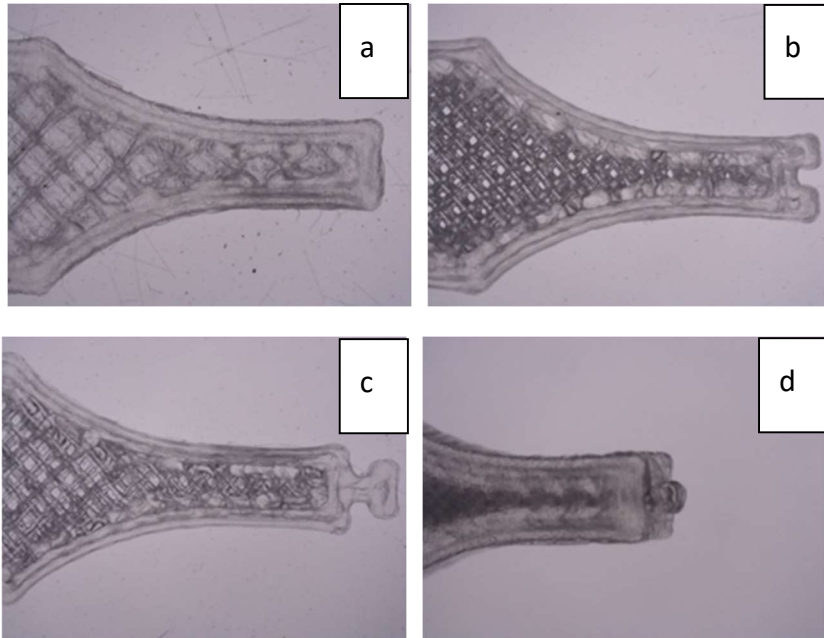
Figure 5-2 Typical FDM inserts employed in overmolding stage, in which (a) HL-NJ 25; (b) HL-FC 50; (c) HL-MT 50; (d) HL-MCO 75.

Table 5-2 shows the results of physical observation for all fabricated samples, which are subjected to the ASTM guidelines. In addition, the lower standard deviations of dimensions in HYM samples indicate FDM's poor dimension control can be improved via IM in overmolding here.

Table 5-2 Dimensions of all fabricated samples.

Parameter	IM specimens	FDM specimens	HYM specimens
Fillet Radius R(mm)	12.7	12.7	12.7
Thickness (mm)	3.2±0.1	3.2±0.2	3.2±0.1
Total length (mm)	64±0.1	64±0.3	64±0.2
Width of joint for injection and FDM (mm)	——	——	3.3±0.2
Width at two ends (mm)	10±0.2	10±0.2	10±0.2

5.2.2 Tensile Performances for all fabricated specimens

To date, several prior studies concluded that FDM-fabricated samples would exhibit worse mechanical performance compared to injection-molded samples, particularly in the tensile test (Boros et al., 2019; Dawoud et al., 2016; Lay et al., 2019). In this context, the tensile performances of PLA material produced by FDM, IM and FDM-IM hybrid manufacturing were compared to emphasize the variations due to the technique applied. The comparison is vital for realizing the full potential of HYM products for improvement of FDM and IM goods in some applications.

The test results, including their average values and standard deviations, of the maximum tensile stress (σ) and Young's Modulus (E) for FDM and IM samples are tabulated in Table 5-3, for HL-series samples in Table 5-4 and for HT-series specimens in Table 5-5.

Table 5-3 Average tensile test results (tensile stress and Young's Modulus) and their standard deviations for IM and FDM batches.

Batch Reference	Tensile Stress, σ(MPa)	Young's Modulus, E (MPa)
IM	68.95±1.75	1130.07±18.93
FDM 25	26.21±1.03	612.32±31.80
FDM 50	25.43±2.15	639.33±30.58
FDM 75	38.75±1.92	814.30±39.52

Table 5-4 Average tensile test results (tensile stress and Young's Modulus) and their standard deviations for HL-series specimens.

Batch Name	σ(MPa)	E(MPa)	Batch Name	σ(MPa)	E(MPa)	Batch Name	σ(MPa)	E(MPa)
HL-NJ 25	12.99±5.78	640.88±±50.43	HL-NJ 50	18.41±2.96	720.85±54.68	HL-NJ 75	19.09±7.14	761.48±71.45
HL-MC 25	16.23±5.85	691.29±71.43	HL-MC 50	17.91±3.16	698.54±36.86	HL-MC 75	26.00±5.51	771.53±68.29
HL-FC 25	19.58±6.59	686.38±69.39	HL-FC 50	22.38±4.66	768.16±27.55	HL-FC 75	26.51±2.90	790.26±75.81
HL-MT 25	16.42±2.65	698.56±32.21	HL-MT 50	27.68±2.82	760.57±58.76	HL-MT75	26.76±1.91	796.83±50.03
HL-FT 25	27.97±3.05	701.45±10.15	HL-FT 50	28.94±1.37	771.23±18.22	HL-FT 75	30.11±3.05	837.98±22.20
HL-MCO 25	20.59±4.82	726.07±120.93	HL-MCO 50	20.93±3.89	643.42±63.54	HL-MCO 75	24.48±6.21	739.32±80.75
HL-FCI 25	20.25±5.72	703.08±170.99	HL-FCI 50	21.97±4.89	651.78±121.74	HL-FCI 75	28.24±5.06	814.5±50.62
HL-MTO 25	15.16±4.32	679.98±109.24	HL-MTO 50	16.00±4.03	644.44±82.36	HL-MTO 75	17.83±6.74	720.8±65.17
HL-FTI 25	21.36±3.73	736.65±159.81	HL-FTI 50	21.39±3.51	759.70±47.65	HL-FTI 75	26.96±4.44	820±132.81

Table 5-5 Average tensile test results (tensile stress and Young's Modulus) and their standard deviations for HT-series specimens.

Batch Name	σ(MPa)	E(MPa)	Batch Name	σ(MPa)	E(MPa)	Batch Name	σ(MPa)	E(MPa)
HT-NJ 25	53.83±2.96	1025.69±45.29	HT-NJ 50	55.26±2.98	984.15±31.96	HT-NJ 75	59.92±1.51	1014.46±36.88
HT-MC 25	62.41±1.94	1027.71±34.66	HT-MC 50	57.53±5.69	994.69±75.82	HT-MC 75	64.74±3.57	1057.92±57.45
HT-FC 25	66.65±2.27	1113.19±54.86	HT-FC 50	65.85±1.79	1075.36±49.73	HT-FC 75	68.38±1.03	1103.13±33.28
HT-MT 25	49.79±3.06	873.45±99.05	HT-MT 50	56.53±3.34	948.59±48.07	HT-MT 75	59.51±3.07	1031.50±86.71
HT-FT 25	65.67±0.51	1023.32±35.83	HT-FT 50	64.76±1.57	1029.40±50.00	HT-FT 75	64.16±1.53	1100.29±45.77

The results of all batches of samples ranged as tensile strength went from lowest to highest, σ= [12.99,68.95] MPa respectively., Young's Modulus (E) on the other hand range went from 612.32 MPa to 1130.07 MPa (E=[612.32,1130.07] MPa) due to their varied parameter settings, emphasizing the possibility of mechanical performance and customization possibilities for applications where these performances would be required for parts performance. In addition, larger standard deviations for the maximum tensile stress and Young's Moduli can be found in all specimens in HL- series than HT series ones due to the certain manufacturing condition, which agrees with the findings of the effects on tensile performance based on the variations of building orientations and infill angles for FDM manufactured samples in previous studies (Lanzotti et al., 2015; Rodríguez et al., 2003b; Sood et al., 2010; Tymrak et al., 2014). This indicates a higher reliability in industry for HT series compared to the HL ones.

The effects of parameters applied in the HM technique on the tensile performance of PLA samples are determined below:

Tensile Performances of FDM and IM samples:

One IM batch and three batches of FDM samples (IM, FDM 25, FDM 50 and FDM 75) were compared in Table 5-3 and Figure 5-3 Average stress-strain curves for IM and FDM samples. through their tensile performances. Firstly, IM batch displays the greatest mechanical performance amongst these four batches for tested properties (68.95 MPa for maximum tensile stress and 1130.07 MPa for Young's Modulus). As for the FDM samples, the FDM 75 shows the greatest tensile performance in the group (38.75 MPa in maximum stress and 814.3 MPa for Young's Modulus), but still finds its poor performance if compared with the IM one (38.75 MPa<68.95 MPa in tensile stress and 814.3 MPa<1130.07 MPa). It can be found that the IM samples show better tensile performance compared with the FDM ones, which is caused of the good-quality polymer chain entanglement produced in IM processing and higher material density produced in the uniform heating rate, resulting the molecular chains of these polymers aligning in one direction of the nozzle (Lay et al., 2019; Weng et al., 2016).
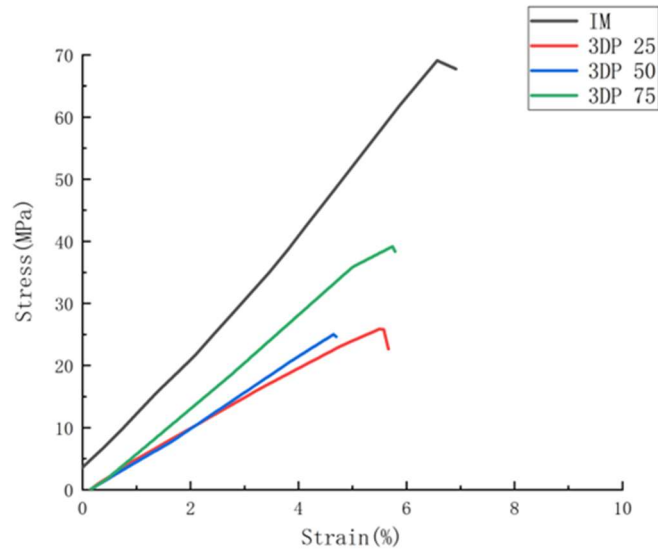
Figure 5-3 Average stress-strain curves for IM and FDM samples.

To figure out the effect of HM on the mechanical performance, two types of HYM samples were taken into account in this study: the half-length samples which were overmolded at a single mid-point along the tensile bar and half-thickness samples which were overmolded along the full length of the FDM inserts. The tensile results for HYM samples displayed in Table 5-4 and Table 5-5 found a gap between half-length series exhibiting tensile stress from 12.99 MPa to 30.11 MPa with half-thickness series ranging from 53.83 MPa to 68.38 MPa.

Effects of infill density on the mechanical performance:

Infill density refers to the quantity of material utilized to fill the interior region of a layer (Qamar Tanveer et al., 2022), which is a critical parameter applied in FDM technique since it affects manufacturing time and mechanical performance (Baich et al., 2015). Hence, infill density is considered in this study to determine its effect in HM samples.

A first glance at the effect of infill density in the FDM samples (Table 5-3 and Figure 5-3), where we found similar performances in FDM 25 and FDM 50 batches (26.21 MPa and 25.43 MPa for maximum tensile stress and 612.32 MPa along with 639.33 MPa for Young's Modulus), but a clear increasing phenomenon can be

observed if infill density sets at 75 % (38.75 MPa for maximum tensile stress and 814.30 MPa for Young's Modulus). This performance transition can be explained by the high-density structure in FDM 75 batch, which provides more material to withstand the loading and thus superior mechanical performance than FDM 25 and FDM 50 batches.

Figure 5-3, Figure 5-4, and Figure 5-5 display the tensile stress as a function of infill density in FDM, HL-NJ and HT-NJ samples, where we found the same trend in HL-NJ and HT-NJ that the higher infill density contributed to an increasing tensile stress.
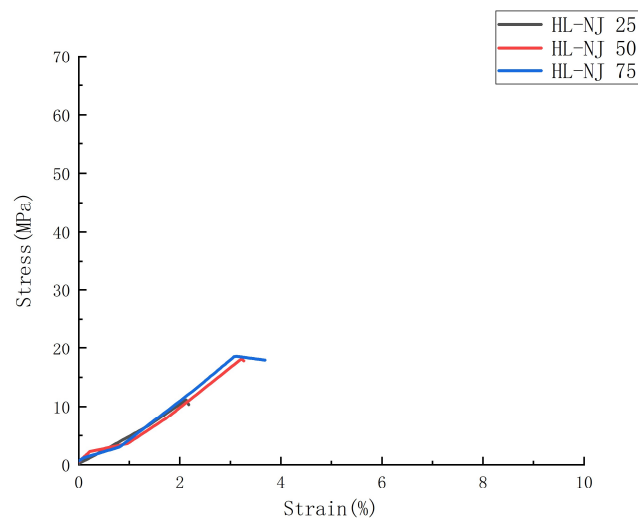
Figure 5-4 Average stress-strain curves for HL-NJ specimens in function of infill density.
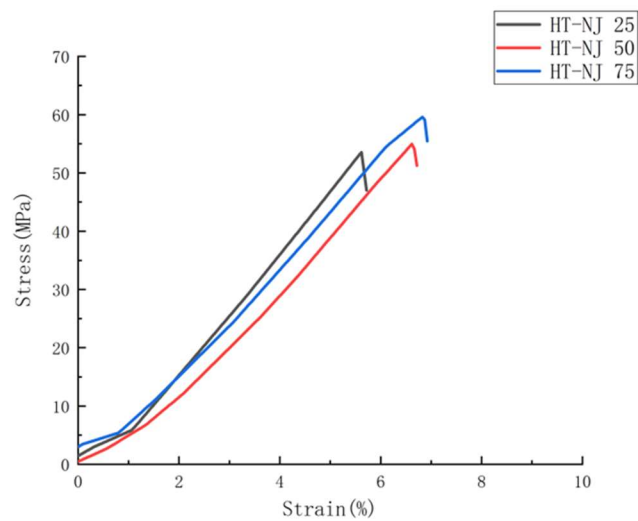
Figure 5-5 Average stress-strain curves for HT-NJ specimens in function of infill density.

Figure 5-6 displays the stress-strain curves for HL-MC and HL-FC series specimens with 25 %, 50 %, and 75 % infill density, respectively. It can be found from Figure 5-6 (a) and (b) that the batch with 75 % infill density are offered the greatest tensile performance (26.00 MPa for maximum tensile strength in HL-MC series and 26.51 MPa for maximum tensile strength in HL-FC series) amongst all. In addition, the performances of maximum tensile strength show increasing tendency in both series if the infill density increases, in which the maximum tensile strength value of HL-MC 25 is 16.23 MPa, and the one for HL-MC 50 is 17.91 MPa. In the case of HL-FC series, the maximum tensile strength value of HL-FC 25 is 19.58 MPa, and the one for HL-FC 50 is 22.38 MPa, which agree with the conditions in HL-NJ series and HT-NJ series.
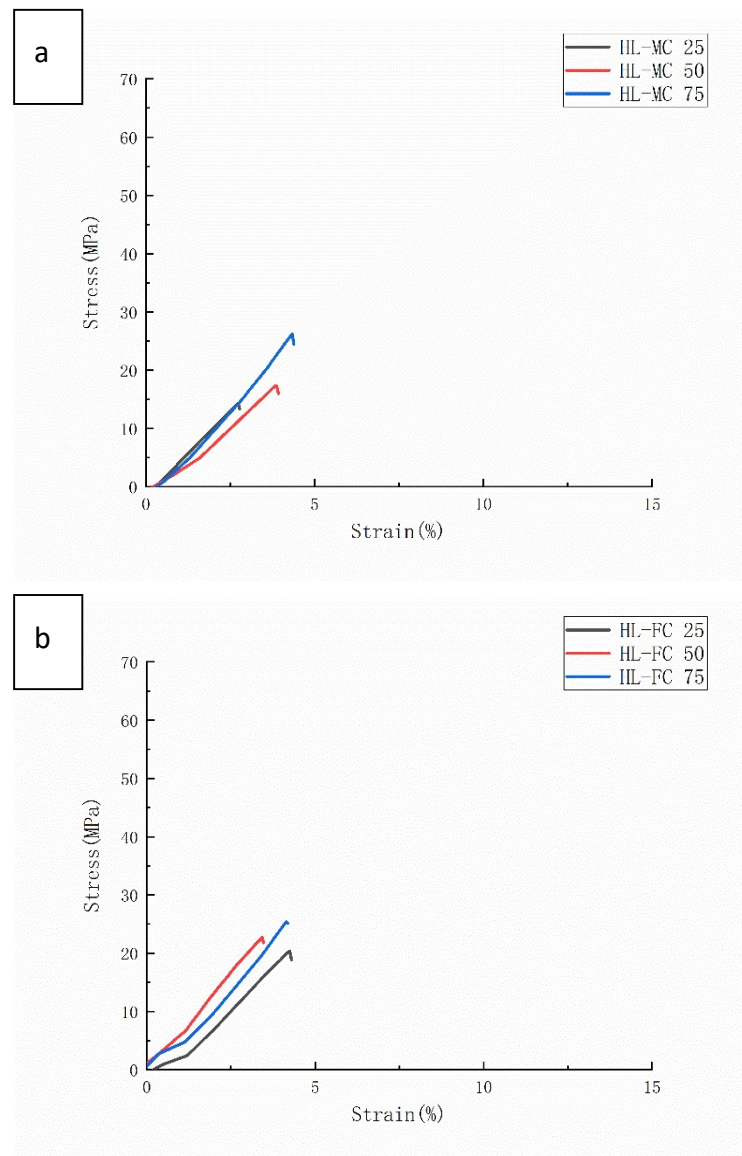
Figure 5-6 Representative stress-strain curves for tensile test amongst half-length series with

cube joint configuration: (a) male ones; (b) female ones.

Regarding to the tensile behaviors for HL-MT and HL-FT series, Figure 5-7 exhibits the stress-strain curves of these specimens, in which HL-MT 50 shows the greatest tensile strength (27.68 MPa) compared to HL-MT 25 (16.42 MPa) and HL-MT 75 (26.76 MPa). Similar to the HL series specimens with cube joint design and the HL-NJ series, the HL-FT series exhibits an increase in individual maximum tensile strengths as the infill density of preforms increases. The highest value of maximum tensile strength can be discovered in HL-FT 75 (30.11 MPa) and following with 28.94 MPa for HL-FT 50 and 27.97 MPa for HL-FT 25. An interesting phenomenon can be determined here is the similar value of HL-MT 50 between HL-MT 75 and those for HL-FT 25 and HL-FT 50.
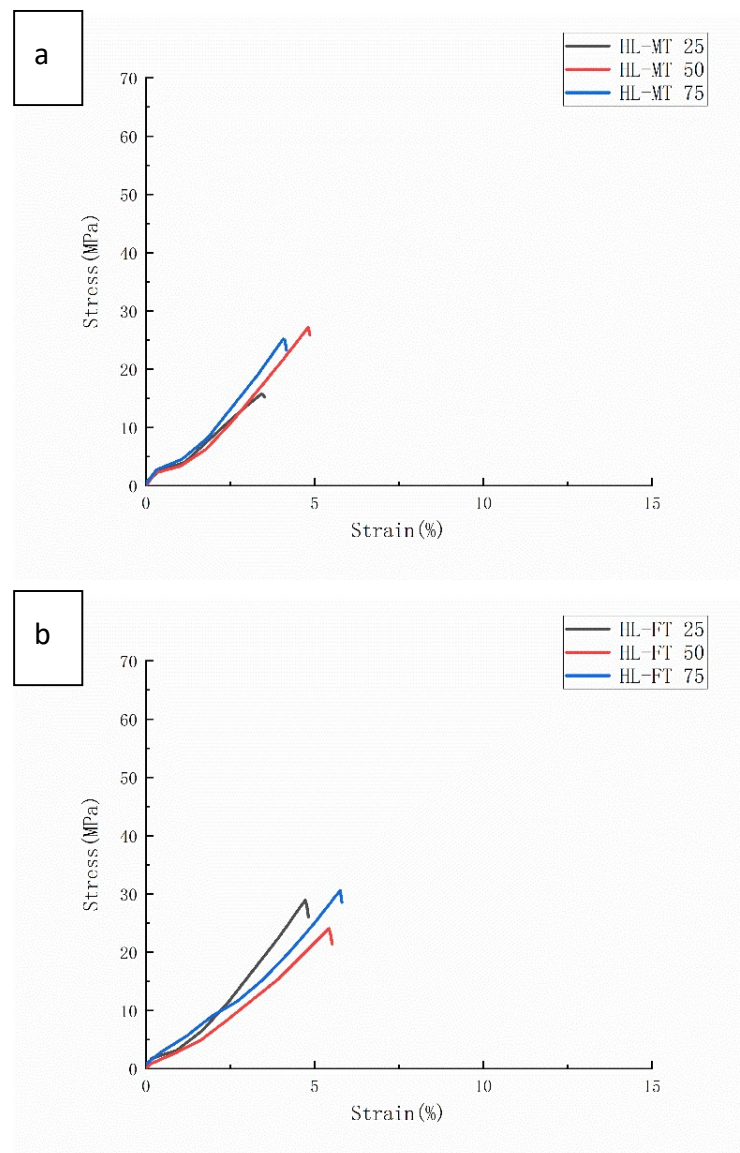
Figure 5-7 Representative stress-strain curves for tensile test amongst half-length series with

T joint configuration: (a) male ones; (b) female ones.

Figure 5-8 displays the stress-strain curves for HL-MCO and HL-FCI series specimens with 25 %, 50 %, and 75 % infill density, respectively. It can be found from Figure 5-8 (a) and (b) that the batch with 75 % infill density are offered the greatest tensile performance (24.48 MPa for maximum tensile strength in HL-MCO series and 28.24 MPa for maximum tensile strength in HL-FCI series) amongst all. Moreover, the performances of maximum tensile strength show increasing tendency in both series if the infill density increases, in which the maximum tensile strength value of HL-MCO 25 is 20.59 MPa, and the one for HL-MCO 50 is 20.93 MPa. In the case of HL-FCI series, the maximum tensile strength value of HL-FCI 25 is 20.25 MPa, and the one for HL-FCI 50 is 21.97 MPa.
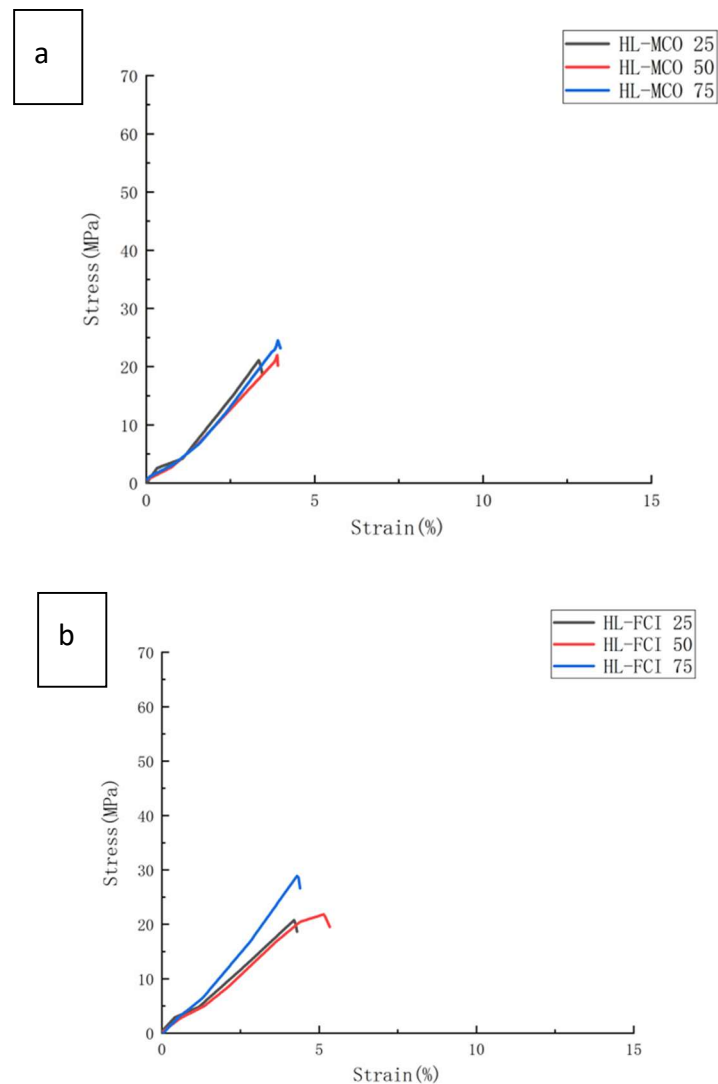
Figure 5-8 Representative stress-strain curves for tensile test amongst half-length series with

cube (outset and inset) joint configuration: (a) male ones; (b) female ones.

As can be found in Figure 5-9 (a) and (b), HL-MTO and HL-FTI series, similar tendency can be determined here that the increase of infill density in FDM preforms results in a higher value in maximum tensile strength. In case of the HL-MTO series, maximum tensile strength values are comparable (15.16 MPa for HL-MTO 25 and 16.00 MPa for HL-MTO 50), with a larger difference between HL-MTO 50 and HL-MTO 75, reaching until 17.83 MPa in HL-MTO 75. Regarding to HL-FTI series, a large gap in tensile strength can be found between the samples with 50 % and 75 %. However, a similar phenomenon shows in samples with 25 % and 50 % (21.36 MPa for HL-FTI 25 and 21.39 MPa for HL-FTI 50).
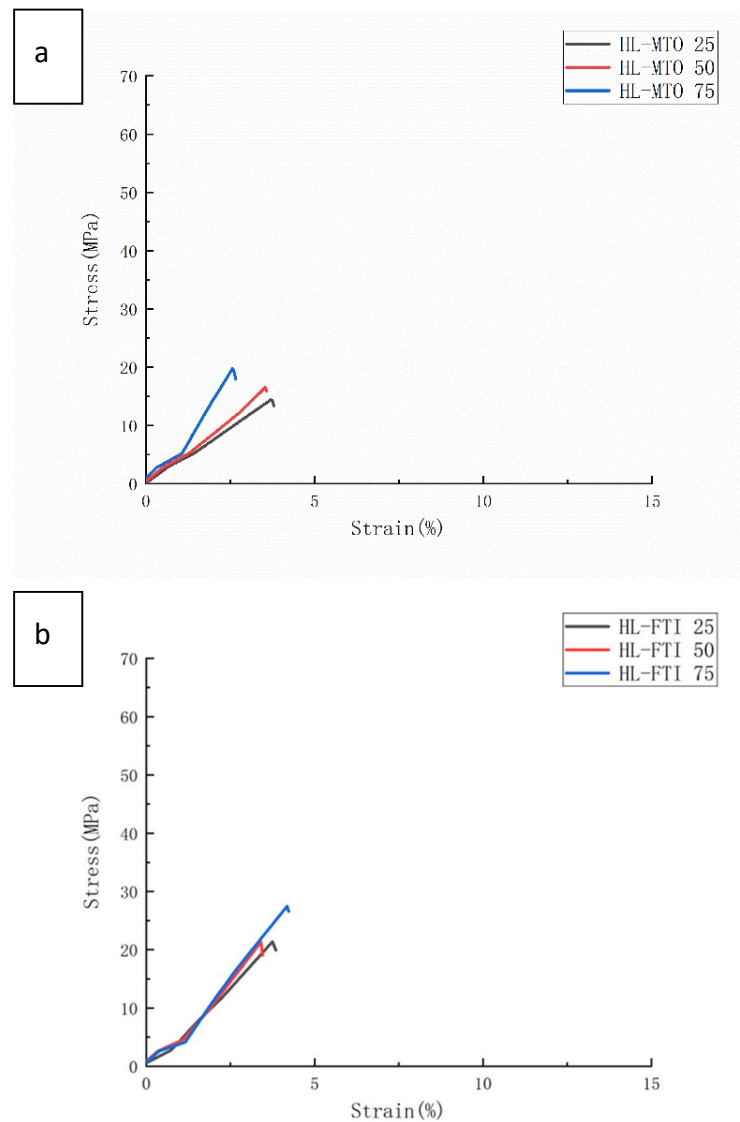
Figure 5-9 Representative stress-strain curves for tensile test amongst half-length series with

T (outset and inset) joint configuration: (a) male ones; (b) female ones.

    Figure 5-10 displays the stress-strain curves for HT-MC and HT-FC series specimens with 25 %, 50 %, and 75 % infill density, respectively. It can be found from Figure 5-10 (a) and (b) that the batch with 75 % infill density are offered the greatest tensile performance (64.74 MPa for maximum tensile strength in HT-MC series and 68.38 MPa for maximum tensile strength in HT-FC series) amongst all. In addition, a higher value in tensile strength can be found in the specimens with 25 % infill density if compared to those with 50 % infill density, in which the maximum tensile strength value of HT-MC 25 is 62.41 MPa, and that for HT-MC 50 is 57.53 MPa. In case of HT-FC series, the maximum tensile strength value of HT-FC 25 is 66.65 MPa, and that for HT-FC 50 is 65.85 MPa.
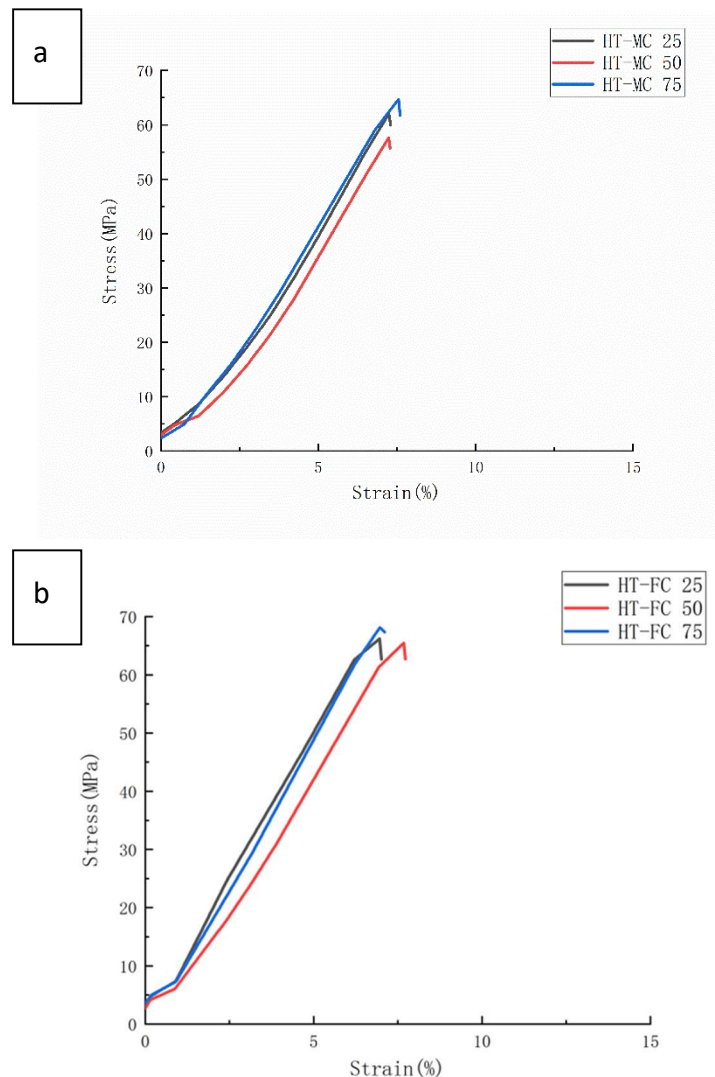
Figure 5-10 Representative stress-strain curves for tensile test amongst half-thickness series

Regarding to the impact of infill density in FDM preform on the tensile performance of finished specimens. The following two conditions are displayed in Figure 5-11 (a) and (b): An increasing infill density of FDM results in a higher value of maximum tensile strength for HT-MT series, where the value of HT-MT 25 is 49.79 MPa and following with 56.53 MPa and 59.51 MPa for HT-MT 50 and HT-MT 75, respectively. However, an opposite phenomenon can be found in the series of HT-FT, in which the value of maximum tensile strength for HT-FT 25 is 65.67 MPa and following with 64.76 MPa and 64.16 MPa for HT-FT 50 and HT-FT 75, respectively.
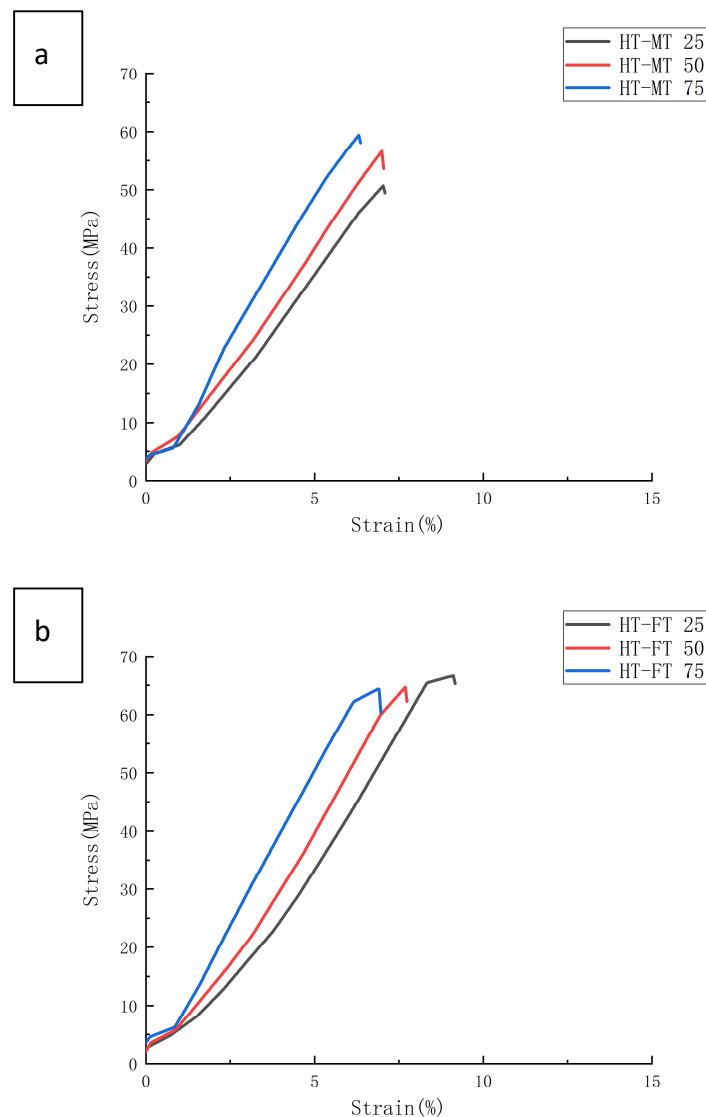
Figure 5-11 Representative stress-strain curves for tensile test amongst half-thickness series with cube joint configuration: (a) male ones; (b) female ones.

In summary, a higher infill density of preform will normally result in greater tensile performances of finished specimens, which agrees with the phenomenon in FDM specimens. The following paragraphs made full explanations in this condition.

For the HYM samples, the FDM inserts with higher infill density were provided better internal structure than those with lower infill. The higher-infill inserts, such as (a-c) and (d-f) shown in Figure 5-12 could produce stronger molecular bonding compared with those inserts with lower infill density, resulting in better joining between FDM inserts and injection-molded polymer. One phenomenon, Figure 5-12(a), which should be thoroughly considered in the HL-NJ 25 manufacturing process is the damage to the FDM insert caused by injection-molded material; this is another indicator of worse mechanical performance in specimens with lower infill density since this insert at this joint configuration and infill density could not withstand the compressive forces of the injection molding volume during manufacturing. Meanwhile, it could be clearly seen from the SEM images in Figure 5-12(a-c) that FDM technique had resulted in void and uneven distribution of molten polymer for the internal structure of FDM area during the 3D printing process, drawing low interlaminar adhesion for FDM parts, which supported that the lower-infill density FDM samples provided worse mechanical properties.
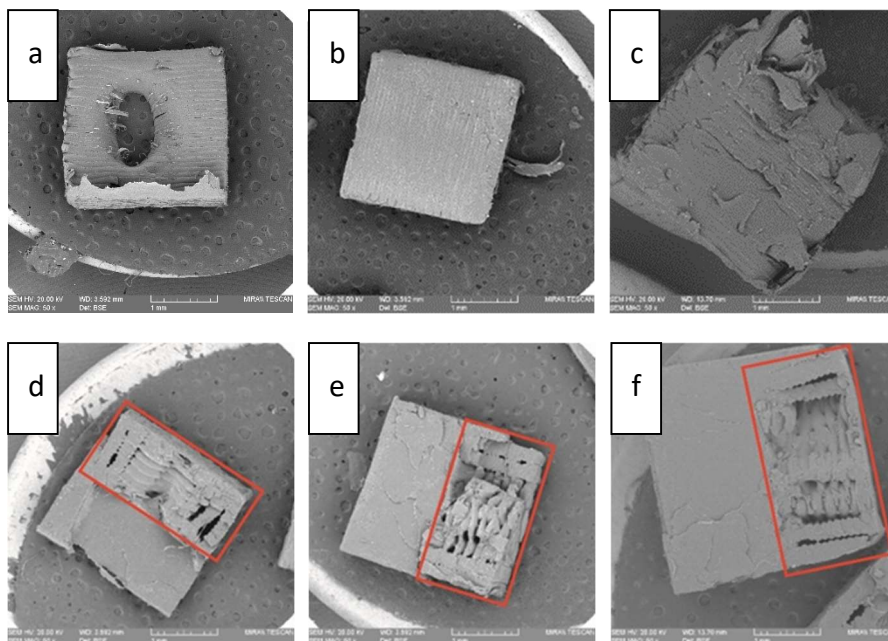
Figure 5-12 SEM observations on the fractured surfaces of (a)HL-NJ 25; (b)HL-NJ 50; (c)HL-

NJ 75; (d)HT-NJ 25; (e)HT-NJ 50; (f)HT-NJ 75, in which the FDM preforms have been contoured using red square for HT series.

In short, infill density shows its crucial impact in tensile performance (stress, stiffness and deformation at fracture). Thus, the high infill density (75 %) exhibits the greatest mechanical performance in the tensile stress for FDM-75, HL-NJ 75 and HT-NJ 75, respectively. In addition, we can figure out a ductile behavior in HL-NJ 75 and HT-NJ 75 if compared with the ones with 25 % and 50 % infill density in Figure 5-12. This indicates a varied mechanical performance of HYM specimen can be resulted from a bespoken characteristics (infill density) in the manufacturing industry.

Effects of interface direction on the mechanical performance:

A large tensile result gap can be found between the HL series samples with the HT series samples, indicating two series of FDM inserts played anisotropic roles in the mechanical performances (maximum tensile stress) of finished HYM samples. For instance, it can be found that the three batches of HT-NJ show their greater mechanical performances in comparison with the HL-NJ 25 to 75, approximately from 76 % (HT-NJ 25 with HL-NJ 25) down to 66.7 % (HT-NJ 50 with HL-NJ 25) for maximum tensile stress, which can be found in the comparison between Table 5-4 and Table 5-5, Figure 5-4 and Figure 5-5. The results of stiffness were in line with the value related to the maximum tensile stress as well, that the Young's Modulus values for half thickness series are larger than the ones for half-length series, ranging from 24.9 % (HT-NJ 75 with HL-NJ 75) to 37.5% (HT-NJ 25 with HL-NJ 25). The same findings can be determined in specimens with cube and T joint configurations in function of two interface directions, which are displayed in Table 5-4 and Table 5-5.

This kind of phenomenon can be explained through the failure modes in the tensile test: inter-layer failure and trans-layer failure, which agreed with some previous pieces of literature related to the building orientations for FDM samples (Casavola et al., 2016; Chacón et al., 2017; Domingo-Espin et al., 2015; Lanzotti et al., 2015; Tymrak et al., 2014). For the half-length series samples, the tensile load was loaded perpendicular to the interface, leading to an inter-layer failure. In these cases,

interfaces between the inserts and overmolded parts withstood most tensile loadings, leading to the low strain values in Figure 5-4 and brittle behaviors in Figure 5-12(a-c), with a schematic graph in Figure 5-13(a). However, there showed an opposite reaction in HT-NJ series, the interface directions were parallel to the tensile loading for these samples, resulting in a trans-layer failure (Figure 5-13(b)). Figure 5-12(d-f) found several breakages since the materials were applied to withstand the tensile loading. Meanwhile, ductile behaviors were found in HT-NJ series since some greater strain values were exhibited in Figure 5-5 for these specimens (5 %-7 %) than the HL-NJ ones (2 %-3.5 %) which shown in Figure 5-4. It can be expected that the HT-NJ series will display a poor tensile performance if these samples were pulled in manufacturing direction (Chacón et al., 2017). Finally, Table 5-4 found larger standard deviations in HL-NJ 25, 50 and 75 than HT-NJ 25, 50 and 75 (Table 5-5), which indicate a greater function of flexibility in half-thickness series samples (Zhai et al., 2021).
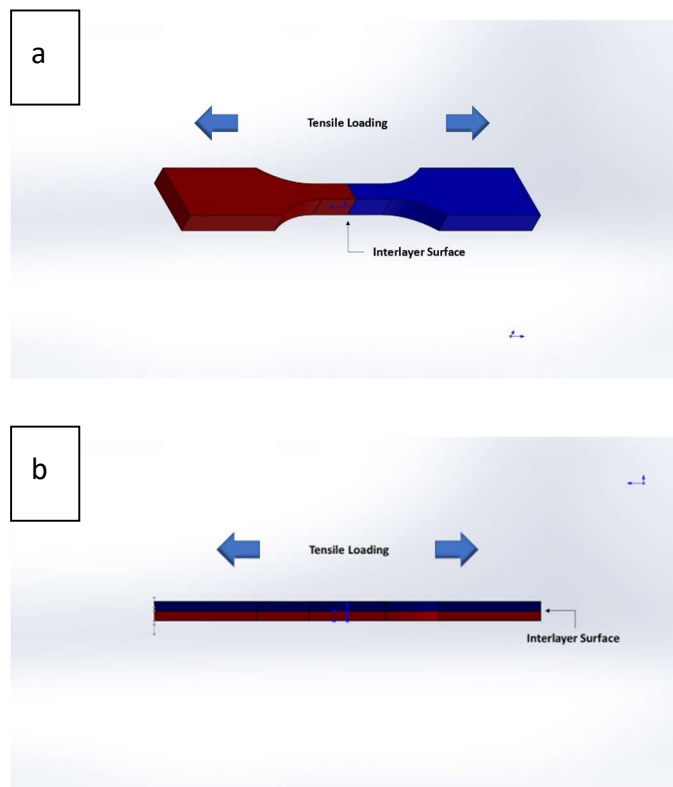
Figure 5-13 Schematic graph of tensile loading for a) HL-NJ series and b) HT-NJ series.

These results underscored that the interface direction had a significant role in affecting tensile performance for HYM samples and this triggered to a superior tensile

performance in half-thickness series samples. However, a half-length series sample can be more popular in market due to the direct availability of customer-tailored features, even if its mechanical performance is worse to that of half-thickness series.

Effects of joint configuration on the mechanical performance:

According to Figure 5-10, Figure 5-11, Figure 5-14, and Table 5-5, the maximum average tensile stress values for 75 % infill density HT series samples with joint configuration (MC, FC, MT and FT) can reach to 68.38 MPa (FC), which is nearly equal with that for injection molded batch (68.95 MPa). When compared to all batches of HT-NJ series, MT 75, the batch with the lowest tensile stress in HT series having joint configurations, nevertheless exhibits an exceptional stress gap, indicating a significant impact of joint configuration on tensile performance. The stress-strain curves shown in Figure 5-10 and Figure 5-11 revealed that FC 75 and FT 75 had a greater tensile stress than MC 75 and MT 75. Additionally, in the tensile test, the fracture began when the tensile loading was applied but was prevented by the overmolded form, which had superior mechanical properties to the FDM preforms, as shown in Figure 5-15. Later, the on-going pull was affected due to the formations of new cracks, aiming to surmount the restriction from the overmolded construction. Additional cracks were then generated by increasing the tensile tension. Finally, the tear steps were produced by repeating the preceding processes.
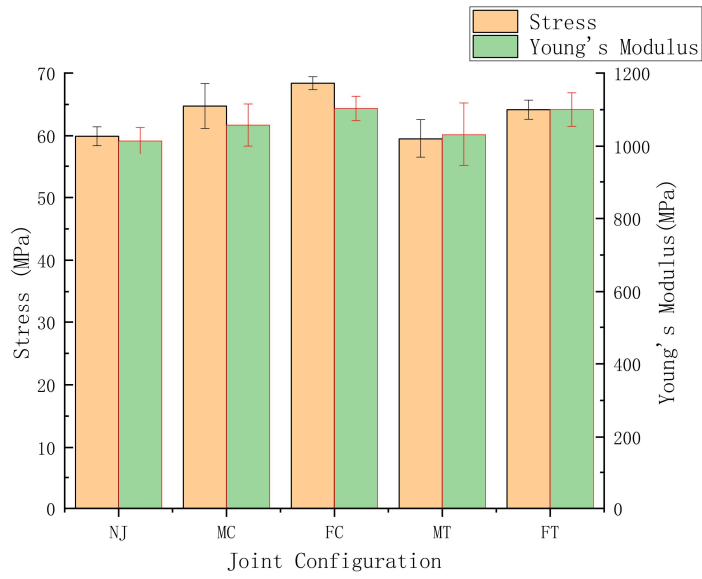
Figure 5-14 Graphical comparison of average stress value and Young's Modulus for the HT series samples (75 % infill density) as a function of joint configuration.
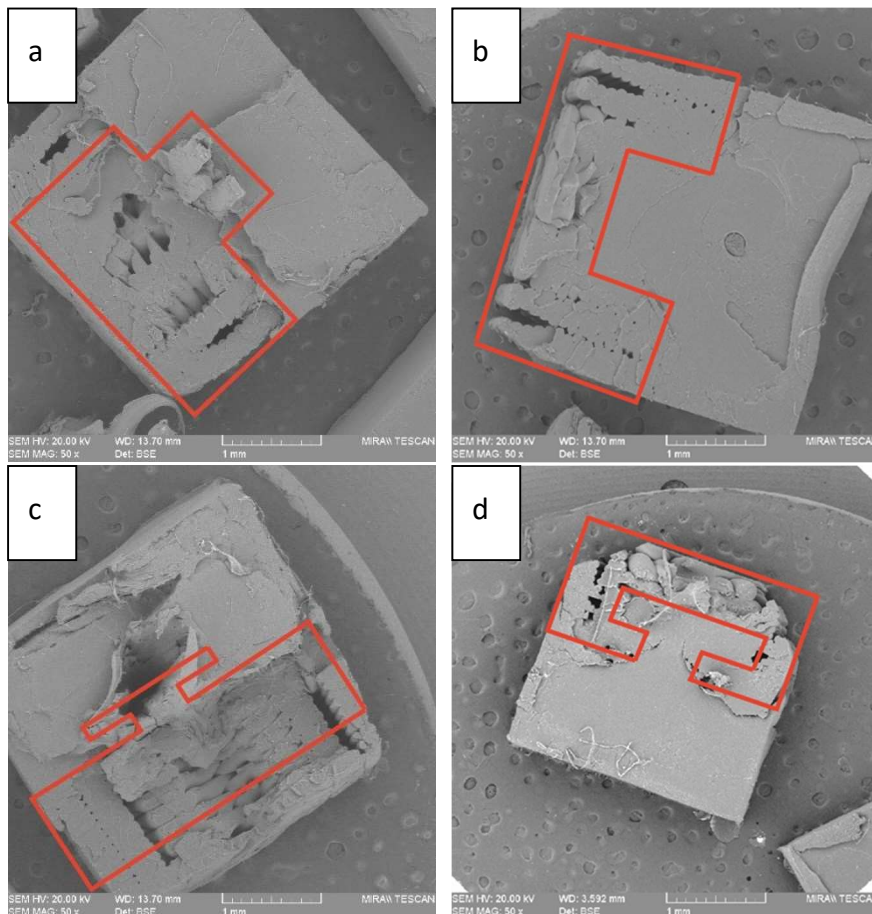
Figure 5-15 SEM observations on the fractured surfaces of (a)HT-MC 75; (b)HT-FC 75; (c)HT-MT 75 and (d)HT-FT 75, in which the FDM preforms have been indicated in red.

In case of the conditions in half-length series samples, the following statements can be determined from the results shown in Figure 5-4, Figure 5-6, Figure 5-7, Figure 5-8, Figure 5-9, and Table 5-4: 1. female joint configuration, which had been shown in Figure 5-16 (b) and (d) would offer stronger mechanical interlock based on the overmolding processing than the male cube shown in Figure 5-16(a) and (c); 2. T joint configuration would result in a worse fusion bond from the overmolding stage due to the greater quantity of pores and therefore the stress concentration would occur in the period of tensile loading; 3. more contact areas for overmolding stage can be found for the HL-MC, HL-FC, HL-MT, and HL-FT series if compared to the HL-MCO, HL-FCI, HL-MTO, and HL-FTI series, resulting in larger area to withstand the tensile loading and thus a greater tensile performance can be attained.
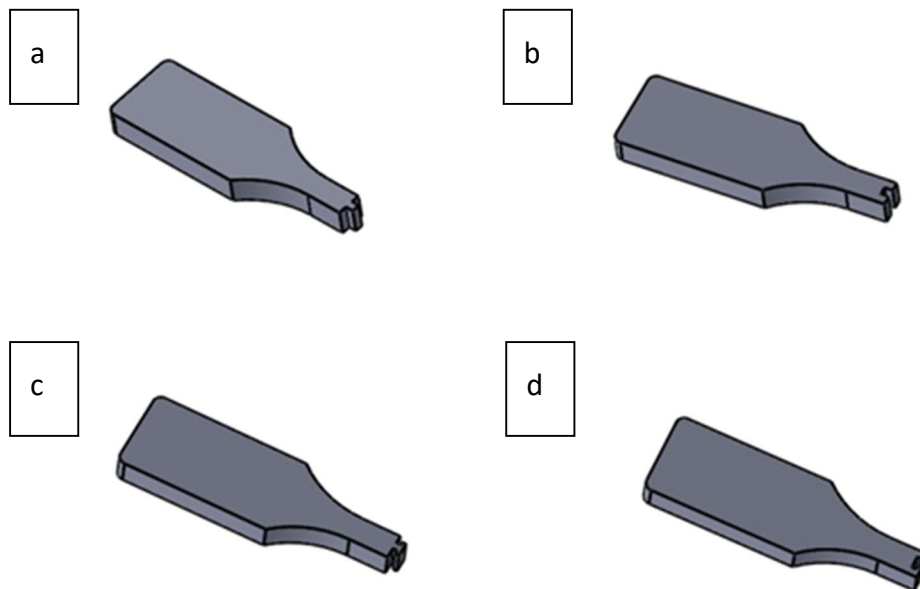
Figure 5-16 CAD graphs for half-length series: a) male cube; b) female cube; c) male T; d) female T.

5.2.3 Statistical Analysis

The results of ANOVA shown in Table 5-6 determined the degree of freedom, sum of squares, mean square, F-ratio and p-value for tensile stress and found the varied joint configurations were statistically significant with the p-values < 0.05 for tensile stress. Moreover, the results of Tukey Test displayed in Table 5-7 indicated 4 levels of

significant effect based on joint configurations while the comparison of HT-NJ 75 with HT-MT 75 and HT-MC 75 with HT-FT 75 showed no significant effect on tensile stress values. These statements are in line with the tensile performances shown in Table 5-5 and make it clear that the selection of joint configurations show a crucial effect in mechanical properties.

Table 5-6 Analysis of variance (ANOVA) of model in tensile stress for HT series specimens with joint configurations. Degree of freedom (DF); sum of squares (SS); mean square (MS); F-ratio (F); p-value (p).

| Source | DF | Ultimate Tensile Stress | | | |
		SS	MS	F	P
Model	4	544	135.998	21.98	0
Residual	45	278.5	6.189		
Total	49	822.5			

Table 5-7 Results of Tukey Test for 75% infill density HT series specimens with joint configurations.

Tukey's multiple comparisons test	Mean Diff.	95.00% CI of diff.	Summary	Adjusted P Value
NJ75 vs. MC75	-4.82	-7.981 to -1.659	***	0.0007
NJ75 vs. FC75	-8.46	-11.62 to -5.299	****	<0.0001
NJ75 vs. MT75	0.41	-2.751 to 3.571	ns	0.9959
NJ75 vs. FT75	-4.24	-7.401 to -1.079	**	0.0036
MC75 vs. FC75	-3.64	-6.801 to -0.4788	*	0.0167
MC75 vs. MT75	5.23	2.069 to 8.391	***	0.0002
MC75 vs. FT75	0.58	-2.581 to 3.741	ns	0.9847
FC75 vs. MT75	8.87	5.709 to 12.03	****	<0.0001
FC75 vs. FT75	4.22	1.059 to 7.381	**	0.0038
MT75 vs. FT75	-4.65	-7.811 to -1.489	**	0.0012

5.3 Summary

In total 46 batches of samples (42 batches of HYM, 3 batches of FDM and 1 batch

of IM samples) were fabricated and tested in this study. Two types of HYM specimens, half-length series which were overmolded at a single mid-point along the tensile sample and half-thickness series samples occurred along the full length of the substrate were mainly assessed. The determination of mechanical performance for all samples were carried out through dimensional accuracy, tensile test and fractographic analysis to figure out the effect of FDM-IM hybrid manufacturing on the final samples.

The tensile test found IM batch provided the best mechanical properties amongst all batches. The half-thickness series samples, especially FC 75 in the study, showed similar tensile strength and stiffness compared with the IM samples. The mechanical properties of FDM samples were better than half-length series samples but worse than the half-thickness series batches. The outstanding mechanical performance for half-thickness series samples along with their great bespoken character have shown their advantages here and these will do more in some daily appliances, such as chopping boards, fridge handles etc.

The SEM found that the half-length series samples were fractured in their joining surfaces and half-thickness series samples were firstly broken in the joining areas and then cracks diffused to the brittle areas, which finally resulted in the fracture. The HYM samples' tensile performance could be explained through the following statements: 1) the direction of interface and tensile loading would significantly affect the tensile be-haviour (parallel direction is recommended); 2) voids located in the joining of HYM samples reduce mechanical strength; 3) the crack inhibition during the tensile loading was brought by the overmolded polymer in HYM samples with joint configurations and this provided HT-FC 75 the greatest tensile behaviour; 4) the bonding condition varies the final mechanical performance (cube shape is recommended).

However, the current study still lacks the analysis related to some parameters applied in the HM, such as the injection molding pressure, the nozzle temperature and the printing speed utilized in the FDM technique. In addition, more mechanical tests should be carried on in these HYM specimens, such as impact and flexural tests, in order to explore mechanical performance metrics beyond tensile. These catalogue of

PLA HYM samples and their mechanical properties would help identify industries and products currently lacking customization where this technique could be adopted for a more complete integration of MC philosophies offered by this unique manufacturing strategy.

Chapter 6: Hybrid Manufacturing of Dual-Material Composite through Material Extrusion 3D printing and injection Molding

6.1 Introduction

In the preceding chapters, samples were fabricated from Acrylonitrile Butadiene Styrene (ABS) and Polylactic Acid (PLA) and categorized according to the manufacturing techniques used: Hybrid Manufacturing (HM) combining Fused Deposition Modelling (FDM) and Injection Molding (IM), FDM alone, and IM alone.

The chapters emphasized that HM permits a high level of customization and a rapid manufacturing rate, thereby overcoming the inherent limitations of FDM's slow production process and IM's limited customization capabilities. Mass Customization (MC) is a manufacturing strategy that combines the customization of bespoke products with the efficiency of mass production.

This chapter studies the tensile properties of dual-material specimens produced by the overmolding technique under various conditions. The manufacturing process consisted of two stages: first, distinct substrates were created using PLA filament and the FDM technique, and then, these substrates were inserted into mold cavities and overmolded with ABS. This method illustrates the cost-effectiveness of overmolding.

Specimens of dual-material bilayer overmolding are compared to those discussed in previous chapters in order to determine the effects of material variation on the final products. To evaluate the effect of HM on the specimens, three parameters were varied: infill density, preform geometry, and injection pressure. By varying the infill density and geometry of the preforms using FDM, it was possible to evaluate mechanical properties and demonstrate the design flexibility of HM. In addition, various injection pressures were utilized to evaluate their potential effect on the final products.

Using a three-way Analysis of Variance (ANOVA), the mechanical properties of the resulting bilayer specimens were analyzed to determine the combined effects of the varied parameters. This study provides the foundation for the widespread adoption of the overmolding technique in the production of dual-material components with intricate geometries, including the incorporation of both soft and rigid materials.

6.2 Results and Discussion

In this study, a total of sixteen batches of specimens were manufactured via the overmolding technique, based on the high design freedom offered by FDM in terms of infill density and joint configuration, as well as two levels of injection molding pressure; the design of this study can be found in Table 6-1.

Table 6-1 Design of specimens in this study.

Joint Configurations	25 %, 60 bar	75 %, 60 bar	25 %, 100 bar	75 %, 100 bar
MC	25-MC-60	75-MC-60	25-MC-100	75-MC-100
FC	25-FC-60	75-FC-60	25-FC-100	75-FC-100
MT	25-MT-60	75-MT-60	25-MT-100	75-MT-100
FT	25-FT-60	75-FT-60	25-FT-100	75-FT-100

6.2.1 Manufacturing Cost

A reduced manufacturing cost along with high quality in products has been a concern in manufacturing industry. In this case, a single substrate fabrication took an average of 3 minutes to complete. However, the overmolding processing needs just 40 seconds each cycle to produce two finished specimens. Regarding the manufacturing time for the FDM and IM specimens shown in Section 5.2, it takes 6 minutes to fabricate one PLA specimen using FDM only. In converse, two IM specimens can be fabricated in 90 seconds.

It can be determined that most fabrication time in getting an overmolded specimen is spent on the first stage to fabricate FDM substrates, which is a critical shortcoming of the FDM technology, but can be addressed by IM in the pursuit of overmolding technique. In addition, this overmolding technique can reduce manufacturing cost when compared to FDM while retaining a considerable design freedom, demonstrating the possibility of this manufacturing technique for use in the future industry in business level. Furthermore, an advanced productivity in manufacturing sector can be delivered if more substrates have been prepared in stock

prior to the IM cycle with several offline FDM machines carried out in manufacturing processing.

6.2.2 High Precision in Dimension

The dimensions of all batches of specimens were measured prior to the tensile testing and were shown in Table 6-2. The higher precision dimensions of these overmolded specimens compared to the ones of FDM specimens in our previous work indicate the use of IM can address the low precision dimensions problem of FDM products, which expands the applications of FDM technique in specific industry, such as the spared parts for automobiles, airplanes and even satellites.

Table 6-2 Dimensions of all batches of specimens.

Parameter	FDM Specimens	Overmolded Specimens
Fillet Radius R (mm)	12.7	12.7
Thickness (mm)	3.2±0.2	3.2±0.1
Total length (mm)	64±0.3	64±0.2
Width of joint for IM and FDM (mm)	——	3.3±0.2
Width at two ends (mm)	10±0.2	10±0.2

6.2.3 Tensile Performance

In this experiment, the maximum tensile strength (σ) and Young's Modulus (E) values along with their average and standard deviation values for the batches are listed in Table 6-3. The minimum and maximum average of σ and E showed differences between specimens fabricated under separated parameter sets, which were in the range of σ= [42.1, 46.1] MPa, E= [945.5, 1129.5] MPa, respectively. These results indicated that the varied combinations of parameters would affect the tensile performances of finished specimens. In addition, low standard deviations of maximum tensile strength and Young's Modulus can be found in Table 6-3, which agrees with the tensile behaviors of half thickness series samples in previous publications both for ABS

samples and PLA specimens. This indicates a superior flexibility in these samples, making overmolding technique popularized in manufacturing industry, such as aerospace products and electronic components.

Table 6-3 Results from the tensile test, in which σ is tensile strength and E is Young's Modulus.

Batch	σ (MPa)	E (MPa)	Batch	σ(MPa)	E (MPa)
25-MC-60	43.8±1.7	945.5±127.0	25-MC-100	42.8±1.1	1065.5±25.9
75-MC-60	44.1±0.3	1056.2±51.5	75-MC-100	43.4±0.1	1093.5±44.2
25-FC-60	44.6±0.8	985.2±56.0	25-FC-100	44.5±0.2	1101.8±39.3
75-FC-60	45.9±0.8	1076.5±37.1	75-FC-100	44.2±0.4	1163.9±109.8
25-MT-60	43.9±1.6	1109.7±58.9	25-MT-100	42.1±0.9	1063.4±21.1
75-MT-60	44.9±0.8	1144.7±112.3	75-MT-100	44.2±1.8	1152.6±72.2
25-FT-60	45.4±0.4	1099.5±18.1	25-FT-100	44.4±0.8	1115.5±23.8
75-FT-60	46.1±0.7	1129.5±76.2	75-FT-100	45.8±0.6	1111.3±45.1

To determine the correlation of tensile performances and the parameters employed in fabrications, some graphical representations are shown below: the averaged maximum tensile strength and Young's Modulus varying with the infill density and joint configurations for FDM substrates and IM pressure in overmolding processing. Furthermore, some stress-strain curves of these samples are displayed as follows to indicate the failure mode in the experiments.

The effects of these parameters on the tensile characteristics of finished specimens are discussed briefly in the following paragraphs.

Effects of infill density in substrates on tensile performances

Infill density indicates the quantity of material used for the internal structure of FDM specimens, with a higher value enhancing properties of FDM specimens, such as mechanical properties and fire properties. However, a different phenomenon can be found that a 50 % infill density of substrate results in greater tensile performance for

ABS pieces but a 75 % infill density of substrate can be attributed to higher tensile stress for PLA pieces, which emphasizes the importance to figure out the real explanation conforming to the greater tensile performances of finished specimens.

Table 6-3 and Figure 6-1 reveal that the overmolded specimens with higher infill density of substrates will enhance the average maximum tensile strength for all batches except the 75-FC-100 batch. For example, the maximum tensile strength of 75-MC-60 batch is 44.1 MPa, which is higher than the 25-MC-60 batch. In case of stiffness, the results shown in Table 6-3 indicate a higher value of Young's Modulus can be found in samples with higher infill density. This phenomenon may be explained from the stronger molecular bonding formed in the substrates with higher infill density, more polymers allowing them to join strongly with the overmolded polymer and thus a greater plastic deformation can be withstand in the process of tensile loading, leading to a ductile behavior (Ageyeva et al., 2022; Rajamani et al., 2021; Szuchács et al., 2022), which can be found the difference between Figure 6-2 (a) and (b),(c) and (d), (e) and (f), (g) and (h).
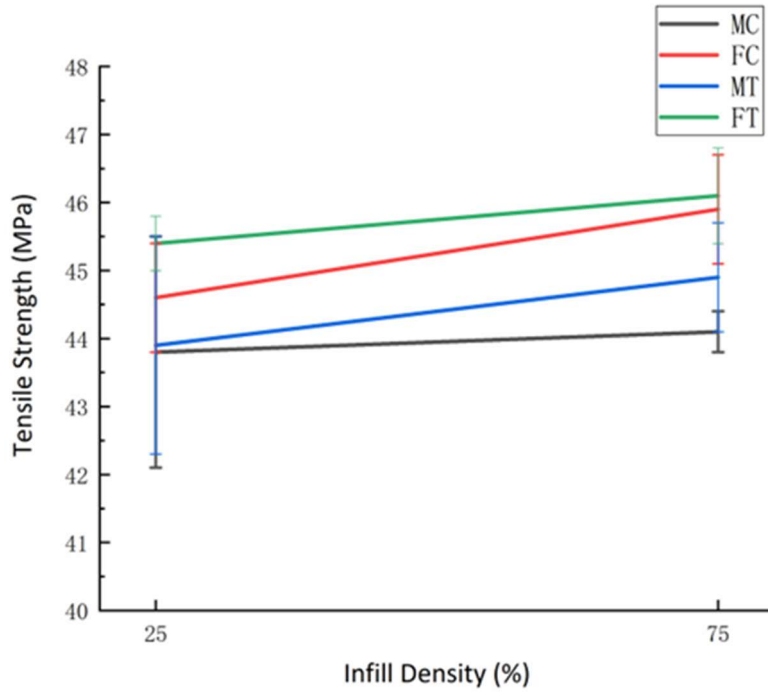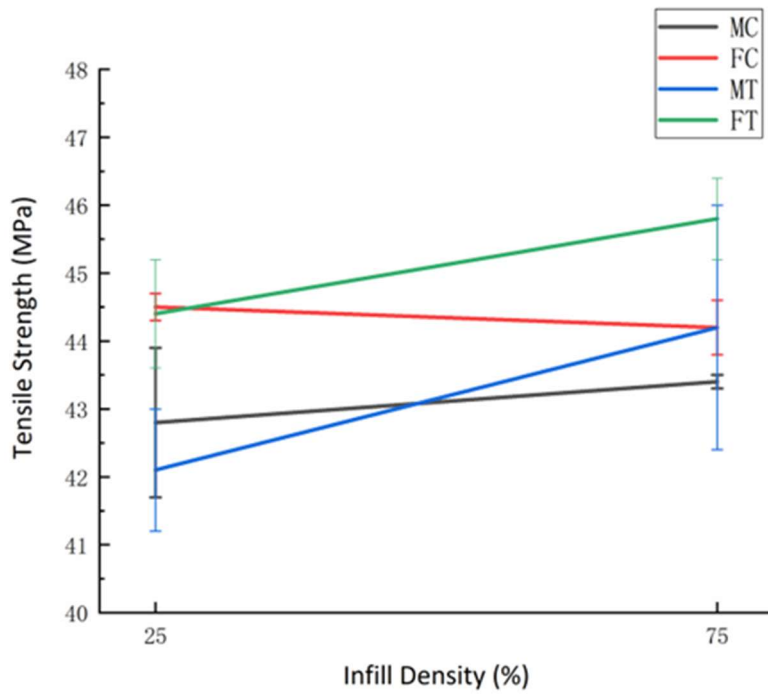
Figure 6-1 Graphical comparison of averaged maximum tensile strength for the specimens as a function of infill density of substrates. (a) overmolding pressure at 60 bar; (b) overmolding pressure at 100 bar.
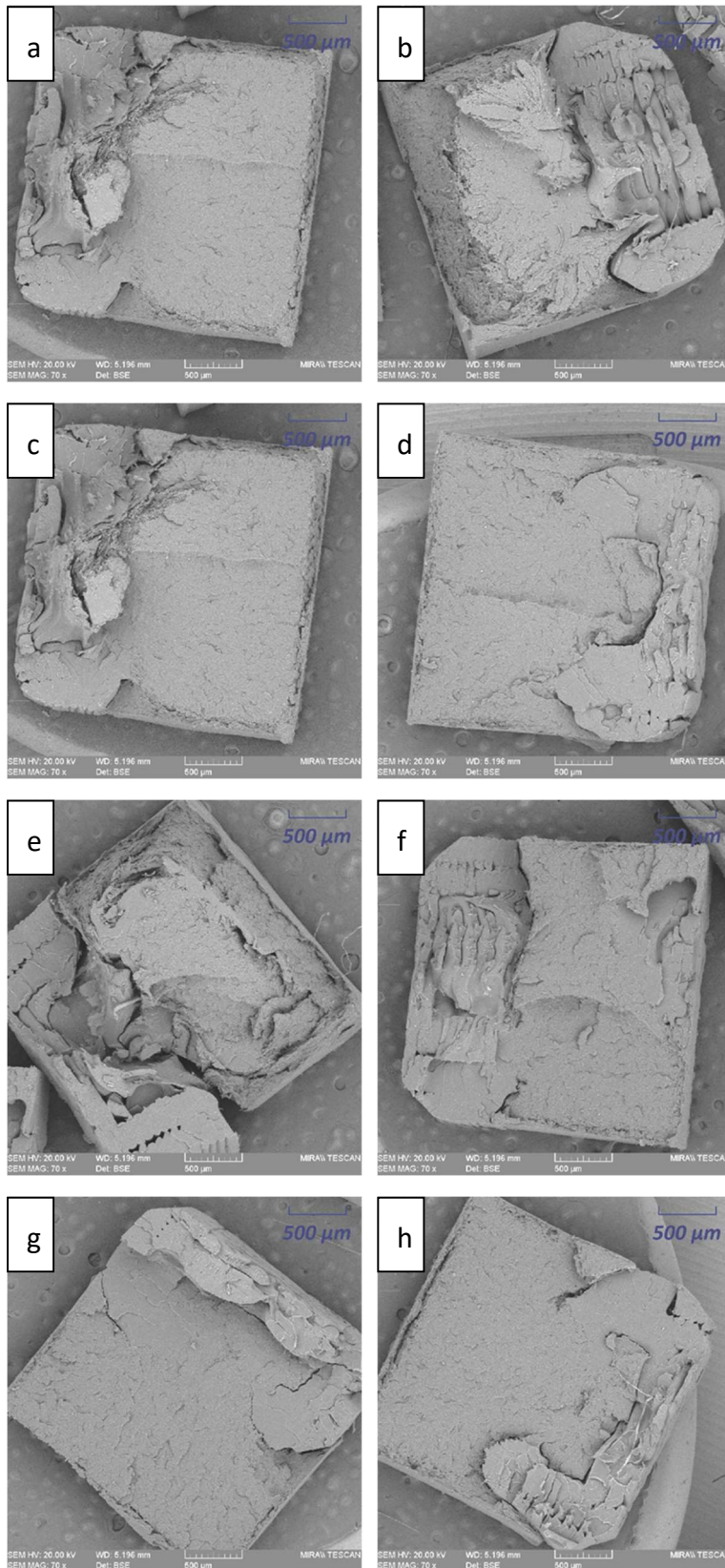
Figure 6-2 SEM images of batches: (a)25-MC-60; (b)75-MC-60; (c)25-FC-60; (d)75-FC-60; (e) 25-MT-60; (f)75-MT-60; (g)25-FT-60; (h)75-FT-60.

These results showed a significant effect from infill density of preforms on the tensile performance, including tensile strength, stiffness, and deformation at fracture. Thus, substrates with higher infill density are recommended employed in the future overmolding manufacturing technique if a higher tensile performance is requested, such as the drive shaft and dental prostheses combined with the characteristic of physically friendly from PLA material.

Effects of overmolding pressure on the tensile performance

IM pressure is an important element in the process of injection molding cycle since it maintains injection speed to confirm the production and affects the manufacturing time in the cycle. In this case, the average maximum tensile strengths of finished specimens are shown in Table 6-3 and Figure 6-3. Figure 6-3 (a) and (b) demonstrate that the maximum tensile strength of samples will decrease if the overmolding pressure is raised from 60 bar to 100 bar. The observed phenomenon may be attributed to the following primary factors in the IM process. Firstly, the high pressure applied in the process will damage the internal structure of substrates. Secondly, the high molding speed results in an inadequate bond between the injection-molded material and the substrates (Tábi et al., 2021). Also, a higher injection molding pressure would lead to a higher crystallization temperature, resulting in a reduced molecular interdiffusion (Giusti & Lucchetta, 2020). These factors contribute to an increased number of cracks and subsequently lead to a decrease in overall strength. These explanations can be determined in the fractured sections shown in Figure 6-2 and Figure 6-4: a brittle fractured mechanism can be found in 25-MC-100 batch (Figure 6-4(a)), whereas a ductile fractured mechanism can be seen in 25-MC-60 batch shown in Figure 6-2(a), particularly, demonstrating a necessity of proper overmolding pressure utilized in this HM approach to produce the finished specimens with desired characteristics in reduced manufacturing cost.
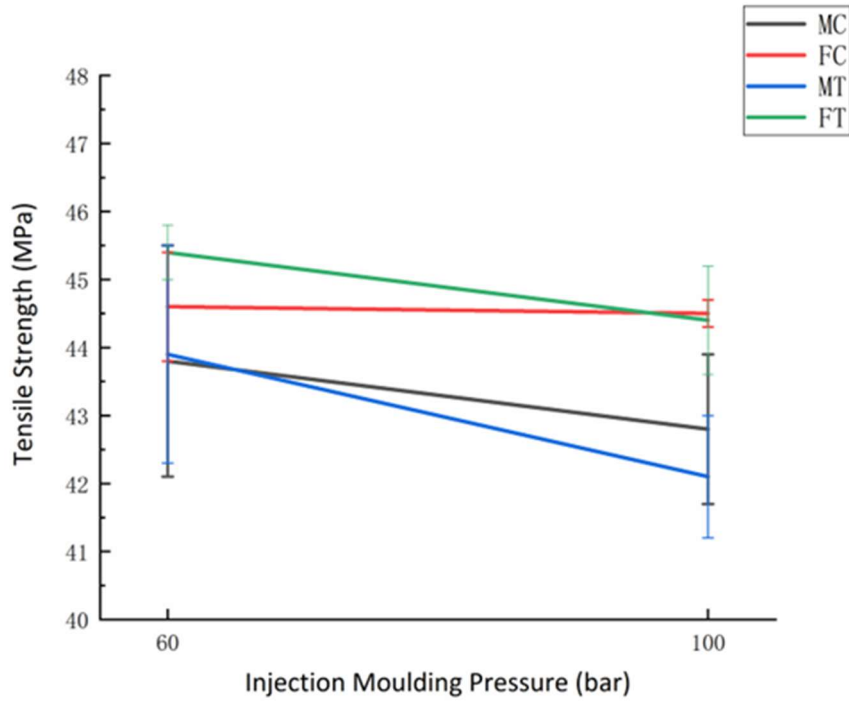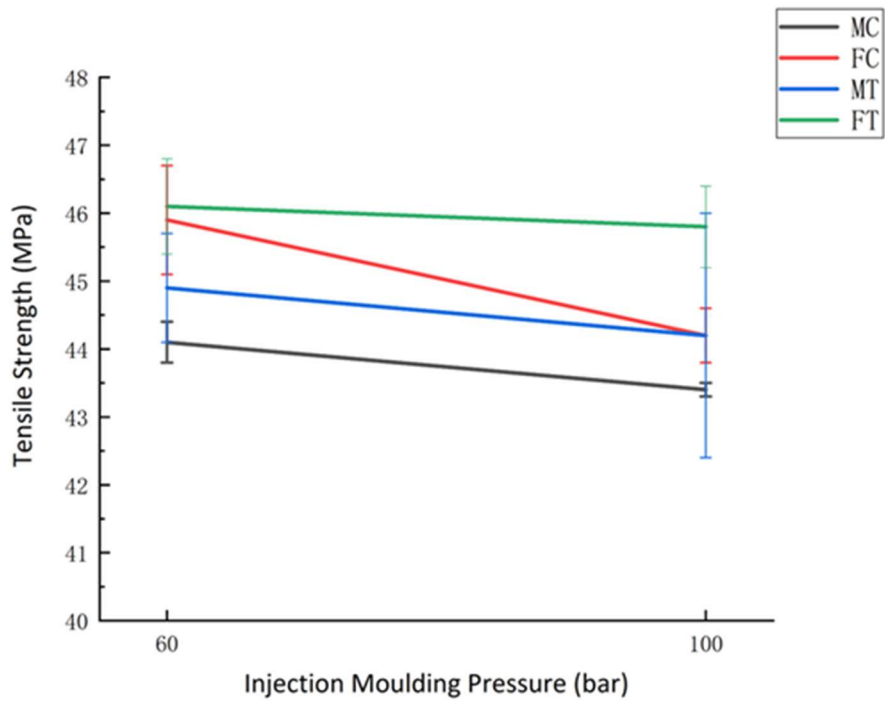
Figure 6-3 Graphical comparison of averaged maximum tensile strength for the specimens as a function of overmolding pressure. (a) infill density of substrates at 25 %; (b) infill density of substrates at 75 %.
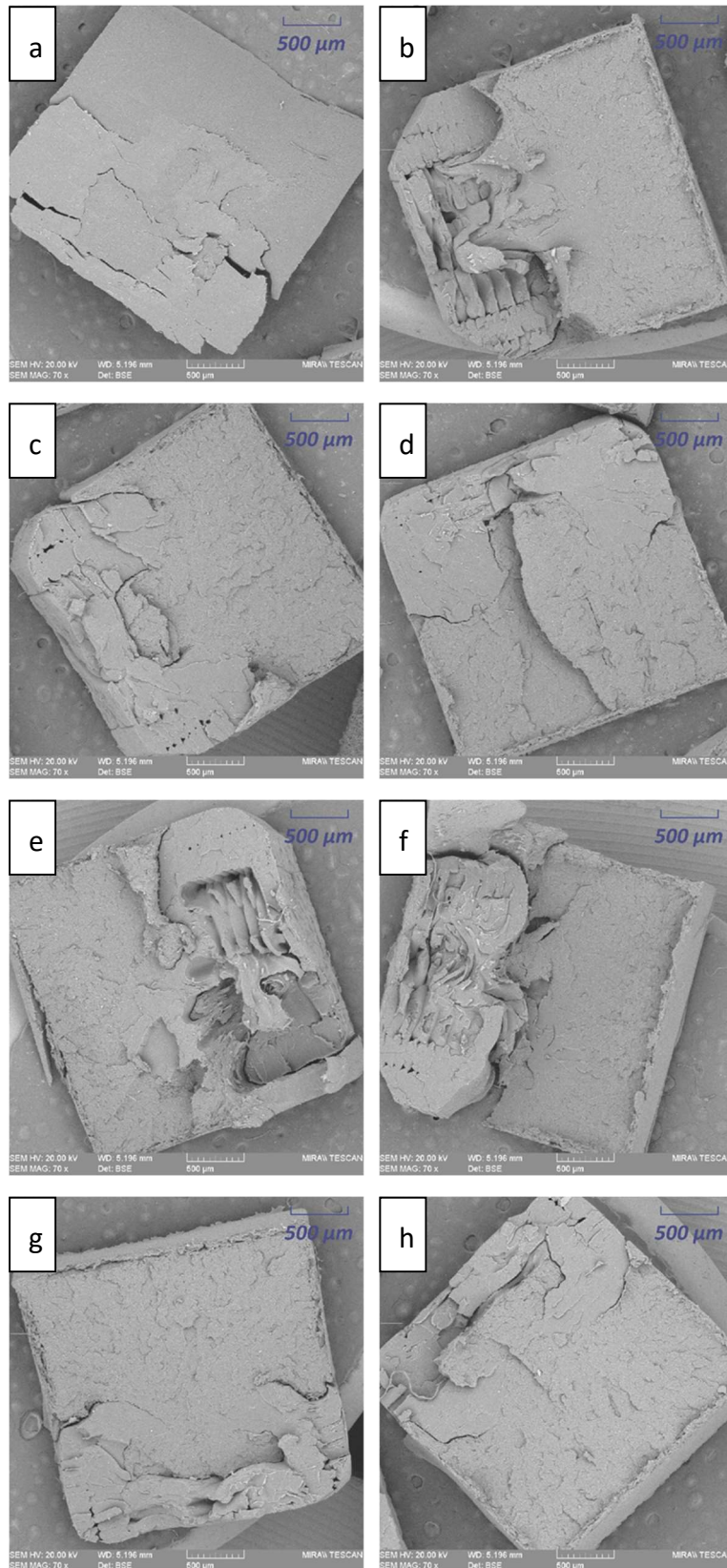
Figure 6-4 SEM images of batches: (a)25-MC-100; (b)75-MC-100; (c)25-FC-100; (d)75-FC-100; (e) 25-MT-100; (f)75-MT-100; (g)25-FT-100; (h)75-FT-100.

6.2.3.3 Effects of joint configurations in the tensile performance

Joint configurations have shown their effects in the mechanical performances in single material overmolded specimens, and this can be modified depending on the customer's preferences using FDM. Table 6-3 and Figure 6-5 indicate that the highest average tensile stress values for overmolded samples under 60 bar and 100 bar can reach to 46.1 MPa (75-FT-60) and 45.8 MPa (75-FT-100). These findings demonstrate the female T joint configuration can result in the highest maximum tensile stress. In addition, the lowest value of maximum tensile stress can be found in the specimens with male cube joint configuration (43.8 MPa at 25-MC-60 batch and 42.8 MPa at 25-MC-100 batch). These results are consistent with the hypothesis found in ABS overmolded specimens shown in Chapter 4, demonstrating the material employed in the overmolding stage will affect the final characteristics due to their individual properties. In addition, (e), (f), (g) and (h) in Figure 6-2 and Figure 6-4 found more gaps in the joining area of substrates and overmolded forms in samples with male joint configuration if compared to those with female joint configuration. This agrees with the low tensile strengths determined in specimens with male joint configuration due to the stress concentration, making it easier to damage the specimen. Besides, greater tensile performance in samples with T joint configurations compared to those with cube joint configurations is accounted from the high ductility of ABS material utilized in overmolding stage, which greatly bonds two materials together and enables the production of a stronger mechanical interlock. Figure 6-2 and Figure 6-4 demonstrate that the fracture started if the tensile was loaded but was then prevented by the overmolded form. Several cracks could be found due to the on-going pull to increase the tensile tension, with the tear steps could be identified during the repeated stages. These results emphasize the major function of FDM technique in this HM approach due to the high design flexibility in manufacturing items with bespoke features in addition to the distinctive mechanical performance. For example, a proper analysis in the geometry of FDM preforms along with the material utilized in the overmolding stage can be carried out prior to the design in finished specimens to allow for a better

mechanical feature.
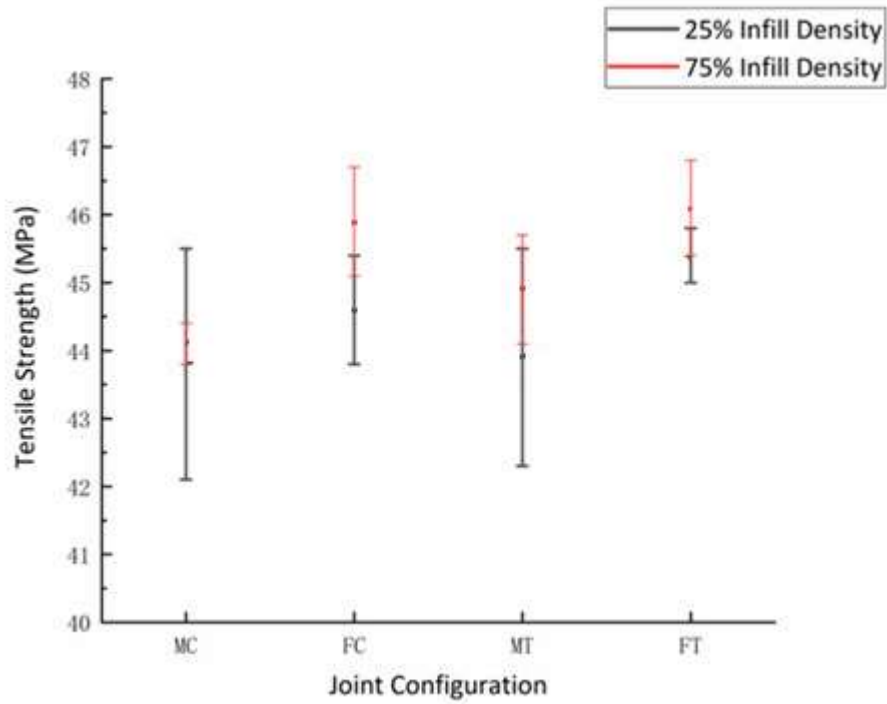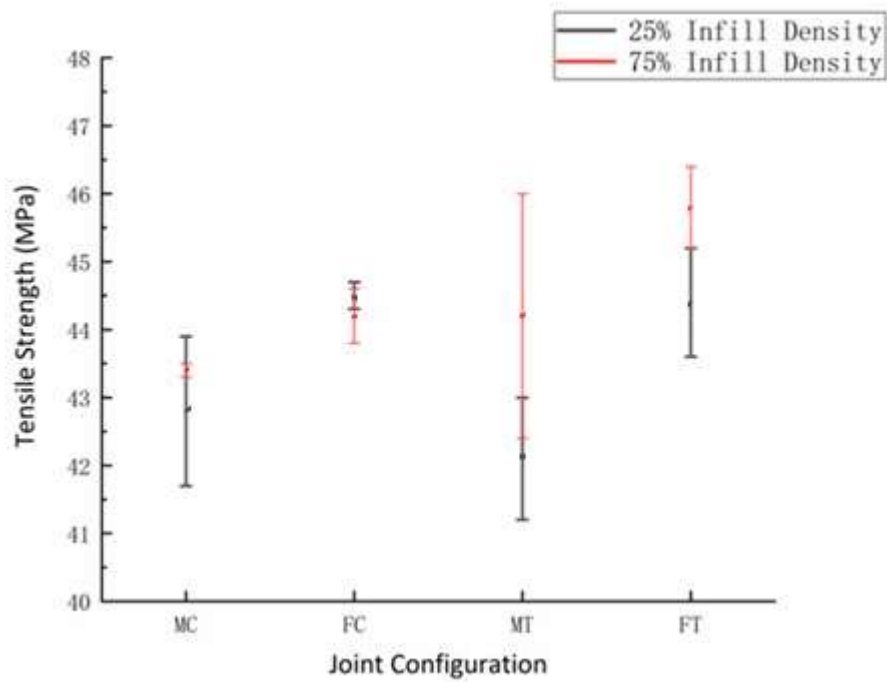
Figure 6-5 Graphical comparison of averaged maximum tensile strength for the specimens as a function of joint configurations. (a) overmolding pressure at 60 bar; (b) overmolding pressure at 100 bar.

6.2.3.4 Mixed-material resulting in a low tensile performance in finished specimens

The tensile performances of these mixed-material specimens were compared to those fabricated using ABS and PLA material only, in which around 2 % lower value of tensile strength can be determined if compared to samples fabricated using ABS only in Chapter 4, but a clear deviation (20 %) can be found in comparison to those PLA specimens in Chapter 5. The phenomenon can primarily be ascribed to insufficient contact between the two materials, leading to weak sections in the finished specimens. Also, the weak sections can be typically found at the transition interface where fractures tend to occur. These hypotheses can be determined from the SEM images of following batches: 75-FC-60 in Figure 6-2(d), 75-FT-60 in Figure 6-2(h), 25-FC-100 in Figure 6-4(c), and 75-FC-100 in Figure 6-4(d), indicating the inadequate contact between the materials with varied features. In terms of PLA overmolded specimens in our previous work, great contacts between the FDM substrates and overmolded material can be observed, which are shown in Figure 6-6. These findings highlight the significance of employing two materials with similar properties throughout the manufacturing process, such as PLA with Polyethylene terephthalate glycol (PETG), providing design insights for multi-material specimens fabricated using overmolding technique.
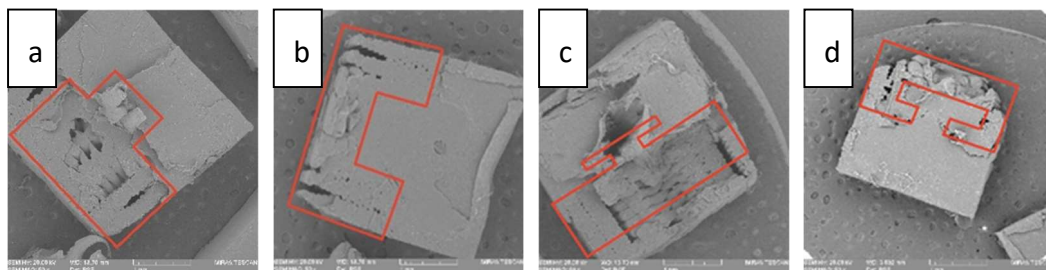
Figure 6-6 SEM images of 75 % infill density PLA overmolded specimens with varied joint configurations, in which (a) MC; (b) FC; (c) MT; (d) FT.

6.2.4 Statistical Analysis of Tensile Performances

Table 6-4 and Table 6-5 indicate the parameters employed in this experiment are statistically significant in the tensile strength since their p-values are lower than 0.05,

in which a higher significance can be found in JC and following with IMP and IDP. However, their interactions (JC x IMP, JC x IDP, IMP x IDP, and JC x IMP x IDP) had no significant effects in the tensile strength as their p-values are above 0.05, indicating a greater impact of FDM technique in the finished specimens if compared to the IM processing.

Table 6-4 ANOVA results, in which JC is joint configuration, IMP is injection molding pressure, and IDP is infill density of substrates.

Source of Variation	Total Variation (%)	P Value	P value Summary	Significant?
JC	29.12	0.0082	**	Yes
IMP	10.43	0.0176	*	Yes
IDP	10.06	0.0191	*	Yes
JC x IMP	0.4519	0.9577	ns	No
JC x IDP	2.235	0.6808	ns	No
IMP x IDP	0.05519	0.8339	ns	No
JC x IMP x IDP	3.015	0.5702	ns	No
Subject	9.401			

Table 6-5 ANOVA results, in which JC is joint configuration, IMP is injection molding pressure, and IDP is infill density of substrates, SS is standard deviation, DF is degree of freedom, MS is mean square, F is F Value, DFn is degrees of freedom in the numerator, DFd is degrees of freedom for the denominator.

Model	SS	DF	MS	F (DFn, DFd)	P value
JC	28.14	3	9.379	F (1.988, 15.90) =6.611	P=0.0082
IMP	10.08	1	10.08	F (1, 8) = 8.879	P=0.0176
IDP	9.72	1	9.72	F (1, 8) = 8.559	P=0.0191
JC x IMP	0.4367	3	0.1456	F (3, 24) = 0.1026	P=0.9577
JC x IDP	2.16	3	0.72	F (3, 24) = 0.5075	P=0.6808
IMP x IDP	0.05333	1	0.05333	F (1, 8) = 0.04696	P=0.8339
JC x IMP x IDP	2.913	3	0.9711	F (3, 24) = 0.6845	P=0.5702
Subject	9.085	8	1.136		
Residual	34.05	24	1.419		

6.3 Summary

This research used a FDM-IM hybrid manufacturing technique to produce mixed-material, bilayer specimens as a function of different parameters (substrate infill density, overmolding pressure, and joint configurations) to learn how these factors affected the final products and to contrast them with single material specimens. Samples were made a two-step process: First, PLA substrates with four different geometries (MC, FC, MT, FT) and two different infill densities (25 % and 75 %) were fabricated using FDM; second, the substrates were inserted into the mold cavity and the overmolding stage was carried out at 60 bar and 100 bar.

Consistent with the phenomenon observed in the PLA overmolded specimens, tensile test results show that specimens with 75 % infill density have superior tensile performance when compared to specimens with 25 % infill density in substrates. Female T joint configuration specimens had the highest tensile strength when compared to other joint configuration specimens, which is in line with the results for ABS overmolded specimens due to the high ductility of ABS material. It was found that the maximum tensile stress in specimens overmolded at 60 bar is higher than those overmolded at 100 bar, indicating a negative effect of overmolding pressure on final tensile performance. Furthermore, mixed-material specimens have low tensile strengths compared to ABS and PLA specimens, with a 2 % decrease compared to ABS ones but a 20 % decrease compared to PLA pieces due to poor contact between the PLA and ABS material.

The results of this study show that the FDM-IM hybrid manufacturing method employed in the mixed-material specimens is a promising technique for rapidly fabricating specimens with superior mechanical properties and a level of customization appropriate for the modern manufacturing sector, especially in the field of home appliances.

Chapter 7: Effect of manufacturing parameters through Taguchi approach on mechanical features of ABS and PLA pieces using overprinting technique

7.1 Introduction

In the previous three chapters, a hybrid approach combining Fused Deposition Modeling (FDM) and Injection Molding (IM) was utilized to fabricate single workstations using the overmolding technique. This involved inserting FDM preforms with varied geometries into mold cavities for overmolding. Acrylonitrile Butadiene Styrene (ABS) and Polylactic Acid (PLA) were used in Chapter 4 and Chapter 5, respectively, to assess the impact of overmolding on the final products. Chapter 6 explored the fabrication of dual-material bilayer specimens by inserting PLA preforms for overmolding, highlighting the technique's potential in the industry. The studies demonstrated that the performance of the finished specimens was influenced by the design flexibility of FDM and the fusion/contact zone between the FDM preforms and the overmolded section from IM. The overmolding technique was identified as having potential applications across various fields.

This chapter introduces the overprinting technique, which is the reverse of overmolding, and hypothesizes its significant utility in the manufacturing industry based on mass customization principles. The overprinting technique is employed to fabricate finished specimens using ABS and PLA, where rigid substrates are printed onto injection-molded preforms. The tensile performance is studied and compared using the Taguchi method. Three parameters are investigated: infill density, printing speed, and extrusion temperature in the FDM process. Taguchi's L9 array, consisting of nine runs with three repeated specimens for each, is used to produce a total of twenty-seven specimens with varied processing settings for one material. The dimensions of all finished specimens adhere to the ASTM D638-III standard.

The results indicate that for optimal tensile strength in PLA specimens, a combination of higher infill density (75%), medium printing speed (70 mm/s), and high extrusion temperature (210°C) is required. For ABS specimens, the optimal parameters are 75% infill density, 40 mm/s printing speed, and 220°C extrusion temperature. This study contributes foundational knowledge of an emerging manufacturing technology capable of producing functional items with exceptional properties.

7.2 Results and Discussion

7.2.1 Dimensional Accuracy

The results of measurements were listed below in Table 7-1, in which the specimen thickness, specimen's total length, gauge width and width at two ends were subjected to the ASTM-638-Ⅲ model. These results indicate a high degree of precision can be provided by the overprinting approach in finished specimens, making it a strong candidate to be employed in some future manufacturing industry requiring a low deviation tolerance.

Table 7-1 The comparisons of the measurements between all batches.

Parameter	Ideal batches	ABS batches	PLA batches
Thickness (mm)	3.2	3.2±0.1	3.2±0.1
Total Length (mm)	64	64±0.2	64±0.2
Gauge Width (mm)	3.3	3.3±0.1	3.3±0.1
Width at two ends (mm)	10	10±0.2	10±0.2

7.2.2 Manufacturing Cost in Fabrication

Manufacturing cost is another topic discussed here. In this experiment, some trials were brought in first to figure out the manufacturing time in fabricating samples by IM and FDM only. Two IM specimens could be fabricated meantime and only need 30 seconds to finish, which applied to ABS and PLA pieces both. As for the FDM specimens, it took an average of 5 mins in fabricating a full size of specimen, both in ABS and PLA. However, as for the samples produced using this hybrid manufacturing, the ABS sample needed 20 seconds in fabricating the IM base and 3 mins in overprinting processing. For PLA pieces, it took 30 seconds in obtaining the IM base but only 2 mins for overprinting approach. Hence, this hybrid manufacturing offers a 100 seconds and 150 seconds reduction in manufacturing for two ABS and PLA pieces fabrication, respectively. This manufacturing time saving made this overprinting technique more practical in business level, especially when IM preforms were in fully

stock and awaiting the overprinting approach.

7.2.3 Tensile Performances

The tensile performances of specimens in this study were analysed through the signal/noise (S/N) ratio. This analysis was determined using the principle of greater is better since these characteristics are supposed to be maximized in the performance. The formula for the S/N ratio is shown below, in which y_i is the results determined in the tests, and n indicates the number of trials in each batch (Phillips, 1995).

$$S/N = -10 \log_{10} [\frac{1}{n} \sum_{i=1}^{n} \frac{1}{y_i^2}$$

Results for ABS pieces

The tensile performances for ABS pieces were shown below in Table 7-2. These results were averaged by three repeated three pieces in a single batch. Three properties were investigated here: tensile strength, Young's Modulus, and the strain at fracture. The individual batch name is decided by the parameters utilized in the FDM technique: 25-40-210 means the infill density at 25 %, printing speed at 40 mm/s and extrusion temperature at 210 °C, etc.

Table 7-2 Tensile performances for ABS pieces, in which the standard deviations of tensile strength and Young's Modulus have been displayed.

Batch	Tensile Strength (MPa)	Young's Modulus (MPa)	Strain (%)
25-40-210	39.9±1.8	940.3±30.4	9.4
25-70-220	47.1±0.5	850.9±70.5	12.8
25-100-230	25.7±1.1	845.6±44.5	11.1
50-40-220	38.9±1.3	1011.7±7.2	14.9
50-70-230	40.8±1.2	1014±40.1	12.0
50-100-210	33.5±1.7	835±13.3	11.3
75-40-230	42.5±1.7	1018.1±73.3	10.5
75-70-210	43.2±0.3	961.3±62.9	8.6
75-100-220	34.1±1.4	925.2±18.9	8.2

As can be found in Figure 7-1(a), slight impacts on the tensile strengths of ABS specimens can be found from infill density and extrusion temperature if compared with that from printing speed. In general, an increasing infill density will boost tensile strength. However, a different phenomenon is seen for printing speed and extrusion temperature, in which the midpoints of both (70 mm/s for printing speed and 220 °C for extrusion temperature) provide the maximum tensile strength value. Furthermore, the printing speed in the overprinting process has a major influence on the tensile strength, since a considerable decrease is seen when the printing speed falls below 100 mm/s. Also, the maximum values of the S/N ratio in tensile strength are largely determined by the printing speed and is similar to the tensile strength, which displays in Figure 7-1(b). This illustrates that a greater emphasis on printing speed is required for an increase in the tensile strength of overprinting specimens and may be used in certain elements due to the high repeatability, such as some assembly-based toys in LEGO brand, gears in manufacturing industry and cup holder tray in coffee machine.

Figure 7-1 Plots of the main effects of the FDM parameters used in the ABS pieces on the (a)tensile strength and (b) tensile strength's S/N ratio, where the dashed line indicates the average result.

The study also made an investigation into the effect of these parameters on the resulting Young's Modulus. The plots of each parameter utilized in DOE are shown in Figure 7-2(a). The values of Young's modulus exhibit a rising trend, which depends on the extrusion temperature. An increased extrusion temperature could reduce the viscosity grade (de Gennes, 2003; Eslami & Grmela, 2008), resulting in a high degree of fusion between each FDM layer and particularly between the first FDM layer and the IM base (Alafaghani & Qattawi, 2018; Hashemi Sanatgar et al., 2017; Sun et al.,

2008). However, the rise in Young's Modulus from 210 °C to 220 °C is less than that from 220 °C to 230 °C, indicating that a stronger fusion can be accomplished if the temperature reaches 220 °C to 230 °C. This phenomenon agrees with some publications (Ahn et al., 2002; Alafaghani et al., 2017) related to the ABS samples that were manufactured using FDM, stating that the mechanical performance of these can be increased via better fusion. As for the printing speed, the value of 40 mm/s leading to the highest Young's Modulus can be found in Figure 7-2(a). In addition, if the printing speed drops from 70 mm/s to 100 mm/s, Young's Modulus decreases dramatically. This can be explained by the filament having insufficient time to melt, and thus triggers to a poor fusion (Nabavi-Kivi et al., 2021). Young's Modulus can be affected by infill density in the FDM stage as well, that a higher infill density offers more material to withstand the loading and this is highly in line with the situation in FDM samples (Baich et al., 2015; Fernandez-Vicente et al., 2016). Furthermore, Figure 7-2(b) pointed out the overprinting specimen with the highest Young's Modulus can be mostly expected under the combination of 75 % infill density, 40 mm/s printing speed, and 230 °C extrusion temperature.
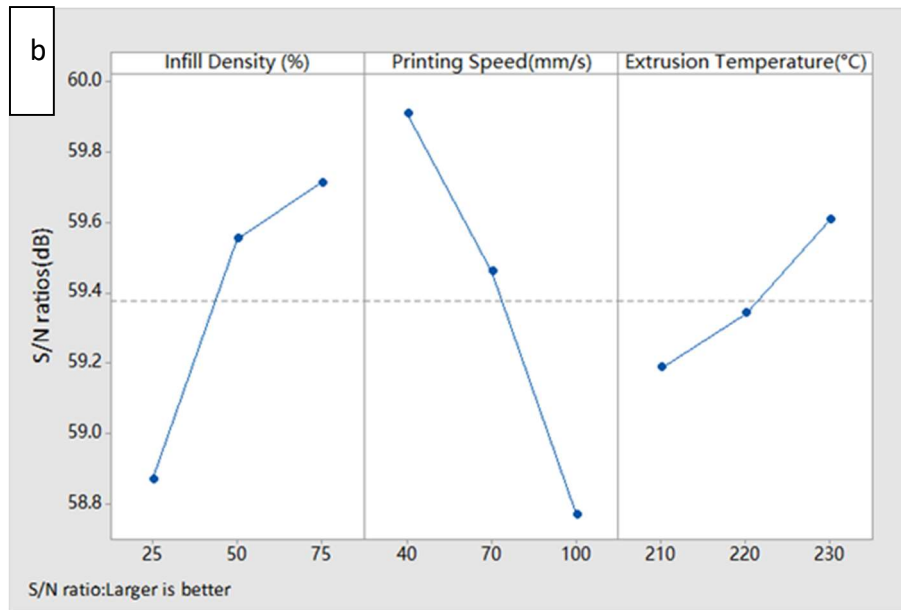
Figure 7-2 Plots of the main effects of the FDM parameters used in the ABS pieces on the (a)Young's Modulus and (b) S/N ratio of Young's Modulus, where the dashed line indicates the average result.

As for the maximum strain in fracture for ABS specimens, it was determined in Figure 7-3(a) that an increase in printing speed decreased the strain value. This phenomenon agrees with the condition of Young's Modulus corresponding to printing speed and is induced by the fusion between each layer (Andreu et al., 2022; Braconnier et al., 2019; S. I. Park et al., 2014). A similar pattern holds for the infill density and extrusion temperature, where the midpoint of both (infill density at 50% and extrusion temperature at 220°C) results in the maximum strain value. The S/N ratio for maximum strain is mostly controlled by infill density as can be seen in Figure 7-3(b), where the S/N ratio rises as the infill density grows from 25% to 50% but decreases dramatically as the infill density increases from 50% to 75%. In addition, the effects of printing speed and extrusion temperature on strain are distinct and will not be observable when compared to the infill density.

Figure 7-3 Plots of the main effects of the FDM parameters utilized in ABS pieces on the (a)maximum strain at fracture and (b) S/N ratio of the strain, where the dashed line indicates the average result.

The reduction in printing speed results in a low S/N ratio; nevertheless, a 220°C extrusion temperature can provide a higher S/N ratio than that from 210°C and 230°C. The phenomena of Young's Modulus and strain deliver a solution in some certain bespoke appliances requiring higher stiffness in several fields, such as the pedal and luggage carrier for bicycles, chairs with some spoken features, television support and even some unique parts in aircraft (Jamir et al., 2018).

Results for PLA pieces

Table 7-3 displays the tensile performances of all PLA pieces. These results were averaged by three repeated three pieces in a single batch. Three properties were investigated here: tensile strength, Young's Modulus, and the strain at fracture. The individual batch name is decided by the parameters utilized in FDM technique: 25-40-190 means the infill density at 25 %, printing speed at 40 mm/s and extrusion temperature at 190 °C, etc.

Table 7-3 Tensile performances for all PLA pieces, in which the standard deviations of tensile strength and Young's Modulus have been displayed.

Batch	Tensile Strength (MPa)	Young's Modulus (MPa)	Strain (%)
25-40-190	37.2±4.3	934.3±10.4	8.1
25-70-200	47.1±0.5	1031.4±112.7	9.3
25-100-210	41.1±7.1	1150.4±25.5	8.9
50-40-200	50.9±2.1	1047.1±141.6	10.1
50-70-210	56.3±0.7	1072.8±64.9	10.1
50-100-190	49.2±2.5	1108.9±54.6	10.3
75-40-210	55.4±1.3	1085.6±184.6	10.2
75-70-190	55.9±1.1	1144.5±40.2	11
75-100-200	54.4±1.9	1126.6±44.4	10.1

Figure 7-4 first analysed the effect of these three parameters on the tensile strengths of PLA pieces, revealing that the infill density has a considerable effect on the tensile strength. A large gap of value in tensile strength can be seen if the infill density increases from 25 % to 50 %. If the infill density increases to 75 %, there is a minor rise in tensile strength, indicating that additional increases in infill density cannot have a significant impact on tensile strength. However, the large variation in tensile strength between 25 % and 75 % infill density shows the influence of this on

the tensile performance, which is consistent with the findings for PLA samples manufactured using FDM (Ebel & Sinnemann, 2014; Lanzotti et al., 2015; Torres et al., 2015). Figure 7-4(a) depicts an alternative trend of tensile strength resulting from the three levels of printing speed. The highest tensile strength can be observed if the printing speed is set as 70 mm/s, and a minimal difference in strength has shown in that for 40 mm/s and 100 mm/s. This indicates a midpoint printing speed is beneficial in the fusion facility. A slow printing speed can offer robust fusion establishment but will trigger excessive accumulation of material and thus stress concentration (Rezaeian et al., 2022). In contrast, the 100 mm/s printing speed will cause insufficient material to collect in each layer, hence increasing the number of voids between layers (the first FDM layer with IM base mainly). As for the extrusion temperature, there is a noticeable difference between 190 °C and 200 °C, but only a tiny change when the temperature reaches 210 °C, which means 200 °C to 210 °C can be a great scope to melt the filament and thus increase the adhesion (Alafaghani & Qattawi, 2018; Lokesh et al., 2021; Mahmood et al., 2018).
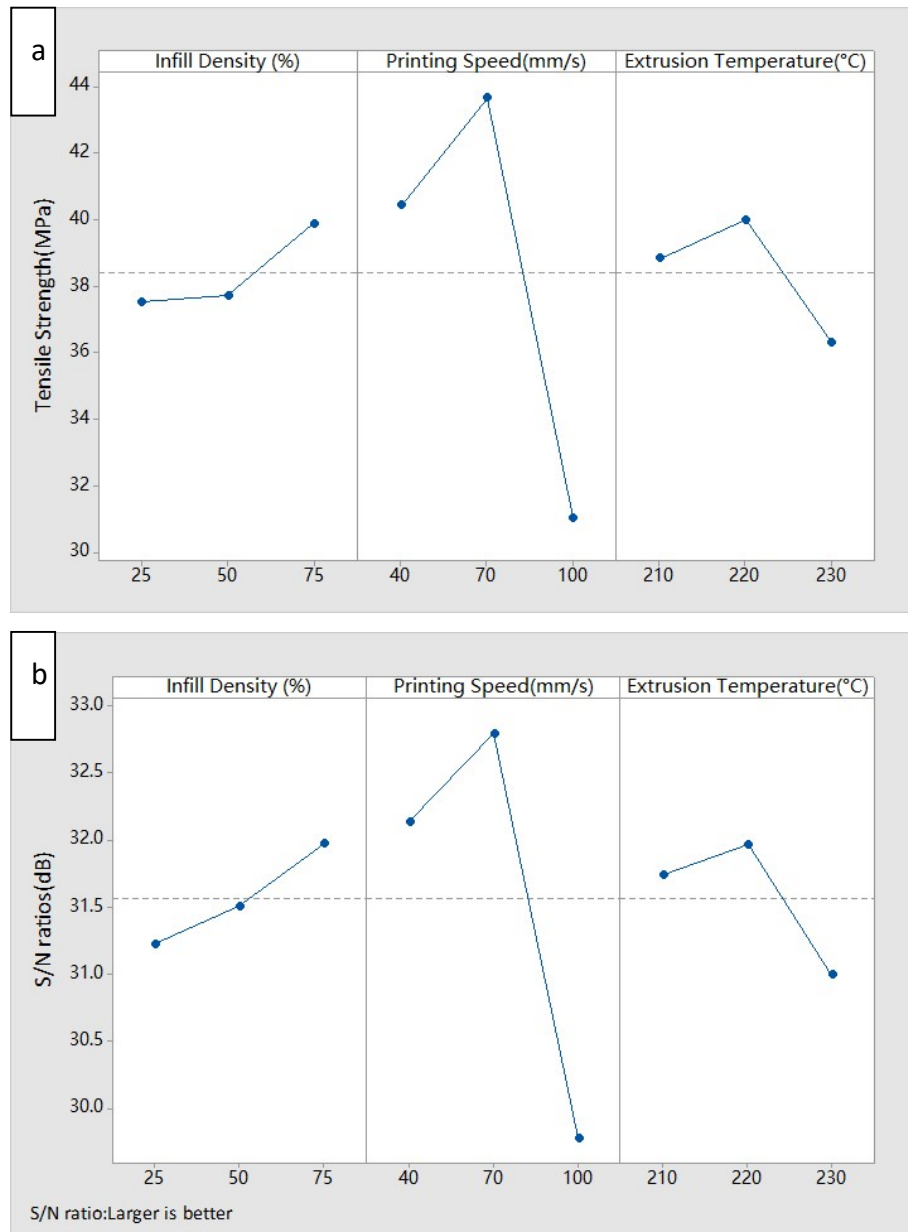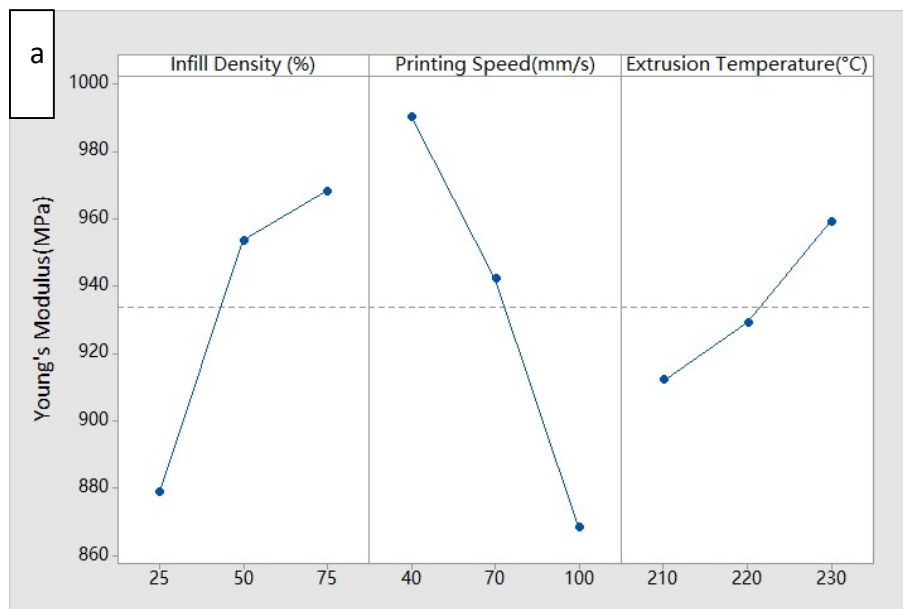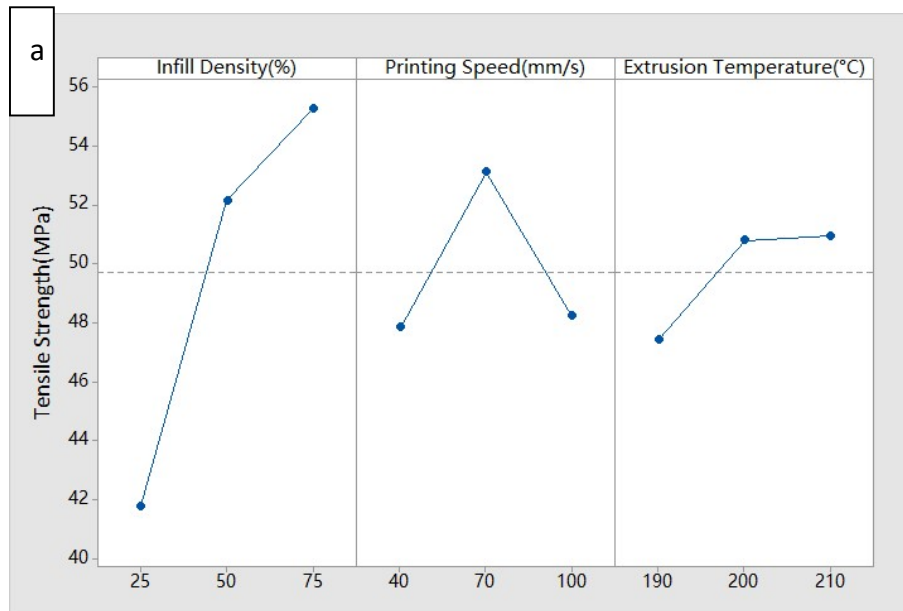
Figure 7-4 Plots of the main effects of the parameters used in PLA pieces on the (a) tensile strength and (b) S/N ratio of the tensile strength, where the dashed line indicates the average result.

For the best S/N ratio, the combination of 75 % infill density, 70 mm/s and 200 °C extrusion temperature yields a high degree of repeatability in tensile strength, which can be found in Figure 7-4(b). These results made it possible for overprinted PLA specimens to be employed in some certain fields, such as the keyboard of laptops with unique tags, lunch box, films in agricultural fields and floor mats in automotive area in combination of some benefits of PLA (safe for use and environmentally friendly).

As for the Young's Modulus for PLA samples, which can be found in Figure 7-5. The increasing infill density shows a linear influence in Young's Modulus. This can be explained by the amount of material required to withstand tensile loading. The printing speed shows a linear effect as well and is getting a more significant role in Young's Modulus, with the 100 mm/s printing speed yields the highest Young's Modulus (Gebisa & Lemu, 2019b; Maurya et al., 2022; Patel et al., 2022). However, the extrusion temperature only shows a slight effect in Young's Modulus, especially from 190 °C to 200 °C. If the temperature reaches to 210 °C, the value of Young's Modulus increases to a higher degree. According to the S/N ratio of Young's Modulus from Figure 7-5, the same level of manufacturing parameters can be utilized in S/N ratio optimization.
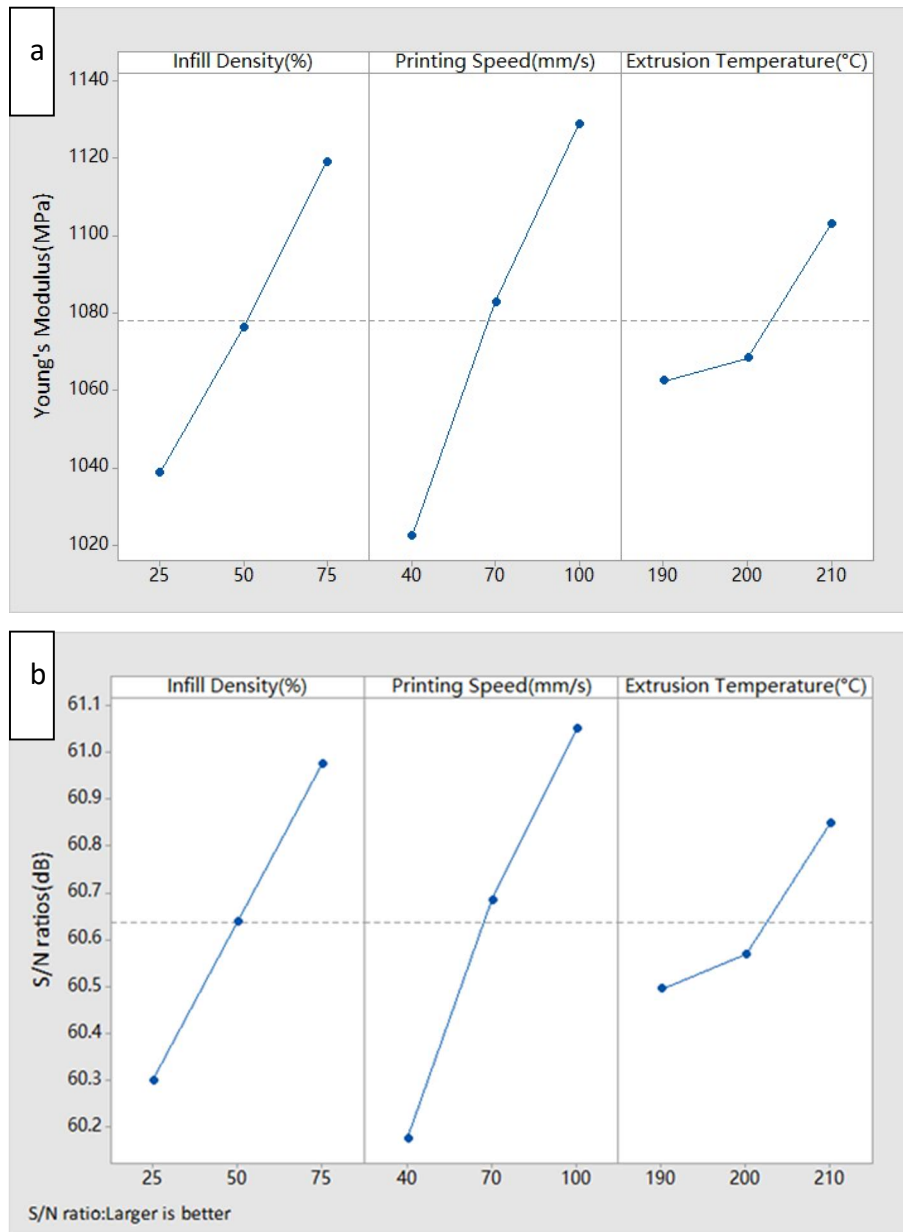
Figure 7-5 Plots of the main effects of the parameters used in PLA pieces on the (a) Young's Modulus and (b) S/N ratio of the Young's Modulus, where the dashed line indicates the average result.

Finally, the results in Figure 7-6 show that the increase of infill density will offer a higher strain at fracture, especially from 25 % to 50 % infill density. However, the increase of infill density from 50 % to 75 % offers a slight increase in the strain (Gebisa & Lemu, 2019a; Patel et al., 2022). This phenomenon shows a similar effort in tensile strength. The printing speed of 70 mm/s finds the greatest strain, and this agrees with the result in tensile strength as well. As for the extrusion temperature, it only shows a negligible influence on the ductility (strain at fracture). The S/N ratio for strain at

fracture is highly affected by infill density and this will be enhanced while infill density increased. The printing speed finds the same effect with the strain, the 70 mm/s printing speed triggers the greatest S/N ratio if compared with that for 40 mm/s and 100 m/s. Last, a varied extrusion temperature has no influence in the strain as well as the S/N ratio. The phenomena found in Young's Modulus and strain at fracture illustrate the availability of overprinted PLA samples in some applications, including drug delivery in medical industry, the scaffolds in bone engineering, and even planting pots for agricultural field.
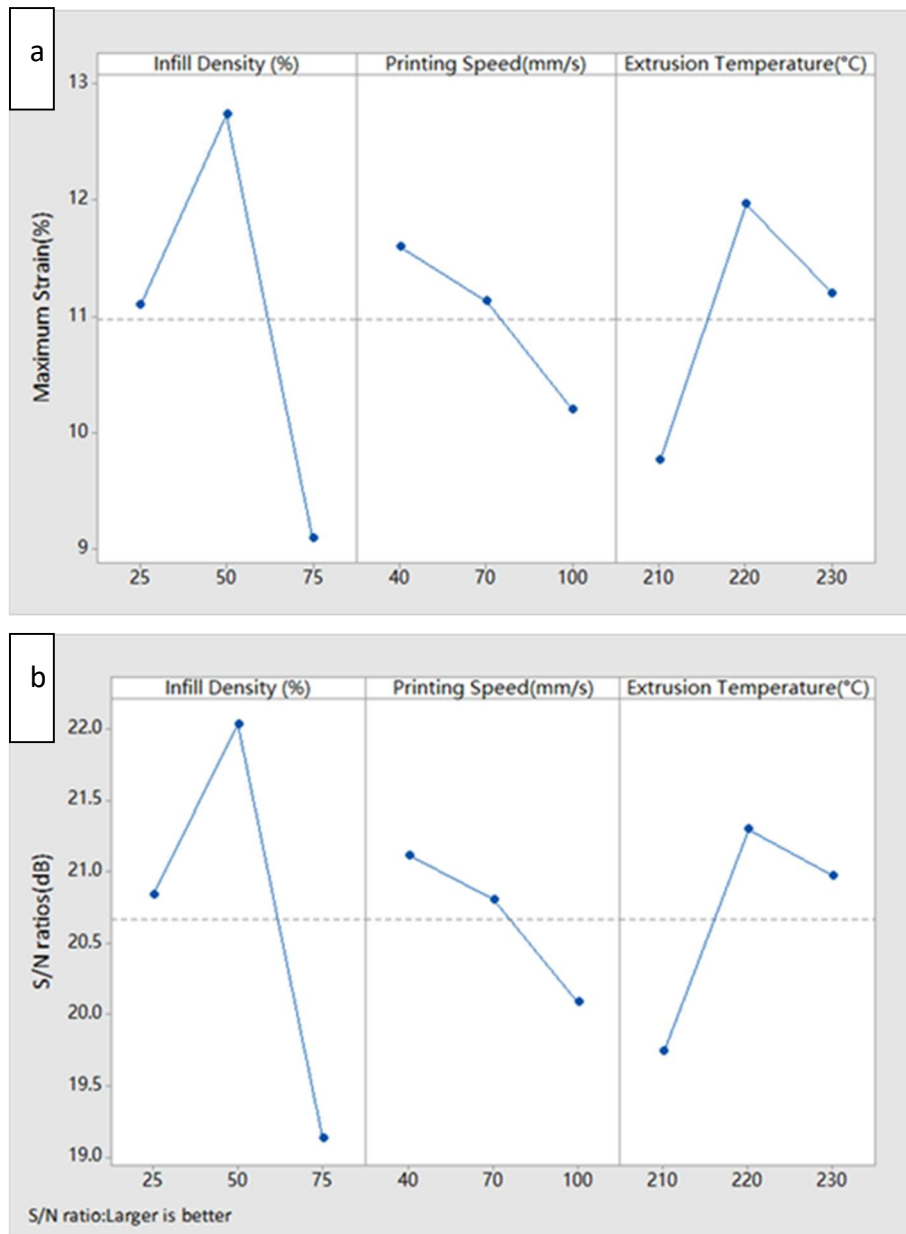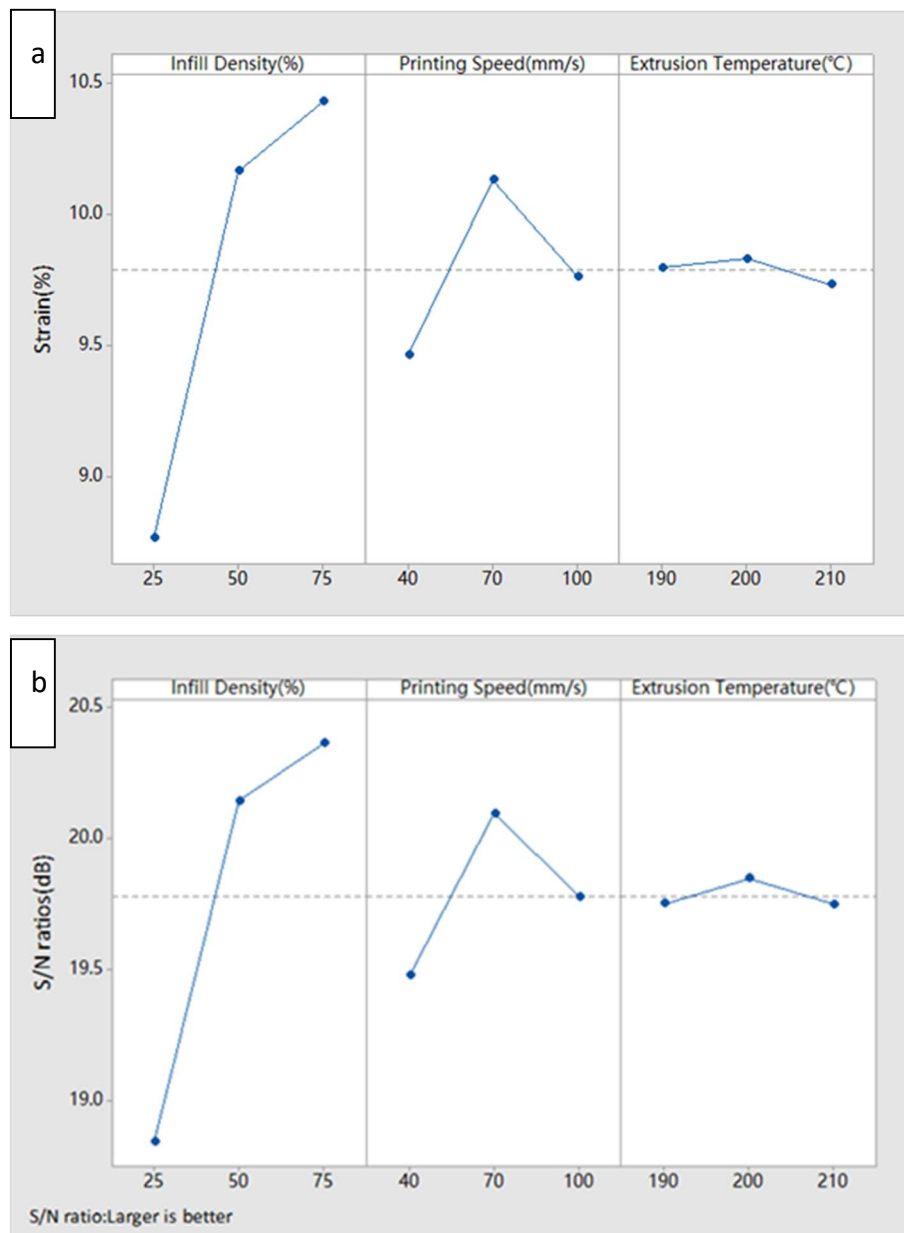

Figure 7-6 Plots of the main effects of the parameters used in PLA pieces on the (a) strain and (b) S/N ratio of the strain, where the dashed line indicates the average result.

7.3 Verification Test

The aforementioned results revealed that the combination of 75 % infill density, 40 mm/s printing speed, and 220 °C extrusion temperature in overprinting stage could result in a finished ABS batch with promising tensile characteristics. In similar, a combination of 75 % infill density, 70 mm/s printing speed, and 210 °C extrusion temperature could lead to a greater tensile strength in PLA pieces. Hence, a verification test was conducted for both pieces to prove the analysis and could be found in Table 7-4.

Table 7-4 Tensile performances for batches in verification test.

	Run	Tensile Strength (MPa)	Young's Modulus (MPa)	Strain (%)
ABS	1	43.6	1021.8	8.8
	2	44.1	984.1	8.1
	3	43.1	1012.3	9.4
	Average	43.6 ± 0.4	1006.1 ± 16	N/A
PLA	1	56.1	1139.4	10.1
	2	55.4	1095.2	10.5
	3	55.8	1172.5	11.2
	Average	55.8 ± 0.3	1135.7 ± 31.7	N/A

The results in verification test found greater tensile performances in comparison with the batches with the greatest tensile properties for both pieces (75-40-230 for ABS batch and 75-70-190 for PLA batch), indicating the improvement of tensile performances benefited from the optimized parameter combination.

7.4 Summary

The IM-FDM hybrid manufacturing of ABS and PLA specimens was investigated in this study. This method was divided into two stages: An iteration of individual material was created using the IM technique, and the material was deposited using the FDM technique, also known as the overprinting technique. This route is opposite to the

extensively studied technique, overmolding, which has offered several advantages for the finished components. Thus, the effect of some key overprinting parameters (infill density, printing speed, and extrusion temperature) on tensile performance was investigated using Taguchi L9 and S/N ratio to determine the possibility of overprinting employed in the future work. Furthermore, other points commonly considered in the manufacturing industry were basically discussed here, such as dimensional accuracy and manufacturing cost. As a result, a total of 54 specimens, 27 ABS specimens and 27 PLA specimens, were first fabricated and tested in this study, with each subjected to three repeated trials.

The first advantage of this overprinting technique in the manufacturing industry is the cost savings at the production stage. The trials in ABS and PLA specimens revealed that the manufacturing costs (time) for producing overprinted samples were half those of FDM samples. This could pave the way for broader acceptance of IM-FDM hybrid manufacturing in the industrial sector. Another positive point identified in this study is the higher dimensional accuracy in finished overprinting batches if compared to the FDM batches. Both characteristics highlight the promising potential of overprinting technique in the competitive market environment, while offering desirable properties via FDM stage.

The tensile performances of two single-material specimens found the PLA specimens produced using the overprinting technique showed more rigidity than ABS ones, which was consistent with IM and FDM specimens in previous studies. Furthermore, when compared to PLA specimens, ABS specimens had greater ductility, which could vary the applications of both specimens.

In terms of the tensile properties of ABS specimens, it has been discovered that increasing the infill density results in higher tensile strength, stiffness (Young's Modulus), and ductility (strain at the fracture). However, increasing the infill density from 25 % to 50 % has no discernible effect on tensile strength. Slow printing speed (40 mm/s) can optimize stiffness and ductility, but 70 mm/s is required for the highest tensile strength. Specimens made at 220 °C have the highest tensile strength and will

degrade if the temperature rises to 230 °C. These may be explained from the following statements: 1. More polymers can be involved in the plastic deformation to withstand the loading; 2. Slow printing speed and a proper extrusion temperature can result in a great reptation, offering a promising degree of fusion between each FDM layer and particularly between the first FDM layer and the IM base (Boros et al., 2019; de Gennes, 2003; Szuchács et al., 2022).

The same phenomenon from infill density can be found in PLA samples, where increasing infill density results in a significant improvement in tensile performance. This is more visible as the infill density increased from low to mid (25 % to 50 %). Furthermore, the optimal printing speed for PLA samples is 70 mm/s, which will provide better tensile performance. Finally, the extrusion temperature has a negligible effect on tensile performance, but it is likely to be 210 °C.

The results for ABS and PLA pieces indicated the varied material employed in the overprinting technique could vary the influence of parameters in the fabrications: 1. Infill density has a more significant impact on the PLA material, whereas ABS is less affected; 2. Similar effects are conducted in the tensile performances for both materials; 3. The extrusion temperature plays a more critical role in ABS pieces compared to PLA pieces, which may due to the higher thermal coefficient of ABS compared to PLA. As a result, the results from both specimens indicate that it is not feasible to optimize all three properties, namely strength, stiffness, and ductility simultaneously. However, for ABS specimens, a combination of 75 % infill density, 40 mm/s printing speed, and 220 °C extrusion temperature is recommended. On the other hand, PLA samples are expected to exhibit excellent tensile performance with 75 % infill density, 70 mm/s printing speed, and 210 °C extrusion temperature.

A verification test based on the analysis for parameters was carried out and found the optimized parameter sets (75-40-220 for ABS batch and 75-70-210 for PLA batch) could result in improved tensile performances for the finished products.

The study shown here builds a foundation on the overprinting technique in engineering aspect. However, more overprinting parameters will be considered in the

future work of this study using the Taguchi's L27 array, which will provide more information on the interactions of manufacturing parameters such as infill pattern and raster angle. Furthermore, in-depth analyses (flexural, compression, and interlayer tests) are required to evaluate the practicality of overprinting batches, while addressing their limitations.

Chapter 8: Conclusion

The main objective of this project was to determine the effect of hybrid manufacturing (HM) combining additive manufacturing (AM) and injection molding (IM) in the finished specimens and the potential feasibility in the future manufacturing industry. The fused deposition modelling (FDM) was selected from the AM techniques due to the high design flexibility, ease in setup and fabrication, low cost and environmental friendliness. In addition, IM technique was employed here since it allows for high-volume fabrications. Thus, the combination of both was carried out in this study and had been processed into two approaches based on the order in the HM: overmolding and overprinting.

The overmolding was first researched here, in which the FDM was utilized first to fabricate the preforms with individual features depending on the parameters employed in the manufacturing process and following with these preforms manually inserted into mold cavity to proceed the overmolding stage. This overmolding technique was studied based on the materials employed, the Acrylonitrile Butadiene Styrene (ABS) and Polylactic Acid (PLA) pieces in Chapter 4 and Chapter 5, respectively. Simultaneously, the dual-material specimens were introduced in Chapter 6 to compare with the single-material specimens shown in Chapter 4 and Chapter 5. The high design flexibility of FDM resulted in the customization feature for all preforms from varied infill density and geometry, while the high-volume characteristic of IM was employed here to allow for minimum manufacturing cost (time), therefore the mass customization can be attained in the finished specimens. These specimens were first compared to the FDM and IM batches and following with the deep analysis in brief based on the varied parameters.

Chapter 7 found another approach of HM in an opposite order, in which we additive manufacture the substances onto the previous IM forms to finish the manufacturing. Three parameters of FDM were varied to determine their effect on the performances of finished specimens. These parameters include extrusion temperature, printing speed, and layer thickness, all of which have been deeply researched and displayed their effect in the FDM-fabricated specimens. The objective of this chapter

was to figure out the effect of these parameters in the finished specimens and compare them to the overmolded specimens, obtaining the specific pros and cons for both approaches.

Manufacturing time is the first topic discussed for all fabricated batches since the low production volume is one tough characteristic for FDM technique, restricting the future applicability, whereas this can be greatly addressed using IM processing. A single tensile specimen fabricated using FDM taking an average of 6 min for PLA pieces and 12 min for ABS pieces to build, depending on processing parameters, particularly infill density, whereas the IM process fabricates two specimens in 1.5 min (this is the molding cycle length). As for the hybrid manufactured specimens, the current HM method took half time in finish the fabrications for hybrid manufactured specimens, indicating that HM manufacturing shows a greater business efficiency than FDM in the future industry.

The dimension accuracy is another section studied here since the stair-step effect in FDM processing results in the poor dimension of finished specimens, while IM allows for a high precision in the manufactured products. As can be found in the studies shown in the previous four chapters, specimens fabricated using both approaches showed a greater dimension precision if compared to the FDM products, which indicate the high dimension effect from hybrid manufacturing.

A comparison between the tensile performances of FDM, IM, and hybrid manufactured specimens are investigated, in which the IM samples surpassed other samples due to the nature of the IM process, which results in strong material compaction and enhanced internal morphology.

The high design flexibility from FDM results in varied features of preforms employed in the overmolding technique and therefore affecting the performances of finished specimens, emphasizing the ease in tailored features from this HM technique:

For ABS and PLA pieces, specimens fabricated using HM can be categorized into two series: half-length (HL) specimens that were overmolded at a single mid-point along the finished sample, and half-thickness (HT) series samples that occurred along

the entire length of the substrate.

The tensile performances of these finished specimens showed an anisotropic behaviour between the HL-series and HT-series specimens, which is resulted from the fusion direction and tensile loading. For the HL series samples, the tensile load was loaded perpendicular to the interface, leading to an inter-layer failure. In these cases, interfaces between the inserts and overmolded parts withstood most tensile loadings, leading to the low strain values and brittle behaviours. However, there showed an opposite reaction in HT series specimens, the interface directions were parallel to the tensile loading for these samples, resulting in a trans-layer failure, in which several breakages can be found since the materials were applied to withstand the tensile loading.

One parameter employed in the fabrication of FDM preforms, infill density, refers to the quantity of material utilized to fill the interior region of a layer, which is a critical parameter applied in FDM technique since it affects manufacturing time and mechanical performance. Hence, infill density is considered in this study to determine its effect in HM samples, therefore it is first briefly discussed here in function of specimen categories:

Regarding to the ABS pieces, a medium (50 %) infill density of FDM preforms results in the greatest tensile performance of finished HT-series specimens due to the good flexibility of ABS material, while a low infill density of preform (25 %) contributes to a greater tensile behaviour in HL-series samples since more material can be injected to the preforms to finish the manufacturing thus decreasing the pores in the joining area. In case of PLA pieces, the FDM inserts with higher infill density were provided better internal structure than those with lower infill. The higher-infill inserts could produce stronger molecular bonding compared with those inserts with lower infill density, resulting in better joining between FDM inserts and injection-molded polymer. In addition, the damage to the FDM insert caused by injection-molded material in the HL-NJ 25 manufacturing process indicates worse mechanical performance in specimens with lower infill density and low infill density preforms could not withstand

the compressive forces of the injection molding volume during manufacturing. Meanwhile, the FDM technique had resulted in void and uneven distribution of molten polymer for the internal structure of FDM area during the 3D printing process, drawing low interlaminar adhesion for FDM parts, which supported that the lower-infill density FDM samples provided worse mechanical properties. Thus, the infill density of preforms can be controlled by FDM and therefore affect the performance of finished specimens.

Furthermore, the outstanding design feasibility brought from FDM technique allows for customization in the preforms and thus the overmolded specimens with unique feel, action, and shape can be attained, which can be found in the batches of specimens with several joint configurations fabricated in the study. Two main joint configuration direction are displayed here, the male and female type with cube and T type, resulting in following interactions: male cube, female cube, male T, and female T in HT-series, whereas extra few batches designed in HL-series specimens.

The findings of studies in ABS and PLA pieces agree with a female joint configuration can be attributed to a greater tensile performance but disagree in female T specimens exhibiting a higher maximum tensile strength for ABS specimens, while female cube specimens performing better for PLA pieces. This phenomenon can be explained from the following claims: 1. female joint configuration would offer stronger mechanical interlock based on the overmolding processing than the male cube; 2. more contact areas can be found in female joint configuration compared to the male one (Kuznetsov et al., 2018b; Ribeiro et al., 2019; Wicaksono et al., 2017). However, a difference in tensile performance can be displayed from the varied joint configuration, in which a cube type leads to a greater behaviour in PLA specimens, while a T joint results in a better tensile performance in ABS pieces, which is caused of T joint configuration resulting in a worse fusion bond from the overmolding stage due to the greater quantity of pores in PLA pieces and therefore the stress concentration would easily occur in the period of tensile loading. However, the high ductility of ABS material benefits the contact with FDM preforms therefore more contact area would result in

greater mechanical locking and thus an enhanced tensile property can be found.

Moreover, the IM pressure utilized in the overmolding stage is varied in the fabrication of dual-material specimens to determine the effect of pressure in the finished specimens. It was discovered that the maximum tensile stress in specimens overmolded under 60 bar is greater than that in specimens overmolded at 100 bar, indicating a proper IM pressure should be considered in the manufacturing, allowing for a minimum waste. Furthermore, low tensile strengths can be found in dual material specimens when compared to ABS and PLA specimens, with a 2 % decrease compared to ABS but a 20 % decrease compared to PLA due to poor contact between the PLA and ABS material.

Regarding to the phenomenon in overprinting technique, it shows a similar behaviour in manufacturing cost decrease exhibits its first benefit in the manufacturing industry, the cost saving in production stage (a half manufacturing time compared to the FDM one), which popularizes this approach in manufacturing industry. As for the tensile performance, it can be found a combination of 75 % infill density, 40 mm/s printing speed, and 220 °C extrusion temperature results in an ideal tensile performance for ABS pieces, while the settings of 75 % infill density, 70 mm/s printing speed, and 210 °C extrusion temperature are expected to fabricate the samples with excellent tensile performance for PLA samples, which are in line with the effect of these parameters in the FDM products, expanding the potential fields of this overprinting technique employed in the manufacturing industry.

Chapter 9: Future work and recommendations

This PhD project tends to investigate the possibility of hybrid manufacturing combining fused deposition modelling (FDM) and injection molding (IM) in the high-volume production of specimens with bespoken features. In this content, the work displayed herein satisfied this purpose and offered significant venues for utilizing a novel manufacturing processing and approach in the production of specimens in customer-tailored manner. However, some limitations can be determined in this study. Some suggestions have been indicated in the following paragraphs to expand the appliances of this project.

One of the most significant approaches in this hybrid manufacturing technique for the employment in manufacturing industry is a proper manufacturing setup, which produces mold efficiently with high design flexibility. The mold fabrication has always been a challenging aspect of setup owing to the several factors that must be considered, including high cost in start up and design changes and long initial lead times. Further investigation on the potential employment of Stereolithography (SLA), another technology of additive manufacturing via solidifying photocurable resin, in the mold design and production, with which more finished specimens can be fabricated using this hybrid manufacturing due to the high design flexibility of SLA technique and short time in mold fabrications. At the meantime, more tests, such as flexural test, compressive test, interlayer test can be introduced in the assessment of the characteristics for the finished specimens, expanding the fields that can be exploited in the finished items. In the stage of fabrication, other technologies of additive manufacturing with higher resolution, such as Arburg Plastics Freeforming (APF) and SLA, can be employed in fabricating preforms in overmolding technique or the second stage of overprinting technique, offering advanced precisions for the finished specimens.

Future work can expand to higher design flexibility in fabricating preforms employed in overmolding technique, such as structural arrangement design and multi-material possibility, allowing for a greater degree of mass customization and flexibility. In addition, some reinforced polymers can be utilized in this hybrid manufacturing

164

technique to enhance the characteristics of finished specimens, allowing for greater quality in finished products. In terms of the recommendations in overprinting technique, the possibility of multiple materials employed in a single specimen can be observed in the future to expand the availability of overprinting in the manufacturing industry. Furthermore, an exploration of combining overmolding and overprinting techniques with enhanced interlayer strength remains exploitable for researchers, in particular for the finished single polymer matrixes with several interfaces allowing for a higher degree of mass customization. Another potential avenue for further investigation lies in exploring the potential of metal-polymer hybrid structures, which could offer enhanced properties and reduced weight in the finished matrix.

The study shown in this literature demonstrates the effects of this hybrid manufacturing in the finished specimens while offering mass customization, it is my hope that this approach can be extensively employed to manufacture items with high degree of design flexibility and mechanical characteristics.

Reference

Ageyeva, T., Kovács, J. G., & Tábi, T. (2022). Comparison of the efficiency of the most effective heterogeneous nucleating agents for Poly(lactic acid). *Journal of Thermal Analysis and Calorimetry*, *147*(15), 8199–8211. https://doi.org/10.1007/s10973-021-11145-y

Ahn, S. H., Montero, M., Odell, D., Roundy, S., & Wright, P. K. (2002). Anisotropic material properties of fused deposition modeling ABS. *Rapid Prototyping Journal*, *8*(4), 248–257. https://doi.org/10.1108/13552540210441166

Aigbedo, H. (2007). An assessment of the effect of mass customization on suppliers' inventory levels in a JIT supply chain. *European Journal of Operational Research*, *181*(2), 704–715. https://doi.org/10.1016/j.ejor.2006.06.037

Akessa, A., Lemu, H., & Gebisa, A. (2017). *Mechanical Property Characterization of Additive Manufactured ABS Material Using Design of Experiment Approach*. https://doi.org/10.1115/IMECE2017-70144

Akué Asséko, A. C., Cosson, B., Lafranche, É., Schmidt, F., & Le Maoult, Y. (2016). Effect of the developed temperature field on the molecular interdiffusion at the interface in infrared welding of polycarbonate composites. *Composites Part B: Engineering*, *97*, 53–61. https://doi.org/https://doi.org/10.1016/j.compositesb.2016.04.064

Alafaghani, A., & Qattawi, A. (2018). Investigating the effect of fused deposition modeling processing parameters using Taguchi design of experiment method. *Journal of Manufacturing Processes*, *36*(September), 164–174. https://doi.org/10.1016/j.jmapro.2018.09.025

Alafaghani, A., Qattawi, A., Alrawi, B., & Guzman, A. (2017). Experimental Optimization of Fused Deposition Modelling Processing Parameters:

A Design-for-Manufacturing Approach. *Procedia Manufacturing*, *10*, 791–80
3. https://doi.org/10.1016/j.promfg.2017.07.079

Alford, D., Sackett, P., & Nelder, G. (2000). Mass customization - an automotive perspective. *International Journal of Production Economics*, *65* (1), 99–110. https://doi.org/10.1016/S0925-5273(99)00093-6

Alrashdan, A., Wright, W. J., & Celik, E. (2020, November 16). Light Assisted Hybrid Direct Write Additive Manufacturing of Thermosets. *Volume 2A: Advanced Manufacturing*. https://doi.org/10.1115/IMECE2020-24525

Additive manufacturing — General principles — Fundamentals and v ocabulary, (2021).

Anandkumar, R., Ramesh Babu, S., & Sathyamurthy, R. (2021). Investi gations on the Mechanical Properties of Natural Fiber Granulated Compo site Using Hybrid Additive Manufacturing: A Novel Approach. *Advances in Materials Science and Engineering*, *2021*. https://doi.org/10.1155/2021/55 36171

Andreu, A., Kim, S., Dittus, J., Friedmann, M., Fleischer, J., & Yoon, Y. J. (2022). Hybrid material extrusion 3D printing to strengthen interlaye r adhesion through hot rolling. *Additive Manufacturing*, *55*. https://doi.org /10.1016/j.addma.2022.102773

Anitha, R., Arunachalam, S., & Radhakrishnan, P. (2001). Critical para meters influencing the quality of prototypes in fused deposition modellin g. *Journal of Materials Processing Technology*, *118*(1–3), 385–388. https:// doi.org/10.1016/S0924-0136(01)00980-3

Araghi, B. T., Manco, G. L., Bambach, M., & Hirt, G. (2009). Investig ation into a new hybrid forming process: Incremental sheet forming com bined with stretch forming. *CIRP Annals - Manufacturing Technology*, *58* (1), 225–228. https://doi.org/10.1016/j.cirp.2009.03.101

Araújo, M. R. P., Sa-Barreto, L. L., Gratieri, T., Gelfuso, G. M., & Cu nha-Filho, M. (2019). The digital pharmacies era: How 3D printing techno

logy using fused deposition modeling can become a reality. *Pharmaceutic s, 11*(3). https://doi.org/10.3390/pharmaceutics11030128

Arif, M. F., Kumar, S., Varadarajan, K. M., & Cantwell, W. J. (2018). Performance of biocompatible PEEK processed by fused deposition additiv e manufacturing. *Materials and Design*, *146*, 249–259. https://doi.org/10.1 016/j.matdes.2018.03.015

Aspinwall, D. K., Dewes, R. C., Burrows, J. M., & Paul, M. A. (2001). Hybrid high speed machining (HSM): System design and experimental re sults for grinding / HSM and EDM / HSM. *CIRP Annals - Manufacturing Technology*, *50*(1), 145–148. https://doi.org/10.1016/S0007-8506(07)62091-5

Auras, R. A., Harte, B., Selke, S., & Hernandez, R. (2003). Mechanica l, Physical, and Barrier Properties of Poly(Lactide) Films. *Journal of Plastic Film & Sheeting*, *19*(2), 123–135. https://doi.org/10.1177/8756087903039 702

B Joseph I I, P. (1993). *Mass customization: the new frontier in busi ness competition*. *32*(1).

Baich, L., Manogharan, G., & Marie, H. (2015). Study of infill print design on production cost-time of 3D printed ABS parts. *International Jo urnal of Rapid Manufacturing*, *5*(3/4), 308. https://doi.org/10.1504/ijrapid m.2015.074809

Baranowski, M., Netzer, M., Gönnheimer, P., Coutandin, S., Fleischer, J., Schlotthauer, T., & Middendorf, P. (2022). Functional Integration of Su bcomponents for Hybridization of Fused Filament Fabrication. *International Journal of Mechanical Engineering and Robotics Research*, *11*(5), 319–32 5. https://doi.org/10.18178/ijmerr.11.5.319-325

Barlow, J., Childerhouse, P., Gann, D., Hong-Minh, S., Naim, M., & O zaki, R. (2003). Choice and delivery in housebuilding: Lessons from Japan for UK housebuilders. *Building Research and Information*, *31*(2), 134–145. https://doi.org/10.1080/09613210302003

Bastien, L. J., & Gillespie Jr., J. W. (1991). A non-isothermal healing model for strength and toughness of fusion bonded joints of amorphous thermoplastics. *Polymer Engineering & Science*, *31*(24), 1720–1730. https://doi.org/https://doi.org/10.1002/pen.760312406

Bernasconi, R., Hatami, D., Hosseinabadi, H. N., Zega, V., Corigliano, A., Suriano, R., Levi, M., Langfelder, G., & Magagnin, L. (2022). Hybrid additive manufacturing of a piezopolymer-based inertial sensor. *Additive Manufacturing*, *59*, 103091. https://doi.org/https://doi.org/10.1016/j.addma.2022.103091

Birosz, M. T., Ledenyák, D., & Andó, M. (2022). Effect of FDM infill patterns on mechanical properties. *Polymer Testing*, *113*, 107654. https://doi.org/10.1016/j.polymertesting.2022.107654

Boland, M. (2008). Innovation in the food industry: Personalised nutrition and mass customisation. *Innovation: Management, Policy and Practice*, *10*(1), 53–60. https://doi.org/10.5172/impp.453.10.1.53

Boros, R., Kannan Rajamani, P., & Kovács, J. G. (2019). Combination of 3D printing and injection molding: Overmolding and overprinting. *Express Polymer Letters*, *13*(10), 889–897. https://doi.org/10.3144/expresspolymlett.2019.77

Braconnier, D. J., Jensen, R. E., & Peterson, A. M. (2019). Processing Parameter Correlations in Material Extrusion Additive Manufacturing. *Additive Manufacturing*, 100924. https://doi.org/10.1016/j.addma.2019.100924

Bryce, D. M. (1996). Plastic Injection Molding ...manufacturing process fundamentals. In D. Peterson (Ed.), *Fundamentals of Injection Molding: Vol. I*. Society of Manufacturing Engineers.

Byberg, K. I., Gebisa, A. W., & Lemu, H. G. (2018). Mechanical properties of ULTEM 9085 material processed by fused deposition modeling. *Polymer Testing*, *72*(August), 335–347. https://doi.org/10.1016/j.polymertesting.2018.10.040

Campo, E. A. (2006). *The Complete Part Design Handbook* (E. A. B. T.-C. P. D. H. Campo, Ed.; pp. I–XXI). Hanser. https://doi.org/https://doi.org/10.3139/9783446412927.fm

Cao, Z., Daly, M., Clémence, L., Geever, L. M., Major, I., Higginbotham, C. L., & Devine, D. M. (2016). Chemical surface modification of calcium carbonate particles with stearic acid using different treating methods. *Applied Surface Science*, *378*, 320–329. https://doi.org/10.1016/j.apsusc.2016.03.205

Casavola, C., Cazzato, A., Moramarco, V., & Pappalettere, C. (2016). Orthotropic mechanical properties of fused deposition modelling parts described by classical laminate theory. *Materials and Design*, *90*, 453–458. https://doi.org/10.1016/j.matdes.2015.11.009

Chacón, J. M., Caminero, M. A., García-Plaza, E., & Núñez, P. J. (2017). Additive manufacturing of PLA structures using fused deposition modelling: Effect of process parameters on mechanical properties and their optimal selection. *Materials and Design*, *124*, 143–157. https://doi.org/10.1016/j.matdes.2017.03.065

Chen, P., Wu, H., Zhu, W., Yang, L., Li, Z., Yan, C., Wen, S., & Shi, Y. (2018). Investigation into the processability, recyclability and crystalline structure of selective laser sintered Polyamide 6 in comparison with Polyamide 12. *Polymer Testing*, *69*(April), 366–374. https://doi.org/10.1016/j.polymertesting.2018.05.045

Christiyan, K. G. J., Chandrasekhar, U., & Venkateswarlu, K. (2016). A study on the influence of process parameters on the Mechanical Properties of 3D printed ABS composite. *IOP Conference Series: Materials Science and Engineering*, *114*(1). https://doi.org/10.1088/1757-899X/114/1/012109

Chueh, Y. H., Wei, C., Zhang, X., & Li, L. (2019). Integrated laser-based powder bed fusion and fused filament fabrication for three-dimension

al printing of hybrid metal/polymer objects. *Additive Manufacturing*. https://doi.org/10.1016/j.addma.2019.100928

Cooke MN, Fisher JP, Dean D, Rimnac C, M. AG. (2003). Use of stereolithography to manufacture critical-sized 3D biodegradable scaffolds for bone ingrowth. *J Biomed Mater Res B Appl Biomater*, *64B*(2), 65–69.

Cooperstein, I., Layani, M., & Magdassi, S. (2015). 3D printing of porous structures by UV-curable O/W emulsion for fabrication of conductive objects. *J. Mater. Chem. C*, *3*(9), 2040–2044. https://doi.org/10.1039/C4TC02215G

Crump, S. (1992). Apparatus and method for creating three-dimensional objects Available at: https://patents.google.com/patent/US5121329A/en. *United States Patent*, *19*, 15. https://doi.org/10.2116/bunsekikagaku.28.3_195

Curtis, D. T., Soo, S. L., Aspinwall, D. K., & Sage, C. (2009). Electrochemical superabrasive machining of a nickel-based aeroengine alloy using mounted grinding points. *CIRP Annals - Manufacturing Technology*, *58*(1), 173–176. https://doi.org/10.1016/j.cirp.2009.03.074

Czink, S., Lubkowitz, V., Dietrich, S., & Schulze, V. (2023). Process development for the hybrid additive manufacturing of metallic structures on polymer substrates. *Additive Manufacturing Letters*, 100132. https://doi.org/10.1016/j.addlet.2023.100132

Da Silveira, G., Borenstein, D., & Fogliatto, F. S. (2001). Mass customization: Literature review and research directions. *International Journal of Production Economics*, *72*(1), 1–13. https://doi.org/10.1016/S0925-5273(00)00079-7

Dai, R., & Zou, M. (2002). The cooling time calculation of plastics product in the injection model. *Modern Plastics Processing and Applications*, *15*(1), 24–26.

Dalgarno, K., Stewart, T., & Allport, J. (2001). Layer manufactured pr

oduction tooling incorporating conformal heating channels for transfer mo ulding of elastomer compounds. *Plastics, Rubber and Composites*, *30*, 384 –388. https://doi.org/10.1179/146580101101541778

Dandekar, C. R., Shin, Y. C., & Barnes, J. (2010). Machinability impro vement of titanium alloy (Ti-6Al-4V) via LAM and hybrid machining. *Inter national Journal of Machine Tools and Manufacture*, *50*(2), 174–182. http s://doi.org/10.1016/j.ijmachtools.2009.10.013

Datta, R., & Henry, M. (2006). Lactic Acid: Recent Advances in Prod ucts, Processes and Technologies A Review. *Journal of Chemical Technolog y & Biotechnology*, *81*, 1119–1129. https://doi.org/10.1002/jctb.1486

Davis, S. M. (1989). From "future perfect": Mass customizing. *Planni ng Review*, *17*(2), 16–21. https://doi.org/10.1108/eb054249

Dawoud, M., Taha, I., & Ebeid, S. J. (2016). Mechanical behaviour of ABS: An experimental study using FDM and injection moulding techniqu es. *Journal of Manufacturing Processes*, *21*, 39–45. https://doi.org/10.1016 /j.jmapro.2015.11.002

de Gennes, P. G. (2003). Reptation of a Polymer Chain in the Prese nce of Fixed Obstacles. *The Journal of Chemical Physics*, *55*(2), 572–579. https://doi.org/10.1063/1.1675789

de Hazan, Y., Thänert, M., Trunec, M., & Misak, J. (2012). Robotic d eposition of 3d nanocomposite and ceramic fiber architectures via UV cu rable colloidal inks. *Journal of the European Ceramic Society*, *32*(6), 1187 –1198. https://doi.org/10.1016/j.jeurceramsoc.2011.12.007

De Marzi, A., Giometti, G., Erler, J., Colombo, P., & Franchin, G. (20 22). Hybrid additive manufacturing for the fabrication of freeform transpa rent silica glass components. *Additive Manufacturing*, *54*, 102727. https:// doi.org/https://doi.org/10.1016/j.addma.2022.102727

Deng, X., Zeng, Z., Peng, B., Yan, S., & Ke, W. (2018). Mechanical p roperties optimization of poly-ether-ether-ketone via fused deposition mod

eling. *Materials*, *11*(2). https://doi.org/10.3390/ma11020216

Deradjat, D., & Minshall, T. (2017). Implementation of rapid manufac turing for mass customisation. *Journal of Manufacturing Technology Mana gement*, *28*(1), 95–121. https://doi.org/10.1108/JMTM-01-2016-0007

Deshpande, S., Rao, N., Pradhan, N., & Irwin, J. L. (2016). Hybrid Po lymer Additive Manufacturing of a Darrieus type Vertical Axis Wind Turbi ne Design to improve power generation efficiency. *Proceedings of the AS ME 2016 International Mechanical Engineering Congress and Exposition*, 1 1–17. http://proceedings.asmedigitalcollection.asme.org/pdfaccess.ashx?url=/ data/conferences/asmep/90978/

Dizon, J. R. C., Espera, A. H., Chen, Q., & Advincula, R. C. (2018). Mechanical characterization of 3D-printed polymers. *Additive Manufacturin g*, *20*, 44–67. https://doi.org/10.1016/j.addma.2017.12.002

Domingo-Espin, M., Puigoriol-Forcada, J. M., Garcia-Granada, A. A., Ll umà, J., Borros, S., & Reyes, G. (2015). Mechanical property characterizat ion and simulation of fused deposition modeling Polycarbonate parts. *Ma terials and Design*, *83*, 670–677. https://doi.org/10.1016/j.matdes.2015.06.0 74

Douglas C. Montgomery. (2009). *Design and analysis of experiments* (7th ed.). John Wiley&Sons,Inc. https://books.google.ie/books?hl=en&lr=&id =Py7bDgAAQBAJ&oi=fnd&pg=PA1&ots=X6u5nZQO38&sig=gCEmb_RmhxCOIXLd vNAG6nH3g5o&redir_esc=y#v=onepage&q&f=false

Drummer, D., Cifuentes-Cuéllar, S., & Rietzel, D. (2012). Suitability of PLA/TCP for fused deposition modeling. *Rapid Prototyping Journal*, *18*(6), 500–507. https://doi.org/10.1108/13552541211272045

Duray, R. (2002). Mass customization origins: mass or custom manuf acturing? *International Journal of Operations & Production Management*, *22*(3), 314–328. https://doi.org/10.1108/01443570210417614

Durgun, I., & Ertan, R. (2014). Experimental investigation of FDM pr

ocess for improvement of mechanical properties and production cost. *Rapid Prototyping Journal*, *20*(3), 228–235. https://doi.org/10.1108/RPJ-10-2012-0091

Ebel, E., & Sinnemann, T. (2014). Fabrication of FDM 3D objects with ABS and PLA and determination of their mechanical properties. *RTejournal*. https://www.rtejournal.de/ausgabe11/3872

Englert, L., Heuer, A., Engelskirchen, M. K., Frölich, F., Dietrich, S., Liebig, W. V., Kärger, L., & Schulze, V. (2022). Hybrid material additive manufacturing: interlocking interfaces for fused filament fabrication on laser powder bed fusion substrates. *Virtual and Physical Prototyping*, *17*(3), 508–527. https://doi.org/10.1080/17452759.2022.2048228

Eslami, H., & Grmela, M. (2008). Mesoscopic formulation of reptation. *Rheologica Acta*, *47*(4), 399–415. https://doi.org/10.1007/s00397-007-0239-y

Faes, M., Vleugels, J., Vogeler, F., & Ferraris, E. (2016). Extrusion-based additive manufacturing of ZrO2 using photoinitiated polymerization. *CIRP Journal of Manufacturing Science and Technology*, *14*, 28–34. https://doi.org/10.1016/j.cirpj.2016.05.002

Falck, R., & Amancio-Filho, S. T. (2022). The Influence of Coating and Adhesive Layers on the Mechanical Performance of Additively Manufactured Aluminum–Polymer Hybrid Joints. *Metals*, *13*(1), 34. https://doi.org/10.3390/met13010034

Falck, R., dos Santos, J. F., & Amancio-Filho, S. T. (2019). Microstructure and mechanical performance of additively manufactured aluminum 2024-t3/acrylonitrile butadiene styrene hybrid joints using an addjoining technique. *Materials*, *16*(6). https://doi.org/10.3390/ma12060864

Falck, R., Goushegir, S. M., dos Santos, J. F., & Amancio-Filho, S. T. (2018). AddJoining: A novel additive manufacturing approach for layered metal-polymer hybrid structures. *Materials Letters*, *217*, 211–214. https://

doi.org/10.1016/j.matlet.2018.01.021

Feldhausen, T., Raghavan, N., Saleeby, K., Love, L., & Kurfess, T. (202
1). Mechanical properties and microstructure of 316L stainless steel prod
uced by hybrid manufacturing. *Journal of Materials Processing Technology*,
290(August 2020), 116970. https://doi.org/10.1016/j.jmatprotec.2020.1169
70

Fernandez, E., Edeleva, M., Fiorio, R., Cardon, L., & D'Hooge, D. R.
(2022). Increasing the Sustainability of the Hybrid Mold Technique throug
h Combined Insert Polymeric Material and Additive Manufacturing Metho
d Design. *Sustainability (Switzerland)*, *14*(2). https://doi.org/10.3390/su1402
0877

Fernandez-Vicente, M., Calle, W., Ferrandiz, S., & Conejero, A. (2016).
Effect of Infill Parameters on Tensile Mechanical Behavior in Desktop 3D
Printing. *3D Printing and Additive Manufacturing*, *3*(3), 183–192. https://
doi.org/10.1089/3dp.2015.0036

Florian, M. (2016). *Plastics Resin Production and Consumption in 63
Countries*. *October 2016*, 80.

Fogliatto, F. S., Da Silveira, G. J. C., & Borenstein, D. (2012). The m
ass customization decade: An updated review of the literature. *Internatio
nal Journal of Production Economics*, *138*(1), 14–25. https://doi.org/10.101
6/j.ijpe.2012.03.002

Fuenmayor, E., Donnell, C. O., Gately, N., Doran, P., Devine, D. M., L
yons, J. G., Mcconville, C., & Major, I. (2019). Mass-customization of oral
tablets via the combination of 3D printing and injection molding. *Intern
ational Journal of Pharmaceutics*, *569*(July), 118611. https://doi.org/10.101
6/j.ijpharm.2019.118611

Fuenmayor, E., Forde, M., Healy, A. V., Devine, D. M., Lyons, J. G.,
McConville, C., & Major, I. (2018). Material considerations for fused-filam
ent fabrication of solid dosage forms. *Pharmaceutics*, *10*(2), 1–27. https:/

/doi.org/10.3390/pharmaceutics10020044

Fuenmayor, E., Forde, M., Healy, A. V., Devine, D. M., Lyons, J. G., McConville, C., & Major, I. (2019). Comparison of fused-filament fabricati on to direct compression and injection molding in the manufacture of or al tablets. *International Journal of Pharmaceutics*, *558*(November 2018), 3 28–340. https://doi.org/10.1016/j.ijpharm.2019.01.013

Gackowski, B. M., Phua, H., Sharma, M., & Idapalapati, S. (2022). H ybrid additive manufacturing of polymer composites reinforced with buck ypapers and short carbon fibres. *Composites Part A: Applied Science and Manufacturing*, *154*. https://doi.org/10.1016/j.compositesa.2021.106794

Gao, W., Zhang, Y., Ramanujan, D., Ramani, K., Chen, Y., Williams, C. B., Wang, C. C. L., Shin, Y. C., Zhang, S., & Zavattieri, P. D. (2015). The status, challenges, and future of additive manufacturing in engineering. *CAD Computer Aided Design*, *69*, 65–89. https://doi.org/10.1016/j.cad.2015. 04.001

Gebisa, A. W., & Lemu, H. G. (2019a). Effect of Process Parameters on Compressive Properties of ULTEM 9085 Produced by FDM Process. *Pr ocedia Manufacturing*, *30*, V002T02A056. https://doi.org/10.1115/imece201 8-87523

Gebisa, A. W., & Lemu, H. G. (2019b). Influence of 3D printing FDM process parameters on tensile property of ultem 9085. *Procedia Manufa cturing*, *30*, 331–338. https://doi.org/10.1016/j.promfg.2019.02.047

Ghosh, S., Viana, J., Reis, R. L., & Mano, J. F. (2008). Development of porous lamellar poly(L-lactic acid) scaffolds by conventional injection m olding process. *Acta Biomaterialia*, *4*, 887–896. https://doi.org/10.1016/j.ac tbio.2008.03.001

Giannatsis, J., & Dedoussis, V. (2009). Additive fabrication technologie s applied to medicine and health care: A review. *International Journal of Advanced Manufacturing Technology*, *40*(1–2), 116–127. https://doi.org/10.

1007/s00170-007-1308-1

Giorleo, L., Stampone, B., & Trotta, G. (2022). Micro injection mould ing process with high-temperature resistance resin insert produced with material jetting technology: Effect of part orientation. *Additive Manufactu ring*, *56*, 102947. https://doi.org/https://doi.org/10.1016/j.addma.2022.1029 47

Giusti, R., & Lucchetta, G. (2020). Modeling the adhesion bonding st rength in injection overmolding of polypropylene parts. *Polymers*, *12*(9). https://doi.org/10.3390/POLYM12092063

Gomes, M., Ribeiro, A., Malafaya, P., Reis, R. L., & Cunha, A. (2001). A new approach based on injection moulding to produce biodegradable starch-based polymeric scaffolds: Morphology, mechanical and degradation behaviour. *Biomaterials*, *22*, 883–889. https://doi.org/10.1016/S0142-9612(0 0)00211-8

Govender, R. (2021). *Integrated product and process design for mass customization: a road towards patient access to individualized pharmaceut ical therapy*. Chalmers University of Technology.

Goyanes, A., Robles Martinez, P., Buanz, A., Basit, A. W., & Gaisford, S. (2015a). Effect of geometry on drug release from 3D printed tablets. *International Journal of Pharmaceutics*, *494*(2), 657–663. https://doi.org/10. 1016/j.ijpharm.2015.04.069

Goyanes, A., Robles Martinez, P., Buanz, A., Basit, A. W., & Gaisford, S. (2015b). Effect of geometry on drug release from 3D printed tablets. *International Journal of Pharmaceutics*, *494*(2), 657–663. https://doi.org/10. 1016/j.ijpharm.2015.04.069

Goyanes, A., Scarpa, M., Kamlow, M.-A., Gaisford, S., Basit, A., & Orl u, M. (2017). Patient acceptability of 3D printed medicines. *International Journal of Pharmaceutics*, *530*. https://doi.org/10.1016/j.ijpharm.2017.07.06 4

Grand View Research. (2020). *Injection Molding Market Size, Share & Trends Analysis Report By Material*.

Grewell, D., & Benatar, A. (2008). Semi-empirical, squeeze flow and intermolecular diffusion model. I. Determination of model parameters. *Polymer Engineering & Science*, *48*(5), 860–867. https://doi.org/https://doi.org/10.1002/pen.21021

Grujicic, M., Sellappan, V., Arakere, G., Seyr, N., & Erdmann, M. (2008). Computational feasibility analysis of direct-adhesion polymer-to-metal hybrid technology for load-bearing body-in-white structural components. *Journal of Materials Processing Technology*, *195*(1–3), 282–298. https://doi.org/10.1016/j.jmatprotec.2007.05.016

Grujicic, M., Sellappan, V., Kotrika, S., Arakere, G., Obieglo, A., Erdmann, M., & Holzleitner, J. (2009). Suitability analysis of a polymer-metal hybrid technology based on high-strength steels and direct polymer-to-metal adhesion for use in load-bearing automotive body-in-white applications. *Journal of Materials Processing Technology*, *209*(4), 1877–1890. https://doi.org/10.1016/j.jmatprotec.2008.04.050

Gu, X., & Koren, Y. (2018). Manufacturing system architecture for cost-effective mass-individualization. *Manufacturing Letters*, *16*, 44–48. https://doi.org/10.1016/j.mfglet.2018.04.002

Hart, C. (1995). Mass Customization: conceptual underpinnings, opportunities and limits. *International Journal of Service Industry Management*, *6*, 36–45. https://doi.org/10.1108/09564239510084932

Hashemi Sanatgar, R., Campagne, C., & Nierstrasz, V. (2017). Investigation of the adhesion properties of direct 3D printing of polymers and nanocomposites on textiles: Effect of FDM printing process parameters. *Applied Surface Science*, *403*, 551–563. https://doi.org/10.1016/j.apsusc.2017.01.112

Haugen, H., Will, J., Fuchs, W., & Wintermantel, E. (2006). A novel

processing method for injection-molded polyether-urethane scaffolds. Part 1: Processing. *Journal of Biomedical Materials Research - Part B Applied Biomaterials*, *77*(1), 65–72. https://doi.org/10.1002/jbm.b.30396

Heisel, U., Wallaschek, J., Eisseler, R., & Potthast, C. (2008). Ultrason ic deep hole drilling in electrolytic copper ECu 57. *CIRP Annals - Manufa cturing Technology*, *57*(1), 53–56. https://doi.org/10.1016/j.cirp.2008.03.078

Hinton, J., Basu, D., Mirgkizoudi, M., Flynn, D., Harris, R., & Kay, R. (2019). Hybrid additive manufacturing of precision engineered ceramic co mponents. *Rapid Prototyping Journal*, *25*(6), 1061–1068. https://doi.org/10. 1108/RPJ-01-2019-0025

Hossain, M. S., Espalin, D., Ramos, J., Perez, M., & Wicker, R. (201 4). Improved Mechanical Properties of Fused Deposition Modeling-Manufa ctured Parts Through Build Parameter Modifications. *Journal of Manufactu ring Science and Engineering, Transactions of the ASME*, *136*(6). https://d oi.org/10.1115/1.4028538

Hossain, M. S., Ramos, J., Espalin, D., Perez, M., & Wicker, R. (201 3). Improving Tensile Mechanical Properties of FDM-Manufactured Specim ens via Modifying Build Parameters. *Materials Science*, 165–170.

Hu, S. J. (2013). Evolving paradigms of manufacturing: From mass pr oduction to mass customization and personalization. *Procedia CIRP*, *7*, 3– 8. https://doi.org/10.1016/j.procir.2013.05.002

Hu, S. J., Ko, J., Weyand, L., Elmaraghy, H. A., Lien, T. K., Koren, Y., Bley, H., Chryssolouris, G., Nasr, N., & Shpitalni, M. (2011). Assembly syst em design and operations for product variety. *CIRP Annals - Manufacturi ng Technology*, *60*(2), 715–733. https://doi.org/10.1016/j.cirp.2011.05.004

Huang, B., & Singamneni, S. (2014). Raster angle mechanics in fused deposition modelling. *Journal of Composite Materials*, *49*. https://doi.org /10.1177/0021998313519153

Huang, S. H., Liu, P., Mokasdar, A., & Hou, L. (2013). Additive manu

facturing and its societal impact: a literature review. *The International Journal of Advanced Manufacturing Technology*, *67*(5), 1191–1203. https://doi.org/10.1007/s00170-012-4558-5

Huang, Z., Meng, L., Lin, P., Cao, X., Zhang, Z., & Liu, G. (2023). Formability improvement of hot-pressed Ti/Al laminated sheet by TiAl3 layer growth and crack healing during deformation. *Journal of Alloys and Compounds*, *938*, 168604. https://doi.org/https://doi.org/10.1016/j.jallcom.2022.168604

Hutmacher, D. W., Schantz, T., Zein, I., Ng, K. W., Teoh, S. H., & Tan, K. C. (2001). Mechanical properties and cell cultural response of polycaprolactone scaffolds designed and fabricated via fused deposition modeling. *Journal of Biomedical Materials Research*, *55*(2), 203–216. https://doi.org/10.1002/1097-4636(200105)55:2<203::AID-JBM1007>3.0.CO;2-7

Jamir, M. R. M., Majid, M. S. A., & Khasri, A. (2018). Natural lightweight hybrid composites for aircraft structural applications. In M. Jawaid & M. B. T.-S. C. for A. A. Thariq (Eds.), *Woodhead Publishing Series in Composites Science and Engineering* (pp. 155–170). Woodhead Publishing. https://doi.org/https://doi.org/10.1016/B978-0-08-102131-6.00008-6

Jiao, J., Tseng, M. M., Duffy, V. G., & Lin, F. (1998). Product Family Modeling For Mass Customization. *Computers & Industrial Engineering*, *35*(3–4), 495–498.

Jonušauskas, L., Baravykas, T., Tičkūnas, T., Butkutė, A., Gadišauskas, T., Andrijec, D., Butkutė, A., Gadišauskas, T., Gadišauskas, T., Andrijec, D., & Andrijec, D. (2019). Femtosecond Laser-Enabled Hybrid Additive-Subtractive 3D Manufacturing of Highly Articulated Micromechanical Structures. *Laser Congress 2019 (ASSL, LAC, LS&C)*, JM5A.45. https://doi.org/10.1364/ASSL.2019.JM5A.45

Jonušauskas, L., Rekštyte, S., Buividas, R., Butkus, S., Gadonas, R., Juodkazis, S., & Malinauskas, M. (2017). Hybrid subtractive-additive-welding

microfabrication for lab-on-chip applications via single amplified femtoseco nd laser source. *Optical Engineering*, *56*(9), 094108. https://doi.org/10.111 7/1.OE.56.9.094108

Kalita, S. J., Bose, S., Hosick, H. L., & Bandyopadhyay, A. (2003). De velopment of controlled porosity polymer-ceramic composite scaffolds via fused deposition modeling. *Materials Science and Engineering C*, *23*(5), 6 11–620. https://doi.org/10.1016/S0928-4931(03)00052-3

Kalpakjian, S., & Schmid, S. R. (2010). *Manufacturing engineering an d technology* (6th ed.). Pearson.

Karamanlioglu, M., Preziosi, R., & Robson, G. D. (2017). Abiotic and biotic environmental degradation of the bioplastic polymer poly(lactic aci d): A review. *Polymer Degradation and Stability*, *137*. https://doi.org/10.1 016/j.polymdegradstab.2017.01.009

Karunakaran, K. P., Suryakumar, S., Pushpa, V., & Akula, S. (2010a). L ow cost integration of additive and subtractive processes for hybrid layer ed manufacturing. *Robotics and Computer-Integrated Manufacturing*, *26*(5), 490–499. https://doi.org/10.1016/j.rcim.2010.03.008

Karunakaran, K. P., Suryakumar, S., Pushpa, V., & Akula, S. (2010b). Low cost integration of additive and subtractive processes for hybrid laye red manufacturing. *Robotics and Computer-Integrated Manufacturing*, *26* (5), 490–499. https://doi.org/10.1016/j.rcim.2010.03.008

Karunakaran, K. P., Suryakumar, S., Pushpa, V., & Akula, S. (2010c). L ow cost integration of additive and subtractive processes for hybrid layer ed manufacturing. *Robotics and Computer-Integrated Manufacturing*, *26*(5), 490–499. https://doi.org/10.1016/j.rcim.2010.03.008

Katayama, S., & Kawahito, Y. (2018). Direct Joining of Metal and Pla stic with Laser. In *Joining of Polymer-Metal Hybrid Structures* (pp. 127–14 4). https://doi.org/https://doi.org/10.1002/9781119429807.ch5

Katstra, W. E., Palazzolo, R. D., Rowe, C. W., Giritlioglu, B., Teung, P.,

& Cima, M. J. (2000). Oral dosage forms fabricated by Three Dimension
al Printing(TM). *Journal of Controlled Release*, *66*(1), 1–9. https://doi.org/1
0.1016/S0168-3659(99)00225-4

Kerschbaumer, M., & Ernst, G. (2004). Hybrid manufacturing process
for rapid high performance tooling combining high speed milling and lase
r cladding. *ICALEO 2004 - 23rd International Congress on Applications of
Laser and Electro-Optics, Congress Proceedings*, *1710*(2004). https://doi.org
/10.2351/1.5060234

Khaled, S. A., Burley, J. C., Alexander, M. R., Yang, J., & Roberts, C.
J. (2015). 3D printing of tablets containing multiple drugs with defined r
elease profiles. *International Journal of Pharmaceutics*, *494*(2), 643–650. h
ttps://doi.org/10.1016/j.ijpharm.2015.07.067

Kim, E., Shin, Y. J., & Ahn, S. H. (2016). The effects of moisture an
d temperature on the mechanical properties of additive manufacturing co
mponents: Fused deposition modeling. *Rapid Prototyping Journal*, *22*(6), 8
87–894. https://doi.org/10.1108/RPJ-08-2015-0095

Klocke, F., Roderburg, A., & Zeppenfeld, C. (2011). Design methodolo
gy for hybrid production processes. *Procedia Engineering*, *9*, 417–430. htt
ps://doi.org/10.1016/j.proeng.2011.03.130

Kolleck, R., Vollmer, R., & Veit, R. (2011). Investigation of a combine
d micro-forming and punching process for the realization of tight geomet
rical tolerances of conically formed hole patterns. *CIRP Annals - Manufac
turing Technology*, *60*(1), 331–334. https://doi.org/10.1016/j.cirp.2011.03.14
1

Konasch, J., Riess, A., Mau, R., Teske, M., Rekowska, N., Eickner, T.,
Grabow, N., & Seitz, H. (2019). A novel hybrid additive manufacturing pr
ocess for drug delivery systems with locally incorporated drug depots. *Ph
armaceutics*, *11*(12). https://doi.org/10.3390/pharmaceutics11120661

Koren, Y., Hu, S. J., Gu, P., & Shpitalni, M. (2013). Open-architecture

products. *CIRP Annals - Manufacturing Technology*, *62*(2), 719–729. https://doi.org/10.1016/j.cirp.2013.06.001

Kozak, J., & Rajurkar, K. P. (2000). Hybrid machining process evaluation and development. *Proceedings of 2nd International Conference on Machining and Measurements of Sculptured Surfaces*, 501–536.

Kozior, T., & Kundera, C. (2017). Evaluation of the Influence of Parameters of FDM Technology on the Selected Mechanical Properties of Models. *Procedia Engineering*, *192*, 463–468. https://doi.org/10.1016/j.proeng.2017.06.080

Kramschuster, A., & Turng, L.-S. (2009). An Injection Molding Process for Manufacturing Highly Porous and Interconnected Biodegradable Polymer Matrices for Use as Tissue Engineering Scaffolds. *Journal of Biomedical Materials Research. Part B, Applied Biomaterials*, *92*, 366–376. https://doi.org/10.1002/jbm.b.31523

Kretzschmar, N., Lipponen, S., Klar, V., Pearce, J. M., Ranger, T. L., Seppälä, J., & Partanen, J. (2019). Mechanical properties of ultraviolet-assisted paste extrusion and postextrusion ultraviolet-curing of three-dimensional printed biocomposites. *3D Printing and Additive Manufacturing*, *6*(3), 127–137. https://doi.org/10.1089/3dp.2018.0148

Kruth, J. P., Mercelis, P., Van Vaerenbergh, J., Froyen, L., & Rombouts, M. (2005). Binding mechanisms in selective laser sintering and selective laser melting. *Rapid Prototyping Journal*, *11*(1), 26–36. https://doi.org/10.1108/13552540510573365

Kumar Pokkalla, D., Kumar, V., Jo, E., Hassen, A. A., Cakmak, E., Alwekar, S. P., Kunc, V., Vaidya, U., Baid, H. K., & Kim, S. (2022). Characterization of Anisotropic Mechanical Properties of Polymer Composites Manufactured by a Hybrid Additive Manufacturing-Compression Molding Process using X-ray Computer Tomography. *Conference: SPIE Smart Structures + Nondestructive Evaluation 2022*. http://energy.gov/downloads/doe-public-acce

ss-plan

Kumar, R., Chohan, J. S., Kumar, R., Yadav, A., Piyush, & Kumar, P. (2022). Metal spray layered hybrid additive manufacturing of PLA composite structures: Mechanical, thermal and morphological properties. *Journal of Thermoplastic Composite Materials*, *35*(10), 1387–1407. https://doi.org/10.1177/0892705720932622

Kunwar, P., Xiong, Z., McLoughlin, S. T., & Soman, P. (2020). Oxygen-Permeable Films for Continuous Additive, Subtractive, and Hybrid Additive/Subtractive Manufacturing. *3D Printing and Additive Manufacturing*, *7*(5), 216–221. https://doi.org/10.1089/3dp.2019.0166

Kuznetsov, V. E., Solonin, A. N., Urzhumtsev, O. D., Schilling, R., & Tavitov, A. G. (2018a). Strength of PLA components fabricated with fused deposition technology using a desktop 3D printer as a function of geometrical parameters of the process. *Polymers*, *10*(3), 1–16. https://doi.org/10.3390/polym10030313

Kuznetsov, V. E., Solonin, A. N., Urzhumtsev, O. D., Schilling, R., & Tavitov, A. G. (2018b). Strength of PLA components fabricated with fused deposition technology using a desktop 3D printer as a function of geometrical parameters of the process. *Polymers*, *10*(3). https://doi.org/10.3390/polym10030313

Lanzotti, A., Grasso, M., Staiano, G., & Martorelli, M. (2015). The impact of process parameters on mechanical properties of parts fabricated in PLA with an open-source 3-D printer. *Rapid Prototyping Journal*, *21*(5), 604–617. https://doi.org/10.1108/RPJ-09-2014-0135

Lauwers, B., Klocke, F., & Klink, A. (2010). Advanced manufacturing through the implementation of hybrid and media assisted processes. *Int. Chemnitz Manufacturing Colloquium*, *54*, 205–220.

Lauwers, B., Klocke, F., Klink, A., Tekkaya, A. E., Neugebauer, R., & McIntosh, D. (2014). Hybrid processes in manufacturing. *CIRP Annals - M*

anufacturing Technology, *63*(2), 561–583. https://doi.org/10.1016/j.cirp.201 4.05.003

Lay, M., Thajudin, N. L. N., Hamid, Z. A. A., Rusli, A., Abdullah, M. K., & Shuib, R. K. (2019). Comparison of physical and mechanical propert ies of PLA, ABS and nylon 6 fabricated using fused deposition modeling and injection molding. *Composites Part B: Engineering*, *176*(November 20 18), 107341. https://doi.org/10.1016/j.compositesb.2019.107341

Le, V. T., Paris, H., & Mandil, G. (2017). Process planning for combi ned additive and subtractive manufacturing technologies in a remanufactu ring context. *Journal of Manufacturing Systems*, *44*, 243–254. https://doi.o rg/10.1016/j.jmsy.2017.06.003

Lee, B. H., Abdullah, J., & Khan, Z. A. (2005). Optimization of rapid prototyping parameters for production of flexible ABS object. *Journal of Materials Processing Technology*, *169*(1), 54–61. https://doi.org/10.1016/j.j matprotec.2005.02.259

Liang, H., Hong, H., & Svoboda, J. (2002). A combined 3D linear an d circular interpolation technique for multi-axis CNC machining. In *Journal of Manufacturing Science and Engineering* (Vol. 124, Issue 2, pp. 305–3 12). American Society of Mechanical Engineers(ASME). https://doi.org/10.1 115/1.1445154

Lim, S. H., Chia, S. M. Y., Kang, L., & Yap, K. Y.-L. (2016). Three-Dim ensional Printing of Carbamazepine Sustained-Release Scaffold. *Journal of Pharmaceutical Sciences*, *105*(7), 2155–2163. https://doi.org/https://doi.org/ 10.1016/j.xphs.2016.04.031

Lim, S. H., Kathuria, H., Tan, J. J. Y., & Kang, L. (2018). 3D printed drug delivery and testing systems — a passing fad or the future? *Advan ced Drug Delivery Reviews*, *132*, 139–168. https://doi.org/10.1016/j.addr.20 18.05.006

Lima, L. T., Aurasb, R., & Rubinob, M. (2008). Processing technologie

s for poly(lactic acid). *Prog Polym Sci*, *32*, 820–852.

Liravi, F., Jacob-John, V., Toyserkani, A., & Vlasea, M. (2017). A Hybrid Method for Additive Manufacturing of Silicone Structures. *Proceedings of the 28th Annual International Solid Freeform Fabrication Symposium*.

Liravi, F., & Toyserkani, E. (2018). A hybrid additive manufacturing method for the fabrication of silicone bio-structures: 3D printing optimization and surface characterization. *Materials and Design*, *138*, 46–61. https://doi.org/10.1016/j.matdes.2017.10.051

Liu, C., Huang, N., Xu, F., Tong, J., Chen, Z., Gui, X., Fu, Y., & Lao, C. (2018). 3D printing technologies for flexible tactile sensors toward wearable electronics and electronic skin. *Polymers*, *10*(6), 1–31. https://doi.org/10.3390/polym10060629

Liu, K., Yan, Z., Pan, R., Wang, F., & Chen, S. (2023). Effect of deposition sequence on interfacial characteristics of Inconel–copper functional bimetallic structures fabricated by directed energy deposition-arc. *Materials Letters*, *345*, 134487. https://doi.org/https://doi.org/10.1016/j.matlet.2023.134487

Liu, Y. (1999). Calculation of cooling time of injection molding parts. *Mould Industry*, *4*, 36–38.

Lokesh, N., Praveena, B. A., Sudheer Reddy, J., Vasu, V. K., & Vijaykumar, S. (2021). Evaluation on effect of printing process parameter through Taguchi approach on mechanical properties of 3D printed PLA specimens using FDM at constant printing temperature. *Materials Today: Proceedings*, *xxxx*. https://doi.org/10.1016/j.matpr.2021.11.054

Lu, R. F., Petersen, T. D., & Storch, R. L. (2009). Asynchronous stochastic learning curve effects in engineering-to-order customisation processes. *International Journal of Production Research*, *47*(5), 1309–1329. https://doi.org/10.1080/00207540701484921

Ma, F., Chen, S., Han, L., Wang, Z., & Pu, Y. (2019). Experimental a

nd numerical investigation on the strength of polymer-metal hybrid with laser assisted metal surface treatment. *Journal of Adhesion Science and Technology*, *33*(10), 1112–1129. https://doi.org/10.1080/01694243.2019.1582888

Ma, J., Zhang, Y., Li, J., Cui, D., Wang, Z., & Wang, J. (2021). Microstructure and mechanical properties of forging-additive hybrid manufactured Ti–6Al–4V alloys. *Materials Science and Engineering A*, *811*(March), 140984. https://doi.org/10.1016/j.msea.2021.140984

MacDonald, E., & Wicker, R. (2016). Multiprocess 3D printing for increasing component functionality. *Science*, *353*(6307). https://doi.org/10.1126/science.aaf2093

Mahmood, S., Qureshi, A. J., & Talamona, D. (2018). Taguchi based process optimization for dimension and tolerance control for fused deposition modelling. *Additive Manufacturing*, *21*, 183–190. https://doi.org/10.1016/j.addma.2018.03.009

Martinez, P. R., Goyanes, A., Basit, A. W., & Gaisford, S. (2018). Influence of Geometry on the Drug Release Profiles of Stereolithographic (SLA) 3D-Printed Tablets. *AAPS PharmSciTech*, *19*(8), 3355–3361. https://doi.org/10.1208/s12249-018-1075-3

Masood, S. H., & Song, W. Q. (2004). Development of new metal/polymer materials for rapid tooling using Fused deposition modelling. *Materials and Design*, *25*(7), 587–594. https://doi.org/10.1016/j.matdes.2004.02.009

Maurya, S., Malik, B., Sharma, P., Singh, A., & Chalisgaonkar, R. (2022). Investigation of different parameters of cube printed using PLA by FDM 3D printer. *Materials Today: Proceedings*. https://doi.org/10.1016/j.matpr.2022.03.700

McIntosh, R. I., Matthews, J., Mullineux, G., & Medland, A. J. (2010). Late customisation: Issues of mass customisation in the food industry. *I*

nternational Journal of Production Research, *48*(6), 1557–1574. https://doi.org/10.1080/00207540802577938

Melchels, F. P. W., Domingos, M. A. N., Klein, T. J., Malda, J., Bartolo, P. J., & Hutmacher, D. W. (2012). Additive manufacturing of tissues and organs. *Progress in Polymer Science*, *37*(8), 1079–1104. https://doi.org/10.1016/j.progpolymsci.2011.11.007

Melenka, G. W., Cheung, B. K. O., Schofield, J. S., Dawson, M. R., & Carey, J. P. (2016). Evaluation and prediction of the tensile properties of continuous fiber-reinforced 3D printed structures. *Composite Structures*, *153*, 866–875. https://doi.org/10.1016/j.compstruct.2016.07.018

Menzies, I., & Koshy, P. (2008). Assessment of abrasion-assisted material removal in wire EDM. *CIRP Annals - Manufacturing Technology*, *57*(1), 195–198. https://doi.org/10.1016/j.cirp.2008.03.135

Merklein, M., Junker, D., Schaub, A., & Neubauer, F. (2016a). Hybrid additive manufacturing technologies - An analysis regarding potentials and applications. *Physics Procedia*, *83*, 549–559. https://doi.org/10.1016/j.phpro.2016.08.057

Merklein, M., Junker, D., Schaub, A., & Neubauer, F. (2016b). Hybrid additive manufacturing technologies - An analysis regarding potentials and applications. *Physics Procedia*, *83*, 549–559. https://doi.org/10.1016/j.phpro.2016.08.057

Mital, A., Desai, A., Subramanian, A., & Mital, A. (2014). The Significance of Manufacturing. In *Product Development* (pp. 3–19). Elsevier. https://doi.org/10.1016/b978-0-12-799945-6.00001-6

Moetazedian, A., Allum, J., Gleadall, A., Mele, E., & Silberschmidt, V. V. (2021). MaTrEx AM: A new hybrid additive manufacturing process to selectively control mechanical properties. *Additive Manufacturing*, *47*. https://doi.org/10.1016/j.addma.2021.102337

Mohamed, O. A., Masood, S. H., & Bhowmik, J. L. (2015). Optimizati

on of fused deposition modeling process parameters: a review of current research and future prospects. *Advances in Manufacturing*, *3*, 42–53. https://doi.org/10.1007/s40436-014-0097-7

Molian, R., Neumann, C., Shrotriya, P., & Molian, P. (2008). Novel laser/water-jet hybrid manufacturing process for cutting ceramics. *Journal of Manufacturing Science and Engineering*, *130*(3), 0310081–03100810. https://doi.org/10.1115/1.2844592

Montero, M., Roundy, S., & Odell, D. (2001). Material characterization of fused deposition modeling (FDM) ABS by designed experiments. *Proceedings of Rapid Prototyping & Manufacturing Conference*, 1–21.

Mourtzis, D. (2016). Challenges and future perspectives for the life cycle of manufacturing networks in the mass customisation era. *Logistics Research*, *9*(1), 1–20. https://doi.org/10.1007/s12159-015-0129-0

Nabavi-Kivi, A., Ayatollahi, M. R., Rezaeian, P., & Mohammad Javad Razavi, S. (2021). Investigating the effect of printing speed and mode mixity on the fracture behavior of FDM-ABS specimens. *Theoretical and Applied Fracture Mechanics*, *118*(August 2021), 103223. https://doi.org/10.1016/j.tafmec.2021.103223

Nassehi, A., Newman, S., Dhokia, V., Zhu, Z., & Asrai, R. I. (2011). Using formal methods to model hybrid manufacturing processes. *4th International Conference on Changeable, Agile, Reconfigurable and Virtual Production (CARV2011)*.

Nau, B., Roderburg, A., & Klocke, F. (2011). Ramp-up of hybrid manufacturing technologies. *CIRP Journal of Manufacturing Science and Technology*, *4*(3), 313–316. https://doi.org/10.1016/j.cirpj.2011.04.003

Nielsen, C. V., & Martins, P. A. (2021). *Metal Forming Formability, Simulation, and Tool Design* (1st ed.). Elsevier.

Ning, F., Cong, W., Jia, Z., Wang, F., & Zhang, M. (2016). *Additive Manufacturing of CFRP Composites Using Fused Deposition Modeling: Effe*

cts of Process Parameters. *1989*, 1–7. https://doi.org/10.1115/msec2016-8561

Oliveira, J. P., LaLonde, A. D., & Ma, J. (2020). Processing parameters in laser powder bed fusion metal additive manufacturing. *Materials and Design*, *193*. https://doi.org/10.1016/j.matdes.2020.108762

Onwubolu, G. C., & Rayegani, F. (2014). Characterization and Optimization of Mechanical Properties of ABS Parts Manufactured by the Fused Deposition Modelling Process. *International Journal of Manufacturing Engineering*, *2014*, 1–13. https://doi.org/10.1155/2014/598531

Ozcelik, B., Ozbay, A., & Demirbas, E. (2010). Influence of injection parameters and mold materials on mechanical properties of ABS in plastic injection molding. *International Communications in Heat and Mass Transfer*, *37*(9), 1359–1365. https://doi.org/10.1016/j.icheatmasstransfer.2010.07.001

Ozlati, A., Movahedi, M., Tamizi, M., Tartifzadeh, Z., & Alipour, S. (2019). An alternative additive manufacturing-based joining method to make Metal/Polymer hybrid structures. *Journal of Manufacturing Processes*, *45*, 217–226. https://doi.org/10.1016/j.jmapro.2019.07.002

Pallari, J. H. P., Dalgarno, K. W., & Woodburn, J. (2010). Mass customization of foot orthoses for rheumatoid arthritis using selective laser sintering. *IEEE Transactions on Biomedical Engineering*, *57*(7), 1750–1756. https://doi.org/10.1109/TBME.2010.2044178

Park, H. S., Phuong, D. X., & Kumar, S. (2019). AI Based Injection Molding Process for Consistent Product Quality. *Procedia Manufacturing*, *28*, 102–106. https://doi.org/10.1016/j.promfg.2018.12.017

Park, S. I., Rosen, D. W., Choi, S. kyum, & Duty, C. E. (2014). Effective mechanical properties of lattice material fabricated by material extrusion additive manufacturing. *Additive Manufacturing*, *1*, 12–23. https://doi.org/10.1016/j.addma.2014.07.002

Pashneh-Tala, S., Moorehead, R., & Claeyssens, F. (2020). Hybrid manufacturing strategies for tissue engineering scaffolds using methacrylate functionalised poly(glycerol sebacate). *Journal of Biomaterials Applications*, *34*(8), 1114–1130. https://doi.org/10.1177/0885328219898385

Patel, R., Desai, C., Kushwah, S., & Mangrola, M. H. (2022). A review article on FDM process parameters in 3D printing for composite materials. *Materials Today: Proceedings*. https://doi.org/10.1016/j.matpr.2022.02.385

Patrick, H., J., B. R., A., S. A., & J., S. E. (2017). User entrepreneur business models in 3D printing. *Journal of Manufacturing Technology Management*, *28*(1), 75–94. https://doi.org/10.1108/JMTM-12-2015-0115

Patterson, A. E., Pereira, T. R., Allison, J. T., & Messimer, S. L. (2019). IZOD impact properties of full-density fused deposition modeling polymer materials with respect to raster angle and print orientation. *Proceedings of the Institution of Mechanical Engineers, Part C: Journal of Mechanical Engineering Science*. https://doi.org/10.1177/0954406219840385

Paz, R., Santamarta, J., Monzón, M. D., García, J., & Pei, E. (2018). An analysis of key process parameters for hybrid manufacturing by material extrusion and CNC machining. *Bio-Design and Manufacturing*, *1*(4), 237–244. https://doi.org/10.1007/s42242-018-0023-0

Pei, E., Shen, J., & Watling, J. (2015). Direct 3D printing of polymers onto textiles: Experimental studies and applications. *Rapid Prototyping Journal*, *21*(5), 556–571. https://doi.org/10.1108/RPJ-09-2014-0126

Phillips, R. (1995). *Taguchi Techniques for Quality Engineering* (M.-H. Education, Ed.; second).

Piller, F. T. (2004). Mass Customization: Reflections on the State of the Concept. In *The International Journal of Flexible Manufacturing Systems* (Vol. 16).

Pokkalla, D. K., Hassen, A. A., Nuttall, D., Tsiamis, N., Rencheck, M.

L., Kumar, V., Nandwana, P., Joslin, C. B., Blanchard, P., Tamhankar, S. L., Maloney, P., Kunc, V., & Kim, S. (2023). A novel additive manufacturing c ompression overmolding process for hybrid metal polymer composite stru ctures. *Additive Manufacturing Letters*, *5*, 100128. https://doi.org/10.1016/ j.addlet.2023.100128

Popescu, D., Zapciu, A., Amza, C., Baciu, F., & Marinescu, R. (2018). FDM process parameters influence over the mechanical properties of pol ymer specimens: A review. *Polymer Testing*, *69*(May), 157–166. https://do i.org/10.1016/j.polymertesting.2018.05.020

Pragana, J. P. M., Sampaio, R. F. V., Bragança, I. M. F., Silva, C. M. A., & Martins, P. A. F. (2021). Hybrid metal additive manufacturing: A st ate–of–the-art review. In *Advances in Industrial and Manufacturing Engine ering* (Vol. 2). Elsevier B.V. https://doi.org/10.1016/j.aime.2021.100032

Qamar Tanveer, M., Mishra, G., Mishra, S., & Sharma, R. (2022). Eff ect of infill pattern and infill density on mechanical behaviour of FDM 3 D printed Parts- a current review. *Materials Today: Proceedings*. https://d oi.org/10.1016/j.matpr.2022.02.310

Rajamani, P. K., Ageyeva, T., & Kovács, J. G. (2021). Personalized ma ss production by hybridization of additive manufacturing and injection m olding. *Polymers*, *13*(2), 1–19. https://doi.org/10.3390/polym13020309

Rajurkar, K. P., Zhu, D., McGeough, J. A., Kozak, J., & De Silva, A. (1999). New Developments in Electro-Chemical Machining. *CIRP Annals - Manufacturing Technology*, *48*(2), 567–579.

Rashid, O., Low, K. W. Q., & Pittman, J. F. T. (2020). Mold cooling i n thermoplastics injection molding: Effectiveness and energy efficiency. *Jo urnal of Cleaner Production*, *264*. https://doi.org/10.1016/j.jclepro.2020.121 375

Rezaeian, P., Ayatollahi, M. R., Nabavi-Kivi, A., & Mohammad Javad Razavi, S. (2022). Effect of printing speed on tensile and fracture behavio

r of ABS specimens produced by fused deposition modeling. *Engineering Fracture Mechanics*, *266*. https://doi.org/10.1016/j.engfracmech.2022.108393

Ribeiro, M., Sousa Carneiro, O., & Ferreira da Silva, A. (2019). Interface geometries in 3D multi-material prints by fused filament fabrication. *Rapid Prototyping Journal*, *25*(1), 38–46. https://doi.org/10.1108/RPJ-05-2017-0107

Rivette, M., Hacoët, J. Y., & Mognol, P. (2007). A graph-based methodology for hybrid rapid design. *Proceedings of the Institution of Mechanical Engineers, Part B: Journal of Engineering Manufacture*, *221*(4), 685–697. https://doi.org/10.1243/09544054JEM666

Roach, D. J., Hamel, C. M., Dunn, C. K., Johnson, M. V., Kuang, X., & Qi, H. J. (2019). The m4 3D printer: A multi-material multi-method additive manufacturing platform for future 3D printed structures. *Additive Manufacturing*, *29*. https://doi.org/10.1016/j.addma.2019.100819

Roberson, D. A., Torrado Perez, A. R., Shemelya, C. M., Rivera, A., MacDonald, E., & Wicker, R. B. (2015). Comparison of stress concentrator fabrication for 3D printed polymeric izod impact test specimens. *Additive Manufacturing*, *7*, 1–11. https://doi.org/10.1016/j.addma.2015.05.002

Robert H. Todd, Dell K. Allen, L. A. (1994). *Manufacturing Processes Reference Guide*.

Rocha, C., Torrado Perez, A., Roberson, D., Shemelya, C., MacDonald, E., & Wicker, R. (2014). Novel ABS-based binary and ternary polymer blends for material extrusion 3D printing. *Journal of Materials Research*, *29*(17), 1859–1866.

Rodríguez, J. F., Thomas, J. P., & Renaud, J. E. (2001). Mechanical behavior of acrylonitrile butadiene styrene (ABS) fused deposition materials. Experimental investigation. *Rapid Prototyping Journal*, *7*(3), 148–158. https://doi.org/10.1108/13552540110395547

Rodríguez, J. F., Thomas, J. P., & Renaud, J. E. (2003a). Design of fu sed-deposition ABS components for stiffness and strength. *Journal of Mec hanical Design, Transactions of the ASME*, *125*(3), 545–551. https://doi.or g/10.1115/1.1582499

Rodríguez, J. F., Thomas, J. P., & Renaud, J. E. (2003b). Design of fu sed-deposition ABS components for stiffness and strength. *Journal of Mec hanical Design, Transactions of the ASME*, *125*(3), 545–551. https://doi.or g/10.1115/1.1582499

Rodríguez-Panes, A., Claver, J., & Camacho, A. M. (2018). The influe nce of manufacturing parameters on the mechanical behaviour of PLA an d ABS pieces manufactured by FDM: A comparative analysis. *Materials*, *1 1*(8). https://doi.org/10.3390/ma11081333

Rosas, L. F. V. (2013). *Characterization of Parametric Internal Structur es for Components Built by Fused Deposition Modeling*. University of Win dsor.

Rosato, M., & Rosato, D. (2000). *Injection Molding Handbook*. https:/ /doi.org/10.1007/978-1-4615-4597-2

Rossi, A., & Lanzetta, M. (2020). Integration of hybrid additive/subtra ctive manufacturing planning and scheduling by metaheuristics. *Computers and Industrial Engineering*, *144*(March), 106428. https://doi.org/10.1016/j. cie.2020.106428

Sadia, M., Arafat, B., Ahmed, W., Forbes, R. T., & Alhnan, M. A. (20 18). Channelled tablets: An innovative approach to accelerating drug rele ase from 3D printed tablets. *Journal of Controlled Release*, *269*(November 2017), 355–363. https://doi.org/10.1016/j.jconrel.2017.11.022

Saleh, J. H., Mark, G., & Jordan, N. C. (2009). Flexibility: A multi-dis ciplinary literature review and a research agenda for designing flexible en gineering systems. *Journal of Engineering Design*, *20*(3), 307–323. https:// doi.org/10.1080/09544820701870813

Salvador, F., Martin de Holan, P., & Piller, F. (2009). Cracking the Code of Mass Customization. *MIT Sloan Management Review*, *50*(3), 71–78.

Sammoura, F., Kang, J., Heo, Y. M., Jung, T., & Lin, L. (2007). Polymeric microneedle fabrication using a microinjection molding technique. *Microsystem Technologies*, *13*(5–6), 517–522. https://doi.org/10.1007/s00542-006-0204-1

Sha, B., Dimov, S., Griffiths, C., & Packianather, M. S. (2007). Investigation of micro-injection moulding: Factors affecting the replication quality. *Journal of Materials Processing Technology*, *183*(2–3), 284–296. https://doi.org/10.1016/j.jmatprotec.2006.10.019

Silva, C. G., Campini, P. A. L., Rocha, D. B., & Rosa, D. S. (2019). The influence of treated eucalyptus microfibers on the properties of PLA biocomposites. *Composites Science and Technology*, *179*(January), 54–62. https://doi.org/10.1016/j.compscitech.2019.04.010

Silva, D. F. M., Bragança, I. M. F., Silva, C. M. A., Alves, L. M., & Martins, P. A. F. (2019). Joining by forming of additive manufactured 'mortise-and-tenon' joints. *Proceedings of the Institution of Mechanical Engineers, Part B: Journal of Engineering Manufacture*, *233*(1), 166–173. https://doi.org/10.1177/0954405417720954

Silva, M., Felismina, R., Mateus, A., Parreira, P., & Malça, C. (2017). Application of a Hybrid Additive Manufacturing Methodology to Produce a Metal/Polymer Customized Dental Implant. *Procedia Manufacturing*, *12*, 150–155. https://doi.org/10.1016/j.promfg.2017.08.019

Silva, M. R., Domingues, J., Costa, J., Mateus, A., & Malça, C. (2019). Study of Metal/Polymer Interface of Parts Produced by a Hybrid Additive Manufacturing Approach. *Applied Mechanics and Materials*, *890*, 34–42. https://doi.org/10.4028/www.scientific.net/amm.890.34

Simpson, T. W. (2004). Product platform design and customization: Status and promise. In *Artificial Intelligence for Engineering Design, Analysis*

and Manufacturing: AIEDAM (Vol. 18, Issue 1, pp. 3–20). https://doi.org/10.1017/S0890060404040028

Skowyra, J., Pietrzak, K., & Alhnan, M. A. (2015). Fabrication of extended-release patient-tailored prednisolone tablets via fused deposition modelling (FDM) 3D printing. *European Journal of Pharmaceutical Sciences*, *68*, 11–17. https://doi.org/10.1016/j.ejps.2014.11.009

Society of Manufacturing Engineers. (1994). *Process Reengineering and the New Manufacturing Enterprise Wheel* (SME, Ed.).

Sood, A. K., Ohdar, R. K., & Mahapatra, S. S. (2010). Parametric appraisal of mechanical property of fused deposition modelling processed parts. *Materials and Design*, *31*(1), 287–295. https://doi.org/10.1016/j.matdes.2009.06.016

Sreedharan, J., & Jeevanantham, A. K. (2018). Analysis of Shrinkages in ABS Injection Molding Parts for Automobile Applications. *Materials Today: Proceedings*, *5*(5), 12744–12749. https://doi.org/10.1016/j.matpr.2018.02.258

Sreenathbabu, A., Karunakaran, K. P., & Amarnath, C. (2005). Statistical process design for hybrid adaptive layer manufacturing. *Rapid Prototyping Journal*, *11*(4), 235–248. https://doi.org/10.1108/13552540510612929

Srinivasan, R., Giannikas, V., McFarlane, D., & Thorne, A. (2018). Customising with 3D printing: The role of intelligent control. *Computers in Industry*, *103*, 38–46. https://doi.org/10.1016/j.compind.2018.09.003

Stansbury, J. W., & Idacavage, M. J. (2016). 3D printing with polymers: Challenges among expanding options and opportunities. *Dental Materials*, *32*(1), 54–64. https://doi.org/10.1016/j.dental.2015.09.018

Strong, D., Kay, M., Conner, B., Wakefield, T., & Manogharan, G. (2018). Hybrid manufacturing – integrating traditional manufacturers with additive manufacturing (AM) supply chain. *Additive Manufacturing*, *21*(February), 159–173. https://doi.org/10.1016/j.addma.2018.03.010

Sugavaneswaran, M., & Arumaikkannu, G. (2015). Analytical and expe rimental investigation on elastic modulus of reinforced additive manufactu red structure. *Materials and Design*, *66*(PA), 29–36. https://doi.org/10.101 6/j.matdes.2014.10.029

Sugioka, K., Wu, D., Xu, J., Sima, F., & Midorikawa, K. (2015). Hybri d Subtractive and Additive Micromanufacturing using Femtosecond Laser f or Fabrication of True 3D Biochips. *CLEO: 2015*, ATh4A.3. https://doi.org/ 10.1364/CLEO_AT.2015.ATh4A.3

Sun, Q., Rizvi, G., Bellehumeur, C. T., & Gu, P. (2008). Effect of proc essing conditions on the bonding quality of FDM polymer filaments. *Rapi d Prototyping Journal*, *14*, 72–80. https://doi.org/10.1108/13552540810862 028

Svečko, R., Kusić, D., Kek, T., Sarjaš, A., Hančič, A., & Grum, J. (201 3). Acoustic emission detection of macro-cracks on engraving tool steel i nserts during the injection molding cycle using PZT sensors. *Sensors (Swit zerland)*, *13*(5), 6365–6379. https://doi.org/10.3390/s130506365

Syed, H. M. (1996). Intelligent rapid prototyping with fused depositio n modelling. *Rapid Prototyping Journal*, *2*(1), 24–33. https://doi.org/10.110 8/13552549610109054

Szuchács, A., Ageyeva, T., Boros, R., & Kovács, J. G. (2022). Bonding strength calculation in multicomponent plastic processing technologies. *M aterials and Manufacturing Processes*, *37*(2), 151–159. https://doi.org/10.1 080/10426914.2021.1948052

Tábi, T., Ageyeva, T., & Kovács, J. G. (2021). Improving the ductility and heat deflection temperature of injection molded Poly(lactic acid) pro ducts: A comprehensive review. In *Polymer Testing* (Vol. 101). Elsevier Lt d. https://doi.org/10.1016/j.polymertesting.2021.107282

Taguchi, G. (1990). *Introduction to Quality Engineering*. McGraw Hill Education.

Tang, S. H., Cheng, C. W., Yeh, R. Y., & Hsu, R. Q. (2018). Direct joining of 3D-printed thermoplastic parts to SLM-fabricated metal cellular structures by ultrasonic welding. *International Journal of Advanced Manufacturing Technology*, *99*(1–4), 729–736. https://doi.org/10.1007/s00170-018-2409-8

Tawakoli, T., & Azarhoushang, B. (2008). Influence of ultrasonic vibrations on dry grinding of soft steel. *International Journal of Machine Tools and Manufacture*, *48*(14), 1585–1591. https://doi.org/10.1016/j.ijmachtools.2008.05.010

Tian, X., Jin, J., Yuan, S., Chua, C. K., Tor, S. B., & Zhou, K. (2017). Emerging 3D-Printed Electrochemical Energy Storage Devices: A Critical Review. *Advanced Energy Materials*, *7*(17). https://doi.org/10.1002/aenm.201700127

Tofail, S. A. M., Koumoulos, E. P., Bandyopadhyay, A., Bose, S., O'Donoghue, L., & Charitidis, C. (2018). Additive manufacturing: scientific and technological challenges, market uptake and opportunities. *Materials Today*, *21*(1), 22–37. https://doi.org/10.1016/j.mattod.2017.07.001

Torres, J., Cotelo, J., Karl, J., & Gordon, A. P. (2015). Mechanical property optimization of FDM PLA in shear with multiple objectives. *The Minerals, Metals&Materials Society*, *67*(5), 1183–1193. https://doi.org/10.1007/s11837-015-1367-y

Trattner, A., Hvam, L., Forza, C., & Herbert-Hansen, Z. N. L. (2019). Product complexity and operational performance: A systematic literature review. In *CIRP Journal of Manufacturing Science and Technology* (Vol. 25, pp. 69–83). Elsevier Ltd. https://doi.org/10.1016/j.cirpj.2019.02.001

Tymrak, B. M., Kreiger, M., & Pearce, J. M. (2014). Mechanical properties of components fabricated with open-source 3-D printers under realistic environmental conditions. *Materials and Design*, *58*(June 2014), 242–246. https://doi.org/10.1016/j.matdes.2014.02.038

Vaezi, M., & Chua, C. K. (2011). Effects of layer thickness and binder saturation level parameters on 3D printing process. *International Journal of Advanced Manufacturing Technology*, *53*(1–4), 275–284. https://doi.org/10.1007/s00170-010-2821-1

Van Der Walt, S., Du Preez, S., & Du Plessis, J. L. (2022). Particle emissions and respiratory exposure to hazardous chemical substances associated with binder jetting additive manufacturing utilizing poly methyl methacrylate. *Hygiene and Environmental Health Advances*, *4*, 100033. https://doi.org/10.1016/j.heha.2022.100033

Vidakis, N., Petousis, M., Korlos, A., Mountakis, N., & Kechagias, J. D. (2022). Friction Stir Welding Optimization of 3D-Printed Acrylonitrile Butadiene Styrene in Hybrid Additive Manufacturing. *Polymers*, *14*(12). https://doi.org/10.3390/polym14122474

Wałpuski, B., & Słoma, M. (2021). Additive Manufacturing of Electronics from Silver Nanopowders Sintered on 3D Printed Low-Temperature Substrates. *Advanced Engineering Materials*, *23*(4). https://doi.org/10.1002/adem.202001085

Wang, X., Jiang, M., Zhou, Z., Gou, J., & Hui, D. (2017). 3D printing of polymer matrix composites: A review and prospective. *Composites Part B: Engineering*, *110*, 442–458. https://doi.org/10.1016/j.compositesb.2016.11.034

Wang, X., Li, P., Xu, Z., Song, X., & Liu, H. (2010). Laser transmission joint between PET and titanium for biomedical application. *Journal of Materials Processing Technology*, *210*(13), 1767–1771. https://doi.org/10.1016/j.jmatprotec.2010.06.007

Weflen, E., & Frank, M. C. (2021). Hybrid additive and subtractive manufacturing of multi-material objects. *Rapid Prototyping Journal*, *27*(10), 1860–1871. https://doi.org/10.1108/RPJ-06-2020-0142

Weng, Z., Wang, J., Senthil, T., & Wu, L. (2016). Mechanical and the

rmal properties of ABS/montmorillonite nanocomposites for fused depositi on modeling 3D printing. *Materials and Design*, *102*, 276–283. https://doi.org/10.1016/j.matdes.2016.04.045

Wicaksono, S. T., Ardhyananta, H., & Pambudi, A. I. (2017). influence of internal geometri on mechanical properties of 3D printed polylactic acid (PLA) material. *International Journal of Engineering Sciences & Research Technology*, *6*(8), 74–78.

Wong, J., & Pfahnl, A. (2014). 3D Printing of Surgical Instruments for Long-Duration Space Missions. *Aviation*, *85*. https://doi.org/10.3357/ASEM.3898.2014

Wool, R. P., Yuan, B.-L., & McGarel, O. J. (1989). Welding of polymer interfaces. *Polymer Engineering & Science*, *29*(19), 1340–1367. https://doi.org/https://doi.org/10.1002/pen.760291906

Wu, D., Wu, S. Z., Xu, J., Niu, L. G., Midorikawa, K., & Sugioka, K. (2014). Hybrid femtosecond laser microfabrication to achieve true 3D glass/polymer composite biochips with multiscale features and high performance: The concept of ship-in-a-bottle biochip. *Laser and Photonics Reviews*, *8*(3), 458–467. https://doi.org/10.1002/lpor.201400005

Wu, W., Geng, P., Li, G., Zhao, D., Zhang, H., & Zhao, J. (2015). Influence of layer thickness and raster angle on the mechanical properties of 3D-printed PEEK and a comparative mechanical study between PEEK and ABS. *Materials*, *8*(9), 5834–5846. https://doi.org/10.3390/ma8095271

Wu, W., Wang, H., Wang, J., Liu, Q., Zhang, Z., Li, K., Gong, Y., Zhao, J., Ren, L., & Li, G. (2022). Hybrid Additive Manufacturing of Fused Filament Fabrication and Ultrasonic Consolidation. *Polymers*, *14*(12). https://doi.org/10.3390/polym14122385

Yassin, K., & Hojjati, M. (2017). Processing of thermoplastic matrix composites through automated fiber placement and tape laying methods: A review. *Journal of Thermoplastic Composite Materials*, *31*(12), 1676–172

5. https://doi.org/10.1177/0892705717738305

Zaldivar, R. J., Witkin, D. B., McLouth, T., Patel, D. N., Schmitt, K., & Nokes, J. P. (2017). Influence of processing and orientation print effects on the mechanical and thermal behavior of 3D-Printed ULTEM ® 9085 Material. *Additive Manufacturing*, *13*, 71–80. https://doi.org/10.1016/j.addma.2016.11.007

Zema, L., Loreti, G., Melocchi, A., Maroni, A., & Gazzaniga, A. (2012). Injection Molding and its application to drug delivery. *Journal of Controlled Release*, *159*(3), 324–331. https://doi.org/10.1016/j.jconrel.2012.01.001

Zhai, W., Wang, P., Ng, F. L., Zhou, W., Nai, S. M. L., & Wei, J. (2021). Hybrid manufacturing of γ-TiAl and Ti–6Al–4V bimetal component with enhanced strength using electron beam melting. *Composites Part B: Engineering*, *207*(December 2020), 108587. https://doi.org/10.1016/j.compositesb.2020.108587

Zhang, Y., Brown, K., Siebenaler, K., Determan, A., Dohmeier, D., & Hansen, K. (2011). Development of Lidocaine-Coated Microneedle Product for Rapid, Safe, and Prolonged Local Analgesic Action. *Pharmaceutical Research*, *29*, 170–177. https://doi.org/10.1007/s11095-011-0524-4

Zhang, Y., & Chou, K. (2008). A parametric study of part distortions in fused deposition modelling using three-dimensional finite element analysis. *Proceedings of the Institution of Mechanical Engineers, Part B: Journal of Engineering Manufacture*, *222*(8), 959–967. https://doi.org/10.1243/09544054JEM990

Zhao, Y., Chen, Y., & Zhou, Y. (2019). Novel mechanical models of tensile strength and elastic property of FDM AM PLA materials: Experimental and theoretical analyses. *Materials & Design*, *181*, 108089. https://doi.org/10.1016/j.matdes.2019.108089

Zhu, Z., Dhokia, V. G., Nassehi, A., & Newman, S. T. (2013). A revie

w of hybrid manufacturing processes - State of the art and future persp
ectives. *International Journal of Computer Integrated Manufacturing*, *26*(7),
596–615. https://doi.org/10.1080/0951192X.2012.749530

Zhuo, S., Geever, L. M., Halligan, E., Tie, B. S. H., & Breheny, C. (20
22). A Development of New Material for 4D Printing and the Material P
roperties Comparison between the Conventional and Stereolithography Pol
ymerised NVCL Hydrogels. *Journal of Functional Biomaterials*, *13*(4). https:
//doi.org/10.3390/jfb13040262

Ziemian, C., Sharma, M., & Ziemi, S. (2012). Anisotropic Mechanical
Properties of ABS Parts Fabricated by Fused Deposition Modelling. *Mecha
nical Engineering*. https://doi.org/10.5772/34233